NPS ARCHIVE
1965.06
PYATT, A.

ANALYSIS OF STEADY-STATE PERFORMANCE IN EIGHT SUPERCHARGED, MULTI-CYLINDER, TWO-STROKE DIESEL ENGINES

by

ARNOLD F. PYATT, LIEUTENANT, UNITED STATES NAVY

B.S., United States Naval Academy

(1958)

BARRICK F. TIBBITTS, LIEUTENANT, UNITED STATES NAVY

B.S., United States Naval Academy

(1956)

SUBMITTED IN PARTIAL FULFILLMENT OF THE REQUIREMENTS

FOR THE DEGREE OF NAVAL ENGINEER

AND THE DEGREE OF

MASTER OF SCIENCE IN MECHANICAL ENGINEERING

AT THE

MASSACHUSETTS INSTITUTE OF TECHNOLOGY

June, 1965

Thesis
P98

ANALYSIS OF EXHAUST TURBINE PERFORMANCE IN HIGHLY SUPERCHARGED, MULTI-CYLINDER, TWO-STROKE DIESEL ENGINES

by

ARNOLD F. PYATT, LIEUTENANT, UNITED STATES NAVY

B.S., United States Naval Academy

(1958)

BARRICK F. TIBBITTS, LIEUTENANT, UNITED STATES NAVY

B.S., United States Naval Academy

(1956)

SUBMITTED IN PARTIAL FULFILLMENT OF THE REQUIREMENTS

FOR THE DEGREE OF NAVAL ENGINEER

AND THE DEGREE OF

MASTER OF SCIENCE IN MECHANICAL ENGINEERING

AT THE

MASSACHUSETTS INSTITUTE OF TECHNOLOGY

June, 1965

Library
U. S. Naval Postgraduate School
Monterey, California

ANALYSIS OF EXHAUST TURBINE PERFORMANCE IN HIGHLY SUPERCHARGED, MULTI-CYLINDER, TWO-STROKE DIESEL ENGINES

by

Lt. Arnold F. Pyatt, U.S.N.

and

Lt. Barrick F. Tibbitts, U.S.N.

Submitted to the Department of Mechanical Engineering and to the Department of Naval Architecture and Marine Engineering on 21 May 1965 in partial fulfillment of the requirements for the degree of Master of Science in Mechanical Engineering and for the degree of Naval Engineer.

ABSTRACT

From engine test measurements a thermodynamic study was made to determine the conditions in the cylinder and the exhaust manifold during the exhaust process. The energy theoretically available in the exhaust gas was determined. This energy was compared with the energy actually recovered by the turbine.

This study used data taken from two different diesel engines, four different exhaust turbines and six different exhaust manifolds. A total of ten different engine-manifold-turbine combinations were investigated.

The relative merits of both blow-down and steady-flow energy recovery systems are compared. In addition, the effects of varying exhaust manifold length and cross-section, varying turbine nozzle cross-section, varying exhaust elbow length and cross-section and varying turbine back pressure are discussed.

It is recommended that studies and tests be conducted to determine the manifold size and geometric configuration that will provide the optimum matching of engine and turbine requirements. It is further recommended that an economic study be made of the feasibility of exhaust power recovery systems to recover power for purposes other than turbocharging.

Thesis Supervisor: C. Fayette Taylor
Title: Professor of Automotive Engineering

ACKNOWLEDGMENTS

The authors wish to express their sincere thanks and gratitude to C. Fayette Taylor, Professor of Automotive Engineering, Massachusetts Institute of Technology for his counsel and guidance during the preparation of this thesis.

The authors also wish to express their thanks to Mr. Alan M. Schrader, Head of Mechanical Branch, Machinery Division, of the United States Naval Marine Engineering Laboratory for making available the data which provided the basis for this thesis. The many personal conversations with Mr. Schrader concerning test procedures and results were invaluable.

TABLE OF CONTENTS

LIST OF FIGURES

NOTES

(1) Figures 2a through 34a are plots of Theor. Exhaust HP vs. BHP for various runs.

(2) Figures 2b through 34b are plots of Turbine Recovery Efficiency vs. BHP for various runs.

(3) Figures 35 through 37 are performance plots of the G. E. Turbochargers with Divided and Common Manifolds at various values of P_4/P_6.

(4) Figures 38 through 42 are performance plots of the Elliott Pulse Turbochargers with Divided and Common Manifolds at various values of P_4/P_6.

(5) Figures 43 through 48 are performance plots of the Elliott Steady Flow Turbochargers with Common and Pulse Converter Manifolds at various values of P_4/P_6.

(6) Figures 49 through 53 are performance plots of the Elliott Steady Flow Turbochargers with EES Manifold without Charger Plates at various values of P_4/P_6.

(7) Figures 54 through 59 are performance plots of the Elliott Steady Flow Turbochargers with EES Manifold without Charger Plates and with various length exhaust elbows and various injector tips at various values of P_4/P_6.

(8) Figures 60 through 63 are performance plots of the Elliott Steady Flow Turbochargers with Common, EES and Pulse Conv. Manifolds at various values of P_4/P_6.

(9) Figures 64 through 70 are performance plots of the DeLaval Steady Flow Turbochargers with Pulse Conv. and EES Manifolds at various values of P_4/P_6.

(10) Figures 71 through 77 are performance plots of the DeLaval Steady Flow Turbochargers with EES Manifold at various values of P_4/P_6.

(11) Figures 78 through 81 are performance plots of the DeLaval Steady Flow Turbochargers with the 8-cylinder engine at various values of P_4/P_6.

(12) Figures 82 through 89 and figures 91 and 95 are performance plots with the DeLaval Steady Flow Turbochargers with various parameters individually varied.

(13) Figures 96 and 97 are plots of the amount of Blowdown and Steady Flow Works that are theoretically available.

LIST OF SYMBOLS

C_P = Specific heat at constant pressure $\left(\frac{\text{BTU}}{\text{lbm.}^{\circ}\text{R}}\right)$

e_S = Scavenging efficiency = $\frac{\text{Air mass retained in cylinder}}{\text{Ideal cylinder air mass}}$

$= \frac{\Gamma \dot{M}_a}{N\, V_D\, \rho_S} \quad (r/r\text{-}1)$

f = Residual gas fraction = $\frac{M_R}{M'_a + M_R}$

F = Fuel air ratio = $\frac{\dot{M}_f}{\dot{M}_a}$

F' = Trapped fuel air ratio = $\frac{F}{\Gamma} = \frac{\dot{M}_f}{\Gamma \dot{M}_a}$

F_C = Stoichiometric fuel-air ratio

F_R = Relative fuel air ratio = F/F_C

F_R' = Trapped relative fuel-air ratio = $\frac{F_R}{\Gamma}$

Γ = Trapping efficiency = $\frac{\text{Air Flow Trapped}}{\text{Air Flow Supplied}} = \frac{e_S}{R_S}$

h = % water vapor by mass = $\frac{\dot{m}_v}{\dot{m}_a}$

J = Conversion constant = $\frac{778 \text{ ft. lbf}}{\text{BTU}}$

K = Ratio of specific heats $\frac{C_P}{C_v}$

m_e = Molecular weight of exhaust gases $\left(\frac{\text{lbm}}{\text{lbm.mole}}\right)$

$\dot{M}_a$ = Mass flow of dry air/unit time $\left(\frac{\text{lbm.}}{\text{min.}}\right)$

M_a = Mass of dry air/engine cycle = $\frac{\dot{M}_a}{N}$ $\left(\frac{\text{lbm}}{\text{Cycle}}\right)$

M_a' = Trapped mass of dry air/engine cycle = ΓM_a $\left(\frac{\text{lbm}}{\text{Cycle}}\right)$

M_{CHC} = Mass of trapped cylinder charge during compression/engine cycle = $\Gamma M_a (1+h) + M_R = \frac{M_a'}{(1-f)} \left[1 + h(1-f)\right]$

M_{CHE} = Mass of trapped cylinder charge during expansion/engine cycle $\left(\frac{\text{lbm}}{\text{cycle}}\right) = M_a' \left[(1+h) + \left(\frac{f}{1-f}\right) + F'\right]$

$\dot{M}_i$ = Air flow to engine/unit time (lbm/min.)

$\dot{M}_{EXH}$ = Exhaust flow from engine/unit time $\left(\frac{\text{lbm}}{\text{min}}\right) = \Gamma \dot{M}_a (1+h+F')$

$\dot{M}_f$ = Mass flow of fuel/unit time $\left(\frac{\text{lbm}}{\text{min}}\right)$

M_R = Mass of retained exhaust/engine cycle

$\dot{M}_{SC}$ = Mass flow of untrapped air/unit time ($^{\text{lbm}}/_{\text{min}}$) = $\dot{M}_a(1+h)(1-\Gamma)$

N = Engine cycles (revolutions /unit time)(RPM)

ρ_S = Scavenging air density $\left(\frac{\text{lbm}}{ft^3}\right) = \left(\frac{P_5}{RT_{BX}}\right)$

P_1 = Absolute pressure at start of compression (atm)

P_4 = Absolute pressure at exhaust valve opening (atm)

P_5 = Absolute engine exhaust back pressure = Absolute exhaust turbine inlet pressure (atm)

P_6 = Absolute exhaust turbine discharge pressure (atm)

P_7 = P_{atm} = Atmospheric Pressure (atm)

P_{EXH1} = Theoretical blowdown power in exhaust gas flow (hp) =

$$\frac{\dot{M}_{EXH}\, R_e\, T_4}{3.3 \times 10^4} \left[\frac{1}{k-1} \left(1 - \left(\frac{P_5}{P_4}\right)^{\frac{k-1}{k}}\right) - \left(\left(\frac{P_5}{P_4}\right)^{\frac{k-1}{k}} - \frac{P_5}{P_4}\right)\right]$$

P_{EXH2} = Theoretical steady flow power in exhaust gas flow (hp) =

$$\frac{\dot{M}_{EXH}}{3.3 \times 10^4}\, C_{Pe}\, T_5\, Y_{T1}\, J$$

P_{SC} = Theoretical power in scavenge air flow (hp) =

$$\frac{\dot{M}_{SC}}{3.3 \times 10^4}\, C_P\, T_1\, Y_{T2}\, J$$

P_{EXH} = Total theoretical power available in exhaust gases (hp) =

$$P_{EXH1} + P_{EXH2} + P_{SC}$$

P_T = Power recovered by exhaust turbine (hp) = $\dfrac{\dot{M}_I\, C_{P_a} \left[(RC)^{\frac{k_a - 1}{k_a}} - 1\right] J\, T_A}{\eta_C\, 3.3 \times 10^4}$

η_C = Isentropic compressor efficiency (%)

η_R = Overall exhaust power recovery efficiency (%) = $\dfrac{P_T}{P_{EXH}}$ (100)

r = Engine compression ratio

RC = Compressor pressure ratio = $\dfrac{P_{OUT}}{P_{ATM}}$

R_e = Gas constant for exhaust gases = 53.5 $\dfrac{ft.lbf}{lbm \cdot {}^oR}$

R_S = Scavenging ratio = $\frac{\text{Mass of air supplied}}{\text{Ideal air mass}} = \frac{\dot{M}_I}{N V_C \left(\frac{P_5}{R_e T_{BX}}\right)} =$

$$\frac{\dot{M}_I}{N V_C \rho_S}$$

T_A = Ambient air temperature (^oR)

T_{ID} = Isentropic temperature (^oR)

T_{BX} = Inlet air box temperature (^oR)

T_{DISCH} = Average discharge temperature (^oR)

T_1 = Temperature of mixed cylinder charge at start of compression (^oR)

T_4 = Temperature of cylinder charge at instant of exhaust valve opening (^oR)

T_5 = Temperature of exhaust gases at exhaust turbine inlet (^oR)

T_6 = Temperature of exhaust gases at exhaust turbine outlet (^oR)

V_C = Cylinder volume above piston at bottom center (ft^3)

$Y_{T1} = 1 - \left(P_6/P_5\right) \frac{k_e - 1}{k_e}$

$Y_{T2} = 1 - \left(P_6/P_5\right) \frac{k_\alpha - 1}{k_\alpha}$

CHAPTER I

INTRODUCTION

The experimental results which are analyzed herein were obtained by the U. S. Naval Marine Engineering Laboratory at Annapolis, Maryland. The original purpose of the experimentation was to determine whether the GM 16-278 diesel engine, rated at 1600 BHP, could be successfully supercharged to 3000 BHP with existing hardware. This goal was reached rather quickly and an attempt was made to optimize supercharged engine performance. To this end, four different turbochargers, four different manifold geometries (including two specially designed for this application), and numerous nozzle geometries were tested. The original experiments were designed to help select a compatible package of working hardware. As the tests progressed, the analysis of engine performance became more concerned with improving the hardware selected. This analysis was thorough and well documented as applied to the specific problems they were considering.

In this thesis we have conducted a critical theoretical analysis of the data obtained with the specific intent of applying the lessons learned to the general case. This data represents the culmination of a test program covering several years and costing over a million dollars; it is undoubtedly one of the best documented tests of supercharged multi-cylinder, two stroke, diesel engines available. It is our belief that a critical analysis of these engines' exhaust turbine performance can be of considerable value to future design applications.

Wherever applicable, references to accepted works in the literature will be made in discussing the observed results. Results of the laboratory tests agree quite well with previously postulated theories in a number of instances.

Our primary goal is to present as clearly and concisely as possible the factors to be considered in designing the exhaust system to optimize exhaust power recovery. Although our analysis is taken from supercharged engine installations, the results are generally applicable to any engine of moderate size. The recovery of any significant portion of the power available in the exhaust will greatly improve the overall efficiency of the engine system regardless of the use to which this power is put.

CHAPTER II

THERMODYNAMIC ANALYSIS OF EXHAUST TURBINE AND ENGINE PERFORMANCE

Although we are primarily interested in the exhaust system and the power recovery from the exhaust gases, no realistic evaluation of this phenomenon in an actual engine can be made without a knowledge of the operating conditions within the engine. The determination of these conditions is, at best, only approximate because of the difficulty in identifying and measuring the exact conditions.

We have chosen as our thermodynamic model the constant volume cycle as shown in Figure 91 . The assumptions which we have made to fit this model are: 1) that the pressure at the start of compression (P_1) is equal to the exhaust back pressure (P_5)*, 2) that the inlet air temperature is approximately equal to the average inlet airbox temperature (T_{BX}), 3) that the vapor content of the inlet air flow is constant at 2 mass %, 4) that both air and exhaust gas can be treated as perfect gases with constant specific heats and 5) that the scavenging efficiency (e_S) of this engine can be approximated by Figure 11-7 of Reference 27.

These assumptions are almost sufficient to permit us to enter the charts of the Edson-Taylor paper (Reference 11) and compute the various points of the cycle. For our purposes, we are interested solely in point 4, the point at which the exhaust process begins. In order to use the Edson-Taylor charts a knowledge of the residual gas

*Reference 27, Chapter II, page 275.

fraction (f) is required. When the data under consideration was collected, no measurement of this quantity was made. We must, therefore, approximate the residual gas fraction as follows:

The compressive cylinder charge is composed of air, water vapor and residual exhaust gases. A value of f is assumed; in our particular case, we found f = .12 to be an approximate mean value. With this value of f, the computational procedure of the Edson-Taylor paper is completed and values of T_1 and T_4 are obtained. From T_4, P_4 and P_5, assuming isentropic expansion in accordance with accepted engine analysis procedures, a value of T_5 is obtained. The mixing equation which we have elected to use is a simple approximate enthalpy balance for 1 lb. of mixed cylinder charge. A more sophisticated mixing equation is unwarranted in view of the other assumptions made thus far: $\therefore \quad C_P \; T_1 = C_P \; T_{BX} \; (1-f) + T_5 \; C_{Pe} \; f$. With this equation, an iterative procedure (described in detail in Appendix G.) is used to vary f until T_1 computed by the Edson-Taylor charts is equal to T_1 computed from the mixing equation. When this requirement is met, the exhaust release point temperature and pressure have been determined within the accuracy of the input quantities and necessary assumptions.

After examining the literature concerning properties of exhaust gases, we selected a C_{Pe} of .27 BTU/ lbm.^{o}R, a ratio of specific heats K = 1.35 and a universal gas constant Re = 53.5 $\frac{\text{ft. lbf}}{\text{lbm.}^{o}\text{R}}$ as representative of average conditions in our region of interest. Without specific measurement of exhaust conditions, which were not made, we decided that the validity of the analysis would not be unduly prejudiced by the use of average properties. The gain in simplicity of analysis far outweighs any loss in accuracy. Reliability of results is discussed in detail in Appendix H.

A very critical section of this analysis, and one which is admittedly suspect, is the determination of the trapping efficiency, Γ. This quantity is dependent on the validity of the calculation of e_S since $\Gamma = \frac{e_S}{R_S}$. Our determination of e_S is based on data collected from a similar engine and a limited survey of published test data indicated little variation in this quantity for similar engines. The consistency of our computated results in returning a value of $\Gamma = .688 \pm .018$ lends credence to this assumption. We conclude that whatever error is introduced is reflected uniformly through the reduced data.

Trapping efficiency, Γ, is defined as mass of air supplied/mass of air retained in the cylinders and is equal to unity only in the ideal engine. Therefore, in any real engine all of the air supplied is not

retained in the cylinders, but a portion flows through the engine into the exhaust system. The major portion of this untrapped air is the scavenge air of a two stroke engine; the remainder is forced out of the cylinder through the exhaust valve at the start of the compression stroke. We therefore have two distinct flow paths through the engine: the first, or primary flow, is the trapped air which is the working fluid of the engine and the secondary or "bypass" flow which is the untrapped air. In actuality, there is mixing of these two flows which is extremely complex and poorly understood. In order to bridge this difficulty, we have treated the two flows as completely independent of each other. The trapped flow participates in the combustion process and is exhausted from the cylinders at T_4 and P_4, and is assumed to expand isentropically to P_5, the steady exhaust back pressure. The "bypass" flow is assumed to be in equilibrium with the cylinder charge and has as its properties T_1 and $P_1 = P_5$.

The evaluation of theoretical exhaust energy is in three parts: the first part consists of the isentropic expansion work minus the pv work of the exhaust blowdown between points 4 and 5 as shown in Figure 91. This energy is designated P_{EXH1}. The second part is the steady flow work of the primary flow between points 5 and 6. This work is simply the enthalpy difference between points 5 and 6 and is designated P_{EXH2}. The third part is the work obtained from the "bypass" air flow and is the enthalpy difference between a point T_1 and P_5 and

a point with pressure, P_6 and a temperature corresponding to isentropic expansion across the pressure ratio P_5/P_6. This work is designated P_{SC}. The total theoretical energy is the sum of these three and is designated P_{EXH}. A detailed derivation of the equations for these quantities from basic thermodynamic equalities is contained in Appendix F.

CHAPTER III

EXPERIMENTAL METHODS

This chapter discusses the methods by which and the physical locations at which engine data was measured. The engines, manifolds and turbines are discussed in Chapter V and Appendices A, B, C, D and E.

Figure 93 is a schematic drawing of a typical divided-manifold geometry showing the various points at which measuring instruments were located.

The following equipment was used:

1. The engine power was absorbed by a hydraulic dynamometer.

2. A Foster flow tube was used to measure the air consumption of the engine. This was a modified venturi-type flowmeter.

3. Maximum cylinder pressures were measured by a Control Engineering Model EP-3000 pressure transducer with a Control Engineering Model 3AC amplifier and a Dumont Model 304H oscilloscope. Simultaneous measurements of dynamic pressure in the cylinders, scavenge air box and exhaust manifold were made by means of Control Engineering Models EP-3000 and LP-50 pressure transducers in combination with Consolidated Electrodynamics Corporation Model 105-A oscillator power supply, Model 1-113B amplifiers and Model 5-114P4 oscillograph.

4. The carbon dioxide content of the exhaust gas was determined by a Ranarex meter. The oxygen content was measured by Hays and Pauling-Beckman analyzers.

5. Samples of the combustion chamber gas from the cylinders and exhaust gas from the exhaust valves were obtained by means of a timed Cox sampling valve.

6. Mercury or water filled manometers were used to measure air and exhaust gas pressures. Pertinent temperatures were recorded by means of thermocouples and an automatic temperature recorder. A calibrated rotameter was used to measure fuel flow.

CHAPTER IV

RESULTS

The results of the computer analysis of thermodynamic engine and exhaust turbine performance are plotted on the following figures.

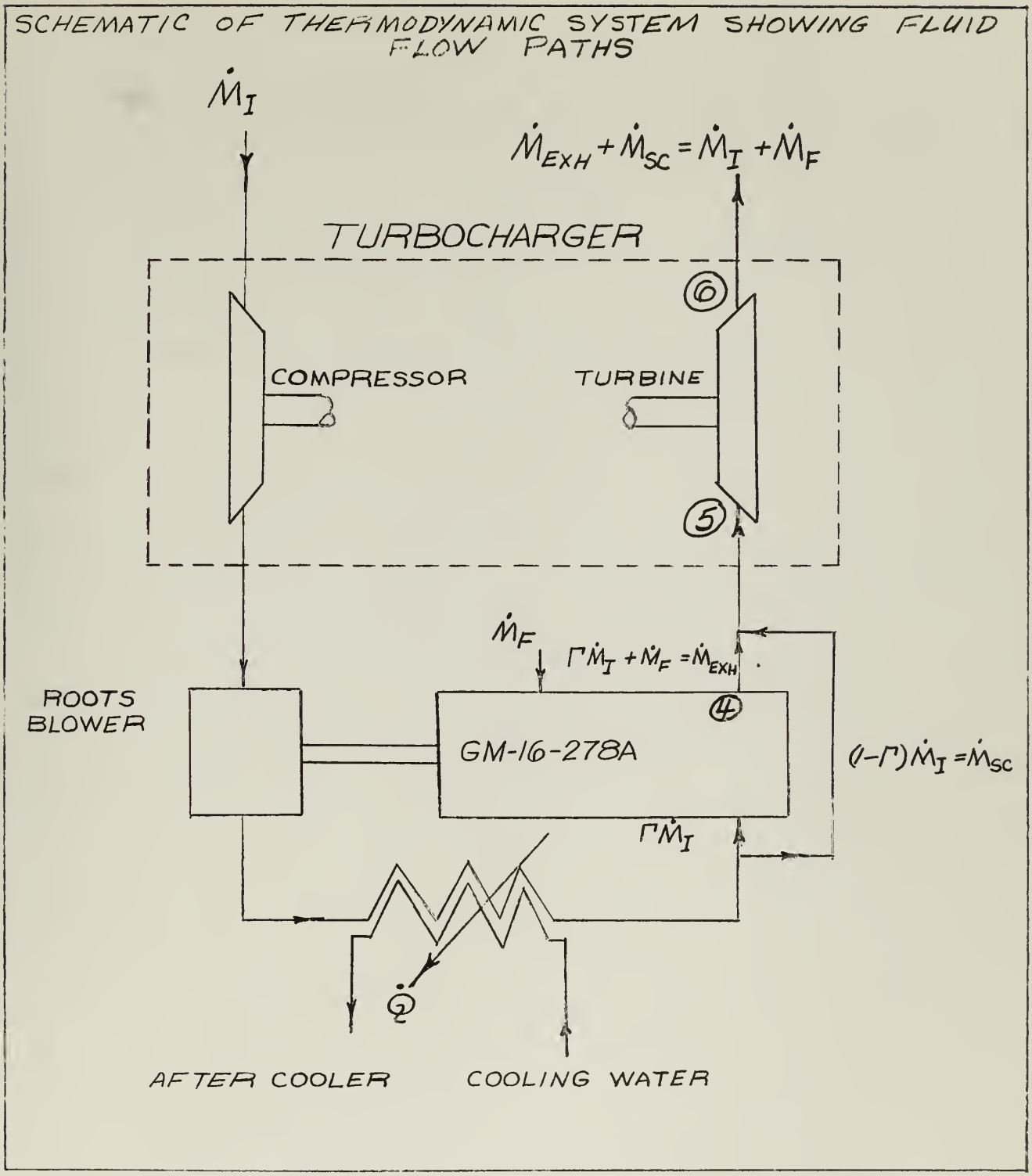
SCHEMATIC OF THERMODYNAMIC SYSTEM SHOWING FLUID FLOW PATHS
$\dot{M}_I$
$\dot{M}_{EXH} + \dot{M}_{SC} = \dot{M}_I + \dot{M}_F$
TURBOCHARGER
6
COMPRESSOR
TURBINE
5
$\dot{M}_F$
$\Gamma\dot{M}_I + \dot{M}_F = \dot{M}_{EXH}$
4
ROOTS BLOWER
GM-16-278A
$(1-\Gamma)\dot{M}_I = \dot{M}_{SC}$
$\Gamma\dot{M}_I$
$\dot{Q}$
AFTER COOLER
COOLING WATER

FIG. 1

FIG. 2A

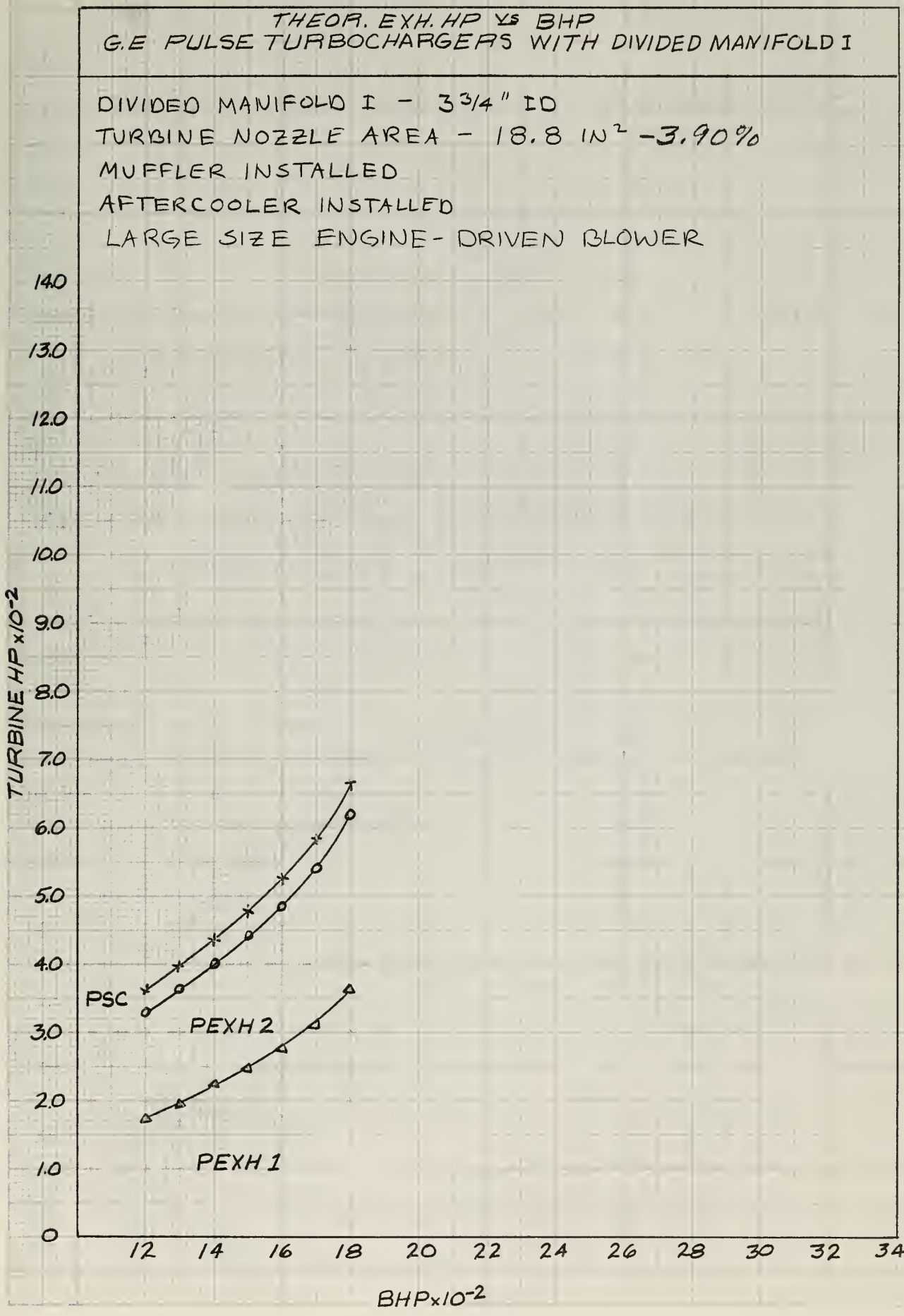
THEOR. EXH. HP Vs BHP
G.E PULSE TURBOCHARGERS WITH DIVIDED MANIFOLD I
DIVIDED MANIFOLD I - 3 3/4" ID
TURBINE NOZZLE AREA - 18.8 IN² -3.90%
MUFFLER INSTALLED
AFTERCOOLER INSTALLED
LARGE SIZE ENGINE-DRIVEN BLOWER
TURBINE HP x10⁻²
14.0
13.0
12.0
11.0
10.0
9.0
8.0
7.0
6.0
5.0
4.0
3.0
2.0
1.0
0
PSC
PEXH 2
PEXH 1
12
14
16
18
20
22
24
26
28
30
32
34
BHP x10⁻²

FIG. 2B

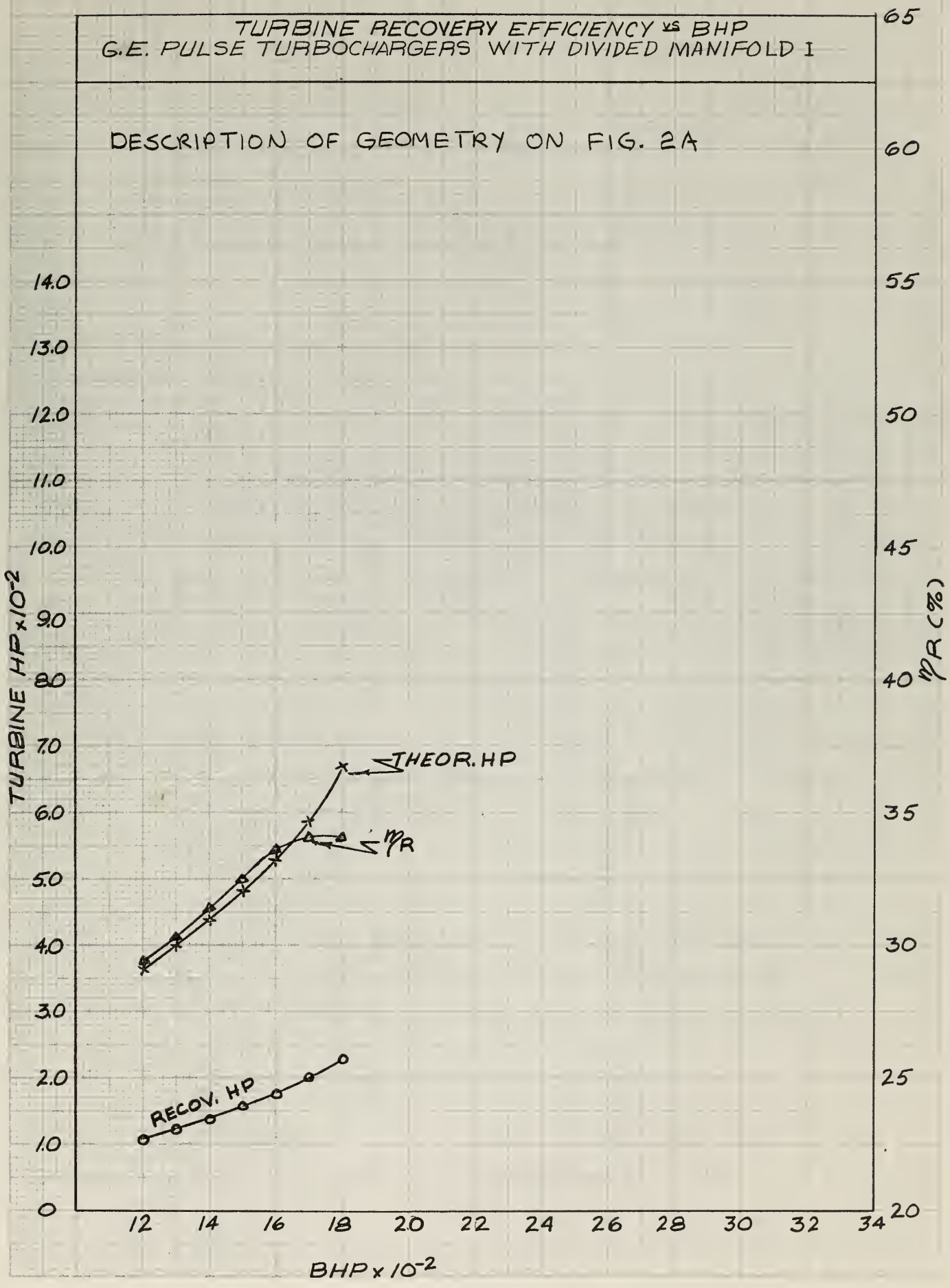
TURBINE RECOVERY EFFICIENCY vs BHP
G.E. PULSE TURBOCHARGERS WITH DIVIDED MANIFOLD I
DESCRIPTION OF GEOMETRY ON FIG. 2A
TURBINE HP x 10-2
ηR (%)
BHP x 10-2
THEOR. HP
ηR
RECOV. HP
0
1.0
2.0
3.0
4.0
5.0
6.0
7.0
8.0
9.0
10.0
11.0
12.0
13.0
14.0
20
25
30
35
40
45
50
55
60
65
12
14
16
18
20
22
24
26
28
30
32
34

FIG. 3A

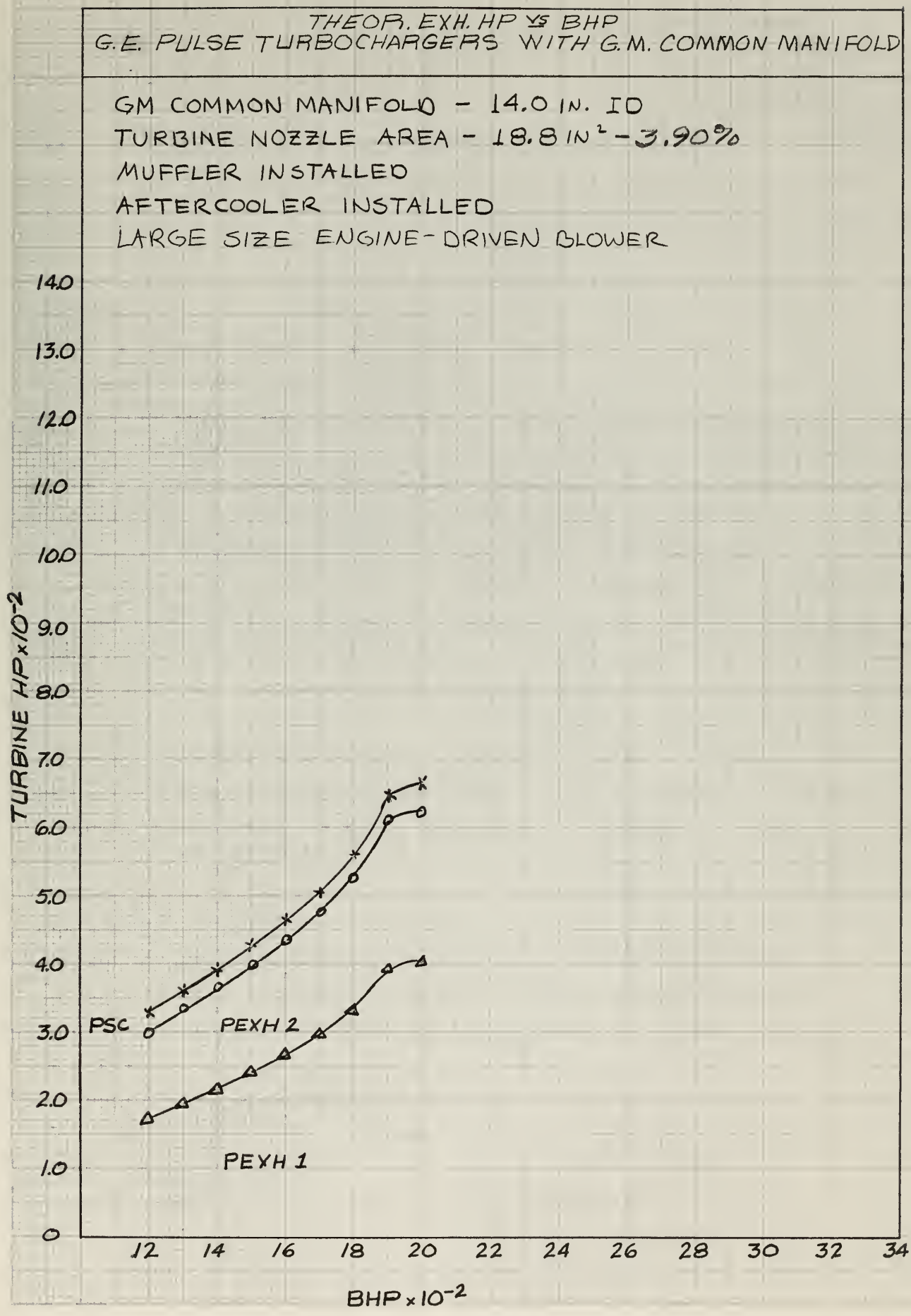
THEOR. EXH. HP VS BHP
G.E. PULSE TURBOCHARGERS WITH G.M. COMMON MANIFOLD
GM COMMON MANIFOLD - 14.0 IN. ID
TURBINE NOZZLE AREA - 18.8 IN² - 3.90%
MUFFLER INSTALLED
AFTERCOOLER INSTALLED
LARGE SIZE ENGINE-DRIVEN BLOWER
TURBINE HP x 10⁻²
14.0
13.0
12.0
11.0
10.0
9.0
8.0
7.0
6.0
5.0
4.0
3.0
2.0
1.0
0
PSC
PEXH 2
PEXH 1
12
14
16
18
20
22
24
26
28
30
32
34
BHP x 10⁻²

FIG. 3B

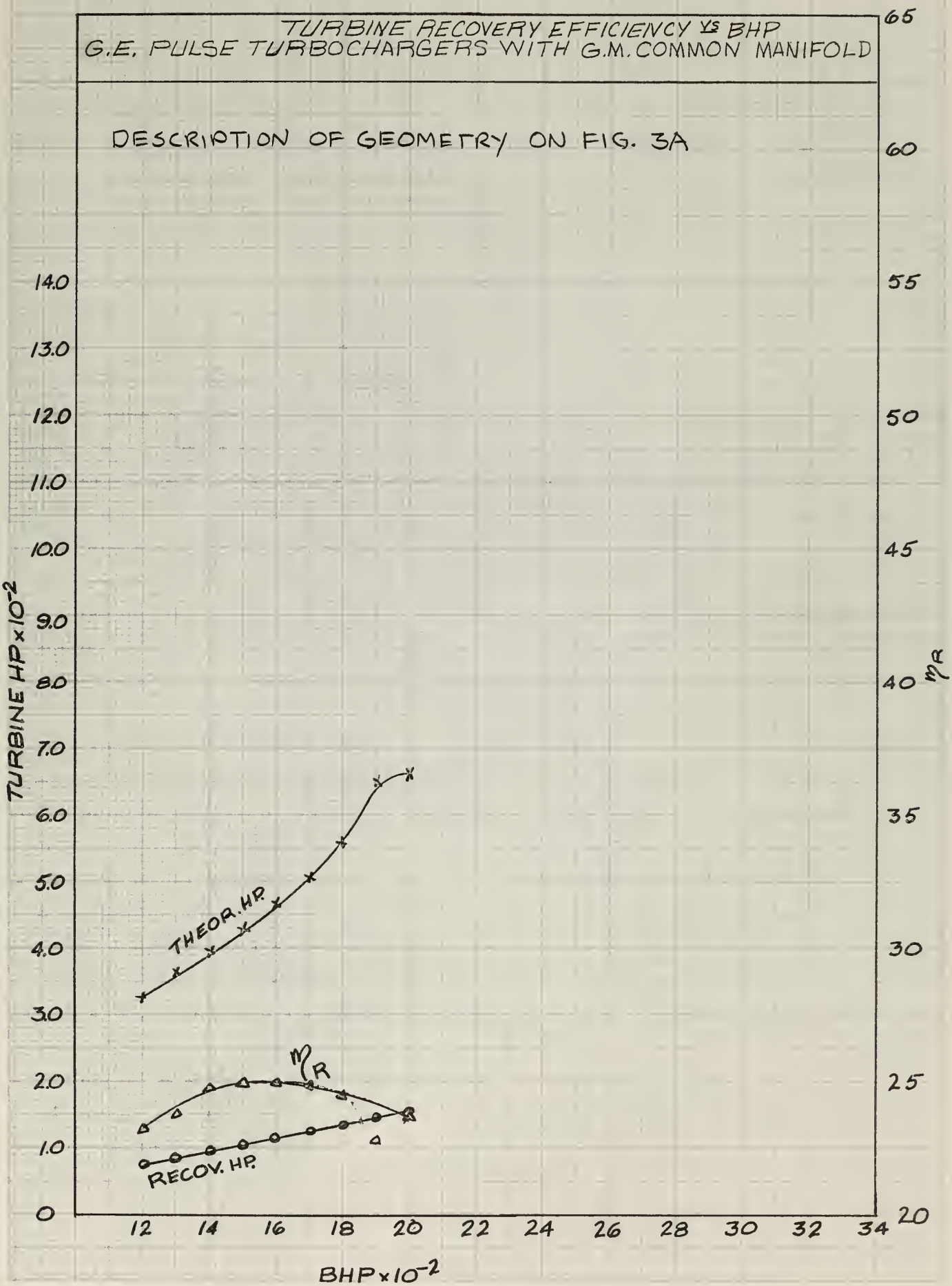
TURBINE RECOVERY EFFICIENCY VS BHP
G.E. PULSE TURBOCHARGERS WITH G.M. COMMON MANIFOLD
DESCRIPTION OF GEOMETRY ON FIG. 3A
TURBINE HP x 10⁻²
14.0
13.0
12.0
11.0
10.0
9.0
8.0
7.0
6.0
5.0
4.0
3.0
2.0
1.0
0
THEOR. HP
MR
RECOV. HP
12
14
16
18
20
22
24
26
28
30
32
34
BHP x 10⁻²
65
60
55
50
45
40
35
30
25
20
MR

FIG. 4A

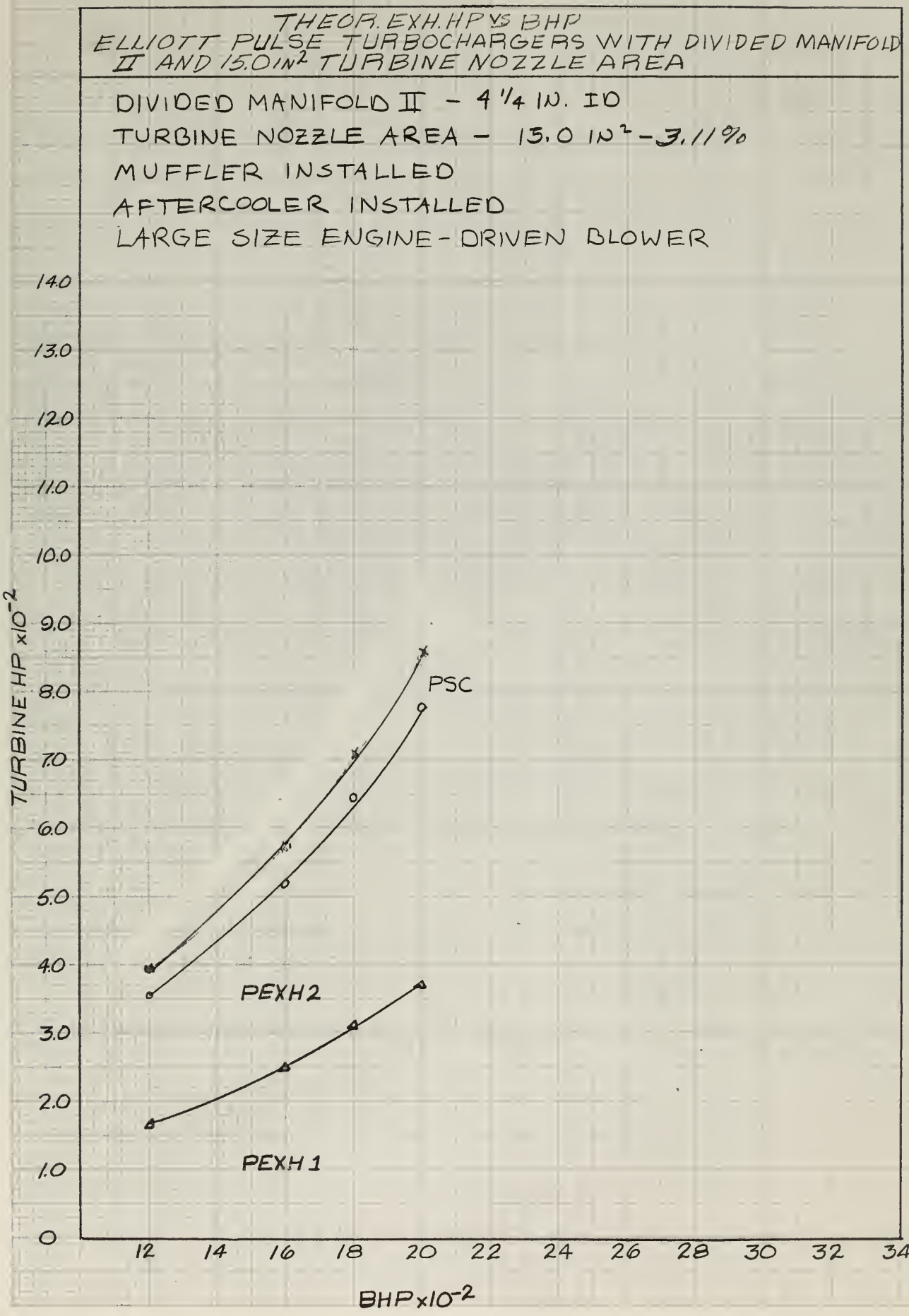
THEOR. EXH. HP VS BHP
ELLIOTT PULSE TURBOCHARGERS WITH DIVIDED MANIFOLD II AND 15.0 IN² TURBINE NOZZLE AREA
DIVIDED MANIFOLD II - 4 1/4 IN. ID
TURBINE NOZZLE AREA - 15.0 IN² - 3.11%
MUFFLER INSTALLED
AFTERCOOLER INSTALLED
LARGE SIZE ENGINE-DRIVEN BLOWER
TURBINE HP x10⁻²
BHP x10⁻²
PSC
PEXH2
PEXH1
14.0
13.0
12.0
11.0
10.0
9.0
8.0
7.0
6.0
5.0
4.0
3.0
2.0
1.0
0
12
14
16
18
20
22
24
26
28
30
32
34

FIG. 4B

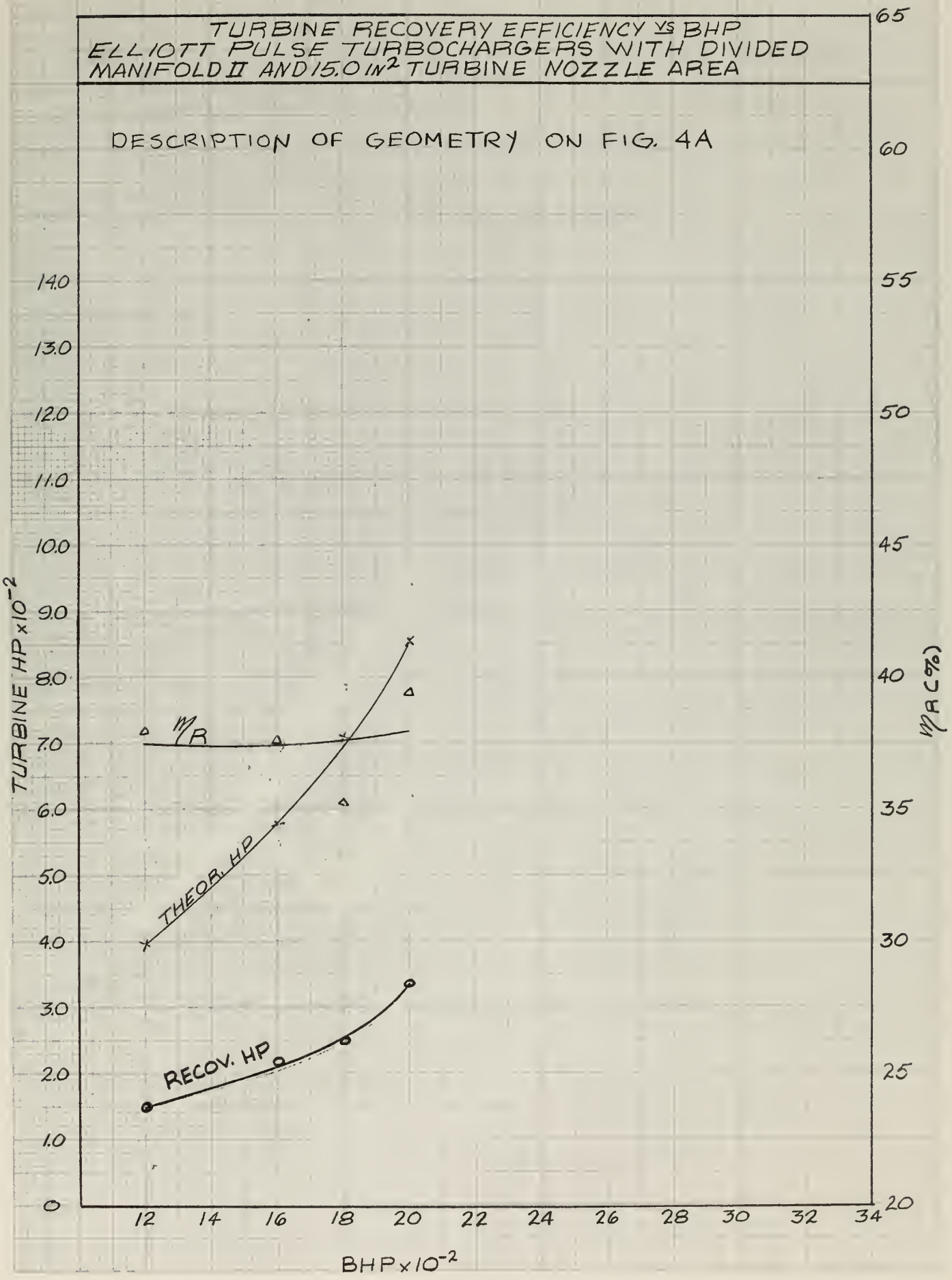
TURBINE RECOVERY EFFICIENCY VS BHP
ELLIOTT PULSE TURBOCHARGERS WITH DIVIDED MANIFOLD II AND 15.0 IN² TURBINE NOZZLE AREA
DESCRIPTION OF GEOMETRY ON FIG. 4A
TURBINE HP x 10⁻²
14.0
13.0
12.0
11.0
10.0
9.0
8.0
7.0
6.0
5.0
4.0
3.0
2.0
1.0
0
65
60
55
50
45
40
35
30
25
20
ηR (%)
ηR
THEOR. HP
RECOV. HP
12
14
16
18
20
22
24
26
28
30
32
34
BHP x 10⁻²

FIG. 5A

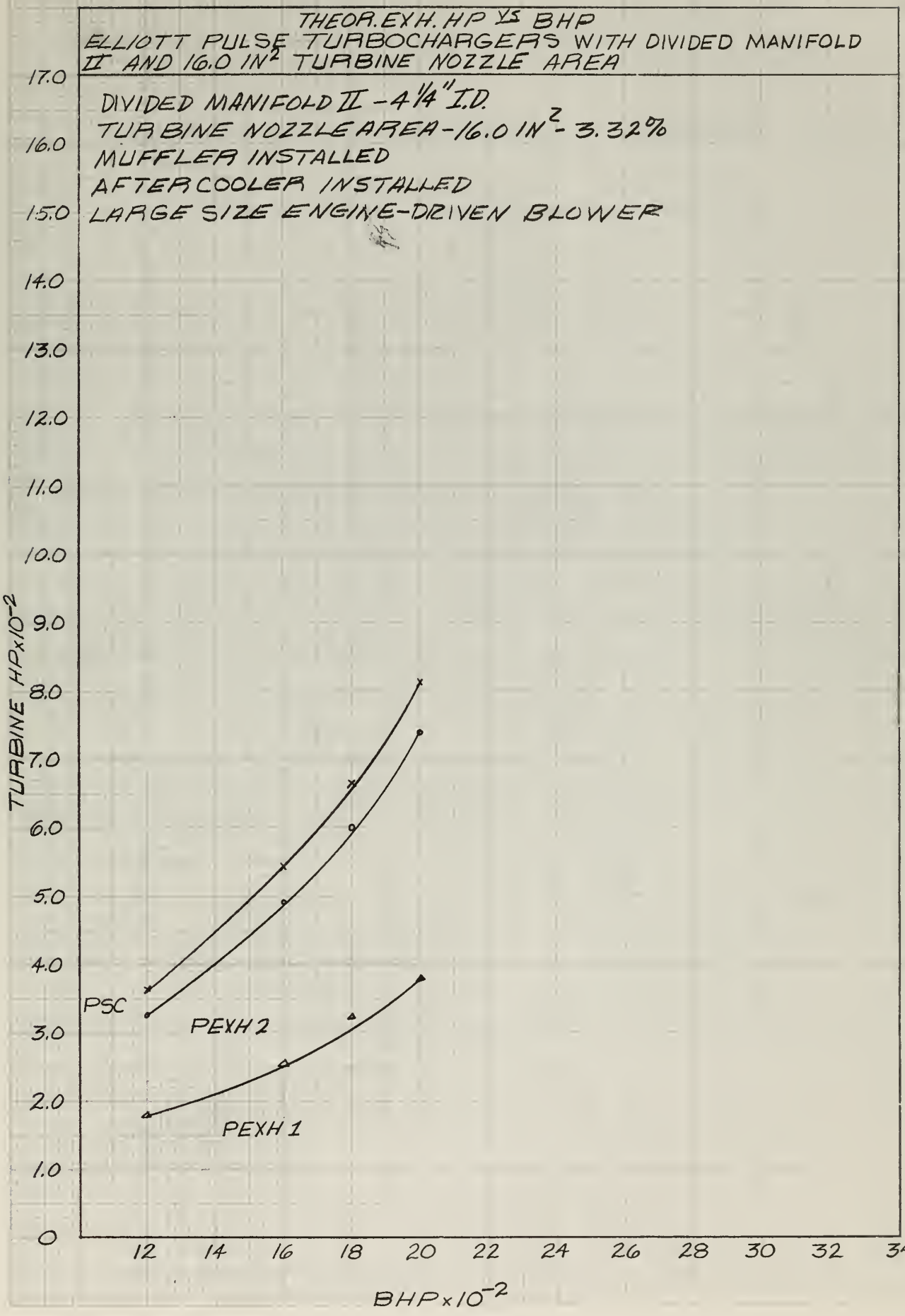
THEOR. EXH. HP VS BHP
ELLIOTT PULSE TURBOCHARGERS WITH DIVIDED MANIFOLD II AND 16.0 IN² TURBINE NOZZLE AREA
DIVIDED MANIFOLD II - 4 1/4" I.D.
TURBINE NOZZLE AREA - 16.0 IN² - 3.32%
MUFFLER INSTALLED
AFTERCOOLER INSTALLED
LARGE SIZE ENGINE-DRIVEN BLOWER
TURBINE HP x 10⁻²
BHP x 10⁻²
PSC
PEXH 2
PEXH 1
17.0
16.0
15.0
14.0
13.0
12.0
11.0
10.0
9.0
8.0
7.0
6.0
5.0
4.0
3.0
2.0
1.0
0
12
14
16
18
20
22
24
26
28
30
32
34

FIG. 5B

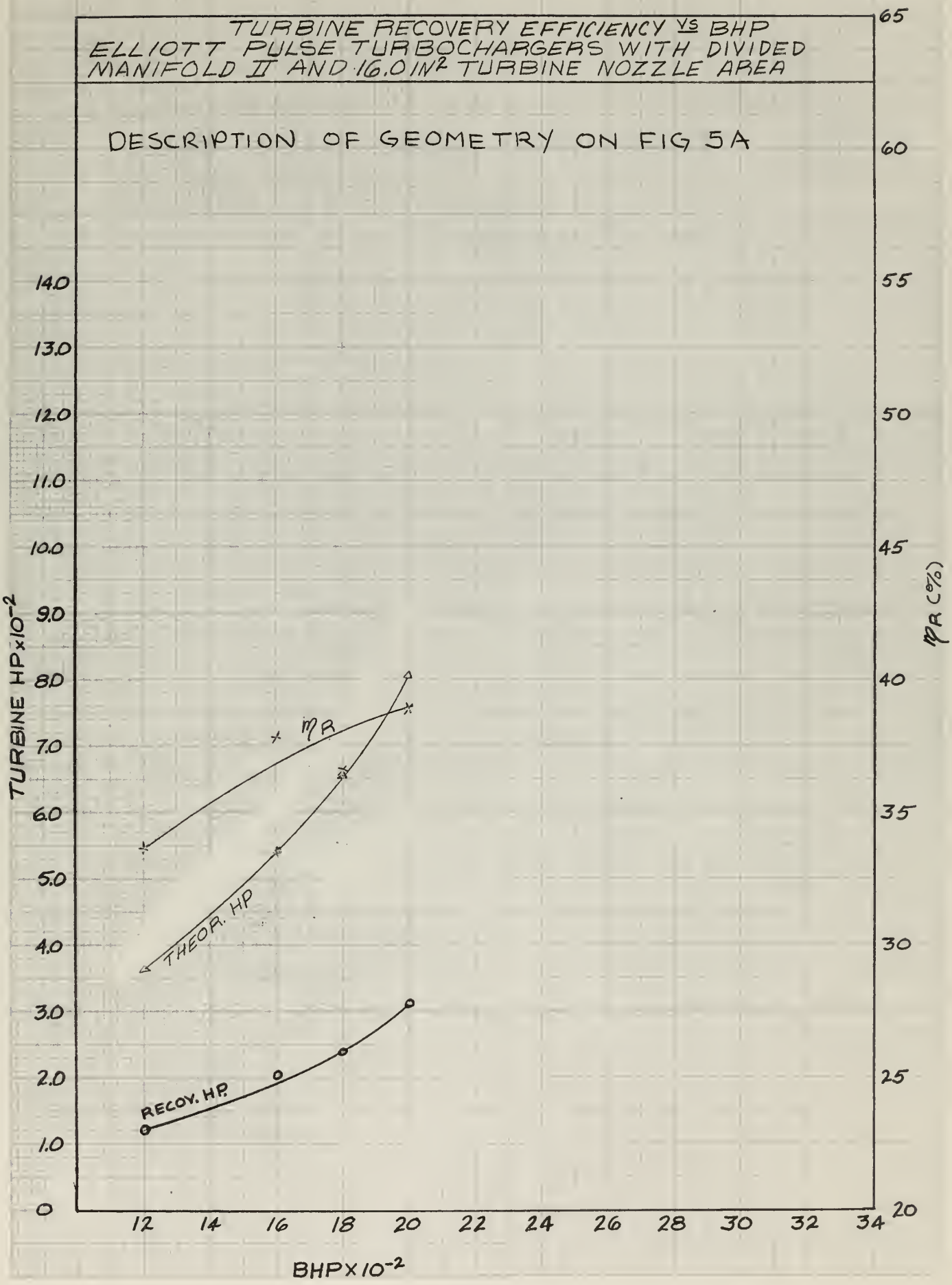
TURBINE RECOVERY EFFICIENCY VS BHP
ELLIOTT PULSE TURBOCHARGERS WITH DIVIDED MANIFOLD II AND 16.0 IN² TURBINE NOZZLE AREA
DESCRIPTION OF GEOMETRY ON FIG 5A
TURBINE HP x 10⁻²
BHP x 10⁻²
ηR (%)
ηR
THEOR. HP
RECOV. HP
0
1.0
2.0
3.0
4.0
5.0
6.0
7.0
8.0
9.0
10.0
11.0
12.0
13.0
14.0
12
14
16
18
20
22
24
26
28
30
32
34
20
25
30
35
40
45
50
55
60
65

FIG. 6A

THEOR. EXH. HP VS BHP
ELLIOTT PULSE TURBOCHARGERS WITH DIVIDED MANIFOLD II AND 18.5 IN^2 TURBINE NOZZLE AREA

DIVIDED MANIFOLD II - 4 1/4 IN. ID
TURBINE NOZZLE AREA - 18.5 IN^2 - 3.84%
MUFFLER INSTALLED
AFTERCOOLER INSTALLED
LARGE SIZE ENGINE-DRIVEN BLOWER

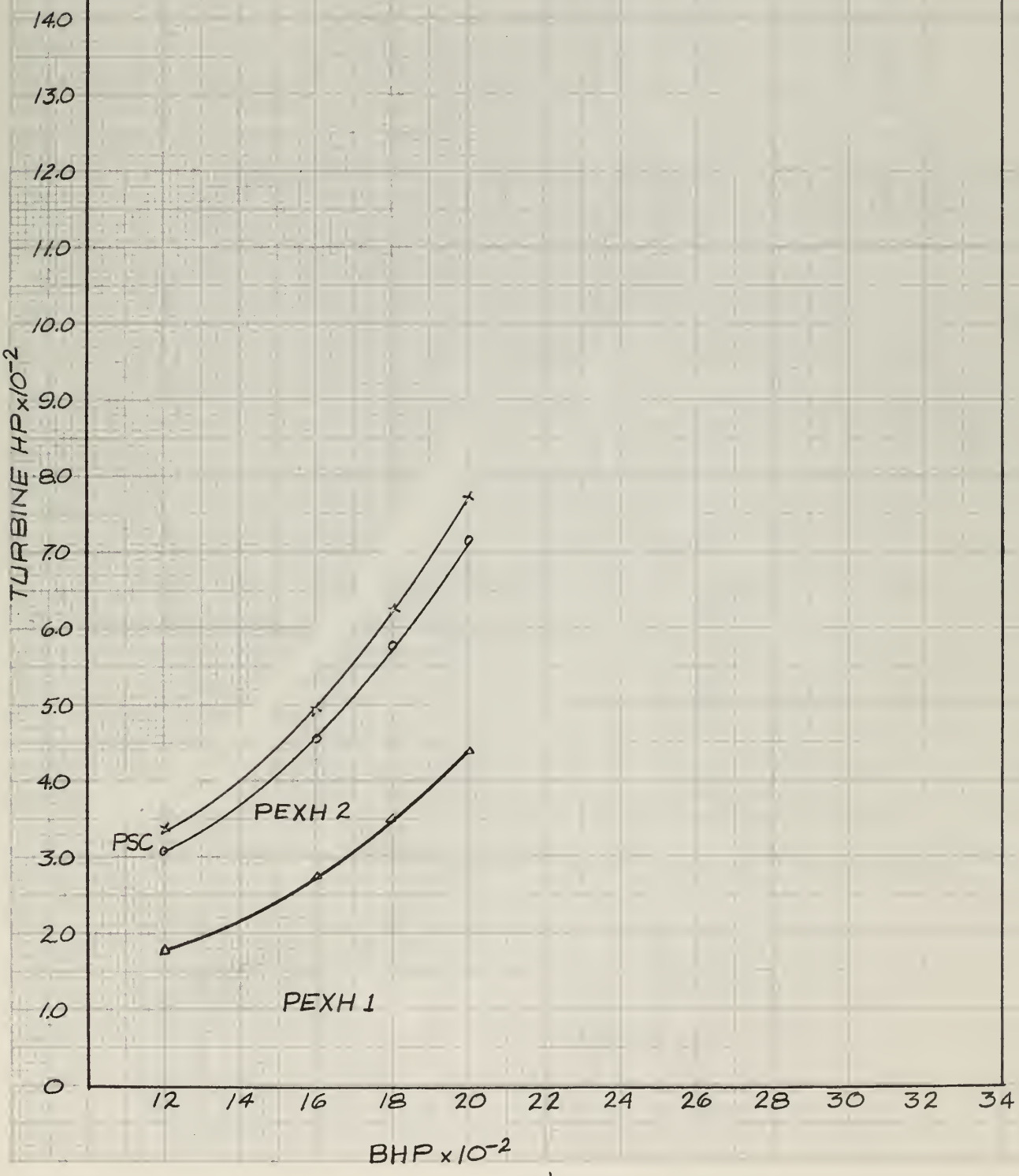

FIG. 6B

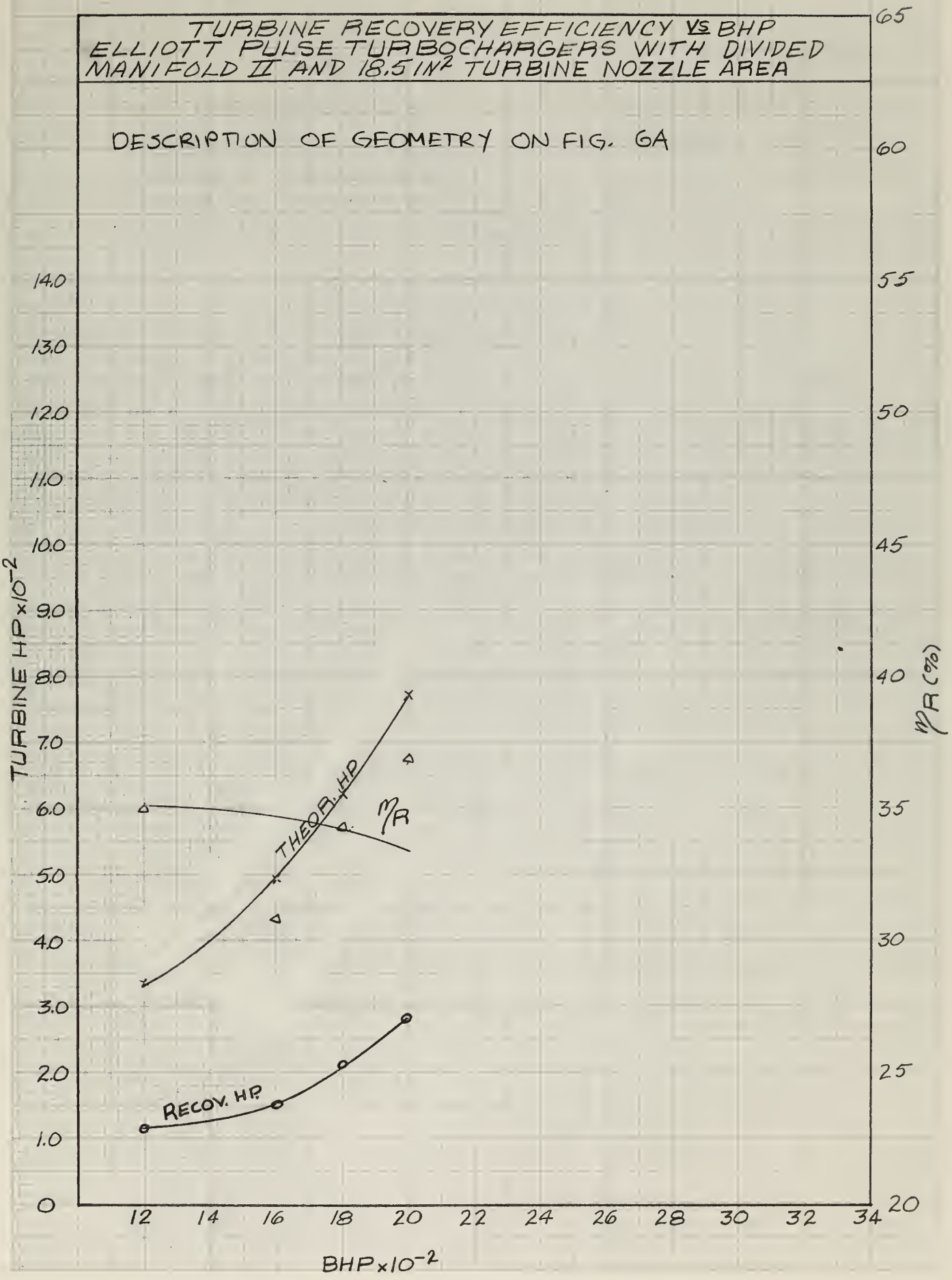
TURBINE RECOVERY EFFICIENCY Vs BHP
ELLIOTT PULSE TURBOCHARGERS WITH DIVIDED MANIFOLD II AND 18.5 IN² TURBINE NOZZLE AREA
DESCRIPTION OF GEOMETRY ON FIG. 6A
TURBINE HP x10⁻²
14.0
13.0
12.0
11.0
10.0
9.0
8.0
7.0
6.0
5.0
4.0
3.0
2.0
1.0
0
65
60
55
50
45
40
35
30
25
20
ηR (%)
THEOR. HP
ηR
RECOV. HP
12
14
16
18
20
22
24
26
28
30
32
34
BHP x10⁻²

FIG. 7A

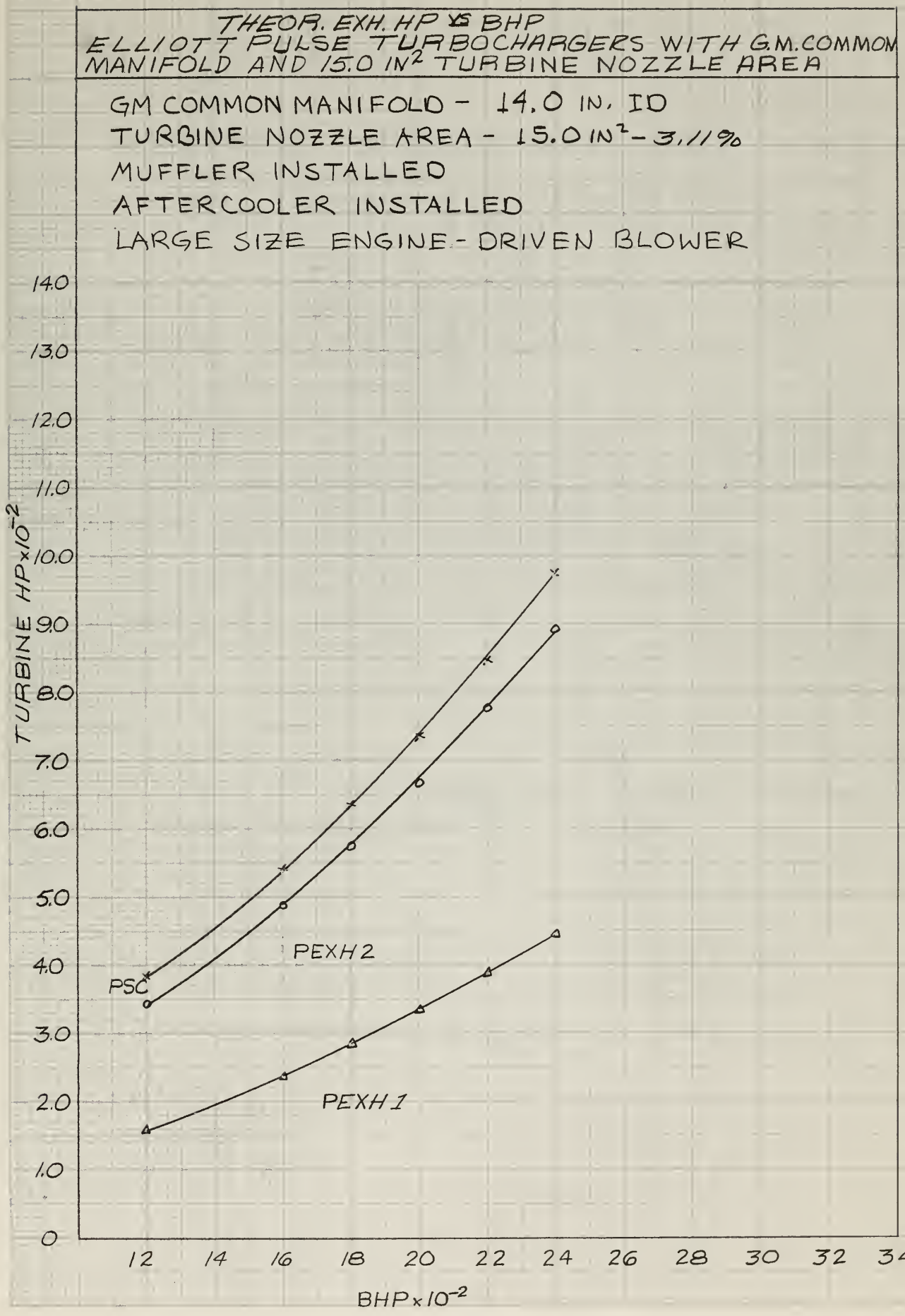
THEOR. EXH. HP VS BHP
ELLIOTT PULSE TURBOCHARGERS WITH G.M.COMMOM MANIFOLD AND 15.0 IN² TURBINE NOZZLE AREA
GM COMMON MANIFOLD - 14.0 IN. ID
TURBINE NOZZLE AREA - 15.0 IN² - 3,11%
MUFFLER INSTALLED
AFTERCOOLER INSTALLED
LARGE SIZE ENGINE-DRIVEN BLOWER
TURBINE HP×10⁻²
14.0
13.0
12.0
11.0
10.0
9.0
8.0
7.0
6.0
5.0
4.0
3.0
2.0
1.0
0
PSC
PEXH 2
PEXH 1
12
14
16
18
20
22
24
26
28
30
32
34
BHP×10⁻²

FIG. 7B

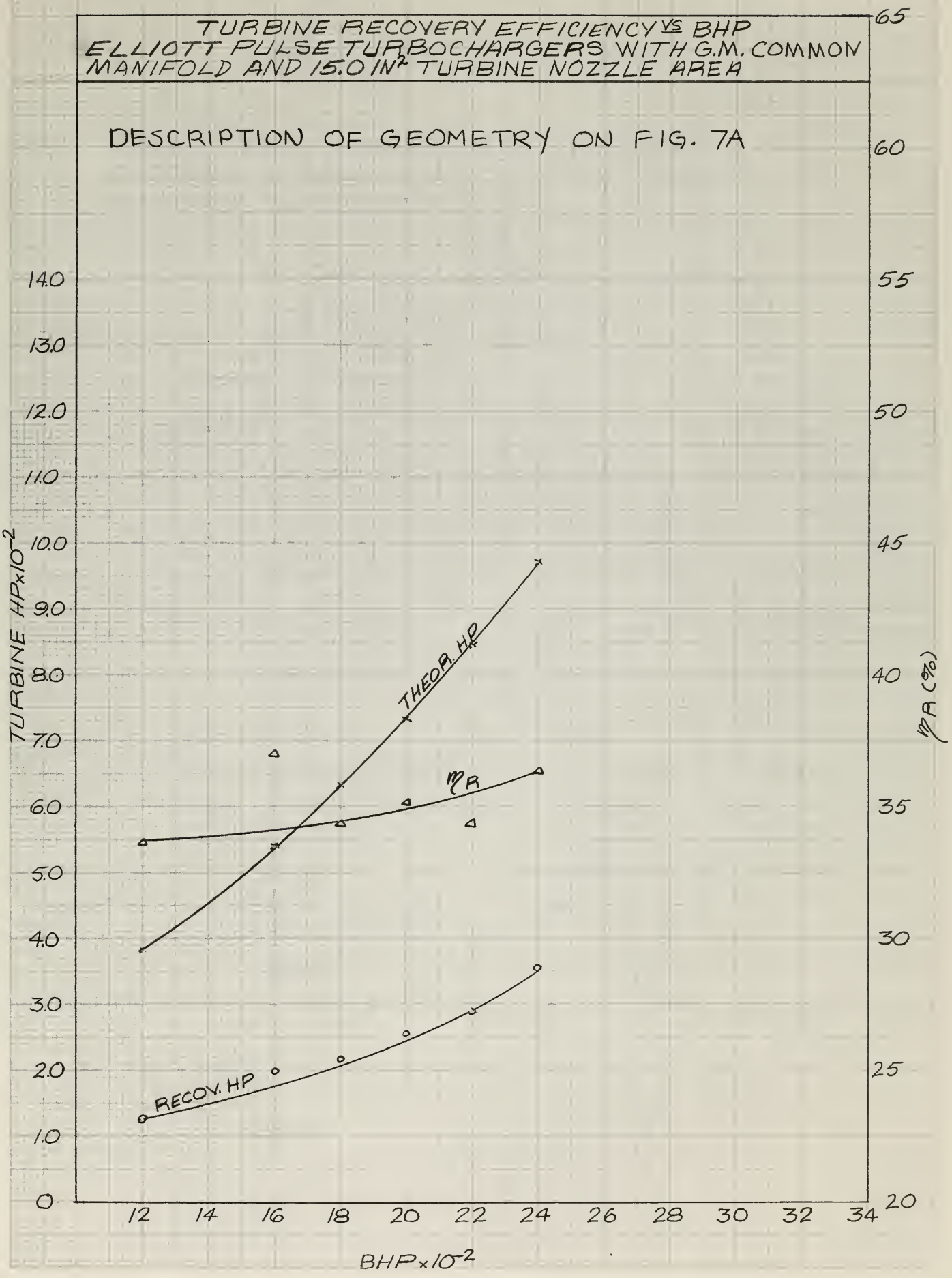
TURBINE RECOVERY EFFICIENCY VS BHP
ELLIOTT PULSE TURBOCHARGERS WITH G.M. COMMON MANIFOLD AND 15.0 IN² TURBINE NOZZLE AREA
DESCRIPTION OF GEOMETRY ON FIG. 7A
TURBINE HP x 10⁻²
14.0
13.0
12.0
11.0
10.0
9.0
8.0
7.0
6.0
5.0
4.0
3.0
2.0
1.0
0
THEOR. HP
ηR
RECOV. HP
12
14
16
18
20
22
24
26
28
30
32
34
BHP x 10⁻²
65
60
55
50
45
40
35
30
25
20
ηA (%)

FIG. 8A

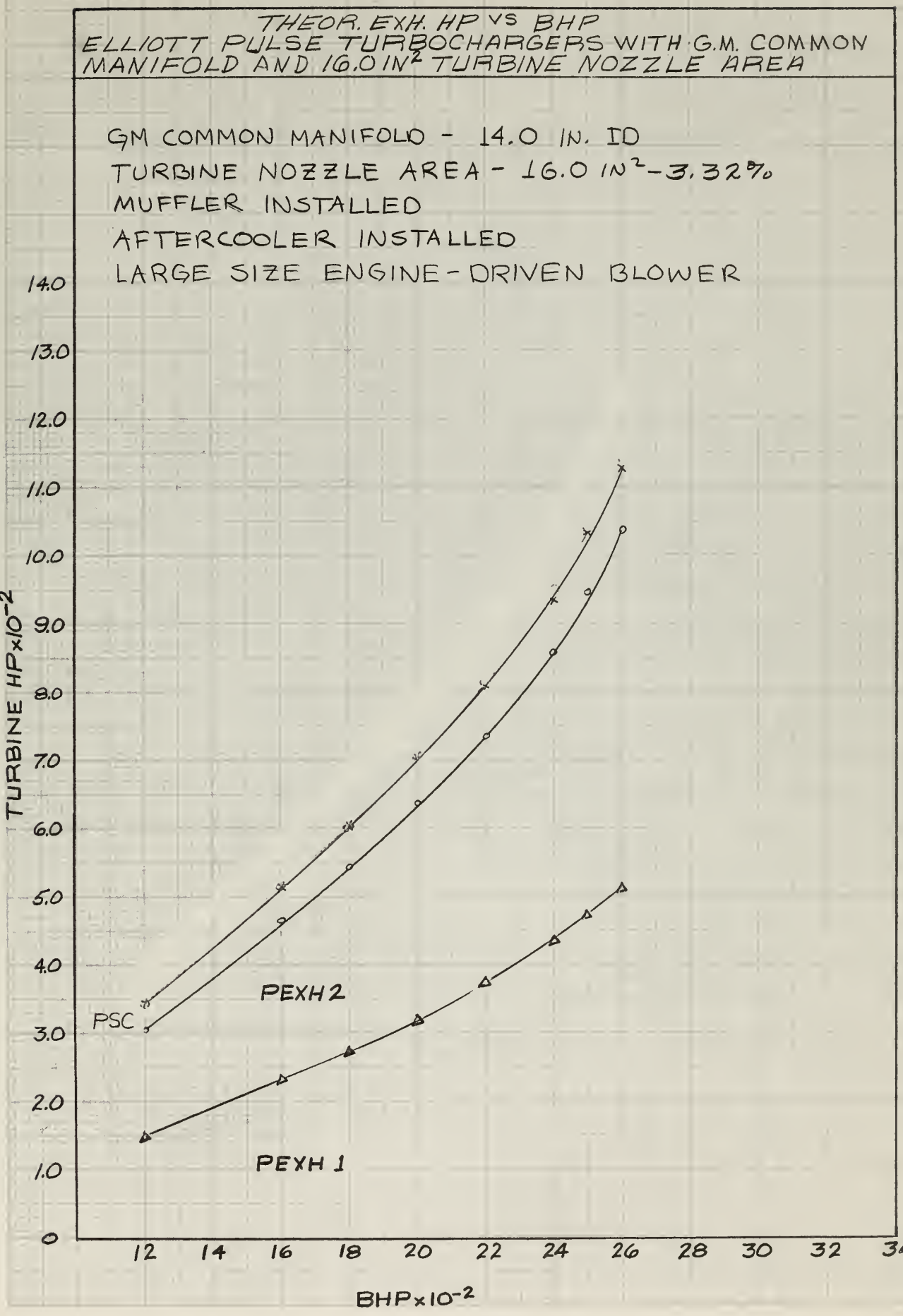
THEOR. EXH. HP VS BHP
ELLIOTT PULSE TURBOCHARGERS WITH G.M. COMMON MANIFOLD AND 16.0 IN² TURBINE NOZZLE AREA
GM COMMON MANIFOLD - 14.0 IN. ID
TURBINE NOZZLE AREA - 16.0 IN² - 3.32%
MUFFLER INSTALLED
AFTERCOOLER INSTALLED
LARGE SIZE ENGINE-DRIVEN BLOWER
TURBINE HP×10⁻²
BHP×10⁻²
PEXH 2
PSC
PEXH 1
0
1.0
2.0
3.0
4.0
5.0
6.0
7.0
8.0
9.0
10.0
11.0
12.0
13.0
14.0
12
14
16
18
20
22
24
26
28
30
32
34

FIG. 8B

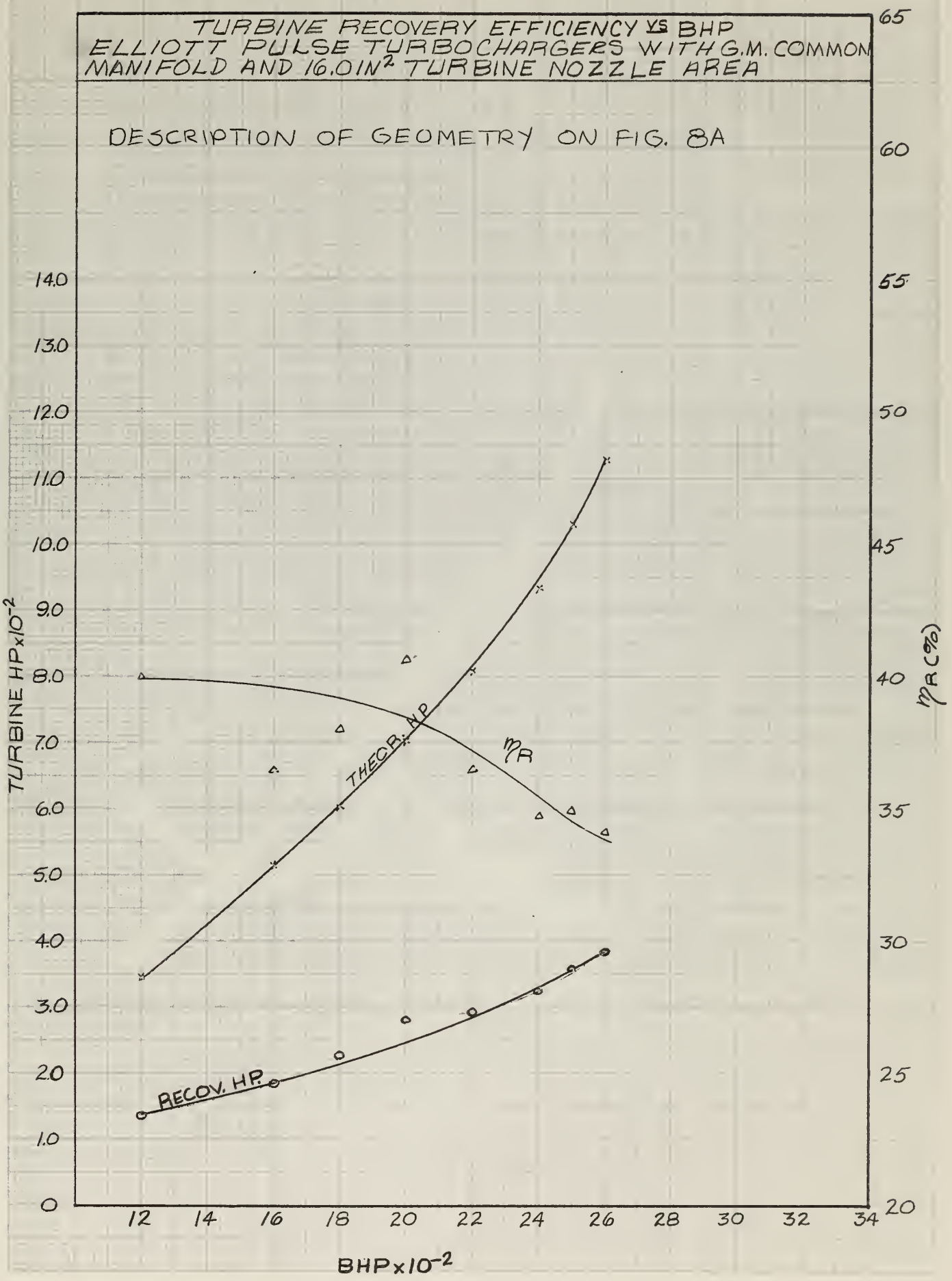
TURBINE RECOVERY EFFICIENCY VS BHP
ELLIOTT PULSE TURBOCHARGERS WITH G.M. COMMON MANIFOLD AND 16.01N² TURBINE NOZZLE AREA
DESCRIPTION OF GEOMETRY ON FIG. 8A
TURBINE HP x 10⁻²
BHP x 10⁻²
ηR (%)
THEOR. H.P.
ηR
RECOV. H.P.
14.0
13.0
12.0
11.0
10.0
9.0
8.0
7.0
6.0
5.0
4.0
3.0
2.0
1.0
0
12
14
16
18
20
22
24
26
28
30
32
34
65
60
55
50
45
40
35
30
25
20

FIG. 9A

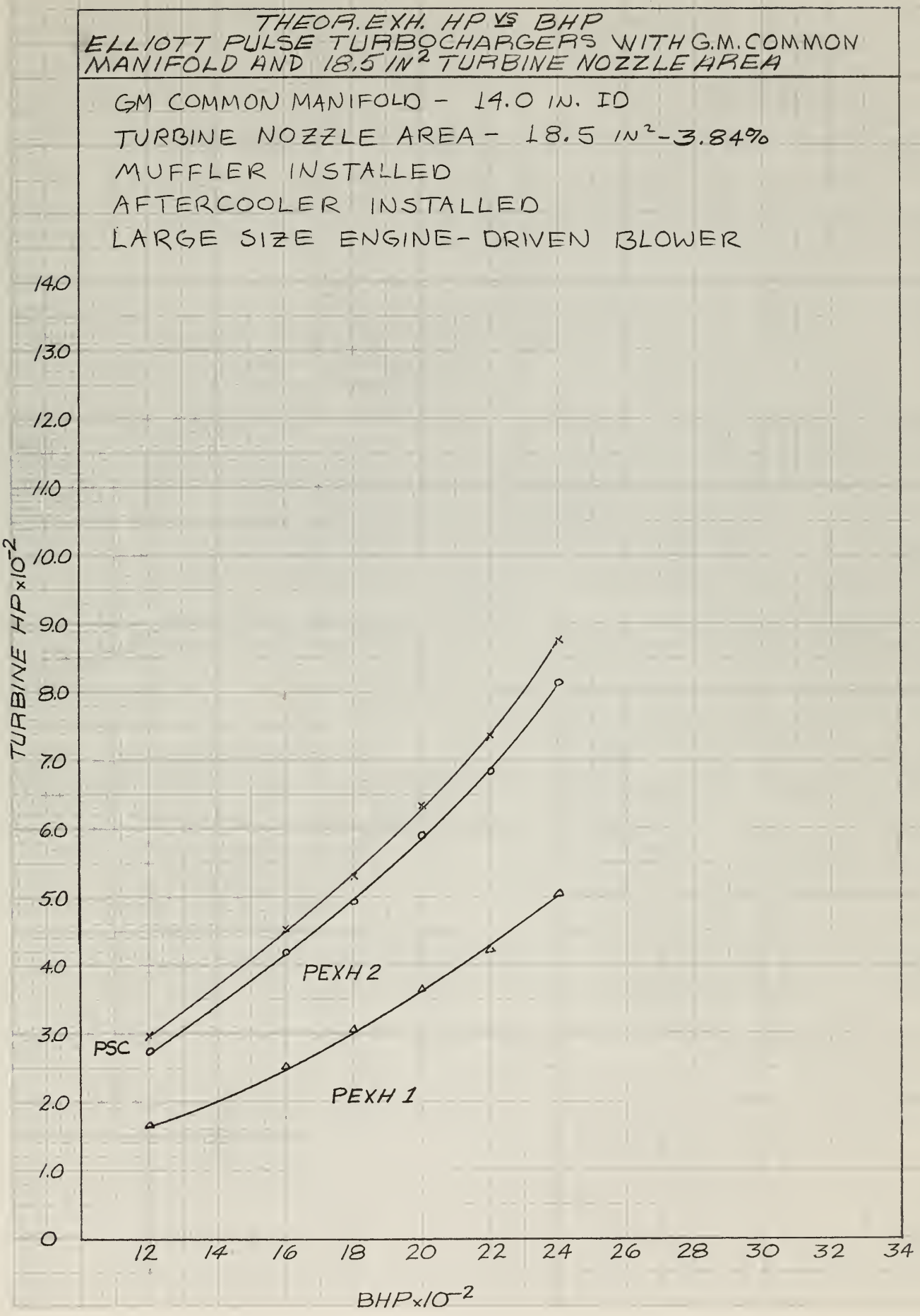
THEOR. EXH. HP VS BHP
ELLIOTT PULSE TURBOCHARGERS WITH G.M. COMMON MANIFOLD AND 18.5 IN² TURBINE NOZZLE AREA
GM COMMON MANIFOLD - 14.0 IN. ID
TURBINE NOZZLE AREA - 18.5 IN² - 3.84%
MUFFLER INSTALLED
AFTERCOOLER INSTALLED
LARGE SIZE ENGINE-DRIVEN BLOWER
TURBINE HP x 10⁻²
14.0
13.0
12.0
11.0
10.0
9.0
8.0
7.0
6.0
5.0
4.0
3.0
2.0
1.0
0
PEXH 2
PSC
PEXH 1
12
14
16
18
20
22
24
26
28
30
32
34
BHP x 10⁻²

FIG. 9B

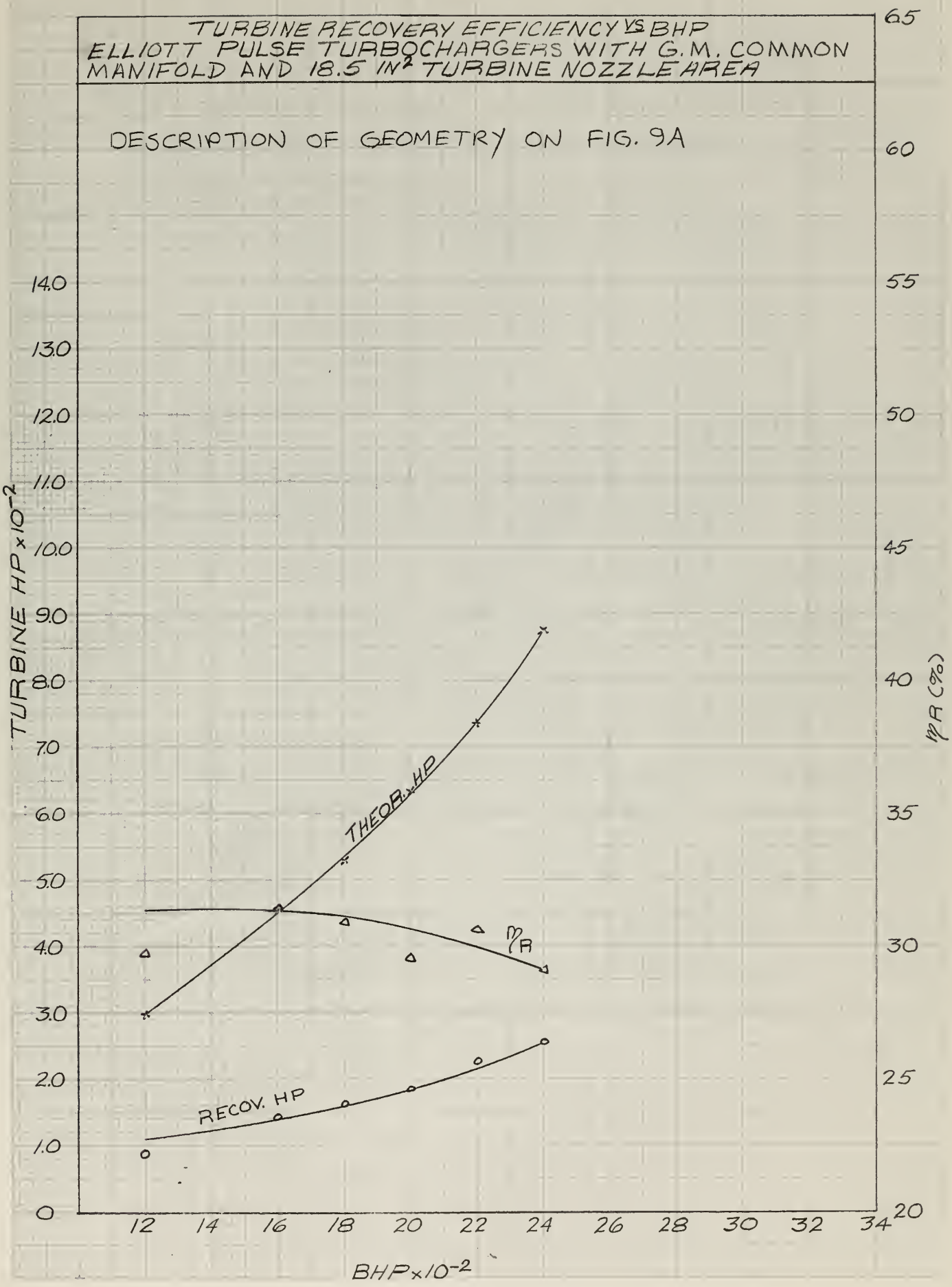
TURBINE RECOVERY EFFICIENCY VS BHP
ELLIOTT PULSE TURBOCHARGERS WITH G.M. COMMON MANIFOLD AND 18.5 IN² TURBINE NOZZLE AREA
DESCRIPTION OF GEOMETRY ON FIG. 9A
TURBINE HP x 10⁻²
14.0
13.0
12.0
11.0
10.0
9.0
8.0
7.0
6.0
5.0
4.0
3.0
2.0
1.0
0
THEOR. HP
RECOV. HP
ηR
65
60
55
50
45
40
35
30
25
20
ηR (%)
12
14
16
18
20
22
24
26
28
30
32
34
BHP x 10⁻²

FIG. 10A

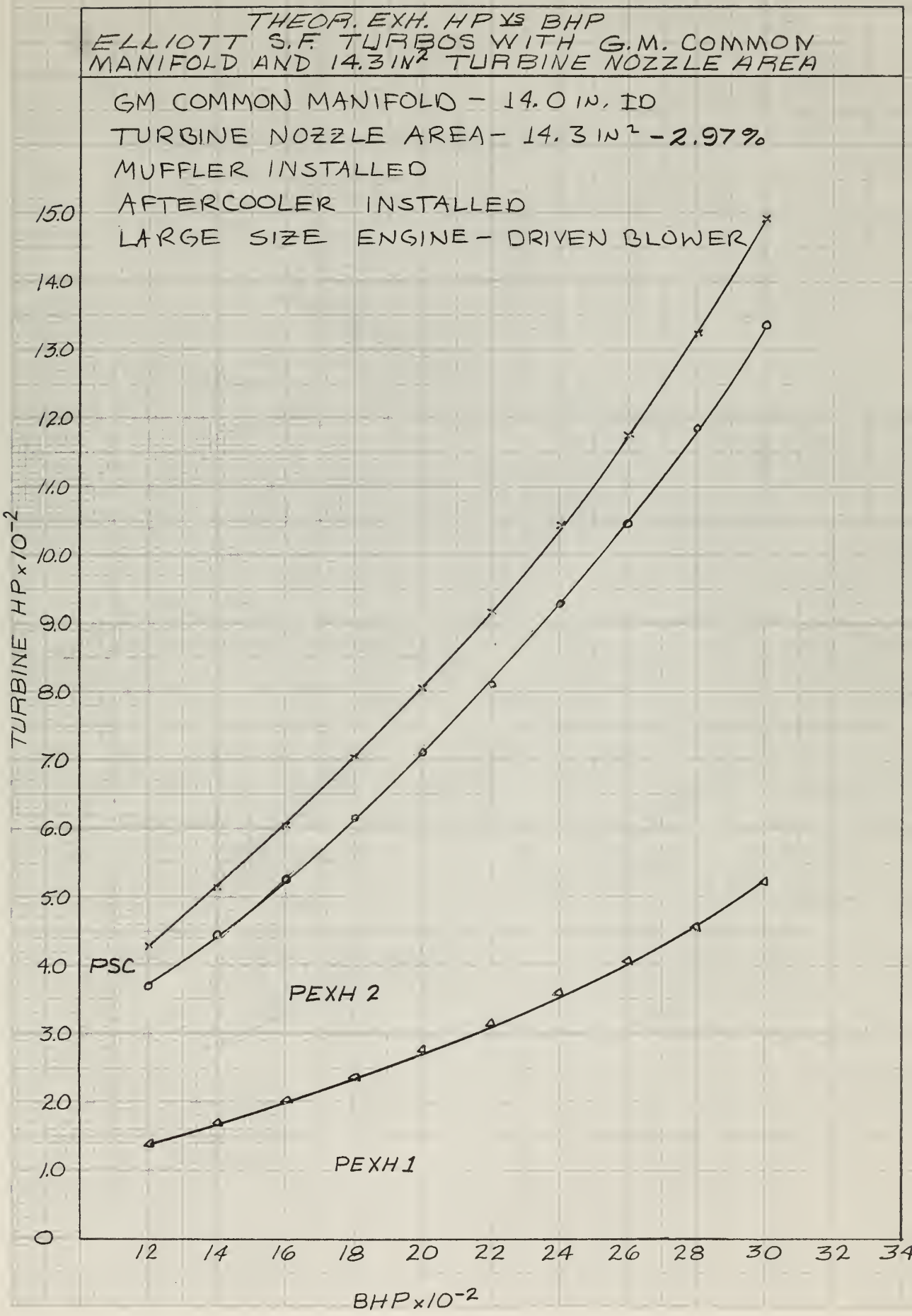
THEOR. EXH. HP VS BHP
ELLIOTT S.F. TURBOS WITH G.M. COMMON MANIFOLD AND 14.3 IN² TURBINE NOZZLE AREA
GM COMMON MANIFOLD - 14.0 IN. ID
TURBINE NOZZLE AREA - 14.3 IN² - 2.97%
MUFFLER INSTALLED
AFTERCOOLER INSTALLED
LARGE SIZE ENGINE - DRIVEN BLOWER
PSC
PEXH 2
PEXH 1
TURBINE HP x 10⁻²
BHP x 10⁻²
0
1.0
2.0
3.0
4.0
5.0
6.0
7.0
8.0
9.0
10.0
11.0
12.0
13.0
14.0
15.0
12
14
16
18
20
22
24
26
28
30
32
34

FIG. 10B

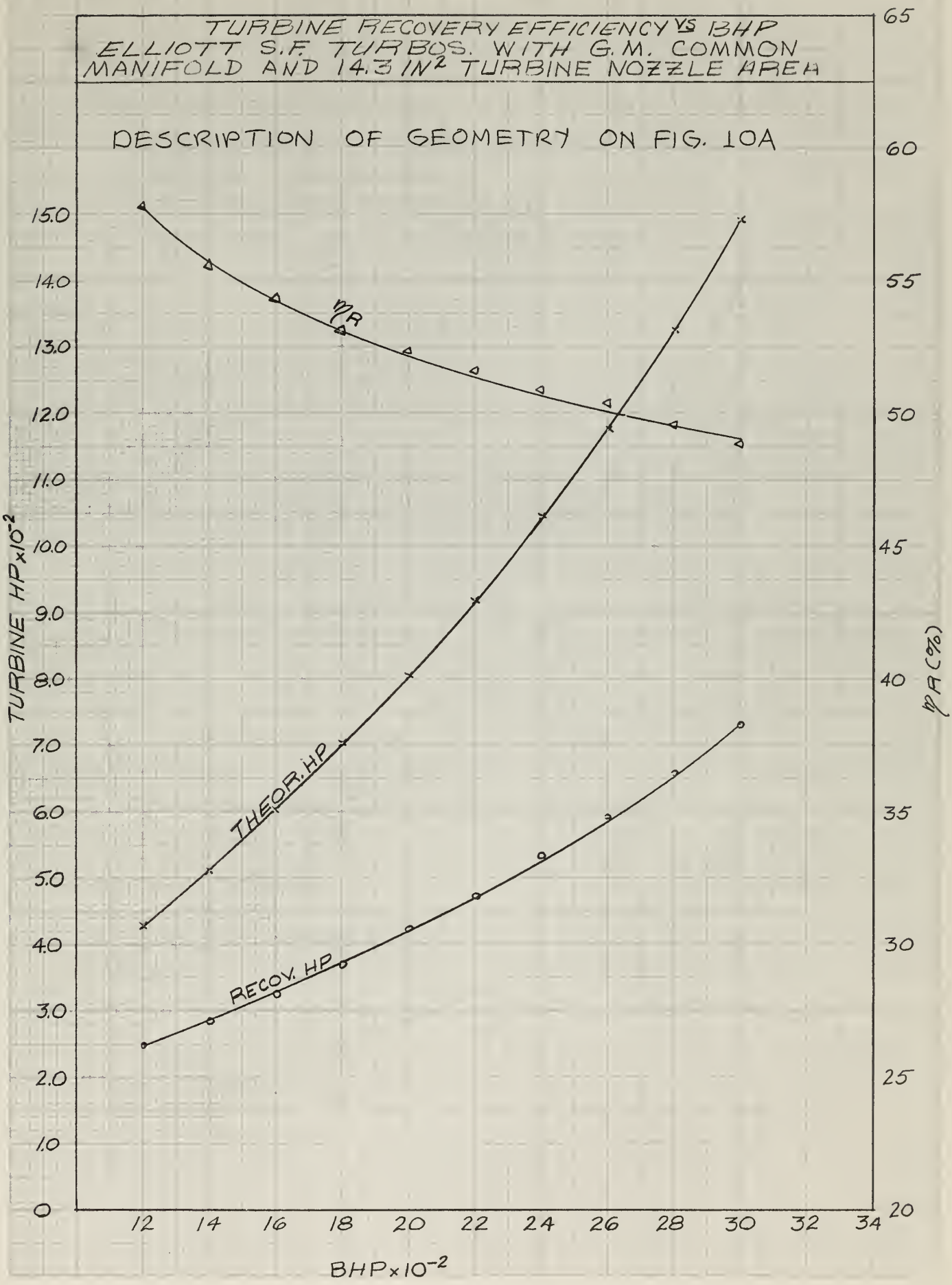
TURBINE RECOVERY EFFICIENCY VS BHP
ELLIOTT S.F. TURBOS. WITH G.M. COMMON MANIFOLD AND 14.3 IN² TURBINE NOZZLE AREA
DESCRIPTION OF GEOMETRY ON FIG. 10A
TURBINE HP x 10⁻²
ηR (%)
BHP x 10⁻²
ηR
THEOR. HP
RECOV. HP
0
1.0
2.0
3.0
4.0
5.0
6.0
7.0
8.0
9.0
10.0
11.0
12.0
13.0
14.0
15.0
20
25
30
35
40
45
50
55
60
65
12
14
16
18
20
22
24
26
28
30
32
34

FIG. 11A

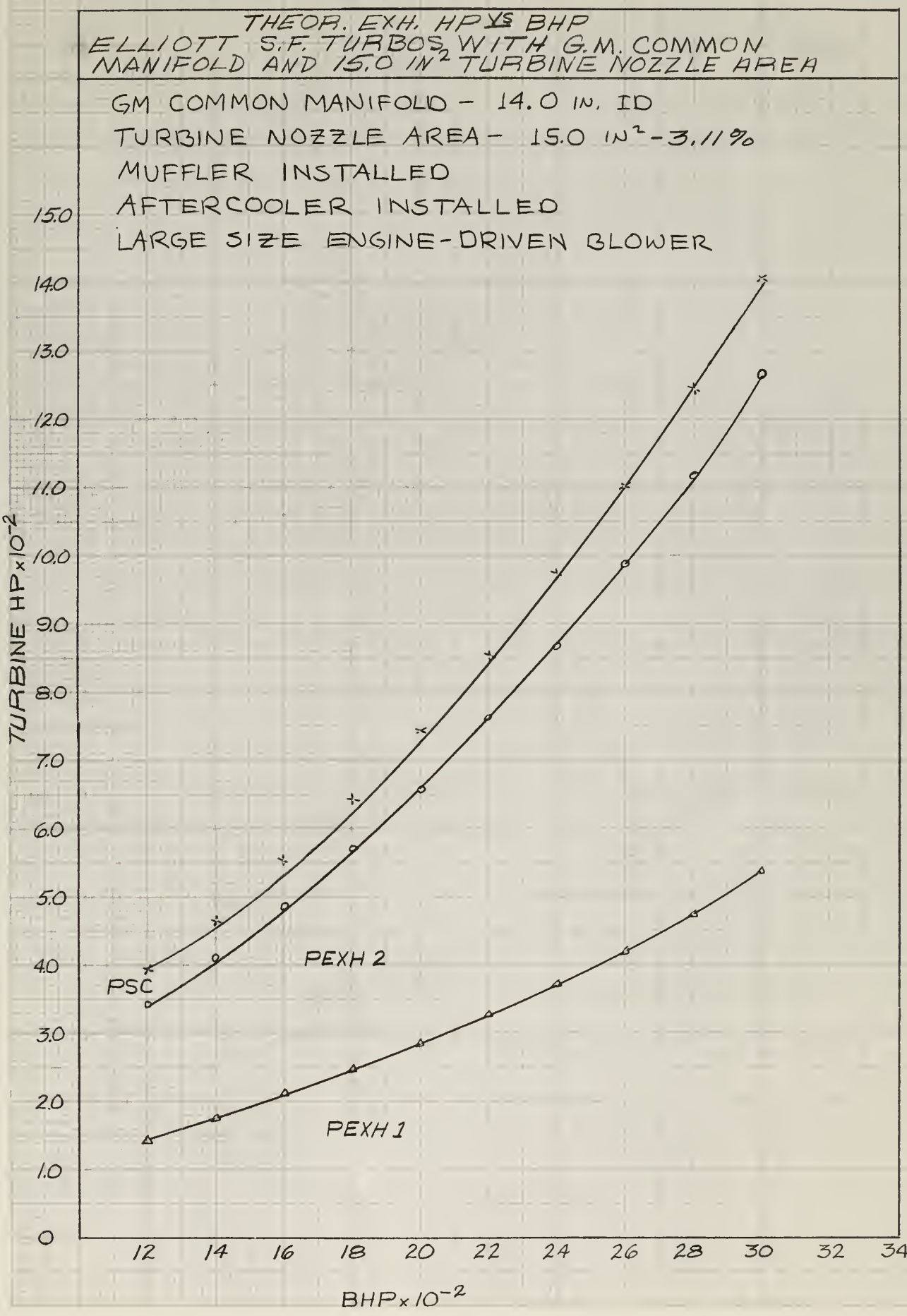
THEOR. EXH. HP VS BHP
ELLIOTT S.F. TURBOS WITH G.M. COMMON MANIFOLD AND 15.0 IN² TURBINE NOZZLE AREA
GM COMMON MANIFOLD - 14.0 IN. ID
TURBINE NOZZLE AREA - 15.0 IN² - 3.11%
MUFFLER INSTALLED
AFTERCOOLER INSTALLED
LARGE SIZE ENGINE-DRIVEN BLOWER
TURBINE HP x 10⁻²
BHP x 10⁻²
PEXH 2
PSC
PEXH 1
0
1.0
2.0
3.0
4.0
5.0
6.0
7.0
8.0
9.0
10.0
11.0
12.0
13.0
14.0
15.0
12
14
16
18
20
22
24
26
28
30
32
34

FIG. 11B

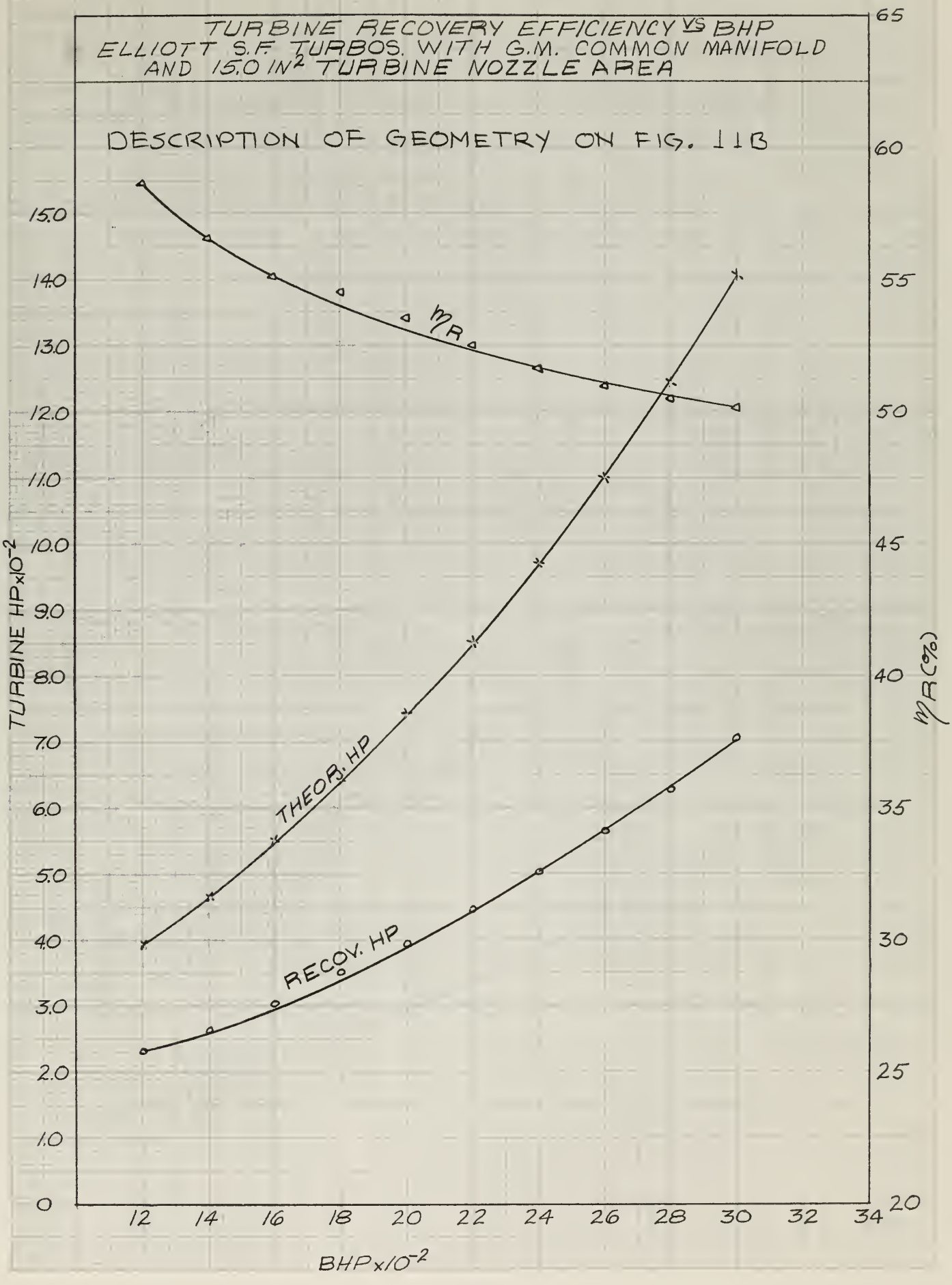
TURBINE RECOVERY EFFICIENCY VS BHP
ELLIOTT S.F. TURBOS. WITH G.M. COMMON MANIFOLD
AND 15.0 IN² TURBINE NOZZLE AREA
DESCRIPTION OF GEOMETRY ON FIG. 11B
η_R
THEOR. HP
RECOV. HP
TURBINE HP x 10⁻²
η_R (%)
BHP x 10⁻²
15.0
14.0
13.0
12.0
11.0
10.0
9.0
8.0
7.0
6.0
5.0
4.0
3.0
2.0
1.0
0
65
60
55
50
45
40
35
30
25
20
12
14
16
18
20
22
24
26
28
30
32
34

FIG. 12A

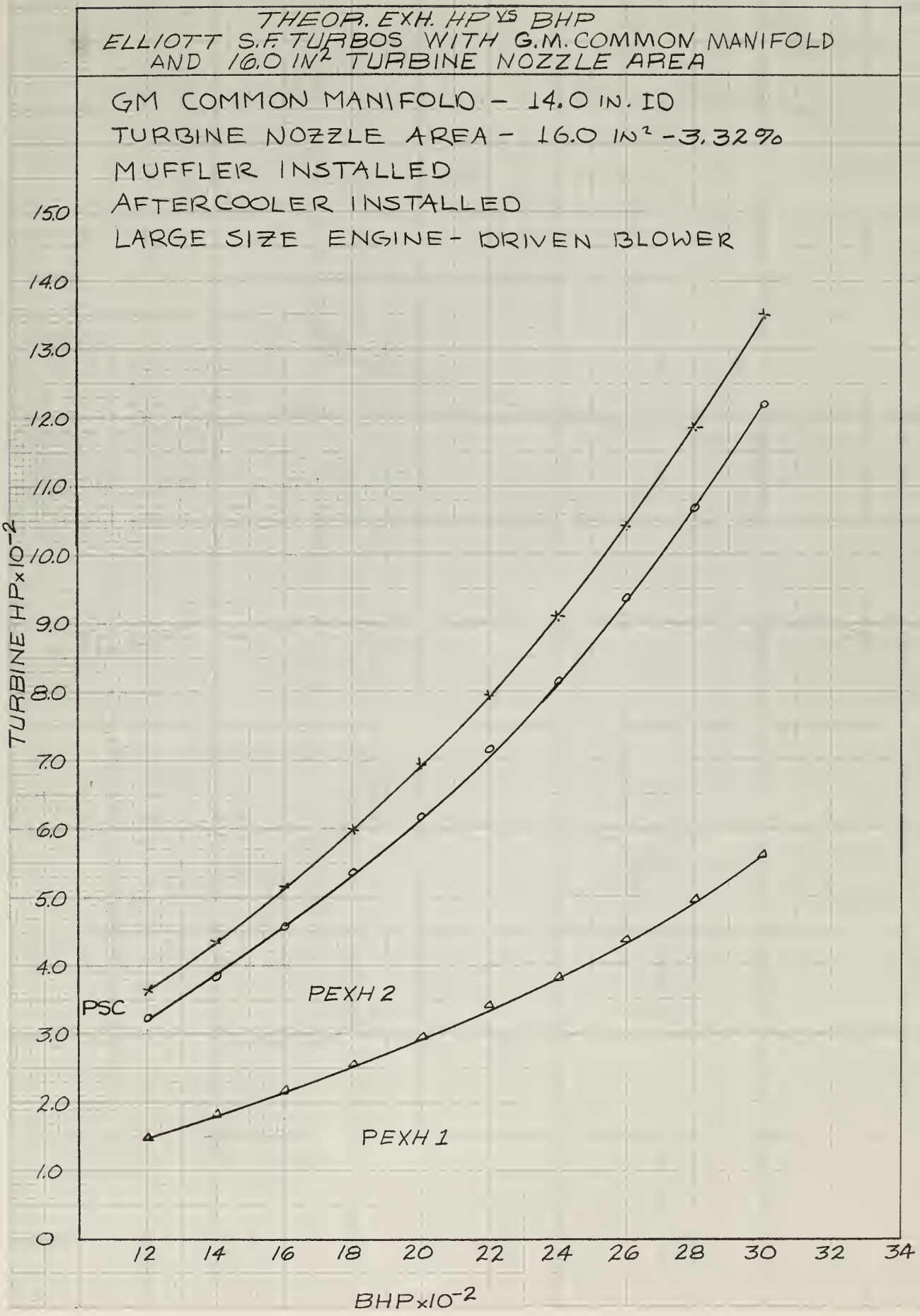
THEOR. EXH. HP VS BHP
ELLIOTT S.F. TURBOS WITH G.M. COMMON MANIFOLD
AND 16.0 IN² TURBINE NOZZLE AREA
GM COMMON MANIFOLD - 14.0 IN. ID
TURBINE NOZZLE AREA - 16.0 IN² - 3.32%
MUFFLER INSTALLED
AFTERCOOLER INSTALLED
LARGE SIZE ENGINE - DRIVEN BLOWER
PSC
PEXH 2
PEXH 1
TURBINE HP x 10⁻²
BHP x 10⁻²
0
1.0
2.0
3.0
4.0
5.0
6.0
7.0
8.0
9.0
10.0
11.0
12.0
13.0
14.0
15.0
12
14
16
18
20
22
24
26
28
30
32
34

FIG. 12B

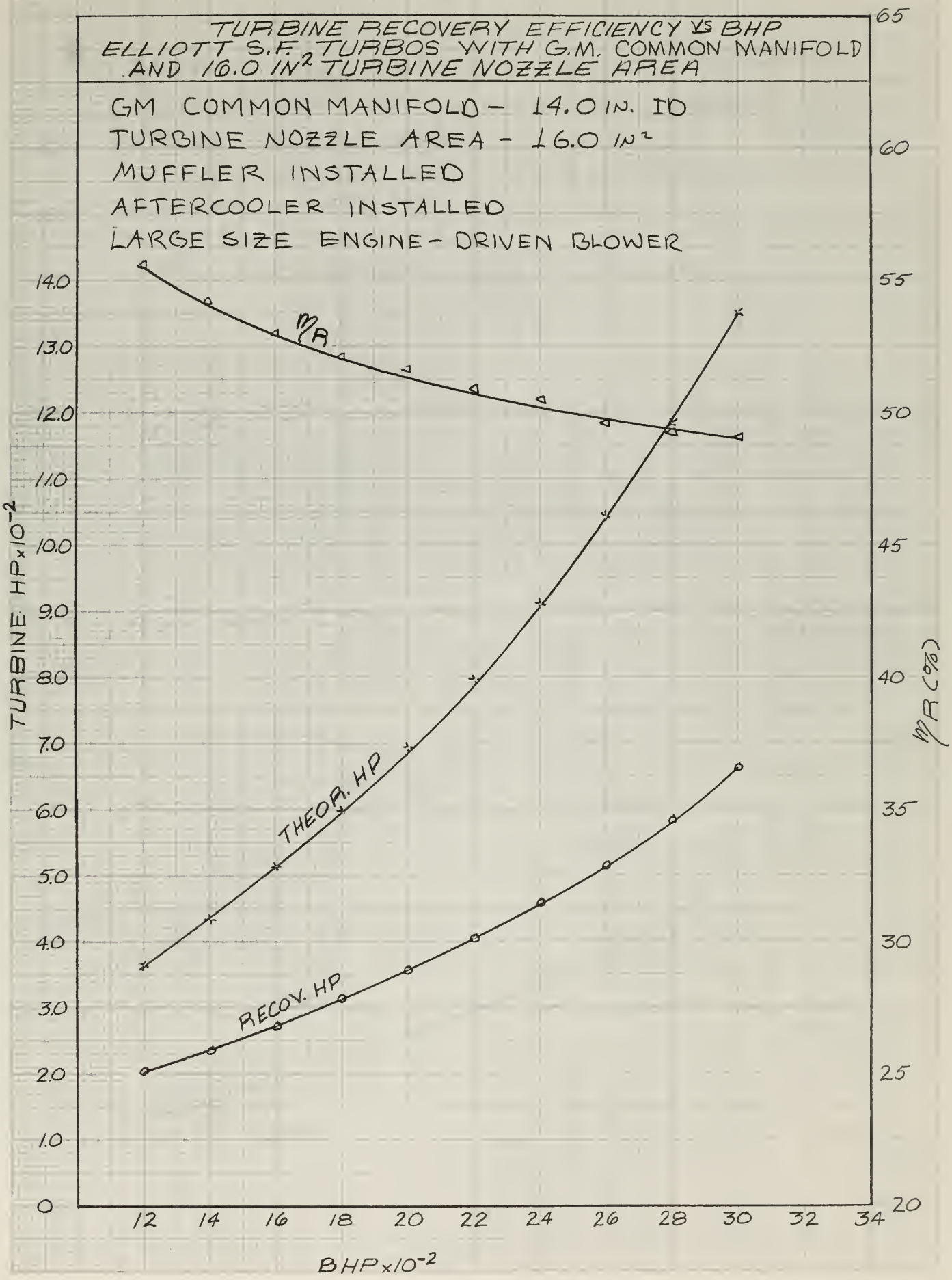
TURBINE RECOVERY EFFICIENCY VS BHP
ELLIOTT S.F. TURBOS WITH G.M. COMMON MANIFOLD AND 16.0 IN² TURBINE NOZZLE AREA
GM COMMON MANIFOLD - 14.0 IN. ID
TURBINE NOZZLE AREA - 16.0 IN²
MUFFLER INSTALLED
AFTERCOOLER INSTALLED
LARGE SIZE ENGINE-DRIVEN BLOWER
ηR
THEOR. HP
RECOV. HP
TURBINE HP x 10⁻²
ηR (%)
BHP x 10⁻²
0
1.0
2.0
3.0
4.0
5.0
6.0
7.0
8.0
9.0
10.0
11.0
12.0
13.0
14.0
20
25
30
35
40
45
50
55
60
65
12
14
16
18
20
22
24
26
28
30
32
34

FIG. 13A

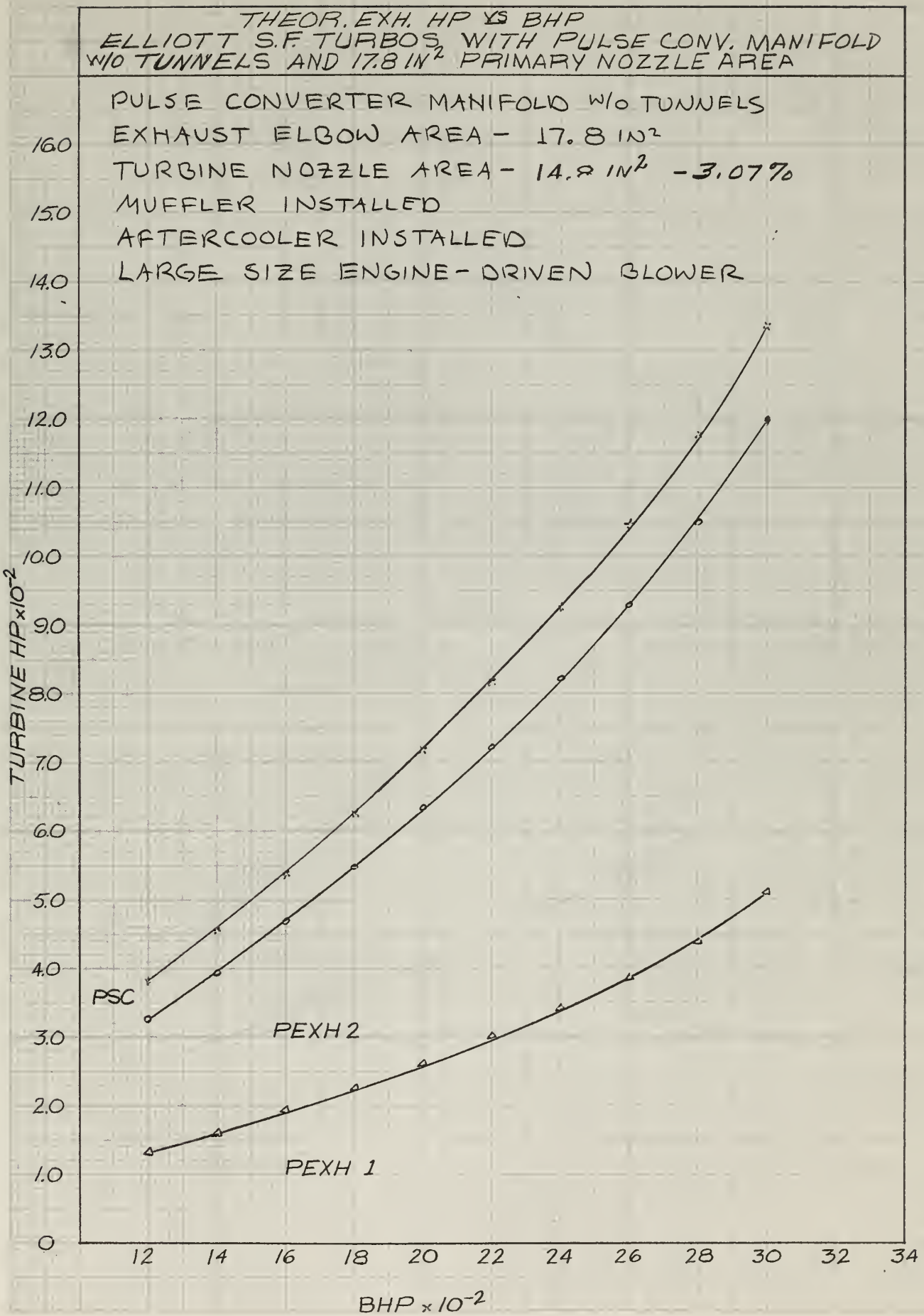
THEOR. EXH. HP VS BHP
ELLIOTT S.F. TURBOS WITH PULSE CONV. MANIFOLD W/O TUNNELS AND 17.8 IN² PRIMARY NOZZLE AREA
PULSE CONVERTER MANIFOLD W/O TUNNELS
EXHAUST ELBOW AREA - 17.8 IN²
TURBINE NOZZLE AREA - 14.8 IN² -3.07%
MUFFLER INSTALLED
AFTERCOOLER INSTALLED
LARGE SIZE ENGINE-DRIVEN BLOWER
TURBINE HP x 10⁻²
BHP x 10⁻²
PSC
PEXH 2
PEXH 1
0
1.0
2.0
3.0
4.0
5.0
6.0
7.0
8.0
9.0
10.0
11.0
12.0
13.0
14.0
15.0
16.0
12
14
16
18
20
22
24
26
28
30
32
34

FIG. 13B

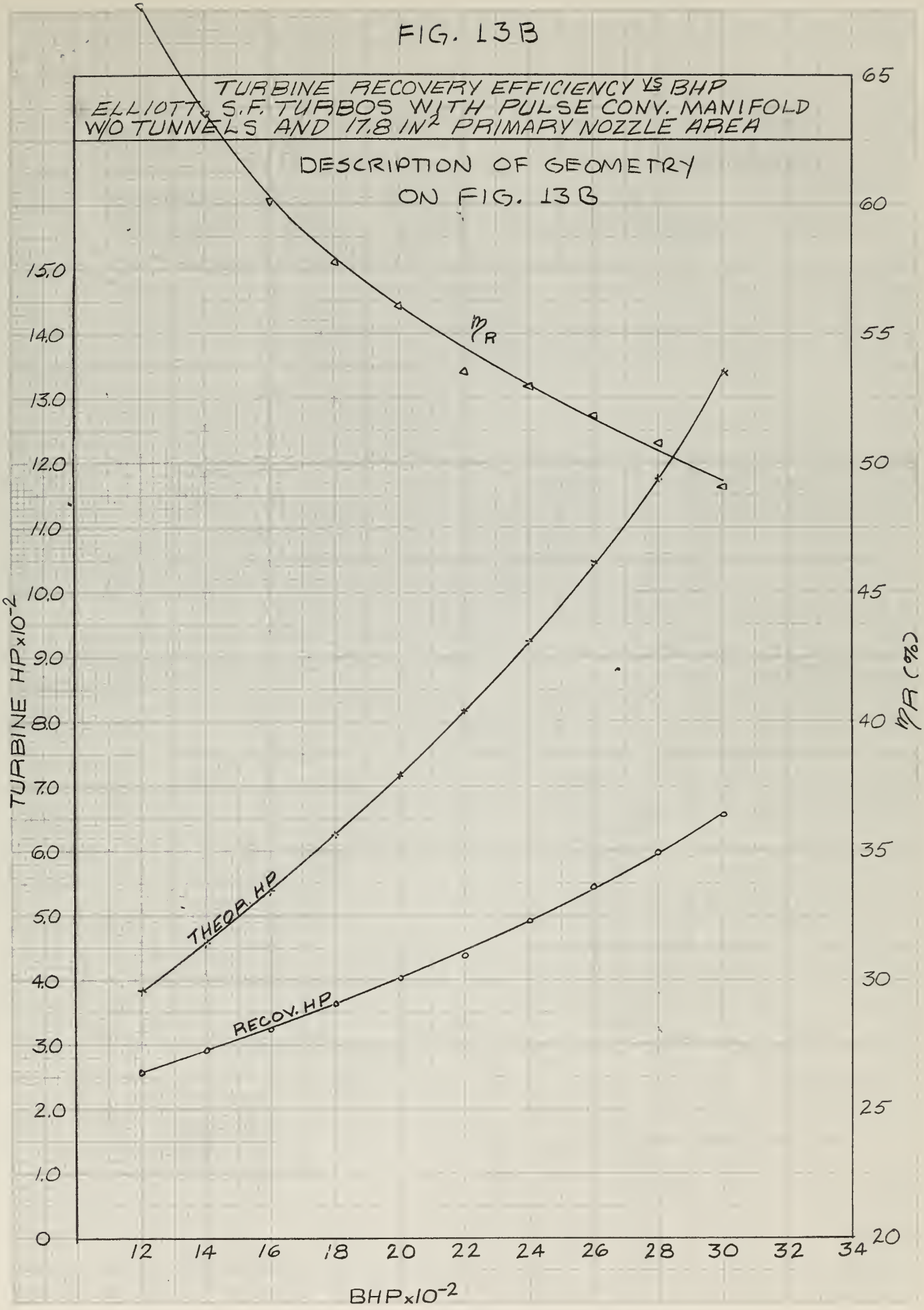
TURBINE RECOVERY EFFICIENCY VS BHP
ELLIOTT S.F. TURBOS WITH PULSE CONV. MANIFOLD
W/O TUNNELS AND 17.8 IN² PRIMARY NOZZLE AREA
DESCRIPTION OF GEOMETRY
ON FIG. 13B
η_R
THEOR. HP
RECOV. HP
TURBINE HP x 10⁻²
BHP x 10⁻²
η_R (%)
0
1.0
2.0
3.0
4.0
5.0
6.0
7.0
8.0
9.0
10.0
11.0
12.0
13.0
14.0
15.0
12
14
16
18
20
22
24
26
28
30
32
34
20
25
30
35
40
45
50
55
60
65

FIG. 14A

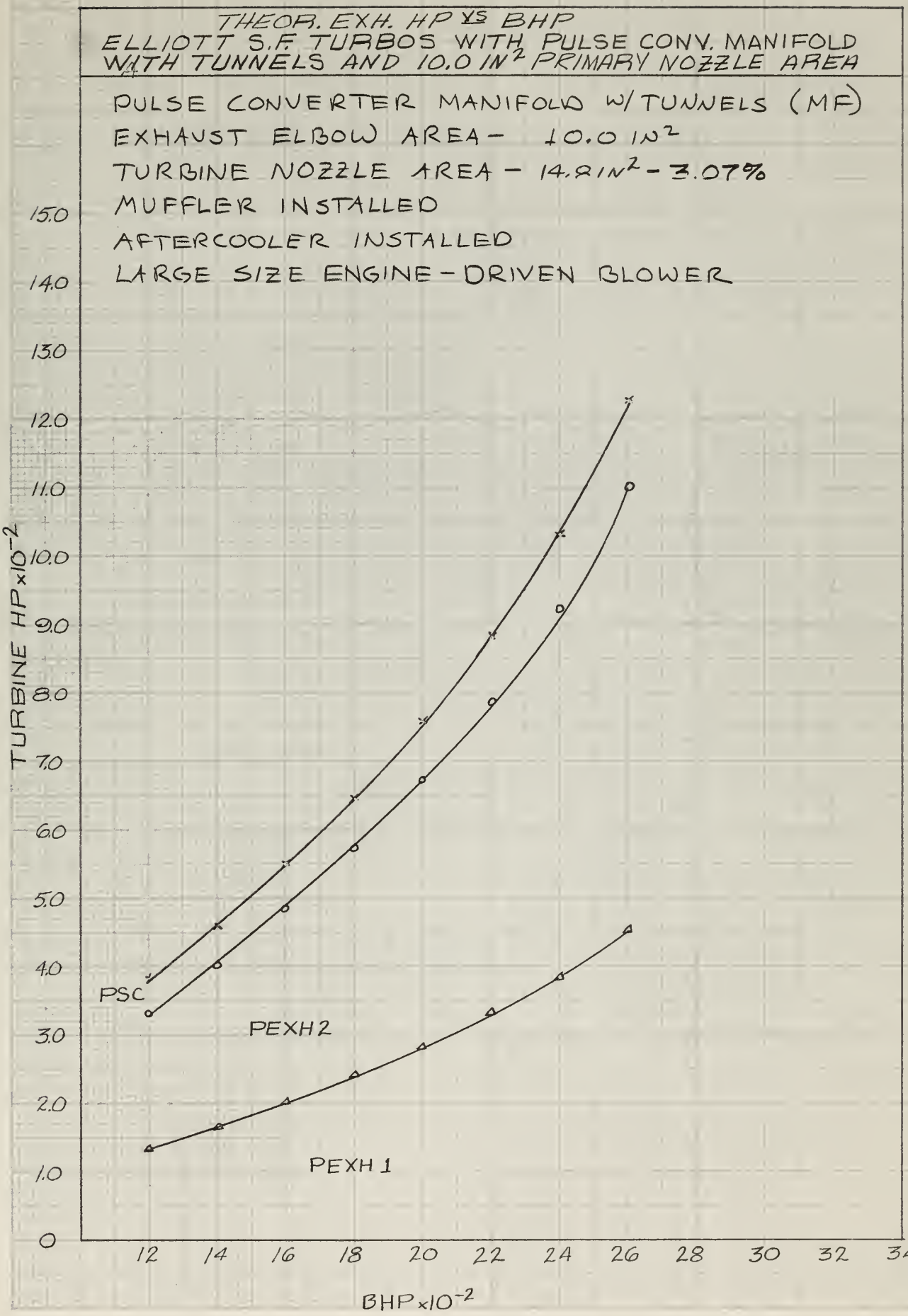
THEOR. EXH. HP VS BHP
ELLIOTT S.F. TURBOS WITH PULSE CONV. MANIFOLD
WITH TUNNELS AND 10.0 IN² PRIMARY NOZZLE AREA
PULSE CONVERTER MANIFOLD W/ TUNNELS (MF)
EXHAUST ELBOW AREA - 10.0 IN²
TURBINE NOZZLE AREA - 14.8 IN² - 3.07%
MUFFLER INSTALLED
AFTERCOOLER INSTALLED
LARGE SIZE ENGINE-DRIVEN BLOWER
TURBINE HP x10⁻²
15.0
14.0
13.0
12.0
11.0
10.0
9.0
8.0
7.0
6.0
5.0
4.0
3.0
2.0
1.0
0
PSC
PEXH 2
PEXH 1
12
14
16
18
20
22
24
26
28
30
32
34
BHP x10⁻²

FIG. 14 B

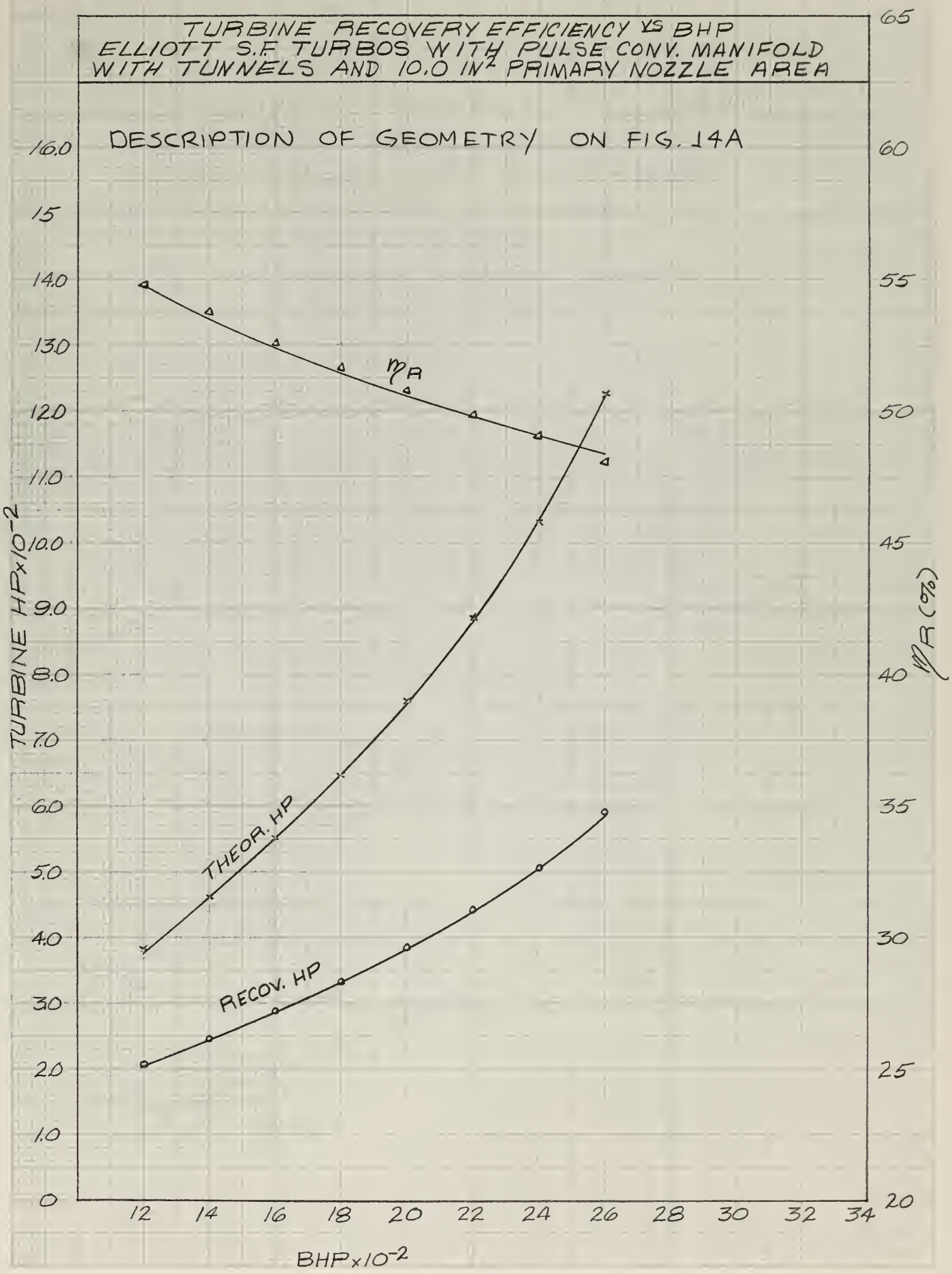
TURBINE RECOVERY EFFICIENCY VS BHP
ELLIOTT S.F. TURBOS WITH PULSE CONV. MANIFOLD
WITH TUNNELS AND 10.0 IN² PRIMARY NOZZLE AREA
DESCRIPTION OF GEOMETRY ON FIG. 14A
η_R
THEOR. HP
RECOV. HP
TURBINE HP×10⁻²
η_R (%)
BHP×10⁻²
16.0
15
14.0
13.0
12.0
11.0
10.0
9.0
8.0
7.0
6.0
5.0
4.0
3.0
2.0
1.0
0
65
60
55
50
45
40
35
30
25
20
12
14
16
18
20
22
24
26
28
30
32
34

FIG. 15A

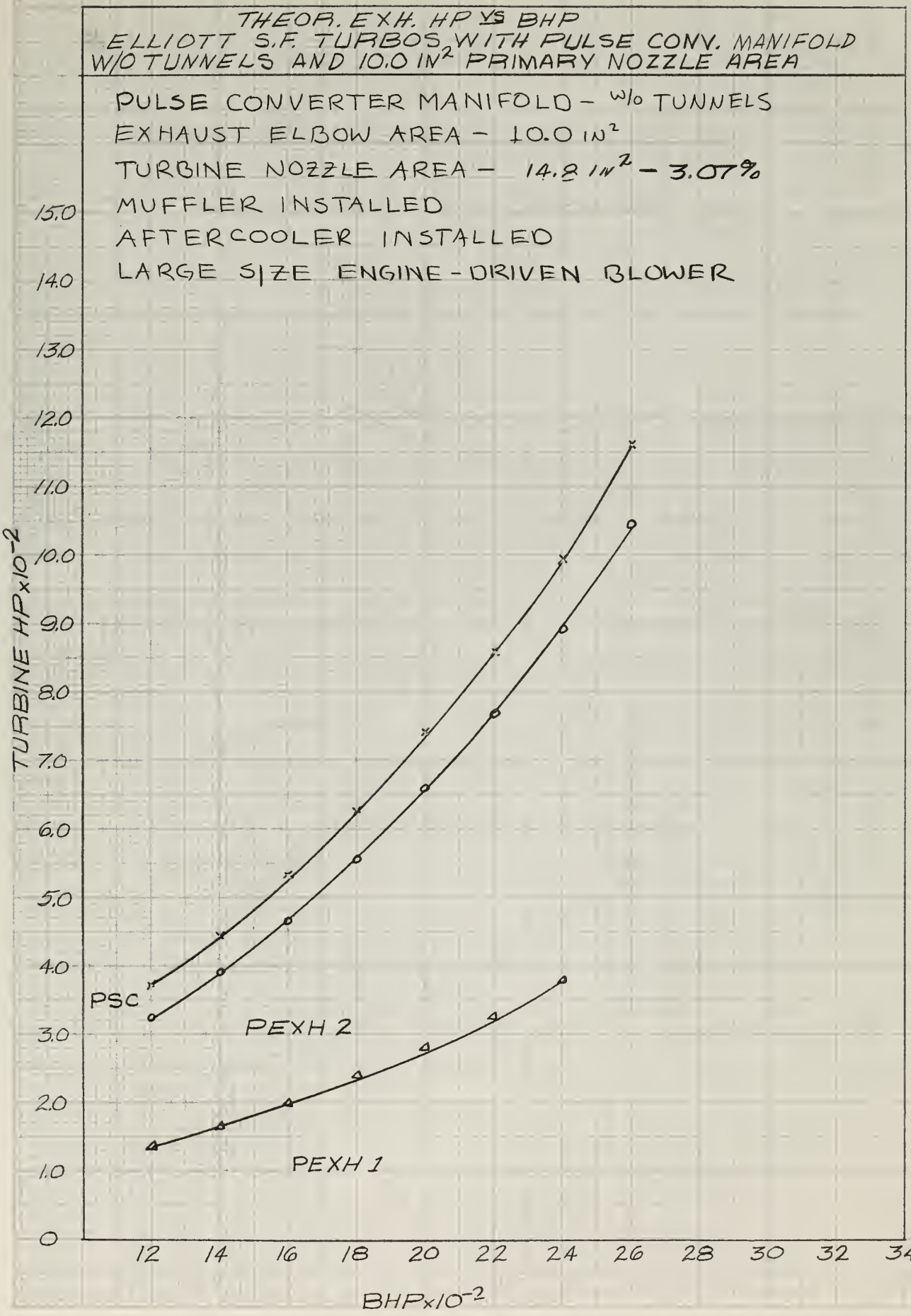
THEOR. EXH. HP VS BHP
ELLIOTT S.F. TURBOS WITH PULSE CONV. MANIFOLD
W/O TUNNELS AND 10.0 IN² PRIMARY NOZZLE AREA
PULSE CONVERTER MANIFOLD – W/O TUNNELS
EXHAUST ELBOW AREA – 10.0 IN²
TURBINE NOZZLE AREA – 14.8 IN² – 3.07%
MUFFLER INSTALLED
AFTERCOOLER INSTALLED
LARGE SIZE ENGINE-DRIVEN BLOWER
TURBINE HP×10⁻²
BHP×10⁻²
PSC
PEXH 2
PEXH 1
0
1.0
2.0
3.0
4.0
5.0
6.0
7.0
8.0
9.0
10.0
11.0
12.0
13.0
14.0
15.0
12
14
16
18
20
22
24
26
28
30
32
34

FIG. 15B

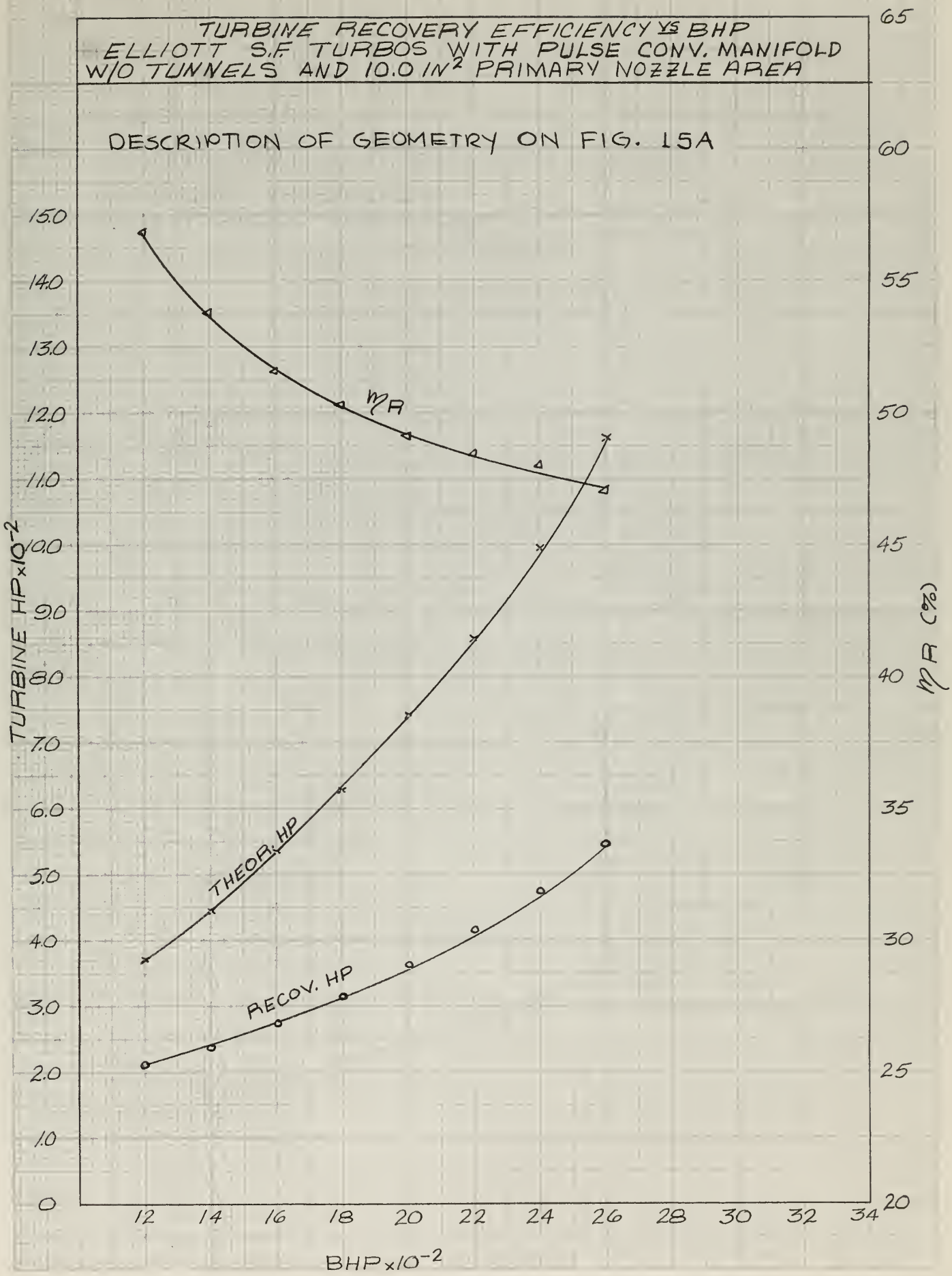
TURBINE RECOVERY EFFICIENCY VS BHP
ELLIOTT S.F. TURBOS WITH PULSE CONV. MANIFOLD
W/O TUNNELS AND 10.0 IN² PRIMARY NOZZLE AREA
DESCRIPTION OF GEOMETRY ON FIG. 15A
TURBINE HP×10⁻²
ηR (%)
BHP×10⁻²
ηR
THEOR. HP
RECOV. HP
15.0
14.0
13.0
12.0
11.0
10.0
9.0
8.0
7.0
6.0
5.0
4.0
3.0
2.0
1.0
0
65
60
55
50
45
40
35
30
25
20
12
14
16
18
20
22
24
26
28
30
32
34

FIG. 16A

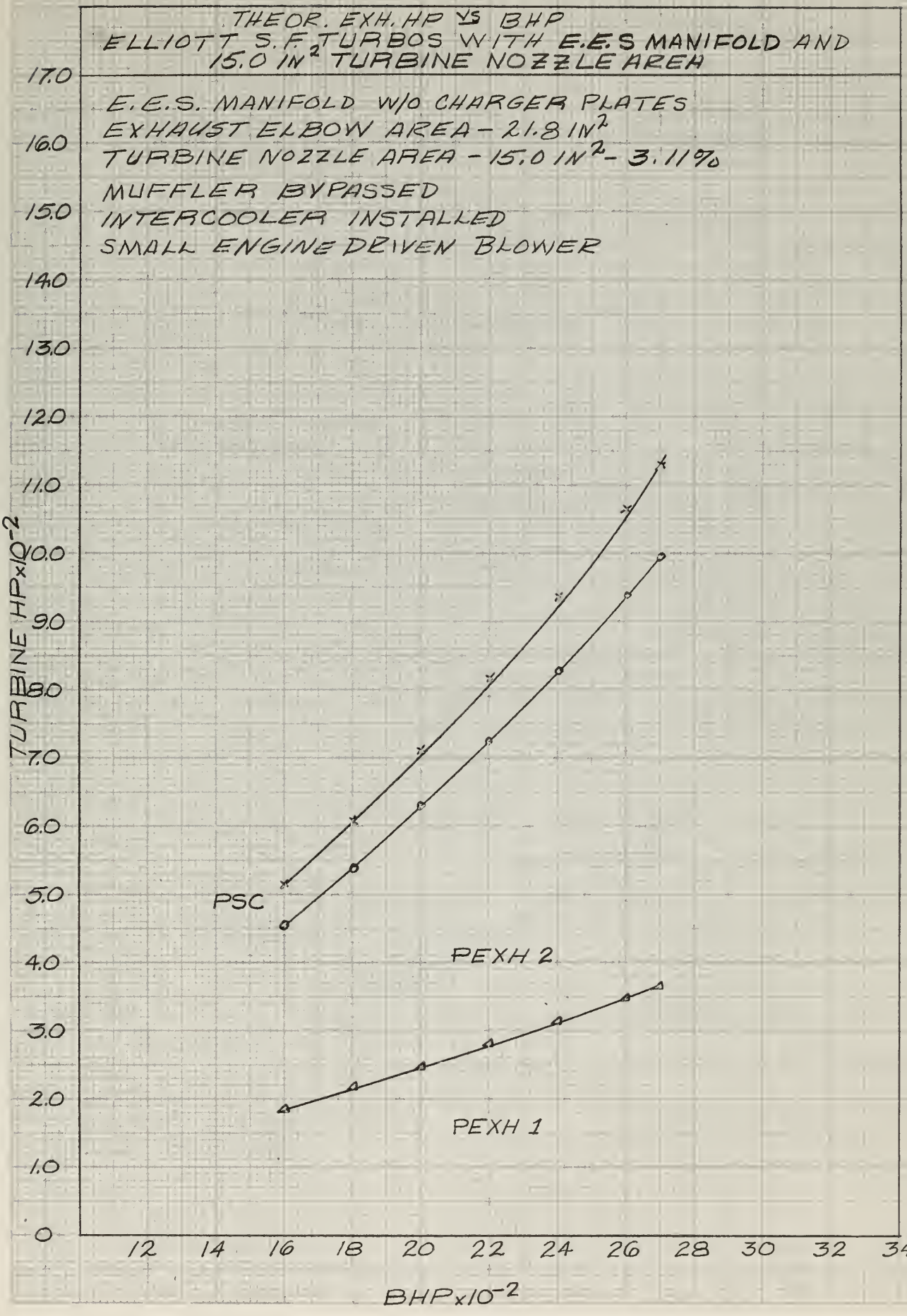
THEOR. EXH. HP VS BHP
ELLIOTT S.F. TURBOS WITH E.E.S MANIFOLD AND
15.0 IN² TURBINE NOZZLE AREA
E.E.S. MANIFOLD W/O CHARGER PLATES
EXHAUST ELBOW AREA - 21.8 IN²
TURBINE NOZZLE AREA - 15.0 IN² - 3.11%
MUFFLER BYPASSED
INTERCOOLER INSTALLED
SMALL ENGINE DRIVEN BLOWER
PSC
PEXH 2
PEXH 1
TURBINE HP x 10⁻²
BHP x 10⁻²
17.0
16.0
15.0
14.0
13.0
12.0
11.0
10.0
9.0
8.0
7.0
6.0
5.0
4.0
3.0
2.0
1.0
0
12
14
16
18
20
22
24
26
28
30
32
34

FIG. 16B

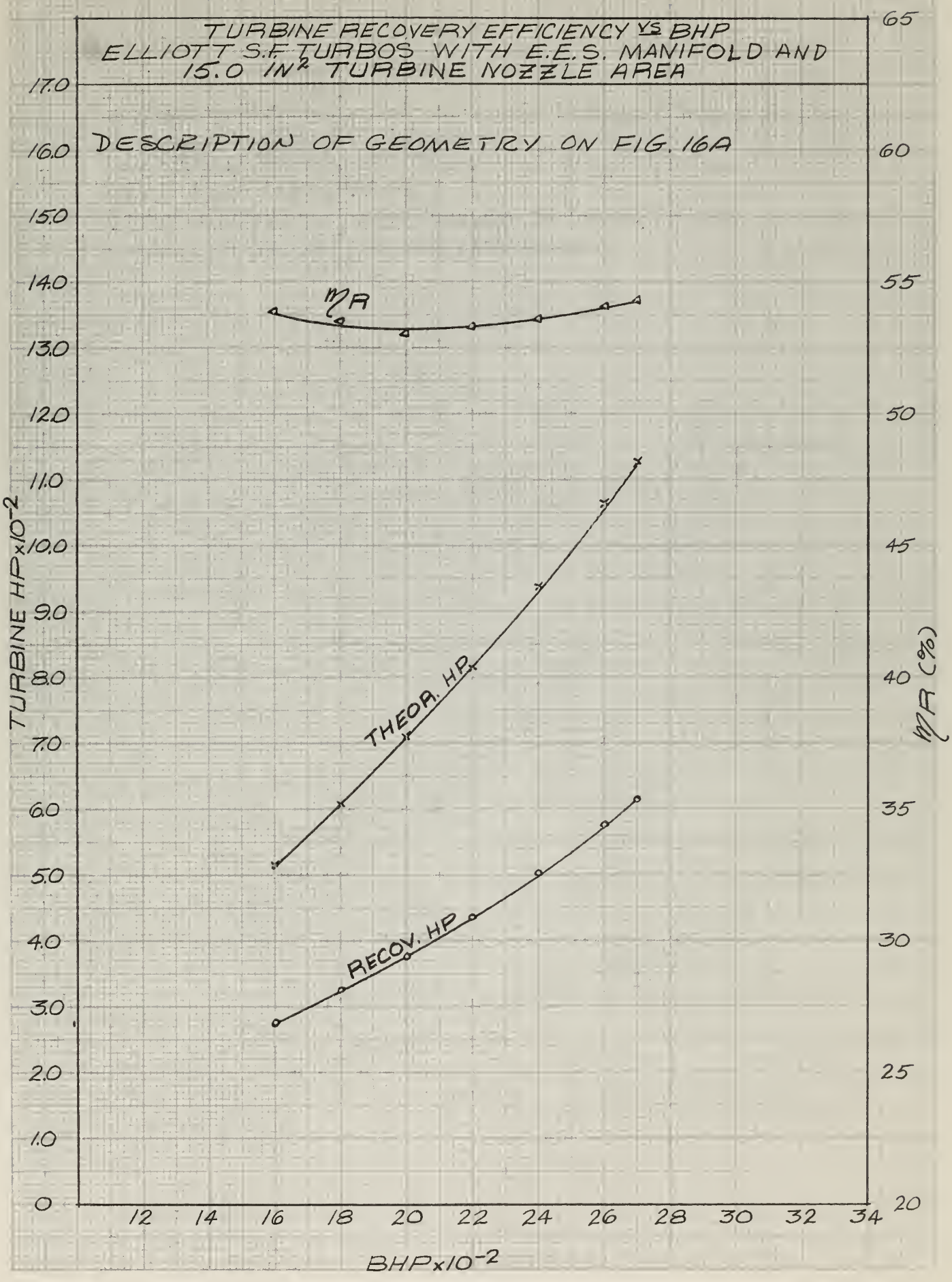
TURBINE RECOVERY EFFICIENCY Vs BHP
ELLIOTT S.F. TURBOS WITH E.E.S. MANIFOLD AND
15.0 IN² TURBINE NOZZLE AREA
DESCRIPTION OF GEOMETRY ON FIG. 16A
ηR
THEOR. HP
RECOV. HP
TURBINE HP x10⁻²
ηR (%)
BHP x10⁻²
17.0
16.0
15.0
14.0
13.0
12.0
11.0
10.0
9.0
8.0
7.0
6.0
5.0
4.0
3.0
2.0
1.0
0
65
60
55
50
45
40
35
30
25
20
12
14
16
18
20
22
24
26
28
30
32
34

FIG. 17A

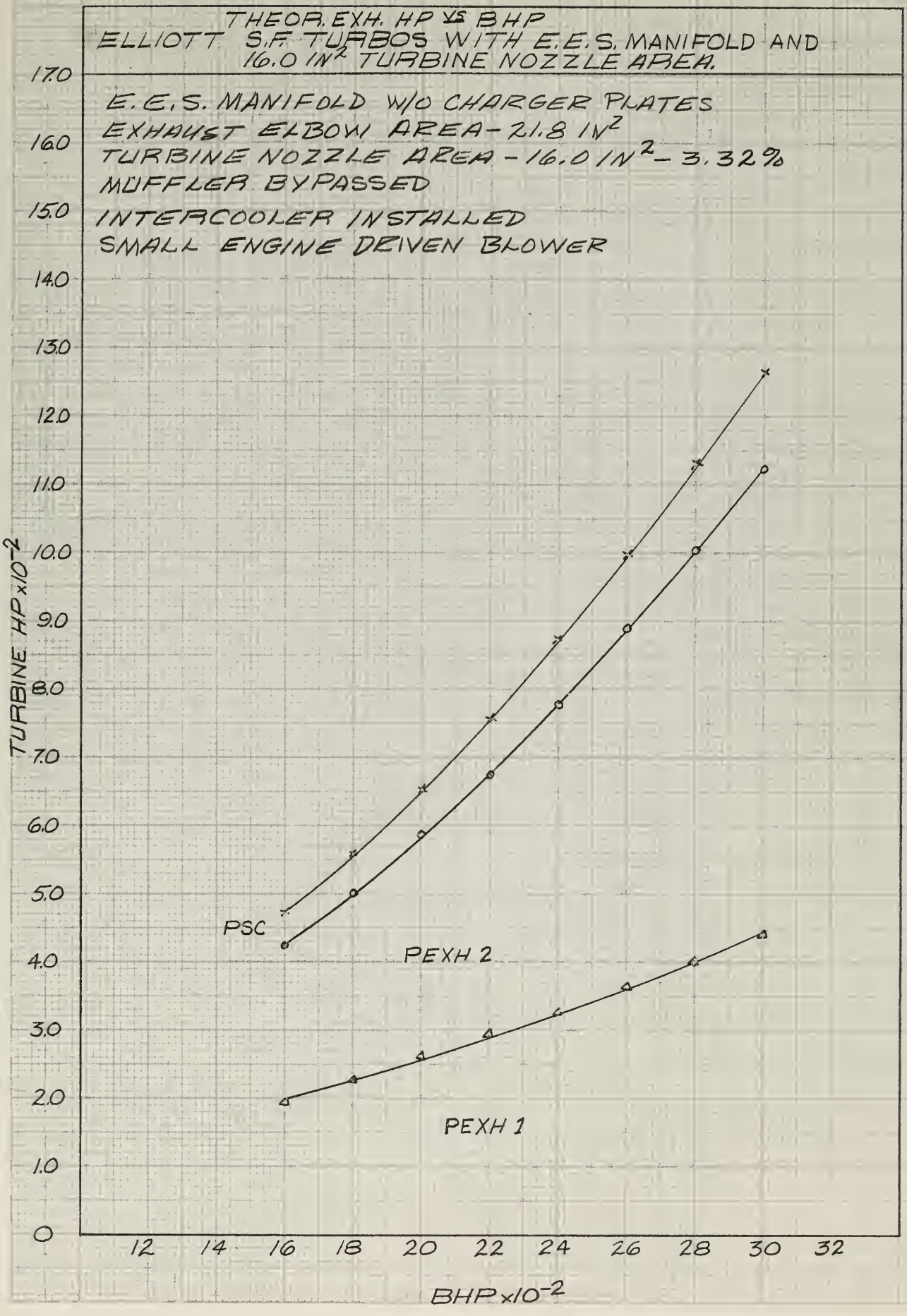
THEOR. EXH. HP VS BHP
ELLIOTT S.F. TURBOS WITH E.E.S. MANIFOLD AND 16.0 IN² TURBINE NOZZLE AREA.
E.E.S. MANIFOLD W/O CHARGER PLATES
EXHAUST ELBOW AREA - 21.8 IN²
TURBINE NOZZLE AREA - 16.0 IN² - 3.32%
MUFFLER BYPASSED
INTERCOOLER INSTALLED
SMALL ENGINE DRIVEN BLOWER
PSC
PEXH 2
PEXH 1
TURBINE HP x10⁻²
BHP x10⁻²
17.0
16.0
15.0
14.0
13.0
12.0
11.0
10.0
9.0
8.0
7.0
6.0
5.0
4.0
3.0
2.0
1.0
0
12
14
16
18
20
22
24
26
28
30
32

FIG. 17 B

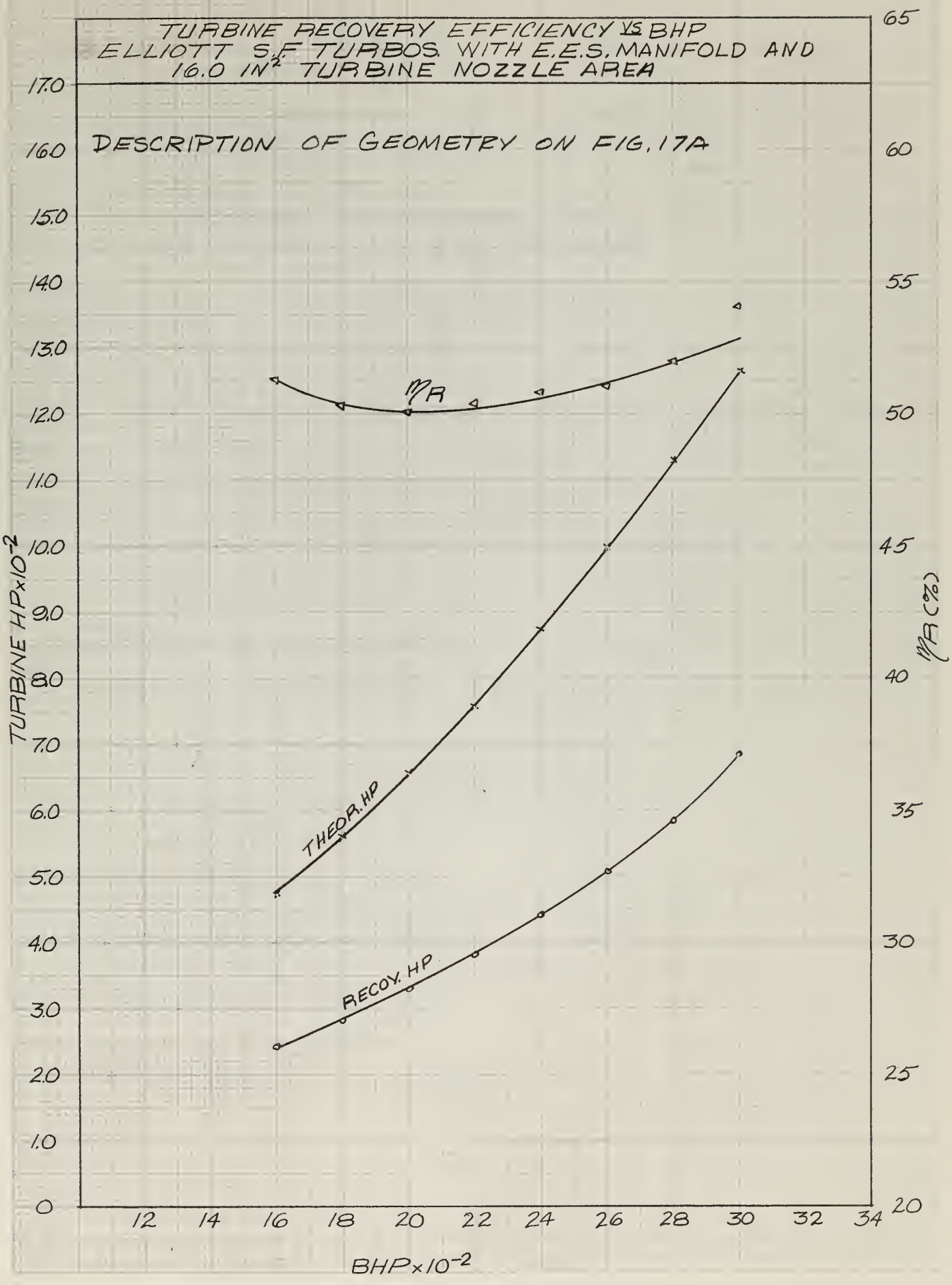
TURBINE RECOVERY EFFICIENCY VS BHP
ELLIOTT S.F TURBOS. WITH E.E.S. MANIFOLD AND
16.0 IN² TURBINE NOZZLE AREA
DESCRIPTION OF GEOMETRY ON FIG. 17A
η_R
THEOR. HP
RECOV. HP
TURBINE HP×10⁻²
η_R (%)
BHP×10⁻²
17.0
16.0
15.0
14.0
13.0
12.0
11.0
10.0
9.0
8.0
7.0
6.0
5.0
4.0
3.0
2.0
1.0
0
65
60
55
50
45
40
35
30
25
20
12
14
16
18
20
22
24
26
28
30
32
34

FIG. 18A

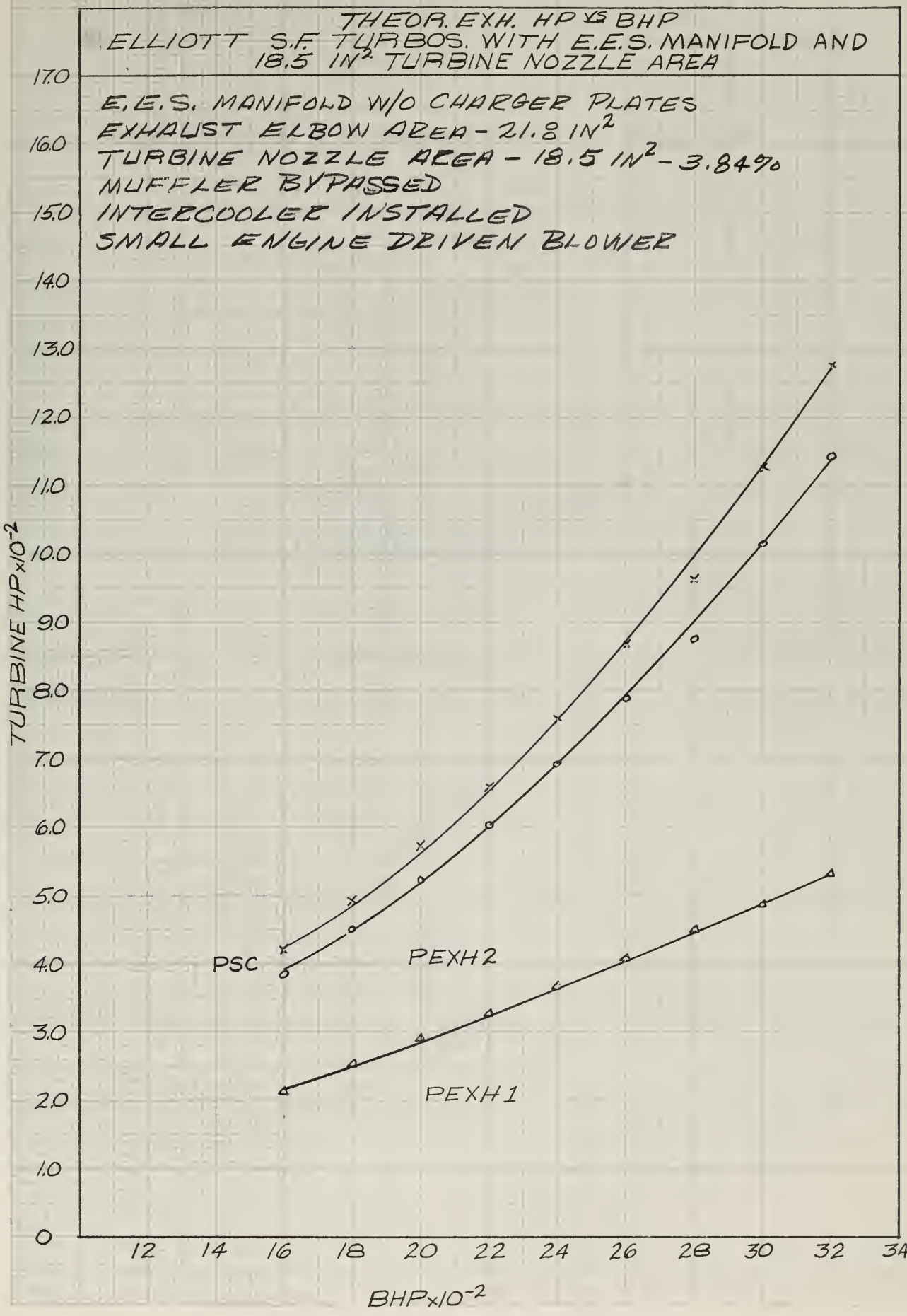
THEOR. EXH. HP VS BHP
ELLIOTT S.F. TURBOS. WITH E.E.S. MANIFOLD AND
18.5 IN² TURBINE NOZZLE AREA
E.E.S. MANIFOLD W/O CHARGER PLATES
EXHAUST ELBOW AREA - 21.8 IN²
TURBINE NOZZLE AREA - 18.5 IN² - 3.84%
MUFFLER BYPASSED
INTERCOOLER INSTALLED
SMALL ENGINE DRIVEN BLOWER
PSC
PEXH2
PEXH1
TURBINE HP×10⁻²
BHP×10⁻²
0
1.0
2.0
3.0
4.0
5.0
6.0
7.0
8.0
9.0
10.0
11.0
12.0
13.0
14.0
16.0
17.0
12
14
16
18
20
22
24
26
28
30
32
34

FIG. 18B

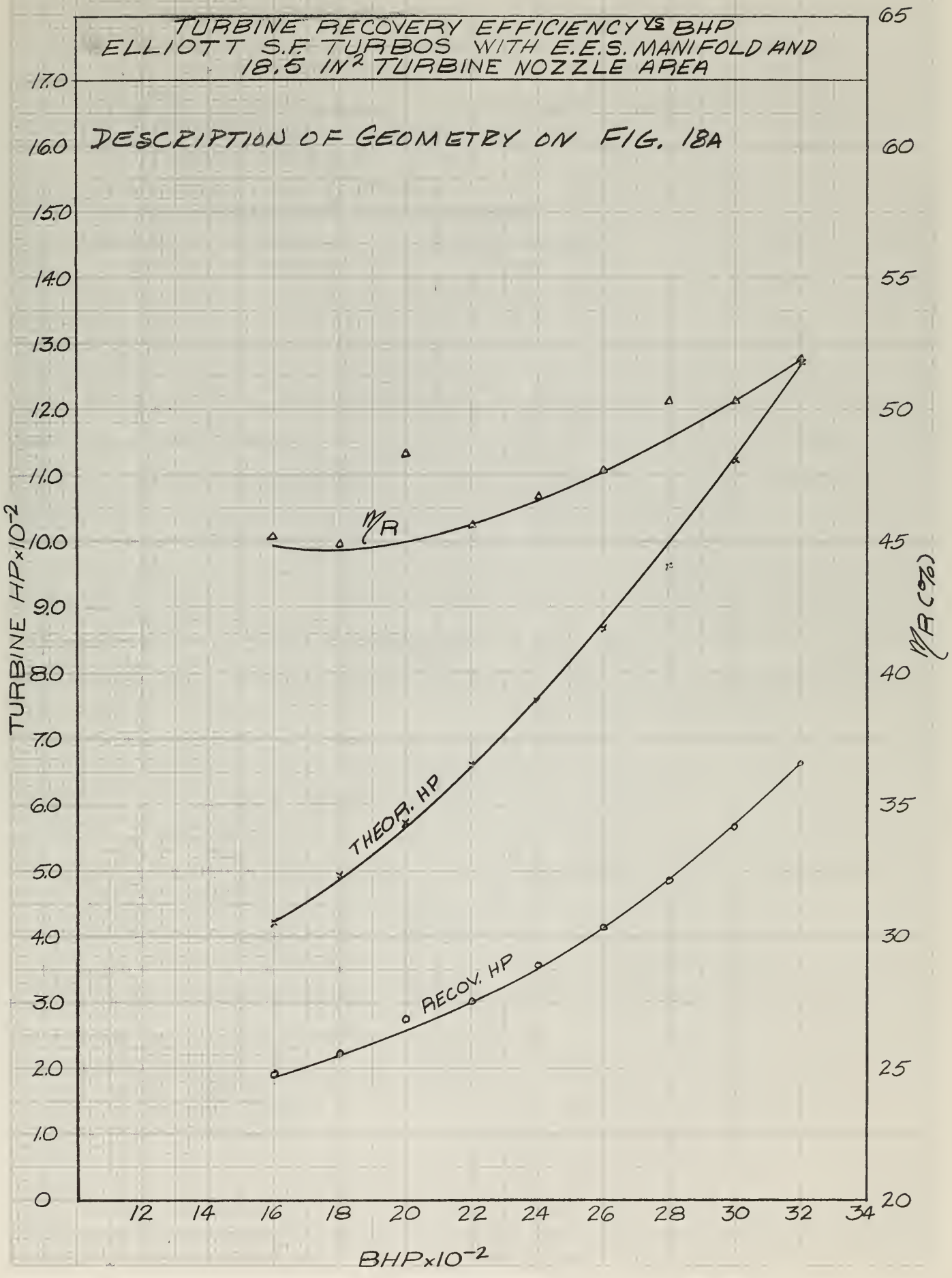
TURBINE RECOVERY EFFICIENCY Vs BHP
ELLIOTT S.F. TURBOS WITH E.E.S. MANIFOLD AND
18.5 IN² TURBINE NOZZLE AREA
DESCRIPTION OF GEOMETRY ON FIG. 18A
TURBINE HP×10⁻²
BHP×10⁻²
ηR (%)
ηR
THEOR. HP
RECOV. HP
17.0
16.0
15.0
14.0
13.0
12.0
11.0
10.0
9.0
8.0
7.0
6.0
5.0
4.0
3.0
2.0
1.0
0
65
60
55
50
45
40
35
30
25
20
12
14
16
18
20
22
24
26
28
30
32
34

FIG. 19A

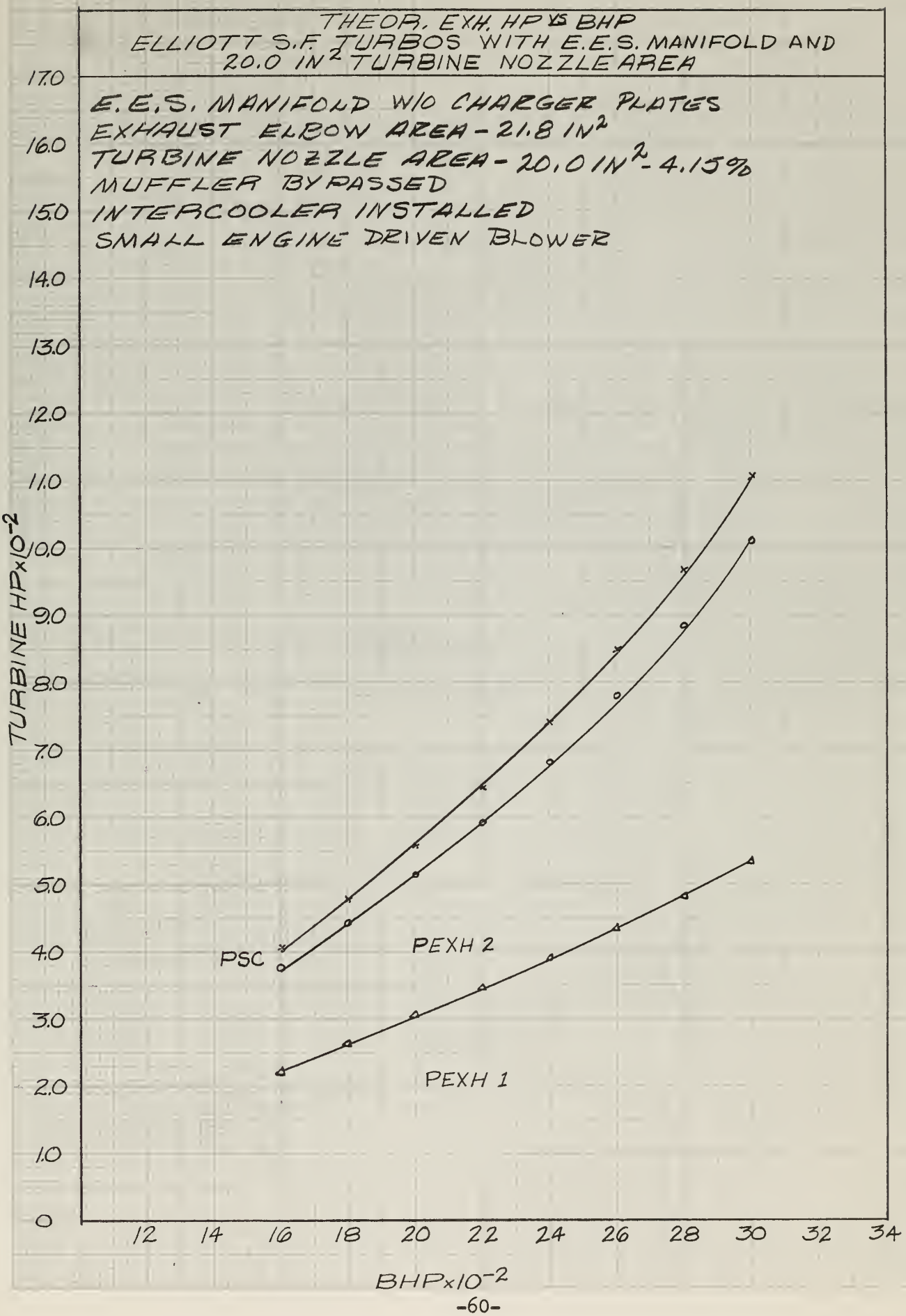
THEOR. EXH. HP VS BHP
ELLIOTT S.F. TURBOS WITH E.E.S. MANIFOLD AND 20.0 IN² TURBINE NOZZLE AREA
E.E.S. MANIFOLD W/O CHARGER PLATES
EXHAUST ELBOW AREA - 21.8 IN²
TURBINE NOZZLE AREA - 20.0 IN² - 4.15%
MUFFLER BYPASSED
INTERCOOLER INSTALLED
SMALL ENGINE DRIVEN BLOWER
PSC
PEXH 2
PEXH 1
TURBINE HP x 10⁻²
BHP x 10⁻²
17.0
16.0
15.0
14.0
13.0
12.0
11.0
10.0
9.0
8.0
7.0
6.0
5.0
4.0
3.0
2.0
1.0
0
12
14
16
18
20
22
24
26
28
30
32
34

FIG. 19B

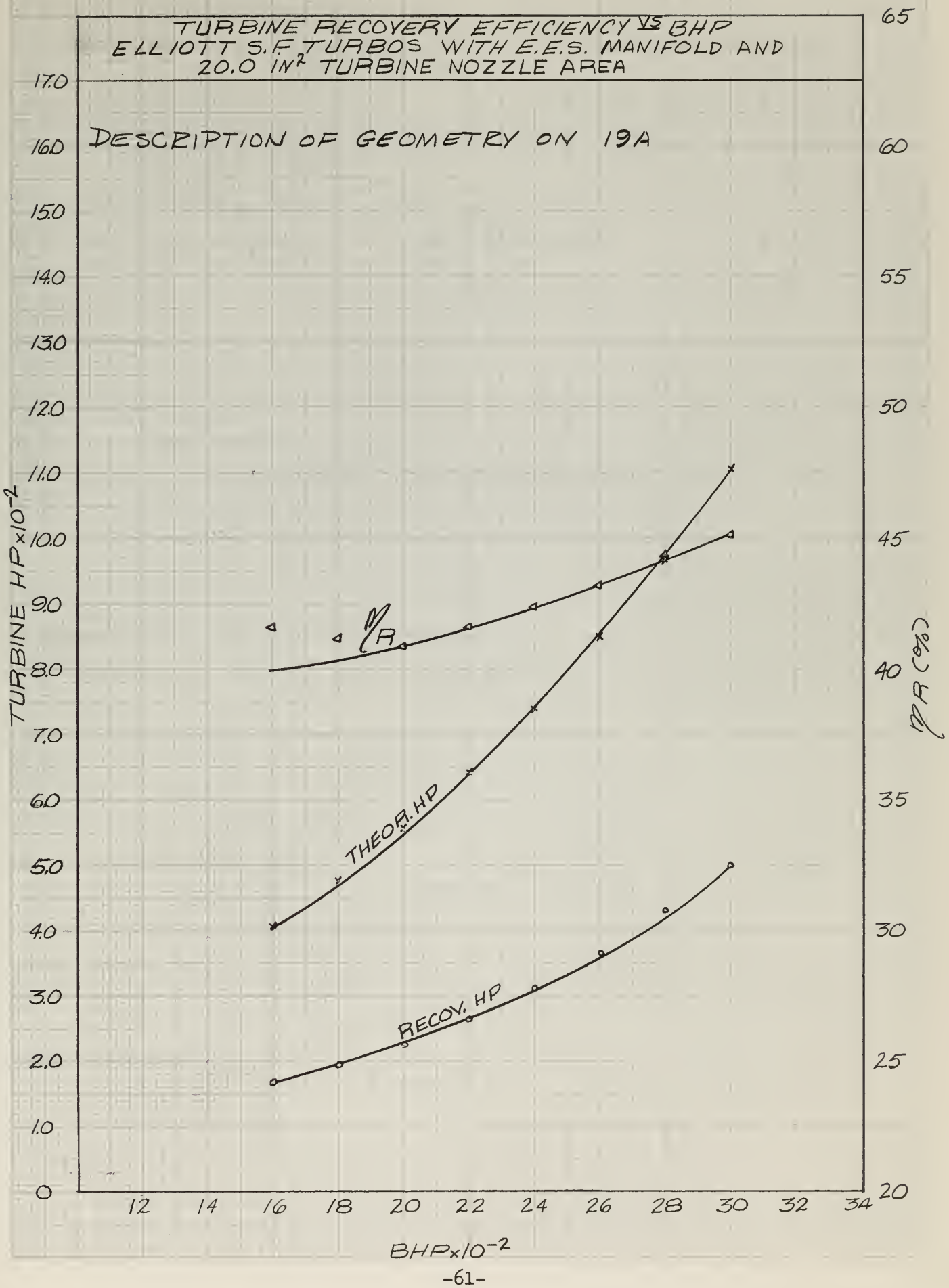
TURBINE RECOVERY EFFICIENCY VS BHP
ELLIOTT S.F. TURBOS WITH E.E.S. MANIFOLD AND
20.0 IN² TURBINE NOZZLE AREA
DESCRIPTION OF GEOMETRY ON 19A
TURBINE HP×10⁻²
17.0
16.0
15.0
14.0
13.0
12.0
11.0
10.0
9.0
8.0
7.0
6.0
5.0
4.0
3.0
2.0
1.0
0
65
60
55
50
45
40
35
30
25
20
η (%)
η
THEOR. HP
RECOV. HP
12
14
16
18
20
22
24
26
28
30
32
34
BHP×10⁻²

FIG. 20A

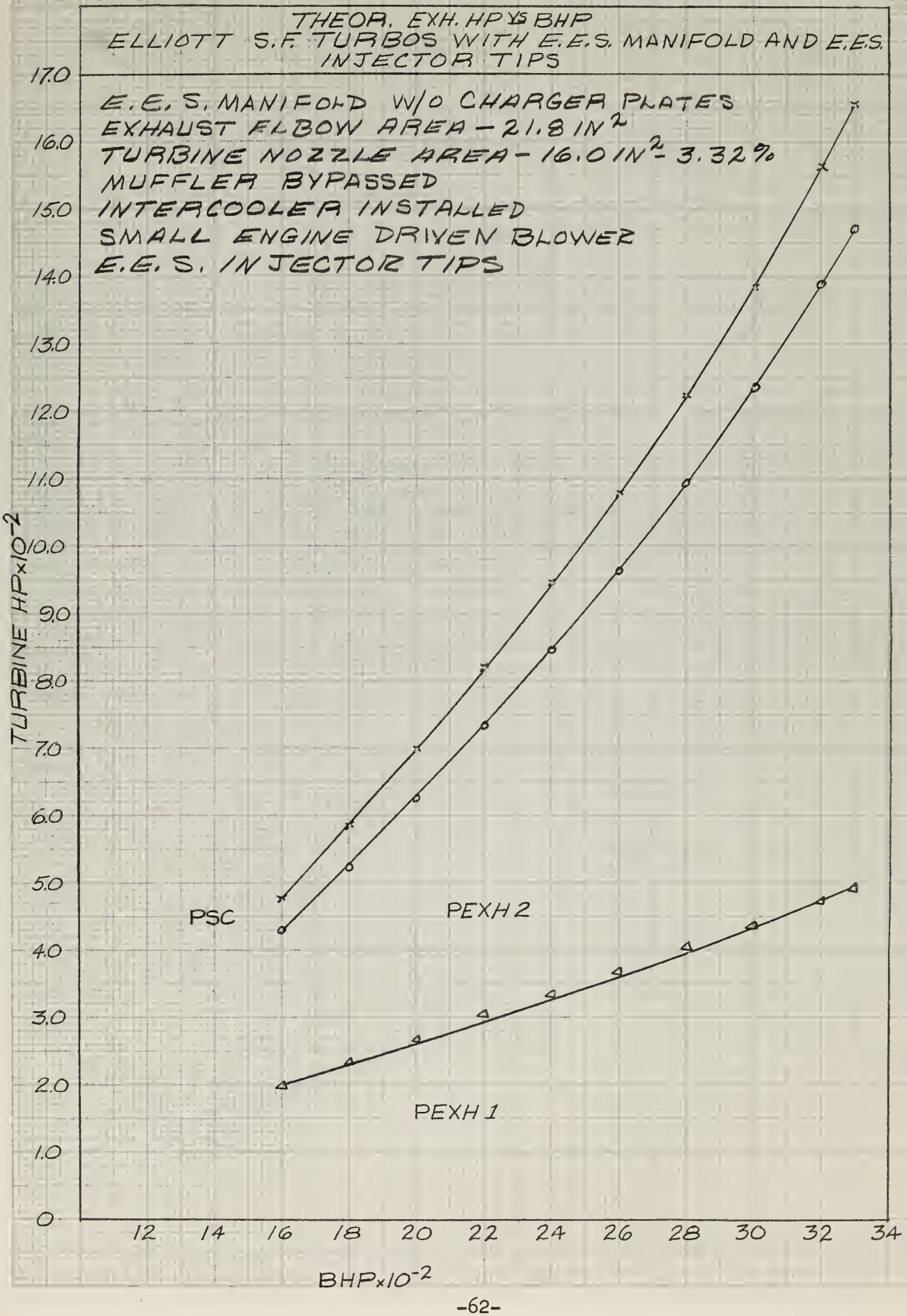
THEOR. EXH. HP VS BHP
ELLIOTT S.F. TURBOS WITH E.E.S. MANIFOLD AND E.E.S. INJECTOR TIPS
E.E.S. MANIFOLD W/O CHARGER PLATES
EXHAUST ELBOW AREA - 21.8 IN²
TURBINE NOZZLE AREA - 16.0 IN² - 3.32%
MUFFLER BYPASSED
INTERCOOLER INSTALLED
SMALL ENGINE DRIVEN BLOWER
E.E.S. INJECTOR TIPS
PSC
PEXH 2
PEXH 1
TURBINE HP x 10⁻²
BHP x 10⁻²
17.0
16.0
15.0
14.0
13.0
12.0
11.0
10.0
9.0
8.0
7.0
6.0
5.0
4.0
3.0
2.0
1.0
0
12
14
16
18
20
22
24
26
28
30
32
34

FIG. 20B

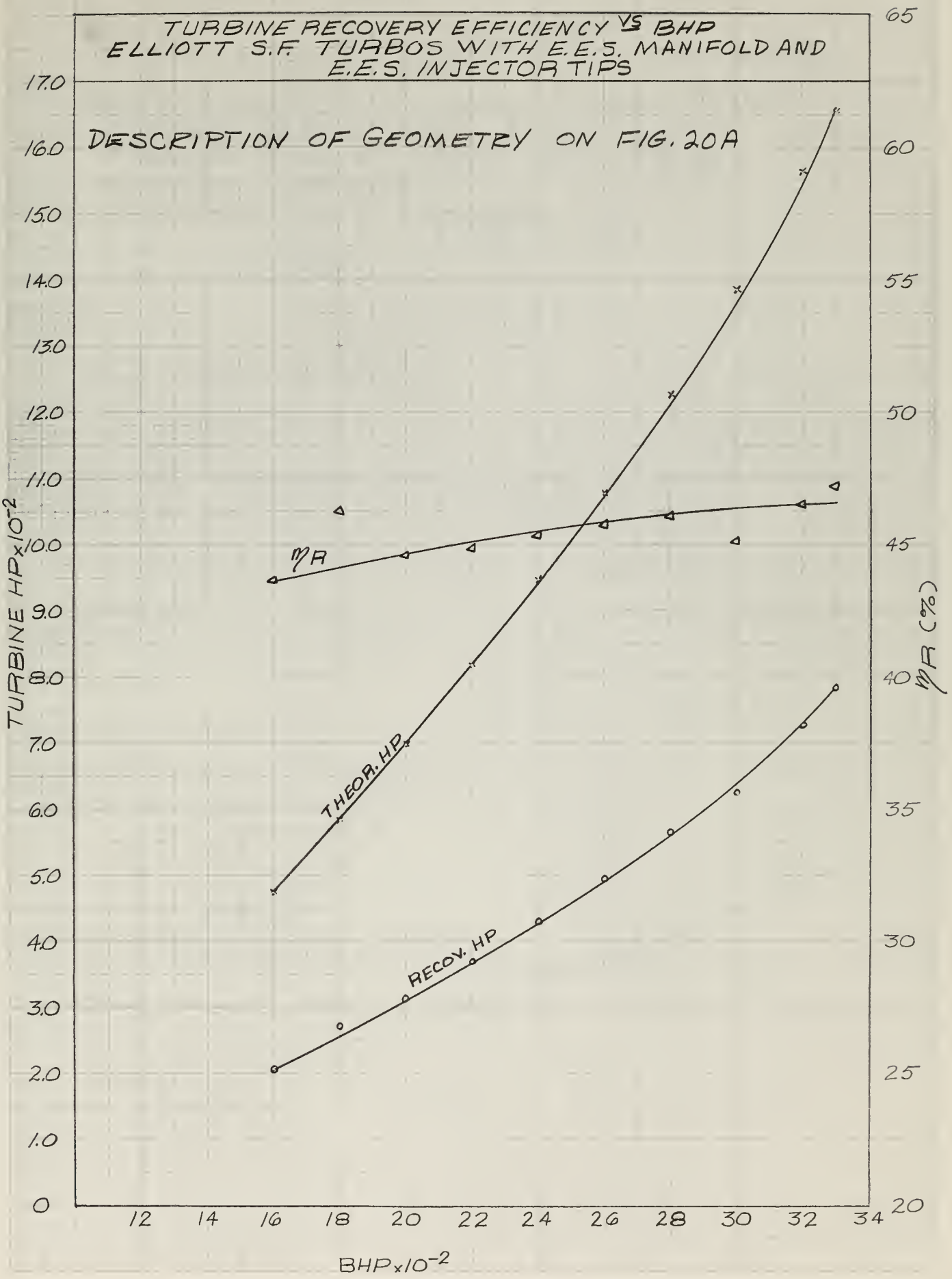
TURBINE RECOVERY EFFICIENCY VS BHP
ELLIOTT S.F. TURBOS WITH E.E.S. MANIFOLD AND E.E.S. INJECTOR TIPS
DESCRIPTION OF GEOMETRY ON FIG. 20A
TURBINE HP x 10⁻²
17.0
16.0
15.0
14.0
13.0
12.0
11.0
10.0
9.0
8.0
7.0
6.0
5.0
4.0
3.0
2.0
1.0
0
65
60
55
50
45
40
35
30
25
20
ηR (%)
ηR
THEOR. HP
RECOV. HP
12
14
16
18
20
22
24
26
28
30
32
34
BHP x 10⁻²

FIG. 21A

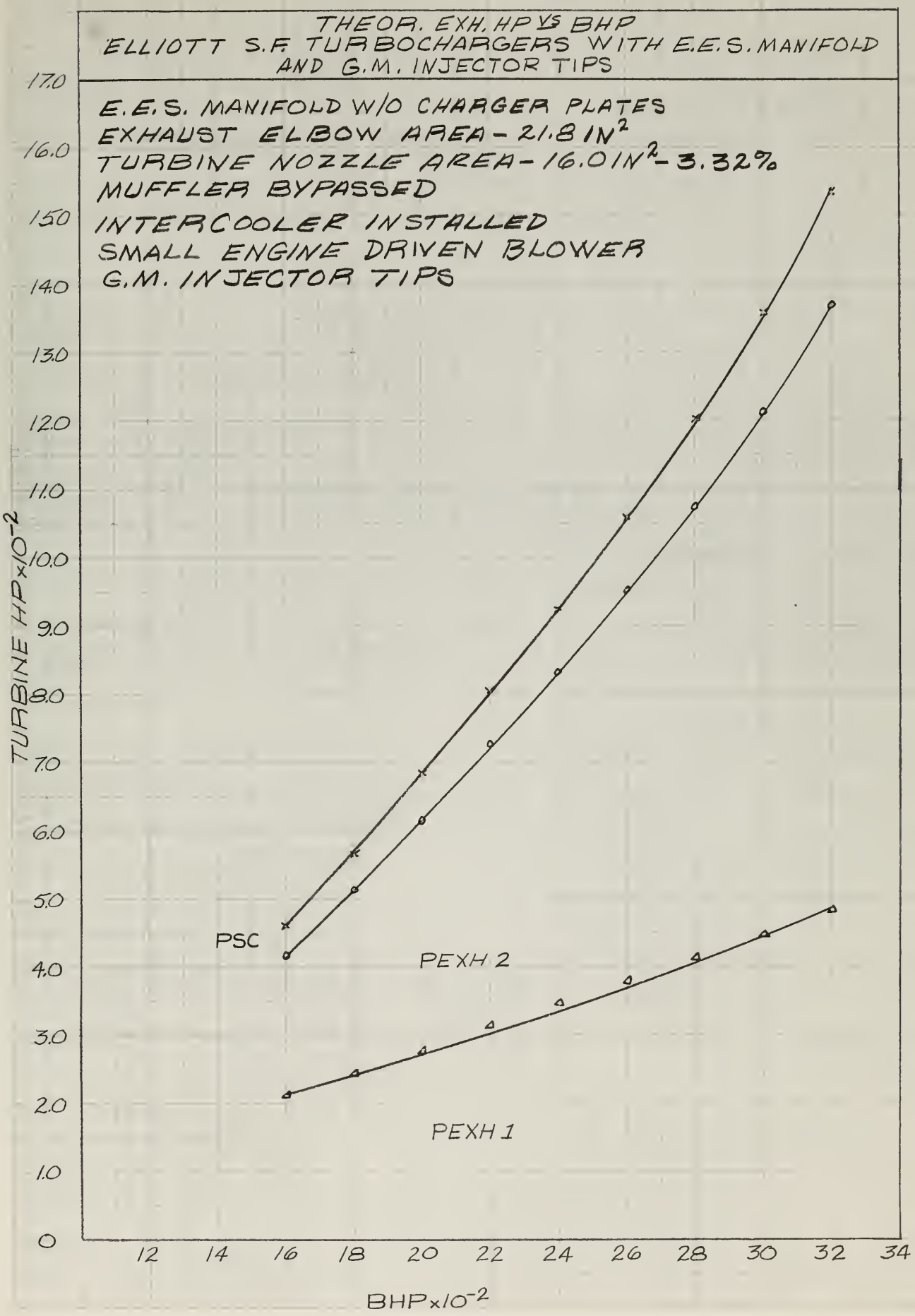
THEOR. EXH. HP VS BHP
ELLIOTT S.F. TURBOCHARGERS WITH E.E.S. MANIFOLD AND G.M. INJECTOR TIPS
E.E.S. MANIFOLD W/O CHARGER PLATES
EXHAUST ELBOW AREA - 21.8 IN²
TURBINE NOZZLE AREA - 16.0 IN² - 3.32%
MUFFLER BYPASSED
INTERCOOLER INSTALLED
SMALL ENGINE DRIVEN BLOWER
G.M. INJECTOR TIPS
PSC
PEXH 2
PEXH 1
TURBINE HP x 10⁻²
BHP x 10⁻²
17.0
16.0
15.0
14.0
13.0
12.0
11.0
10.0
9.0
8.0
7.0
6.0
5.0
4.0
3.0
2.0
1.0
0
12
14
16
18
20
22
24
26
28
30
32
34

FIG. 21B

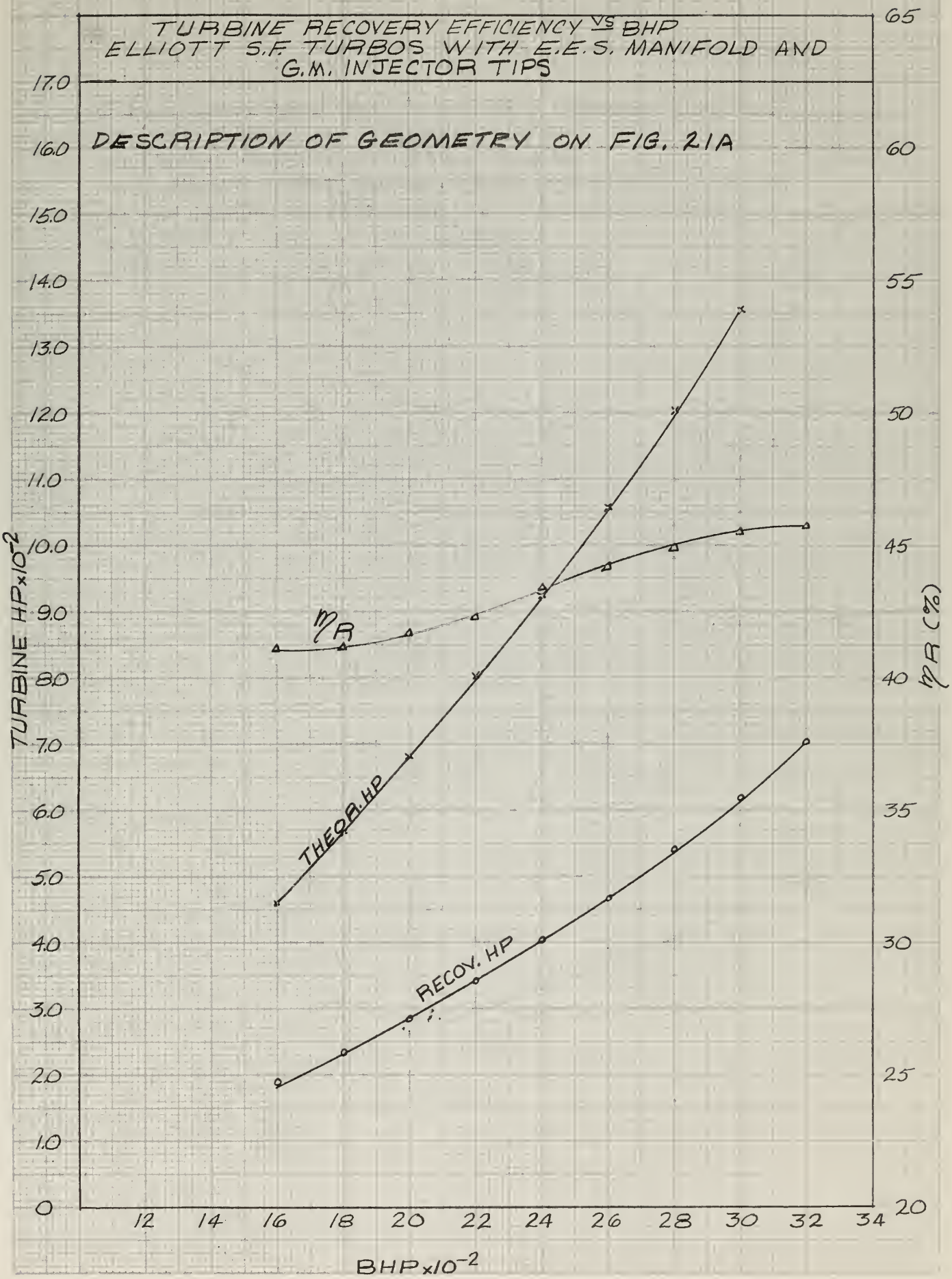
TURBINE RECOVERY EFFICIENCY VS BHP
ELLIOTT S.F. TURBOS WITH E.E.S. MANIFOLD AND G.M. INJECTOR TIPS
DESCRIPTION OF GEOMETRY ON FIG. 21A
TURBINE HP x10⁻²
BHP x10⁻²
η R (%)
η R
THEOR. HP
RECOV. HP
17.0
16.0
15.0
14.0
13.0
12.0
11.0
10.0
9.0
8.0
7.0
6.0
5.0
4.0
3.0
2.0
1.0
0
65
60
55
50
45
40
35
30
25
20
12
14
16
18
20
22
24
26
28
30
32
34

FIG. 22A

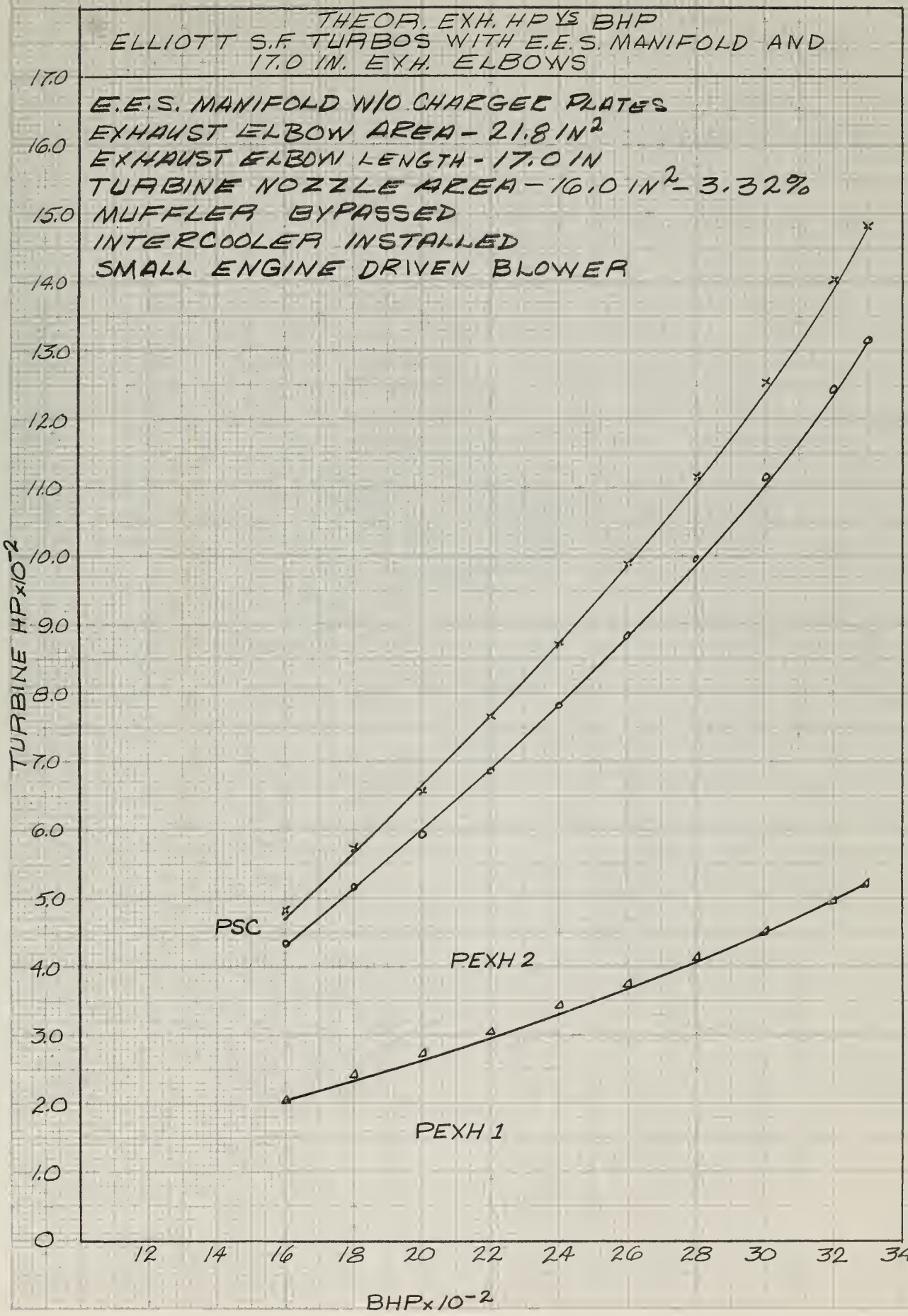
THEOR. EXH. HP VS BHP
ELLIOTT S.F TURBOS WITH E.E.S. MANIFOLD AND
17.0 IN. EXH. ELBOWS
E.E.S. MANIFOLD W/O CHARGEE PLATES
EXHAUST ELBOW AREA - 21.8 IN²
EXHAUST ELBOW LENGTH - 17.0 IN
TURBINE NOZZLE AREA - 16.0 IN² - 3.32%
MUFFLER BYPASSED
INTERCOOLER INSTALLED
SMALL ENGINE DRIVEN BLOWER
PSC
PEXH 2
PEXH 1
TURBINE HP x 10⁻²
BHP x 10⁻²
17.0
16.0
15.0
14.0
13.0
12.0
11.0
10.0
9.0
8.0
7.0
6.0
5.0
4.0
3.0
2.0
1.0
0
12
14
16
18
20
22
24
26
28
30
32
34

FIG. 22B

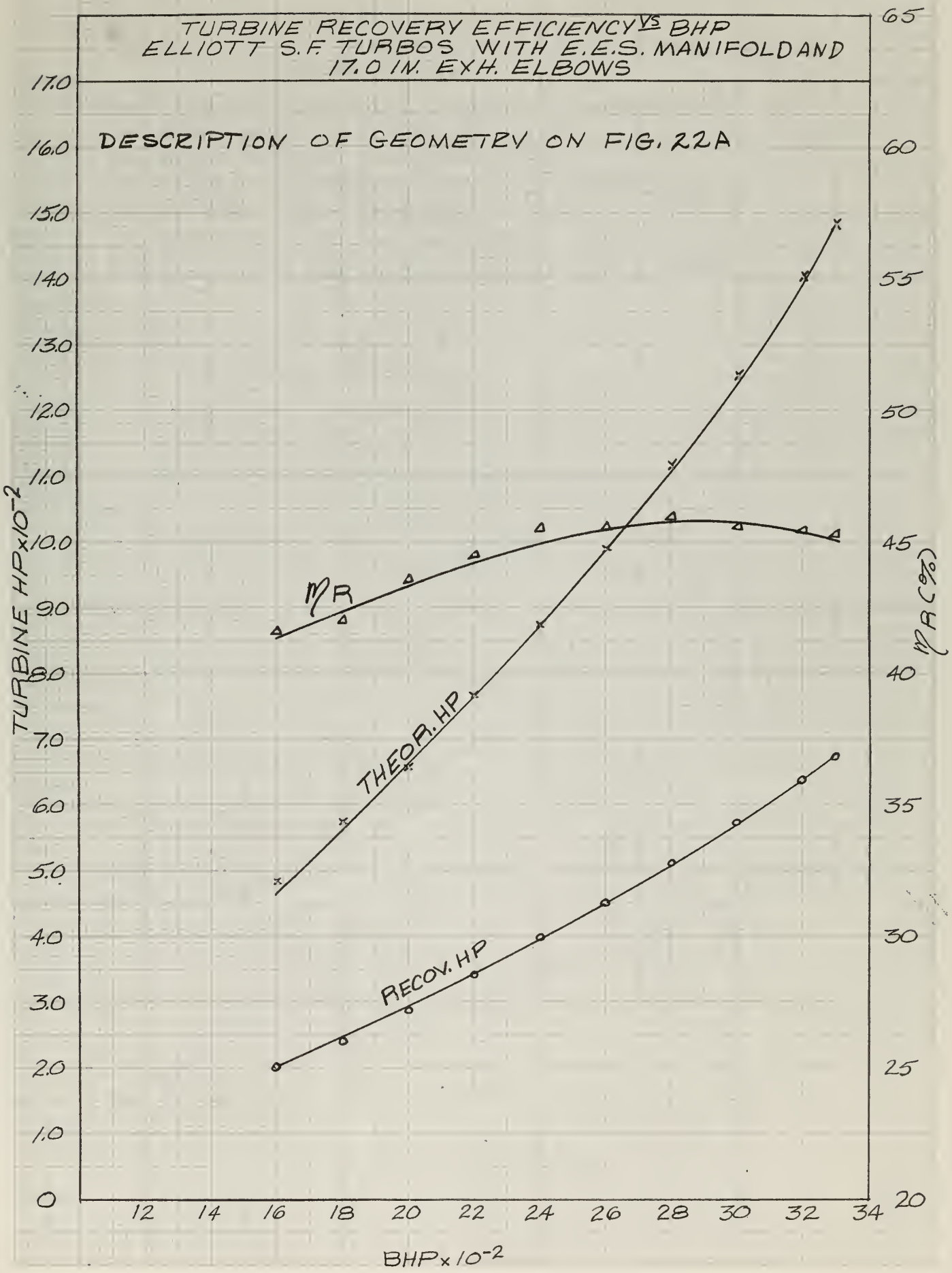
TURBINE RECOVERY EFFICIENCY Vs BHP
ELLIOTT S.F. TURBOS WITH E.E.S. MANIFOLD AND
17.0 IN. EXH. ELBOWS
DESCRIPTION OF GEOMETRY ON FIG. 22A
TURBINE HP x 10⁻²
BHP x 10⁻²
ηR (%)
ηR
THEOR. HP
RECOV. HP
17.0
16.0
15.0
14.0
13.0
12.0
11.0
10.0
9.0
8.0
7.0
6.0
5.0
4.0
3.0
2.0
1.0
0
65
60
55
50
45
40
35
30
25
20
12
14
16
18
20
22
24
26
28
30
32
34

FIG. 23A

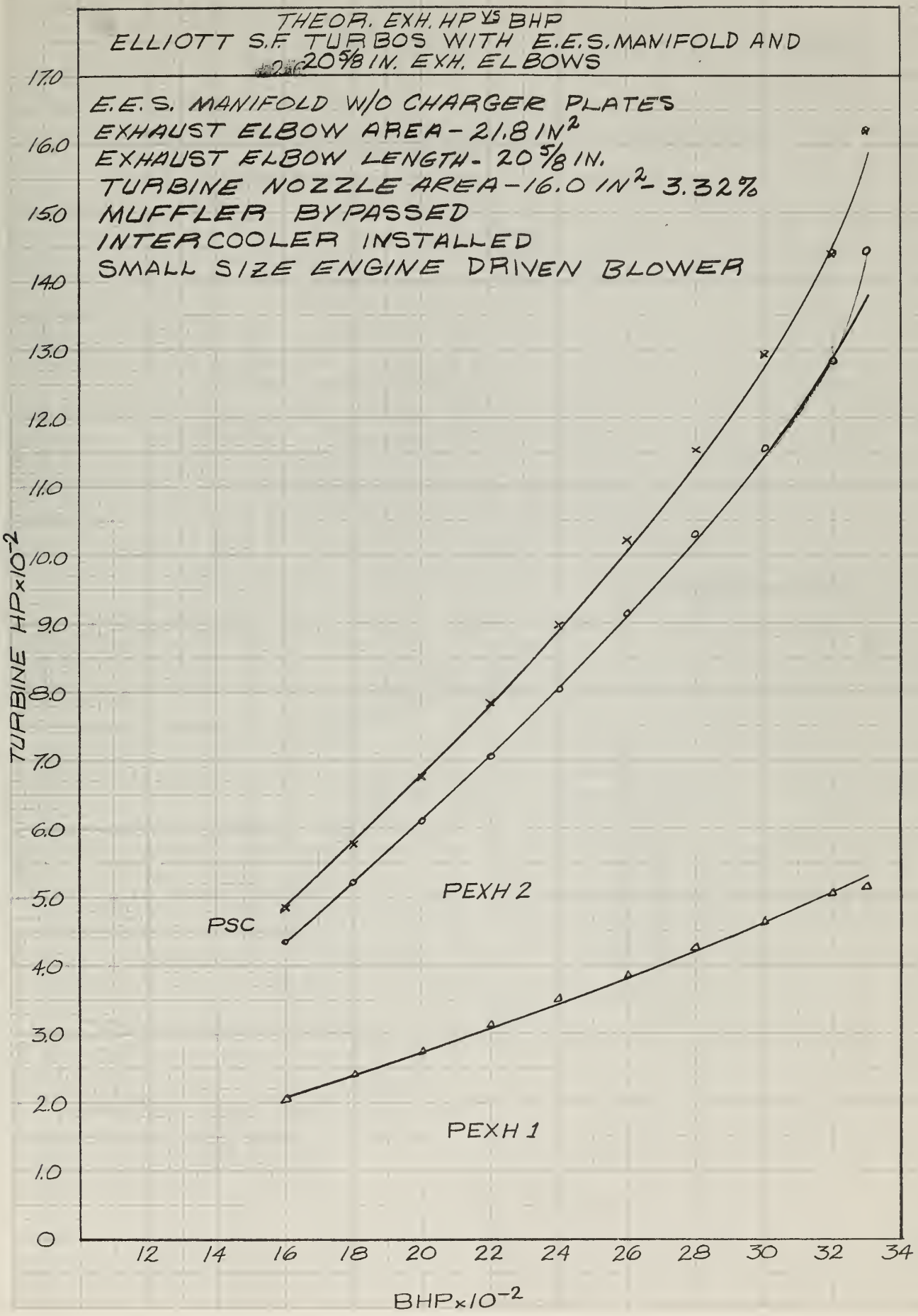
THEOR. EXH. HP VS BHP
ELLIOTT S.F. TURBOS WITH E.E.S. MANIFOLD AND 20 5/8 IN. EXH. ELBOWS
E.E.S. MANIFOLD W/O CHARGER PLATES
EXHAUST ELBOW AREA - 21.8 IN²
EXHAUST ELBOW LENGTH - 20 5/8 IN.
TURBINE NOZZLE AREA - 16.0 IN² - 3.32%
MUFFLER BYPASSED
INTERCOOLER INSTALLED
SMALL SIZE ENGINE DRIVEN BLOWER
PEXH 2
PSC
PEXH 1
TURBINE HP×10⁻²
BHP×10⁻²
17.0
16.0
15.0
14.0
13.0
12.0
11.0
10.0
9.0
8.0
7.0
6.0
5.0
4.0
3.0
2.0
1.0
0
12
14
16
18
20
22
24
26
28
30
32
34

FIG. 23B

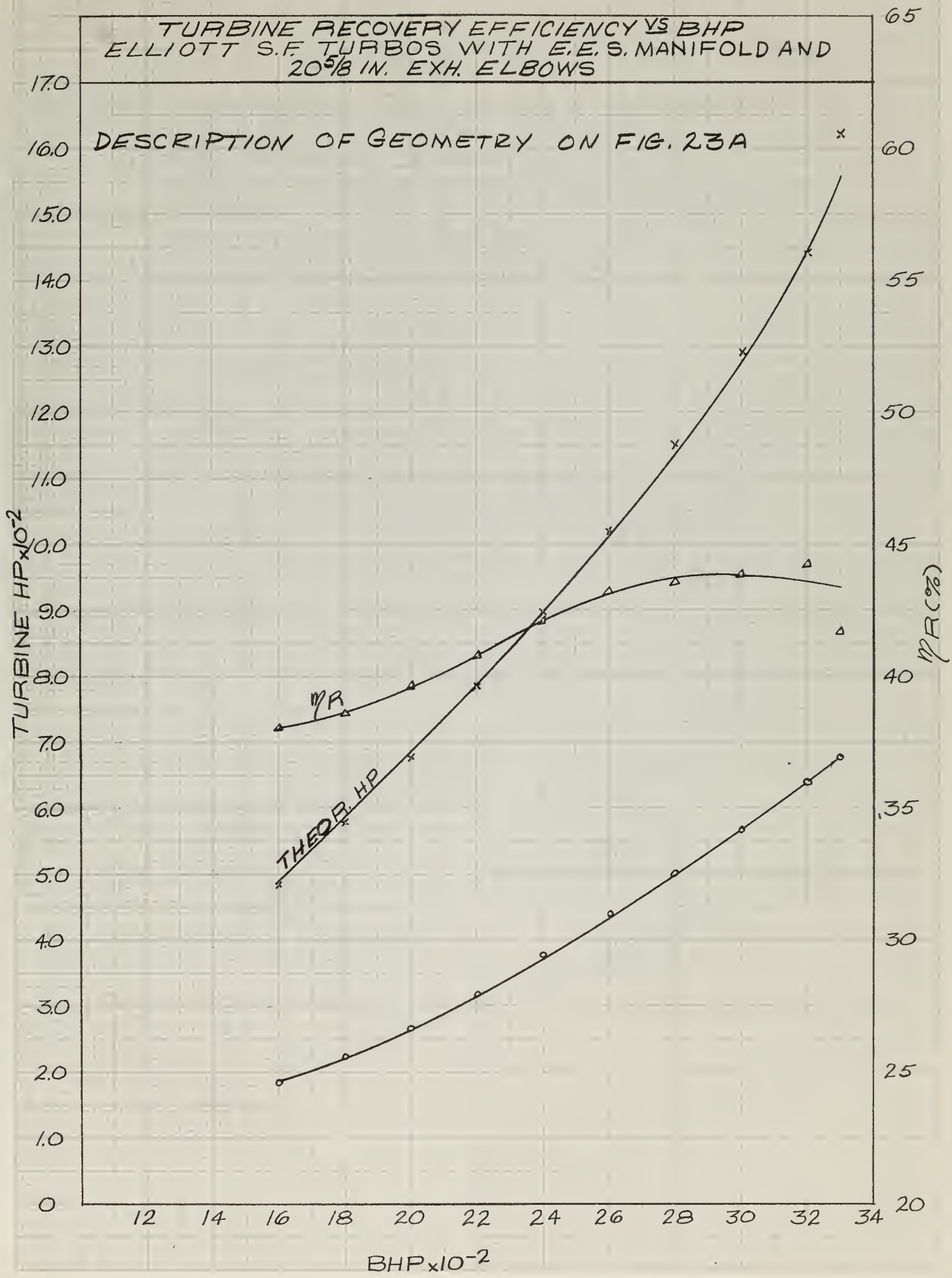
TURBINE RECOVERY EFFICIENCY VS BHP
ELLIOTT S.F. TURBOS WITH E.E.S. MANIFOLD AND
20 5/8 IN. EXH. ELBOWS
DESCRIPTION OF GEOMETRY ON FIG. 23A
TURBINE HP x 10^-2
BHP x 10^-2
η R (%)
η R
THEO. HP
17.0
16.0
15.0
14.0
13.0
12.0
11.0
10.0
9.0
8.0
7.0
6.0
5.0
4.0
3.0
2.0
1.0
0
12
14
16
18
20
22
24
26
28
30
32
34
65
60
55
50
45
40
35
30
25
20

FIG. 24A

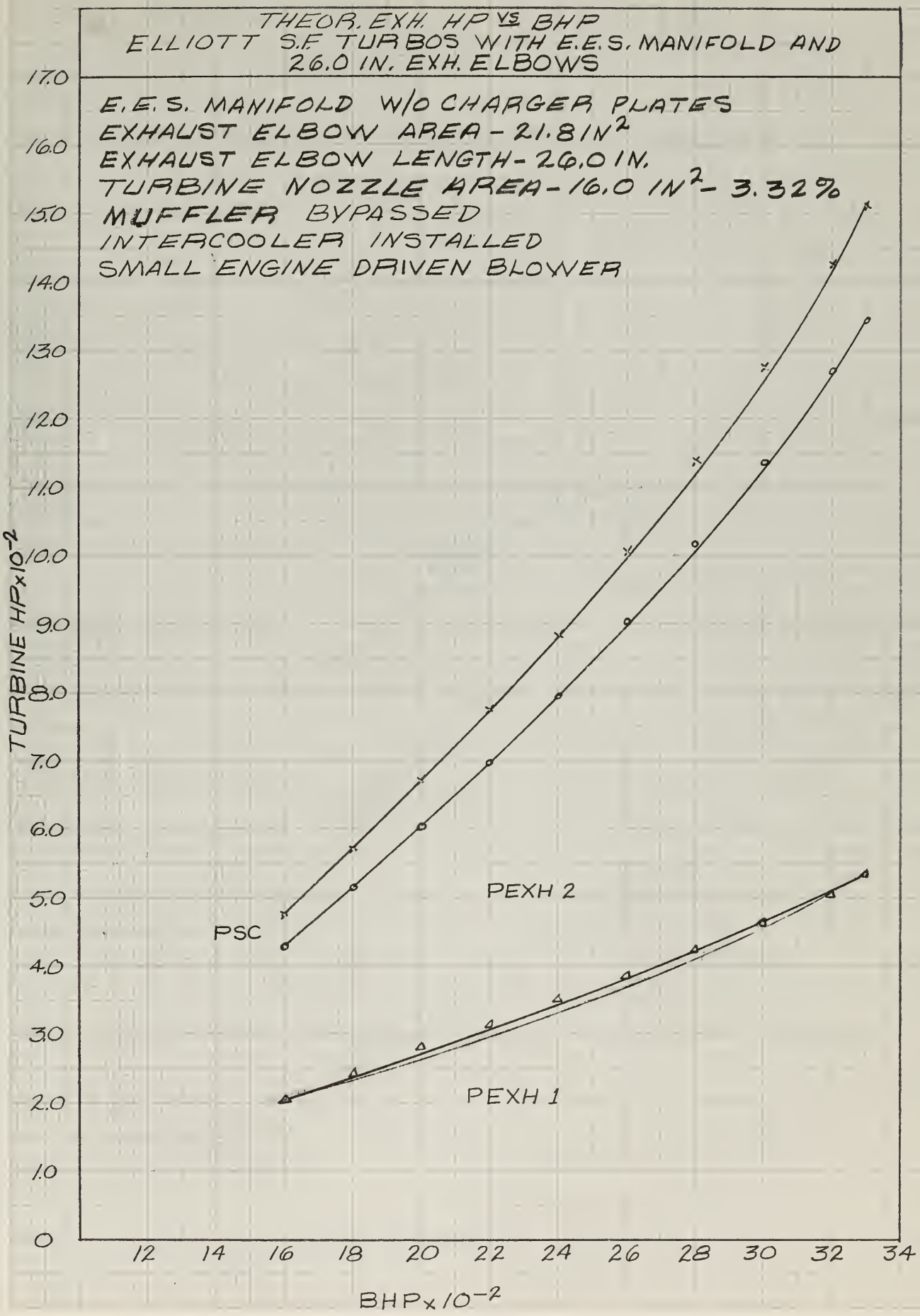
THEOR. EXH. HP VS BHP
ELLIOTT S.F TURBOS WITH E.E.S. MANIFOLD AND 26.0 IN. EXH. ELBOWS
E.E.S. MANIFOLD W/O CHARGER PLATES
EXHAUST ELBOW AREA - 21.8 IN²
EXHAUST ELBOW LENGTH - 26.0 IN.
TURBINE NOZZLE AREA - 16.0 IN² - 3.32%
MUFFLER BYPASSED
INTERCOOLER INSTALLED
SMALL ENGINE DRIVEN BLOWER
PSC
PEXH 2
PEXH 1
TURBINE HP x 10⁻²
BHP x 10⁻²
17.0
16.0
15.0
14.0
13.0
12.0
11.0
10.0
9.0
8.0
7.0
6.0
5.0
4.0
3.0
2.0
1.0
0
12
14
16
18
20
22
24
26
28
30
32
34

FIG. 24B

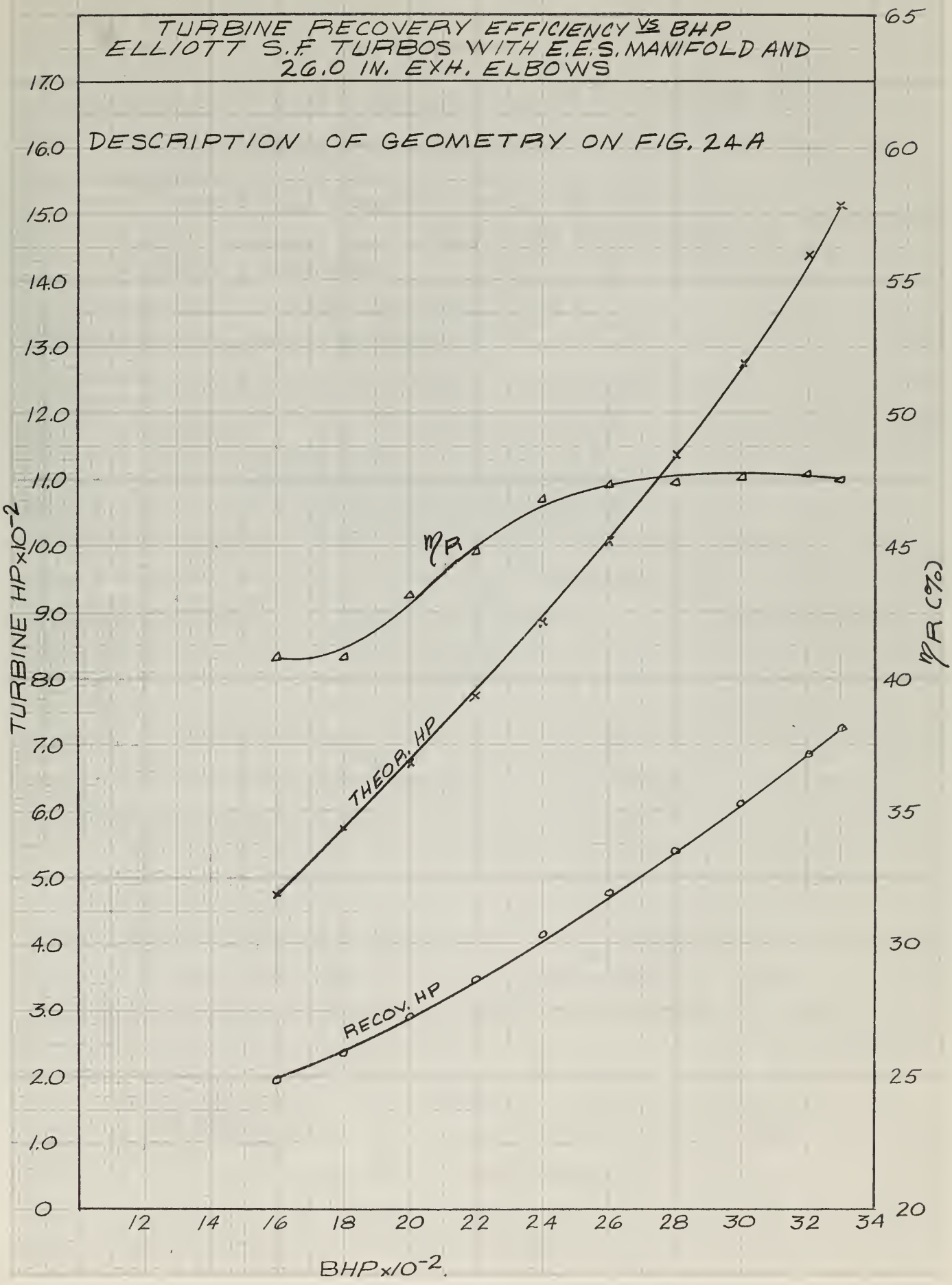
TURBINE RECOVERY EFFICIENCY Vs BHP
ELLIOTT S.F. TURBOS WITH E.E.S. MANIFOLD AND
26.0 IN. EXH. ELBOWS
DESCRIPTION OF GEOMETRY ON FIG. 24A
TURBINE HP x 10⁻²
ηR (%)
BHP x 10⁻².
ηR
THEOR. HP
RECOV. HP
17.0
16.0
15.0
14.0
13.0
12.0
11.0
10.0
9.0
8.0
7.0
6.0
5.0
4.0
3.0
2.0
1.0
0
65
60
55
50
45
40
35
30
25
20
12
14
16
18
20
22
24
26
28
30
32
34

FIG. 25A

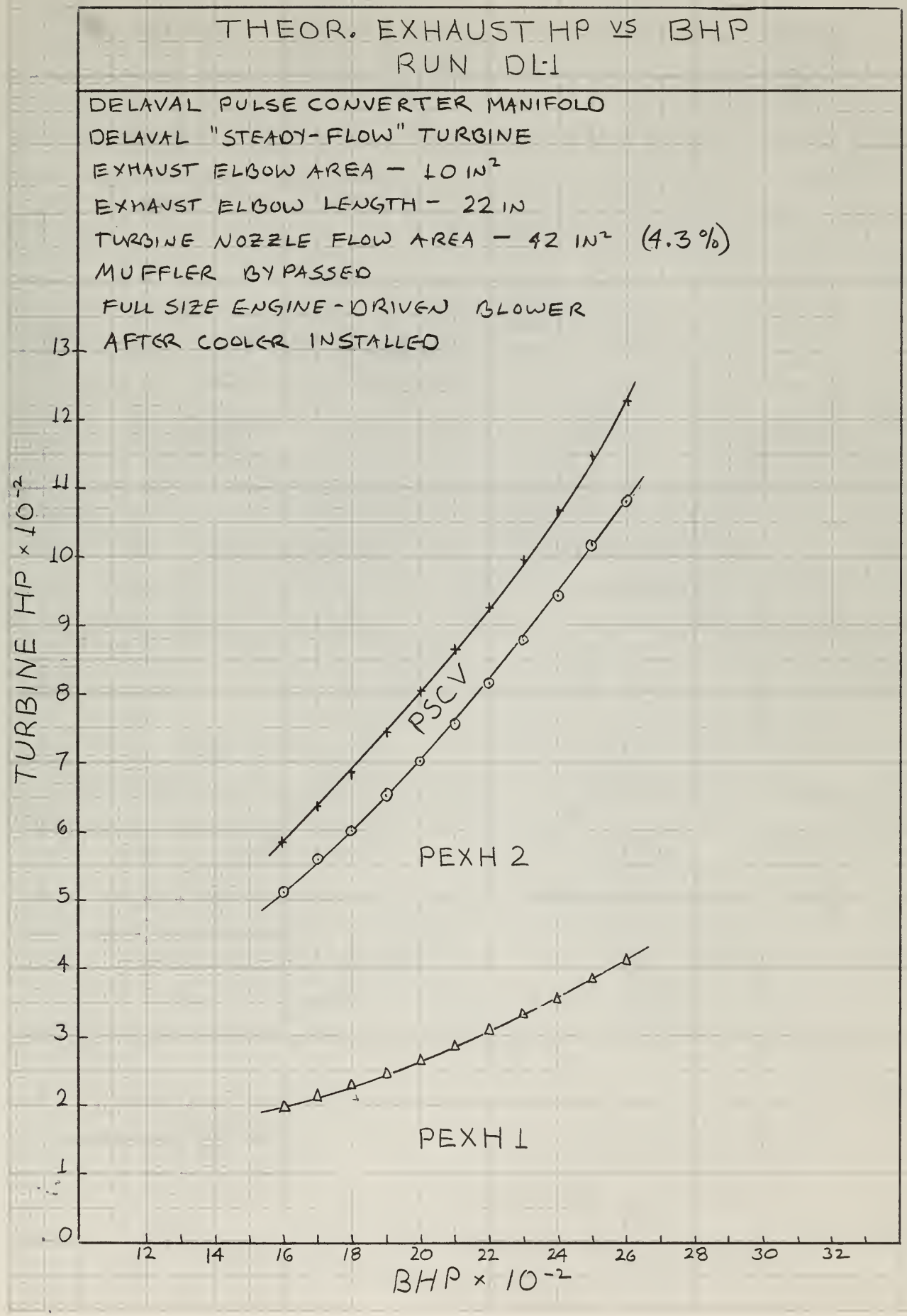
THEOR. EXHAUST HP VS BHP
RUN DL-1
DELAVAL PULSE CONVERTER MANIFOLD
DELAVAL "STEADY-FLOW" TURBINE
EXHAUST ELBOW AREA – 10 IN²
EXHAUST ELBOW LENGTH – 22 IN
TURBINE NOZZLE FLOW AREA – 42 IN² (4.3%)
MUFFLER BYPASSED
FULL SIZE ENGINE-DRIVEN BLOWER
AFTER COOLER INSTALLED
TURBINE HP × 10⁻²
BHP × 10⁻²
PSCV
PEXH 2
PEXH 1
0
1
2
3
4
5
6
7
8
9
10
11
12
13
12
14
16
18
20
22
24
26
28
30
32

FIG. 25B

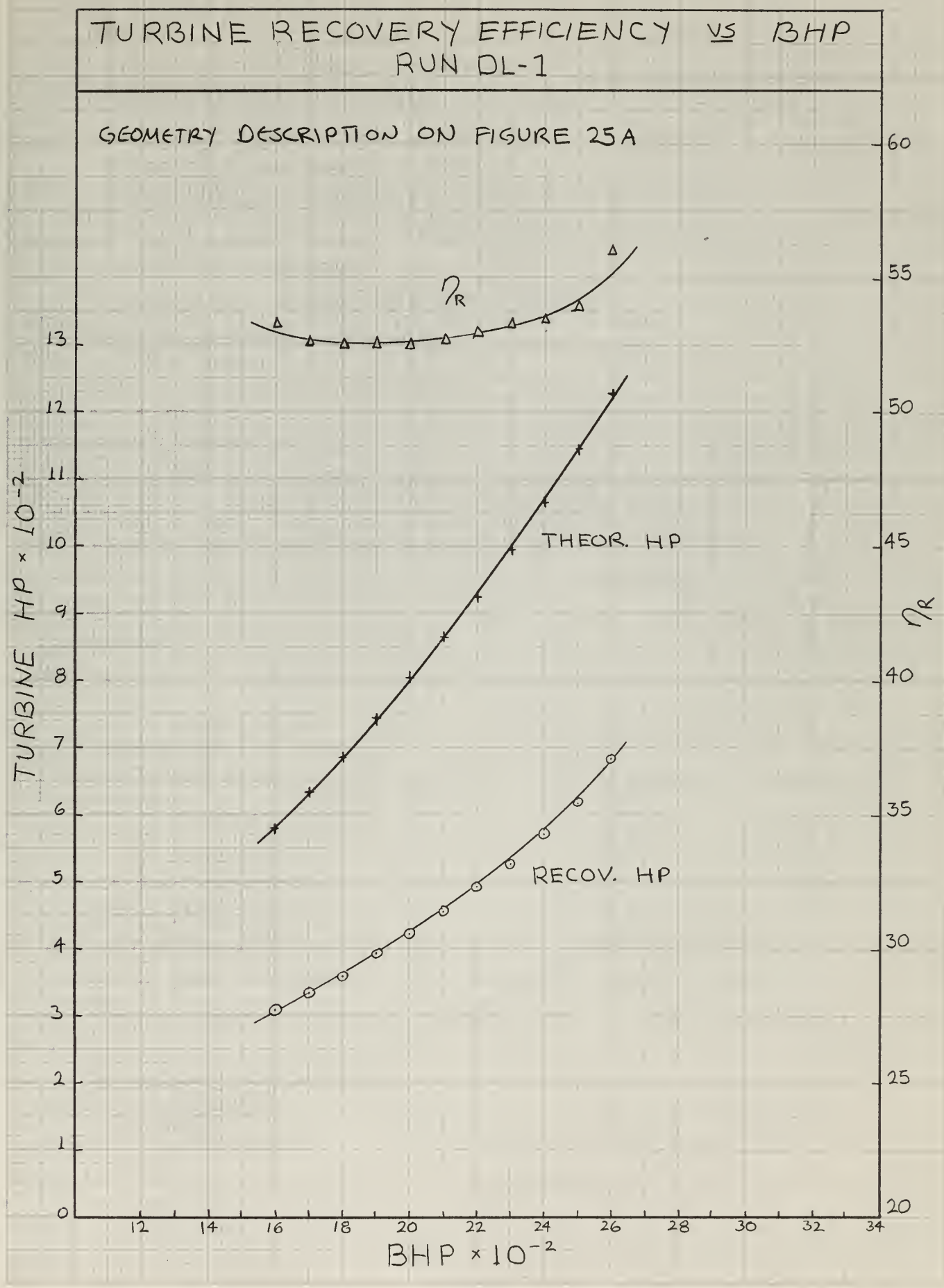
TURBINE RECOVERY EFFICIENCY VS BHP
RUN DL-1
GEOMETRY DESCRIPTION ON FIGURE 25A
η_R
THEOR. HP
RECOV. HP
TURBINE HP × 10⁻²
η_R
BHP × 10⁻²
0
1
2
3
4
5
6
7
8
9
10
11
12
13
20
25
30
35
40
45
50
55
60
12
14
16
18
20
22
24
26
28
30
32
34

FIG. 26A

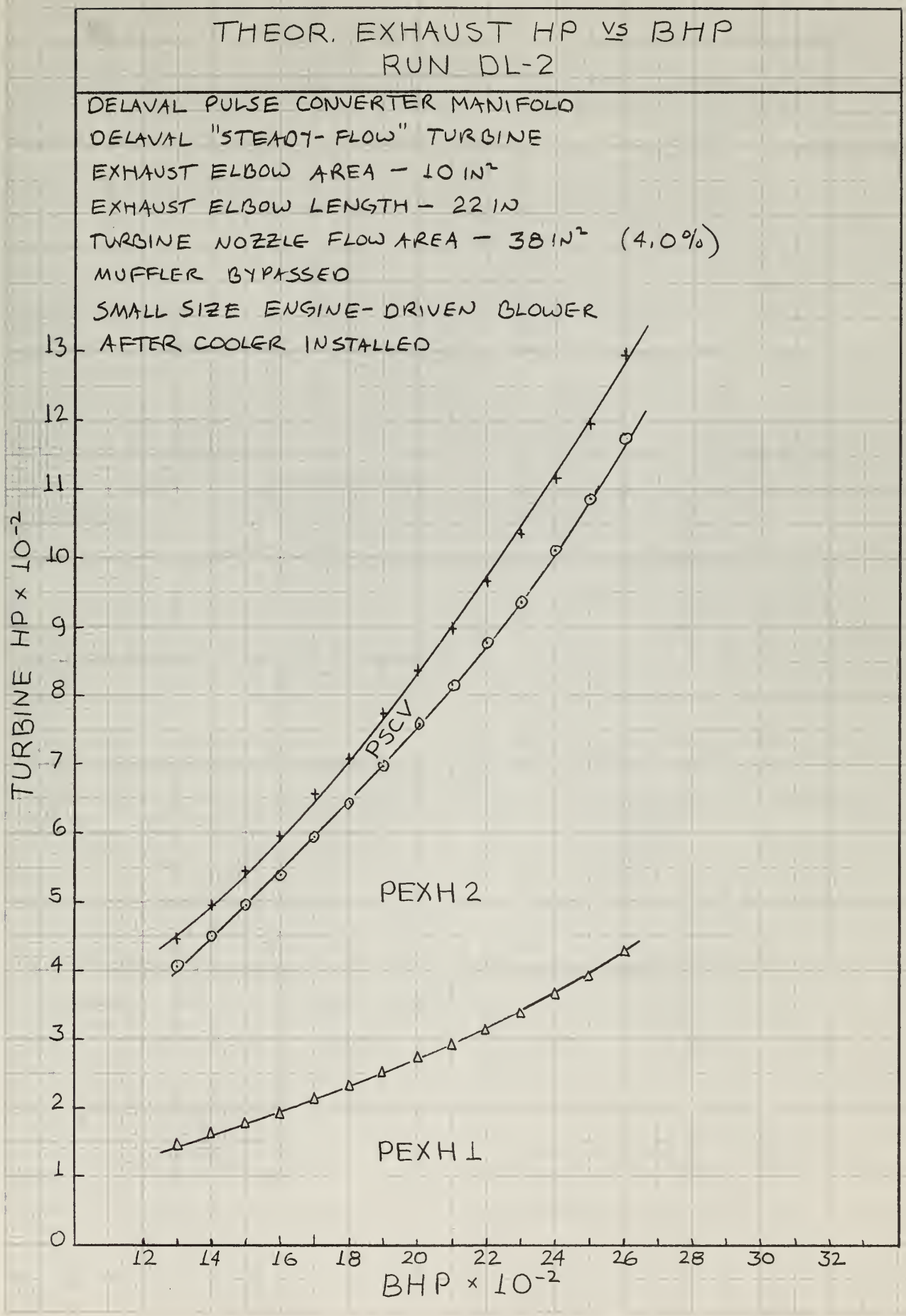
THEOR. EXHAUST HP VS BHP
RUN DL-2
DELAVAL PULSE CONVERTER MANIFOLD
DELAVAL "STEADY-FLOW" TURBINE
EXHAUST ELBOW AREA – 10 IN²
EXHAUST ELBOW LENGTH – 22 IN
TURBINE NOZZLE FLOW AREA – 38 IN² (4.0%)
MUFFLER BYPASSED
SMALL SIZE ENGINE-DRIVEN BLOWER
AFTER COOLER INSTALLED
PSCV
PEXH 2
PEXH 1
TURBINE HP × 10⁻²
BHP × 10⁻²
0
1
2
3
4
5
6
7
8
9
10
11
12
13
12
14
16
18
20
22
24
26
28
30
32

FIG. 26B

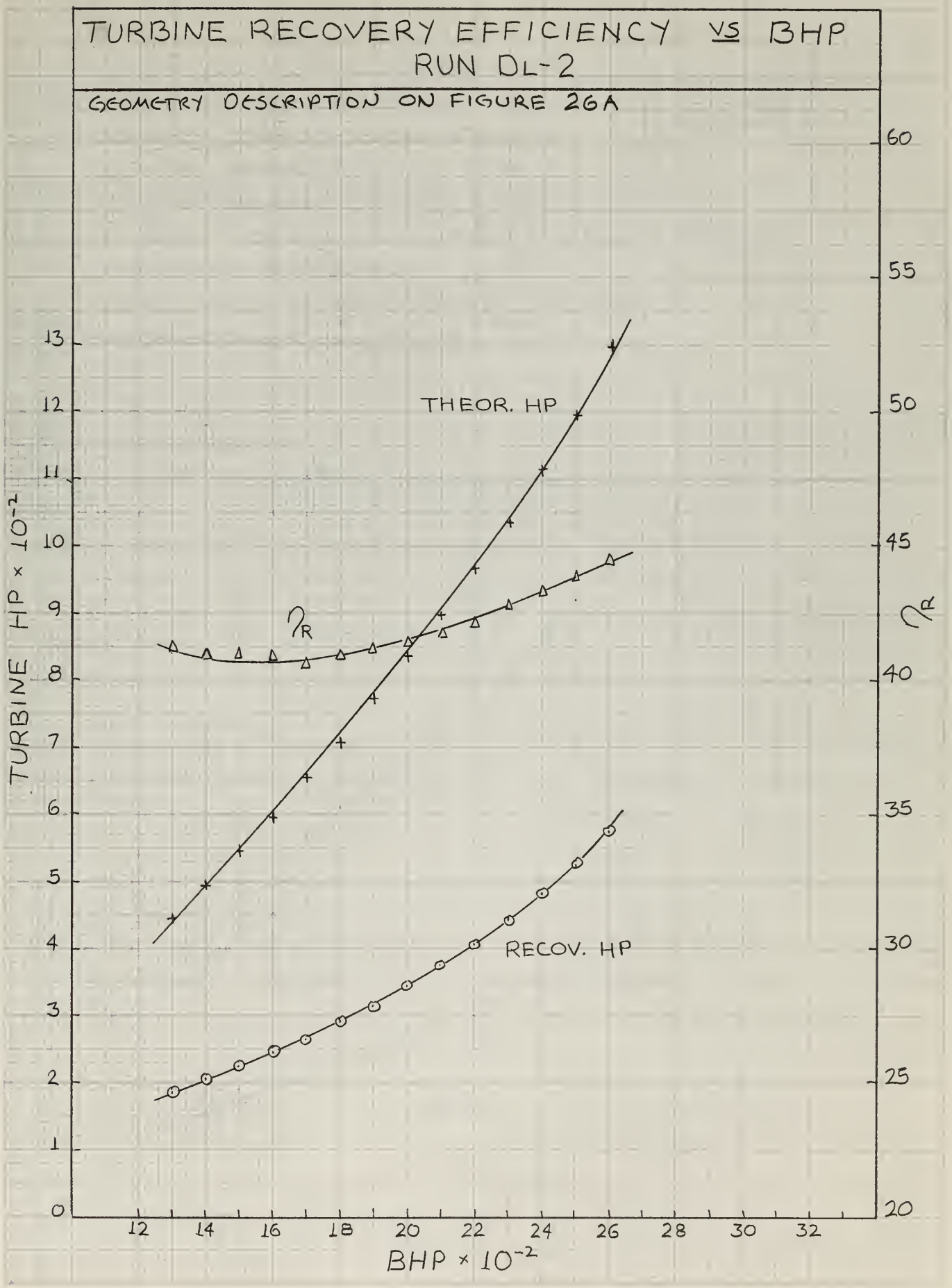
TURBINE RECOVERY EFFICIENCY VS BHP
RUN DL-2
GEOMETRY DESCRIPTION ON FIGURE 26A
THEOR. HP
RECOV. HP
η_R
η_R
TURBINE HP × 10⁻²
BHP × 10⁻²
0
1
2
3
4
5
6
7
8
9
10
11
12
13
20
25
30
35
40
45
50
55
60
12
14
16
18
20
22
24
26
28
30
32

FIG. 27A

THEOR. EXHAUST HP VS BHP
RUN DL-3

DELAVAL PULSE CONVERTER MANIFOLD (TUNNELS REMOVED)
DELAVAL "STEADY-FLOW" TURBINE
EXHAUST ELBOW AREA - 17.8 IN^2
EXHAUST ELBOW LENGTH - 22 IN
TURBINE NOZZLE FLOW AREA - 38 IN^2 (4.0%)
MUFFLER BYPASSED
SMALL SIZE ENGINE-DRIVEN BLOWER
AFTER COOLER INSTALLED

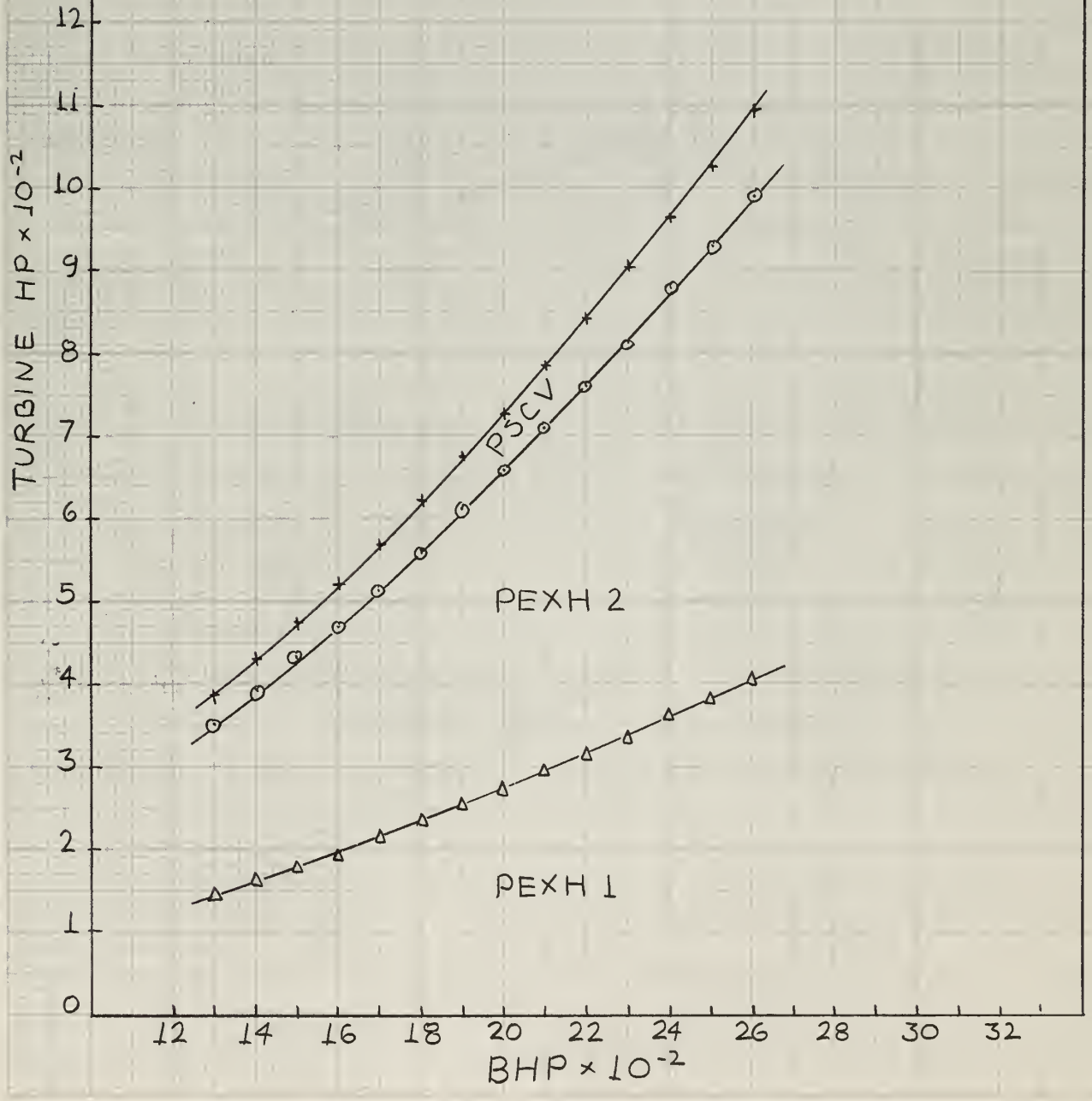

FIG. 27B

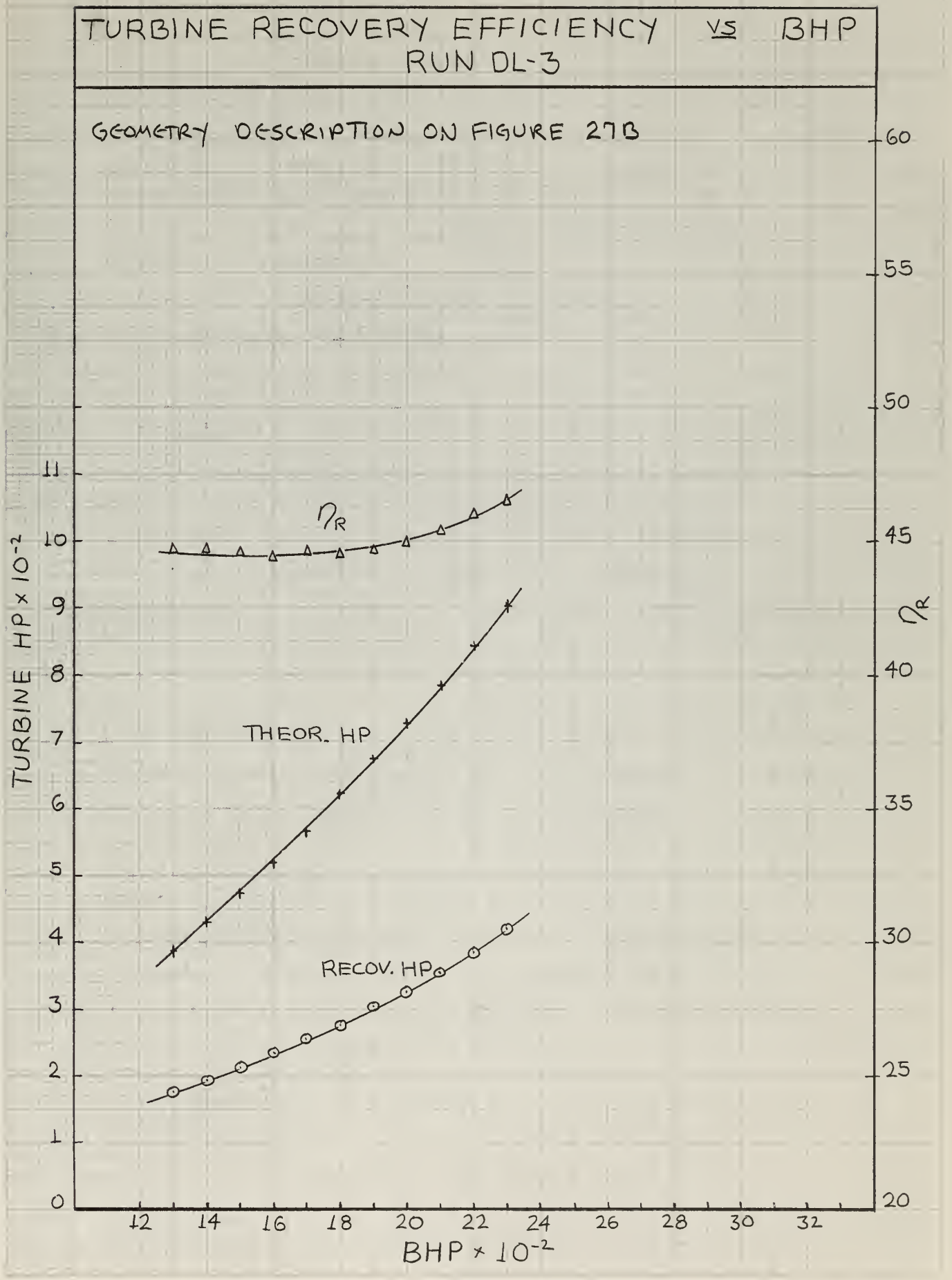
TURBINE RECOVERY EFFICIENCY VS BHP
RUN DL-3
GEOMETRY DESCRIPTION ON FIGURE 27B
η_R
THEOR. HP
RECOV. HP
TURBINE HP × 10^{-2}
η_R
BHP × 10^{-2}
0
1
2
3
4
5
6
7
8
9
10
11
12
14
16
18
20
22
24
26
28
30
32
20
25
30
35
40
45
50
55
60

FIG. 28A

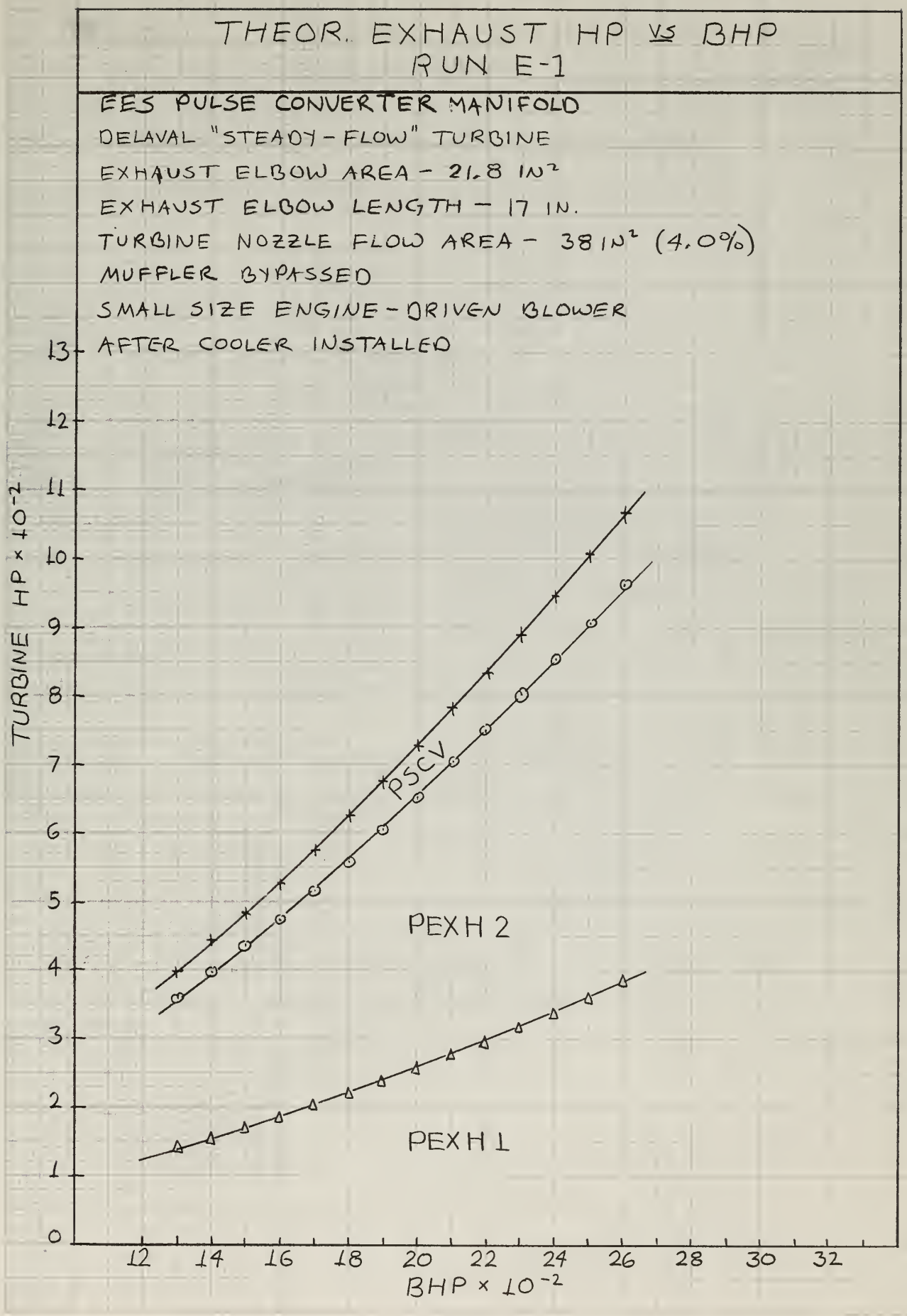
THEOR. EXHAUST HP VS BHP
RUN E-1
EES PULSE CONVERTER MANIFOLD
DELAVAL "STEADY-FLOW" TURBINE
EXHAUST ELBOW AREA - 21.8 IN²
EXHAUST ELBOW LENGTH - 17 IN.
TURBINE NOZZLE FLOW AREA - 381 IN² (4.0%)
MUFFLER BYPASSED
SMALL SIZE ENGINE-DRIVEN BLOWER
AFTER COOLER INSTALLED
TURBINE HP × 10⁻²
BHP × 10⁻²
PSCV
PEXH 2
PEXH 1
0
1
2
3
4
5
6
7
8
9
10
11
12
13
12
14
16
18
20
22
24
26
28
30
32

FIG. 28B

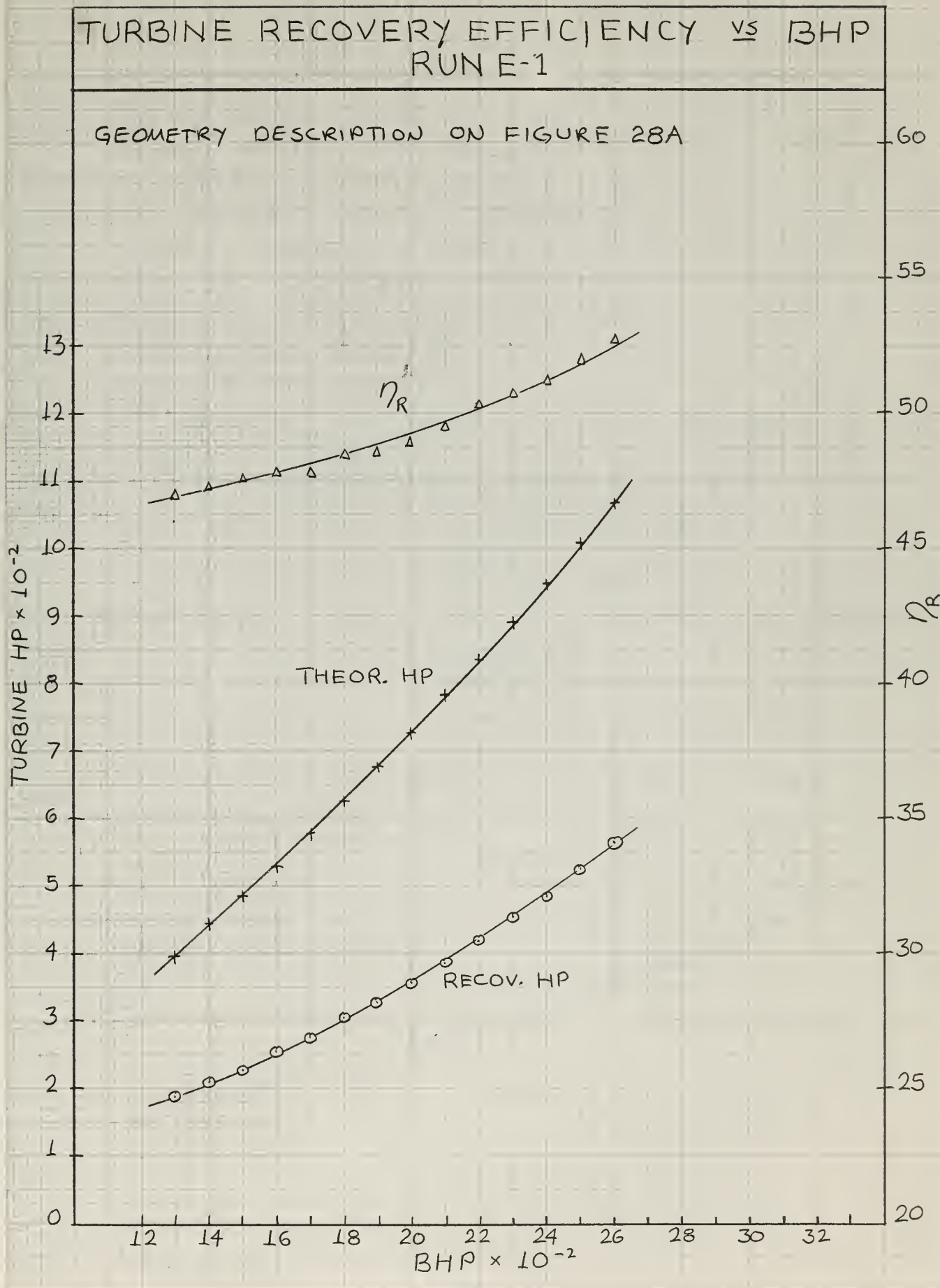
TURBINE RECOVERY EFFICIENCY VS BHP
RUN E-1
GEOMETRY DESCRIPTION ON FIGURE 28A
η_R
THEOR. HP
RECOV. HP
TURBINE HP × 10^{-2}
BHP × 10^{-2}
η_R
0
1
2
3
4
5
6
7
8
9
10
11
12
13
20
25
30
35
40
45
50
55
60
12
14
16
18
20
22
24
26
28
30
32

FIG. 29A

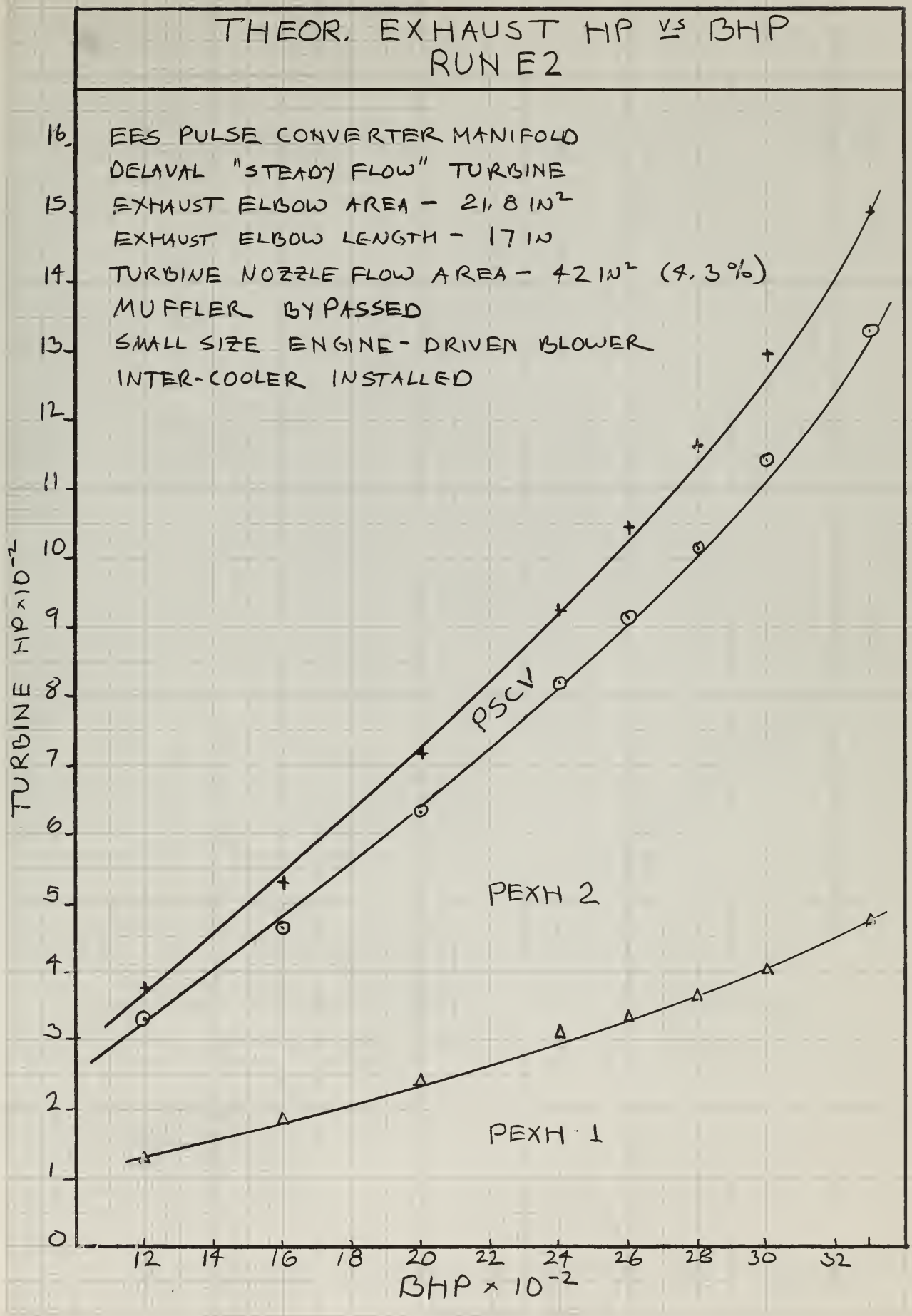
THEOR. EXHAUST HP VS BHP
RUN E2
EES PULSE CONVERTER MANIFOLD
DELAVAL "STEADY FLOW" TURBINE
EXHAUST ELBOW AREA - 21.8 IN²
EXHAUST ELBOW LENGTH - 17 IN
TURBINE NOZZLE FLOW AREA - 42 IN² (4.3%)
MUFFLER BY PASSED
SMALL SIZE ENGINE-DRIVEN BLOWER
INTER-COOLER INSTALLED
PSCV
PEXH 2
PEXH 1
TURBINE HP x 10⁻²
BHP x 10⁻²
0
1
2
3
4
5
6
7
8
9
10
11
12
13
14
15
16
12
14
16
18
20
22
24
26
28
30
32

FIG. 29B

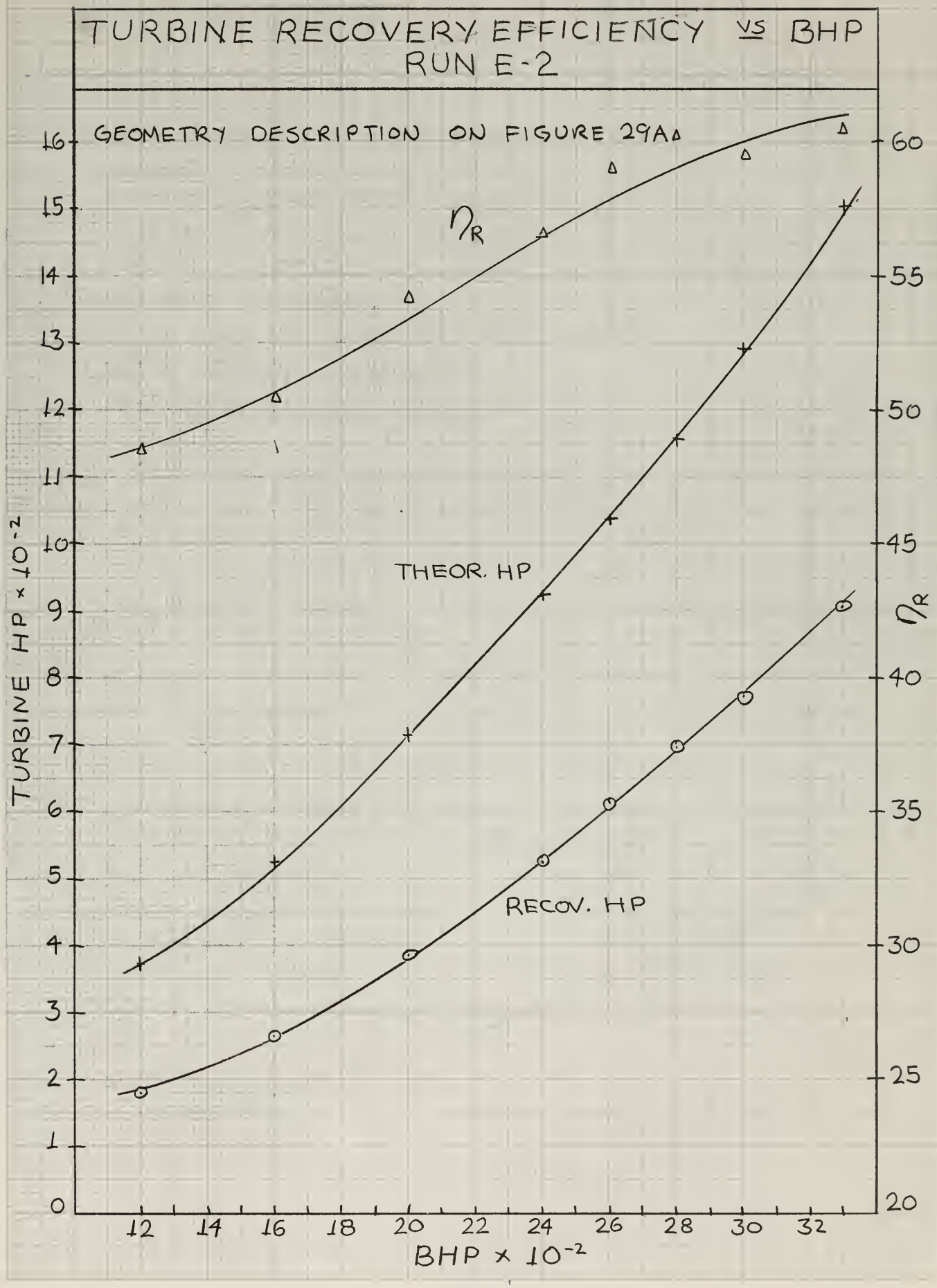
TURBINE RECOVERY EFFICIENCY VS BHP
RUN E-2
GEOMETRY DESCRIPTION ON FIGURE 29A
η_R
THEOR. HP
RECOV. HP
TURBINE HP × 10⁻²
η_R
BHP × 10⁻²
0
1
2
3
4
5
6
7
8
9
10
11
12
13
14
15
16
20
25
30
35
40
45
50
55
60
12
14
16
18
20
22
24
26
28
30
32

FIG. 30A

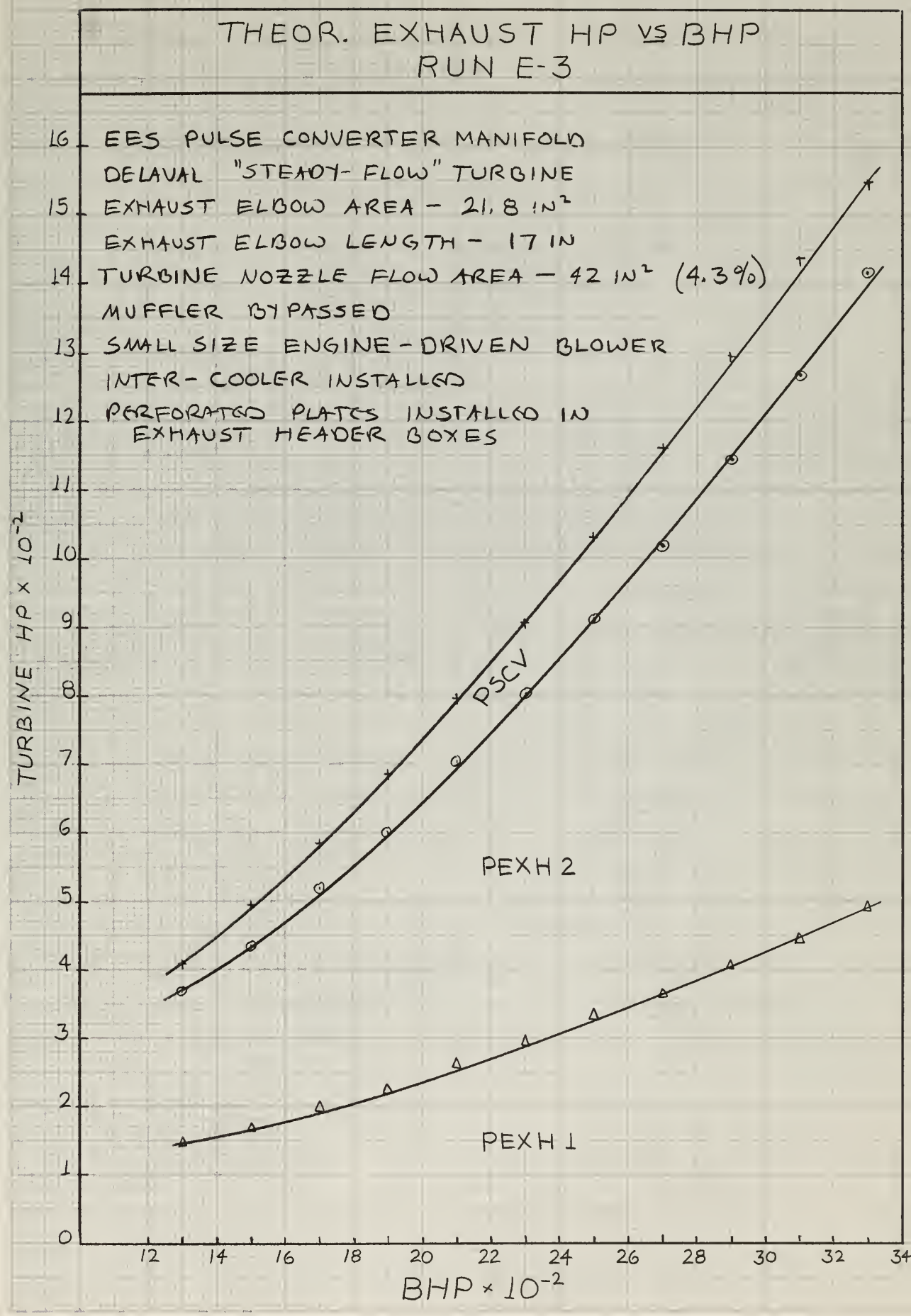
THEOR. EXHAUST HP VS BHP
RUN E-3
EES PULSE CONVERTER MANIFOLD
DELAVAL "STEADY-FLOW" TURBINE
EXHAUST ELBOW AREA - 21.8 IN²
EXHAUST ELBOW LENGTH - 17 IN
TURBINE NOZZLE FLOW AREA - 42 IN² (4.3%)
MUFFLER BYPASSED
SMALL SIZE ENGINE-DRIVEN BLOWER
INTER-COOLER INSTALLED
PERFORATED PLATES INSTALLED IN EXHAUST HEADER BOXES
PSCV
PEXH 2
PEXH 1
TURBINE HP × 10⁻²
BHP × 10⁻²
0
1
2
3
4
5
6
7
8
9
10
11
12
13
14
15
16
12
14
16
18
20
22
24
26
28
30
32
34

FIG. 30B

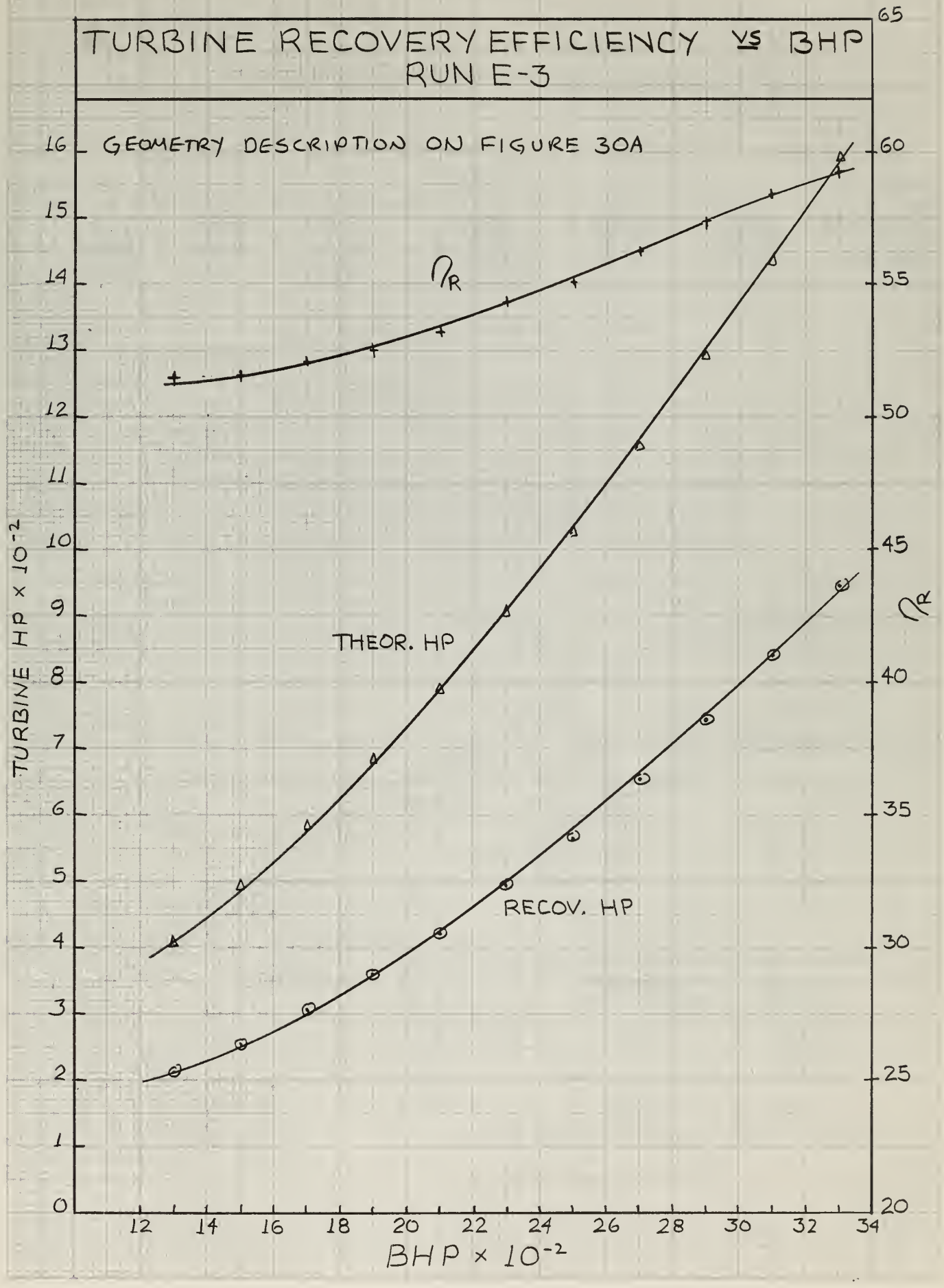
TURBINE RECOVERY EFFICIENCY VS BHP
RUN E-3
GEOMETRY DESCRIPTION ON FIGURE 30A
η_R
THEOR. HP
RECOV. HP
η_α
TURBINE HP × 10^{-2}
BHP × 10^{-2}
0
1
2
3
4
5
6
7
8
9
10
11
12
13
14
15
16
20
25
30
35
40
45
50
55
60
65
12
14
16
18
20
22
24
26
28
30
32
34

FIG. 31B

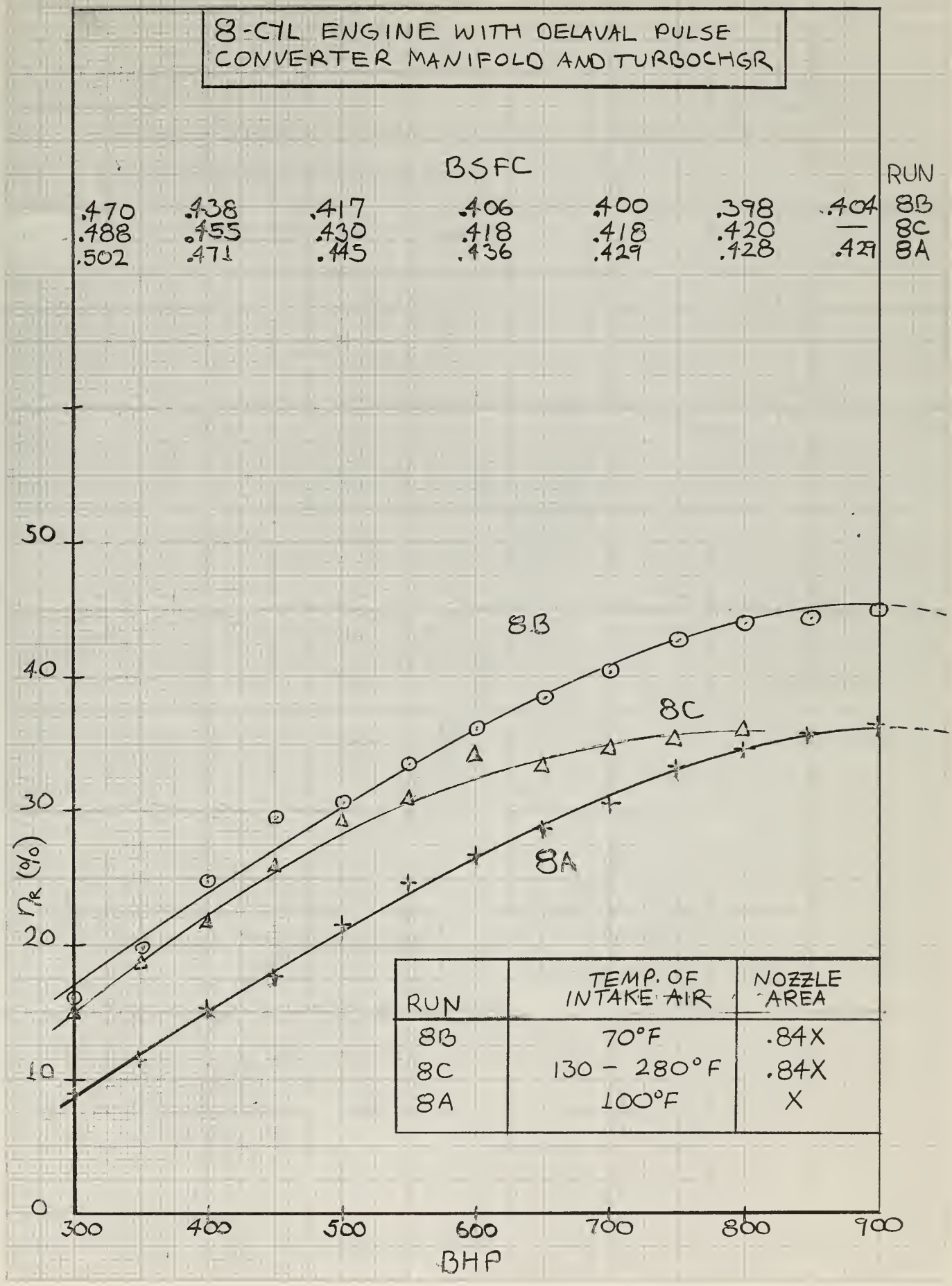
8-CYL ENGINE WITH DELAVAL PULSE CONVERTER MANIFOLD AND TURBOCHGR
BSFC
RUN
.470 .438 .417 .406 .400 .398 .404 8B
.488 .455 .430 .418 .418 .420 — 8C
.502 .471 .445 .436 .429 .428 .429 8A
8B
8C
8A
η_R (%)
0
10
20
30
40
50
300
400
500
600
700
800
900
BHP
RUN | TEMP. OF INTAKE AIR | NOZZLE AREA
8B | 70°F | .84X
8C | 130 - 280°F | .84X
8A | 100°F | X

FIG. 32A

THEOR. EXHAUST HP VS BHP
RUN 8A

DELAVAL "STEADY-FLOW" TURBINE (MODEL B-8)
TEMPERATURE OF INTAKE AIR – 100°F
TURBINE NOZZLE FLOW AREA = X
GM 8-268A DIESEL ENGINE

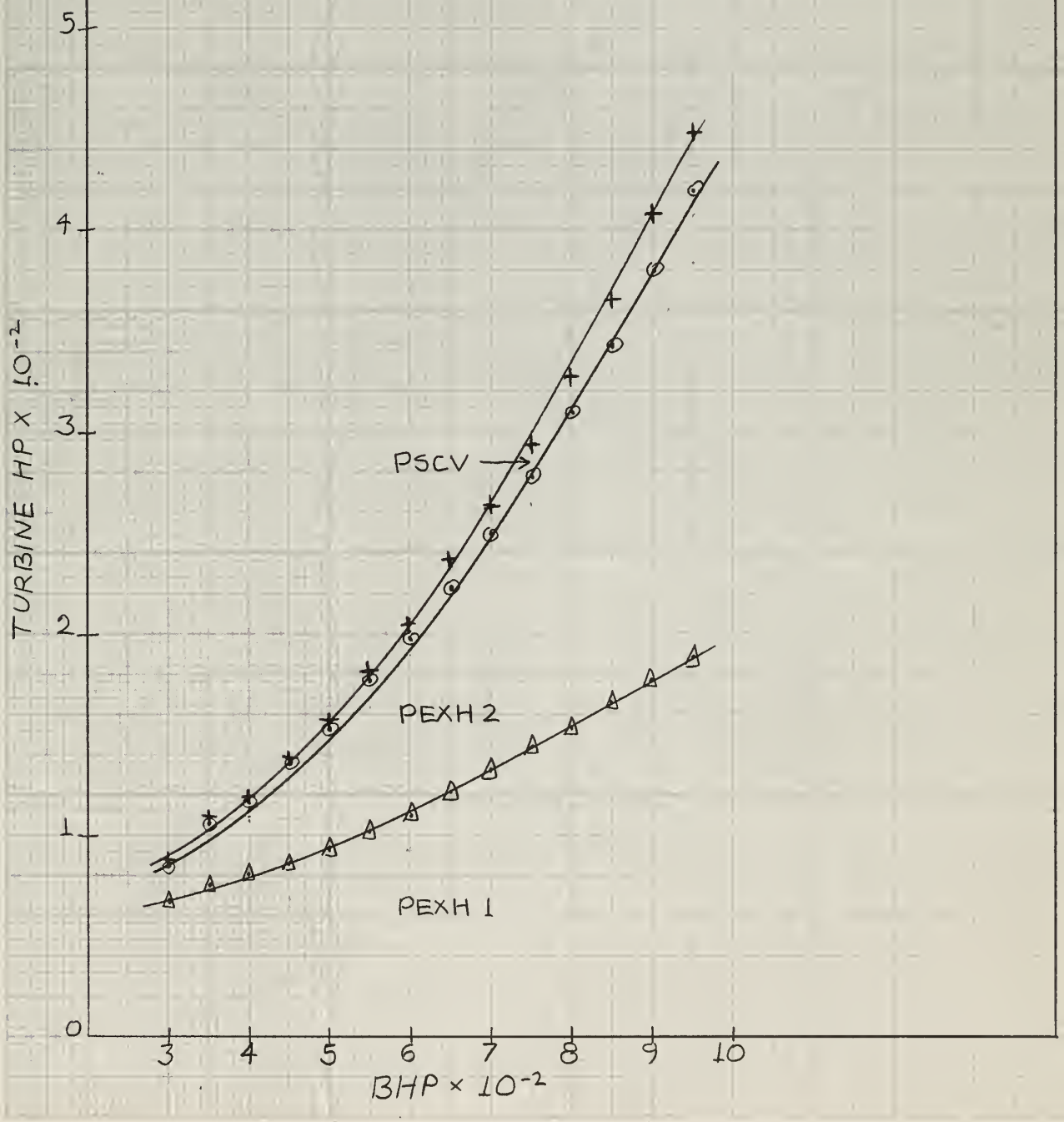

FIG. 32B

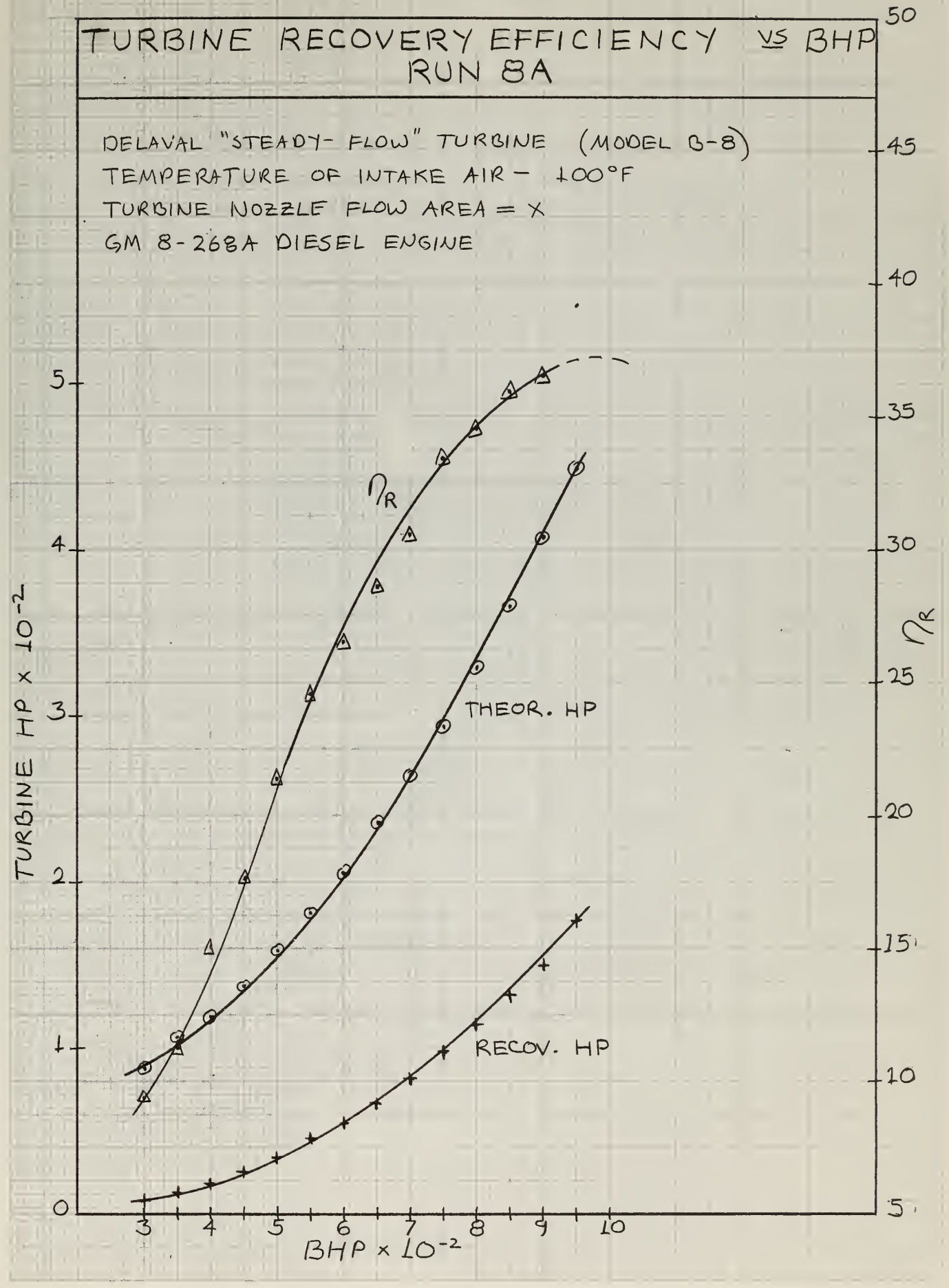
TURBINE RECOVERY EFFICIENCY VS BHP
RUN 8A
DELAVAL "STEADY-FLOW" TURBINE (MODEL B-8)
TEMPERATURE OF INTAKE AIR – 100°F
TURBINE NOZZLE FLOW AREA = X
GM 8-268A DIESEL ENGINE
η_R
THEOR. HP
RECOV. HP
TURBINE HP x 10^{-2}
BHP x 10^{-2}
η_R
0
1
2
3
4
5
3
4
5
6
7
8
9
10
5
10
15
20
25
30
35
40
45
50

FIG. 33A

THEOR. EXHAUST HP VS BHP
RUN 8B

DELAVAL "STEADY-FLOW" TURBINE (MODEL B-8)
TEMPERATURE OF INTAKE AIR = 70°F
TURBINE NOZZLE FLOW AREA = 0.84X
GM 8-268A DIESEL ENGINE

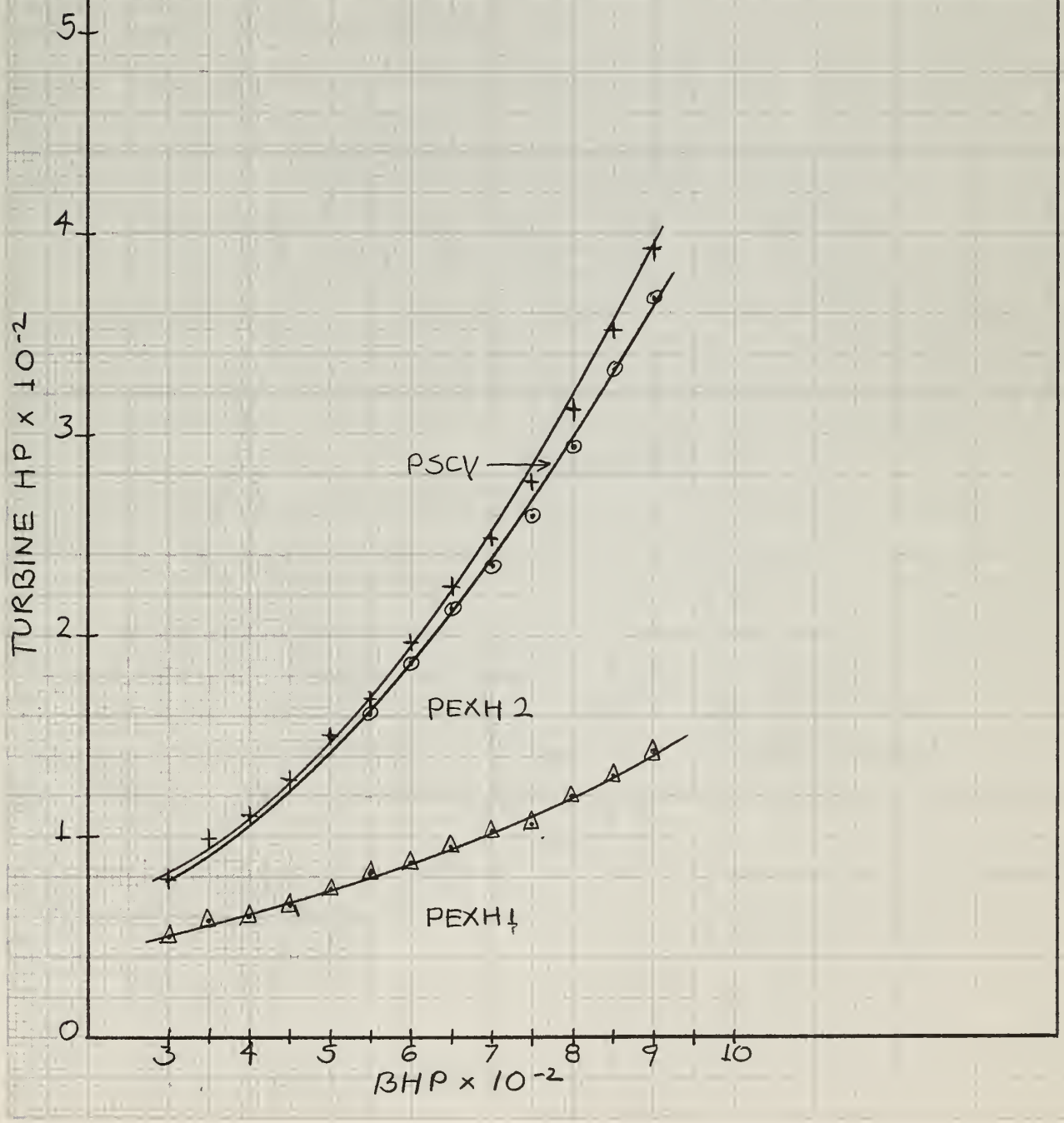

FIG. 33B

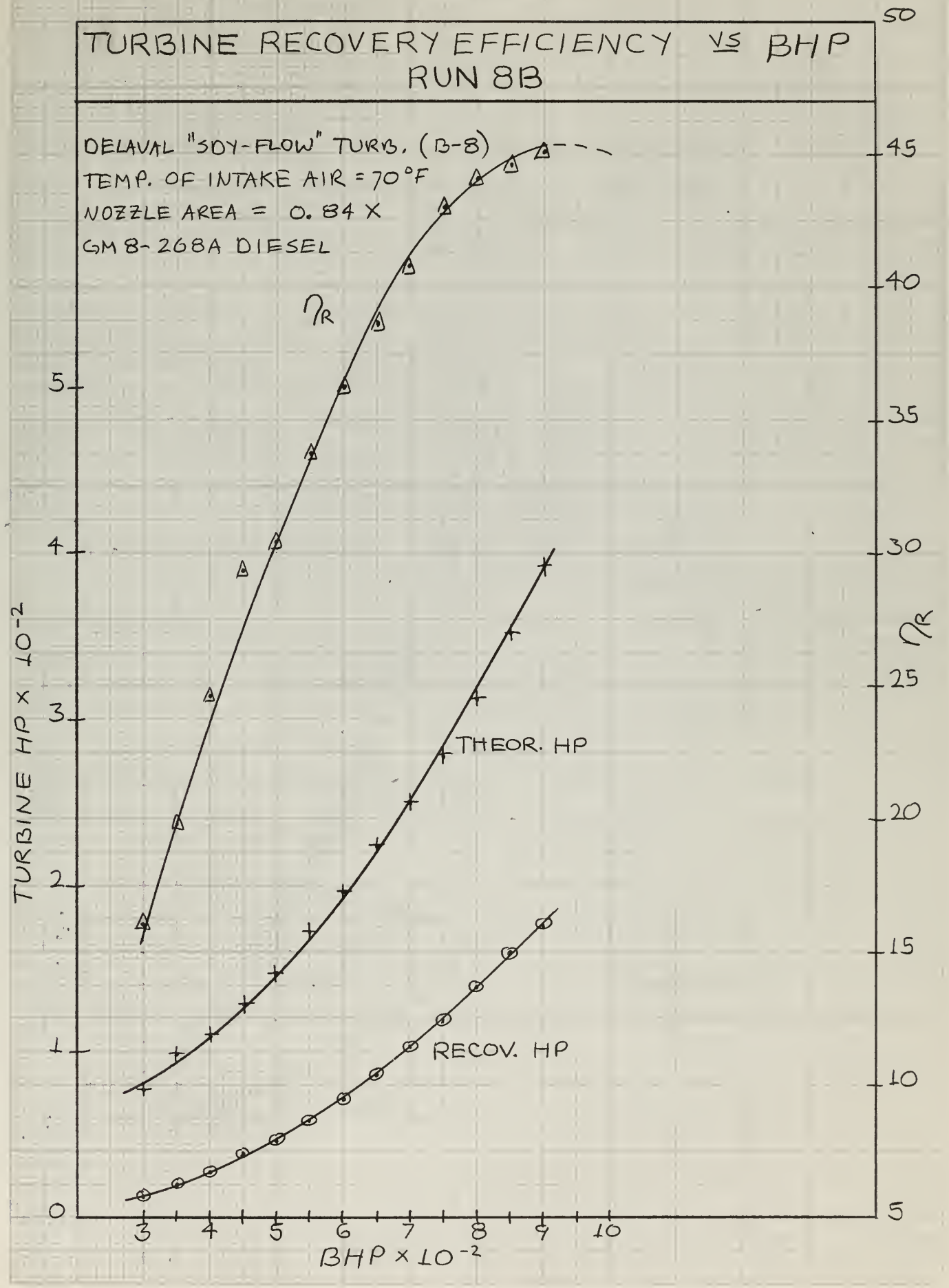
TURBINE RECOVERY EFFICIENCY VS BHP
RUN 8B
DELAVAL "SOY-FLOW" TURB. (B-8)
TEMP. OF INTAKE AIR = 70°F
NOZZLE AREA = 0.84 X
GM 8-268A DIESEL
ηR
THEOR. HP
RECOV. HP
TURBINE HP x 10⁻²
BHP x 10⁻²
ηR
0
1
2
3
4
5
3
4
5
6
7
8
9
10
5
10
15
20
25
30
35
40
45
50

FIG. 34A

THEOR. EXHAUST HP VS BHP
RUN 8C

DELAVAL "STEADY-FLOW" TURBINE (MODEL B-8)
TEMPERATURE OF INTAKE AIR - 130°-280°F
TURBINE NOZZLE AREA = 0.84 X
GM 8-268A DIESEL ENGINE

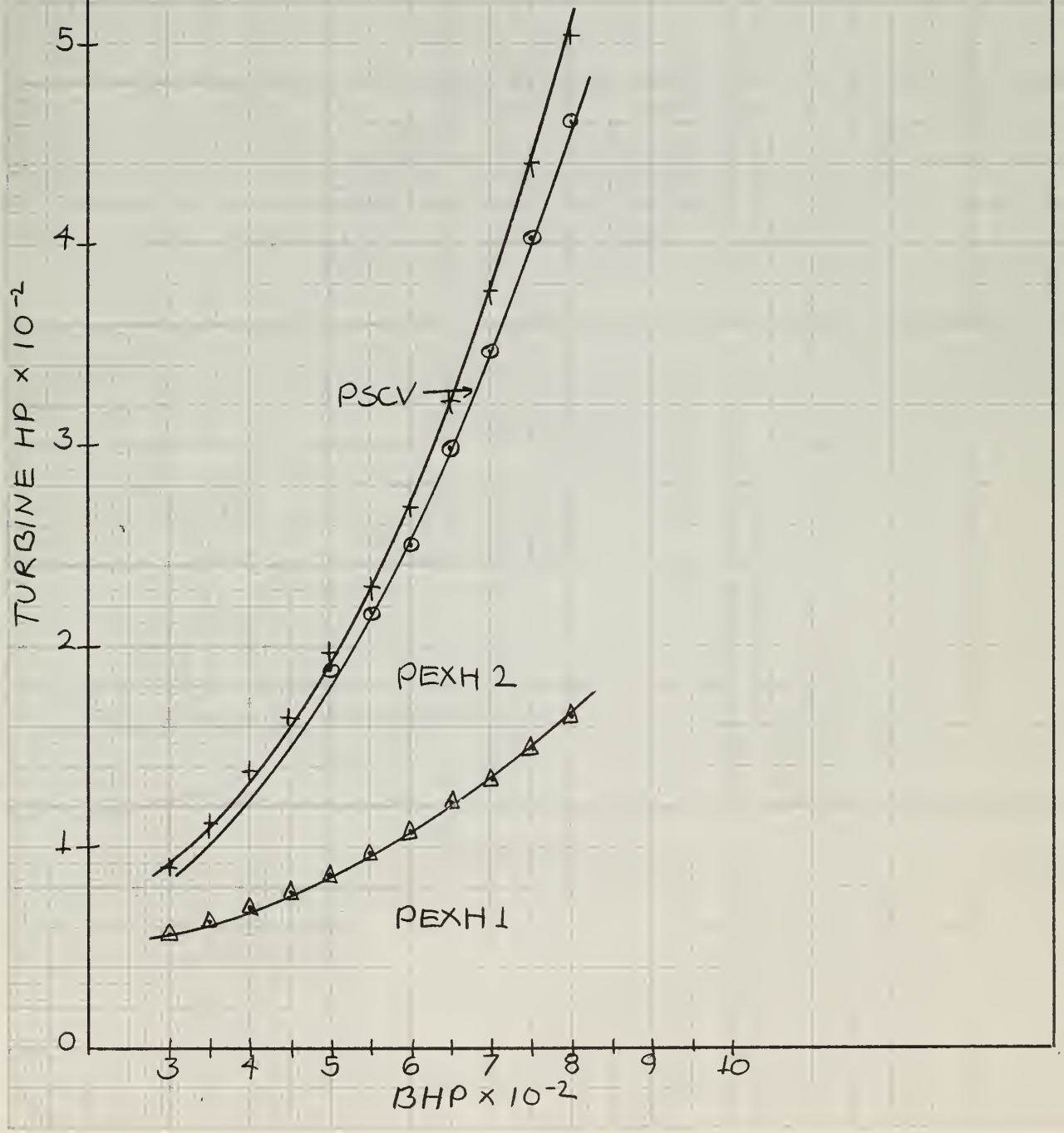

FIG. 34B

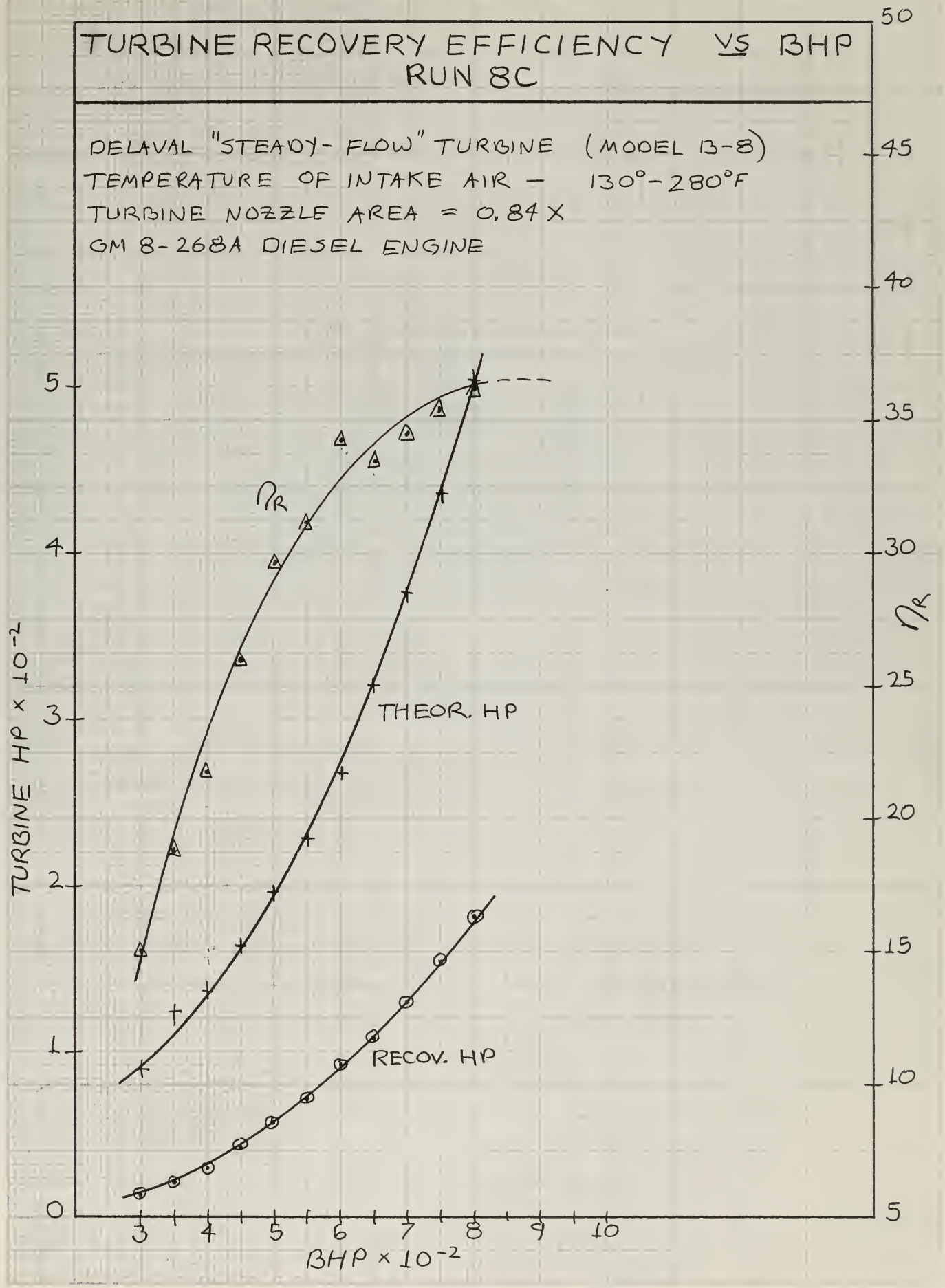
TURBINE RECOVERY EFFICIENCY VS BHP
RUN 8C
DELAVAL "STEADY-FLOW" TURBINE (MODEL B-8)
TEMPERATURE OF INTAKE AIR — 130°-280°F
TURBINE NOZZLE AREA = 0.84 X
GM 8-268A DIESEL ENGINE
η_R
THEOR. HP
RECOV. HP
TURBINE HP x 10^{-2}
BHP x 10^{-2}
η_R
0
1
2
3
4
5
3
4
5
6
7
8
9
10
5
10
15
20
25
30
35
40
45
50

G.E. TURBOCHARGERS FIG 35

$P_4/P_6 = 3.0$

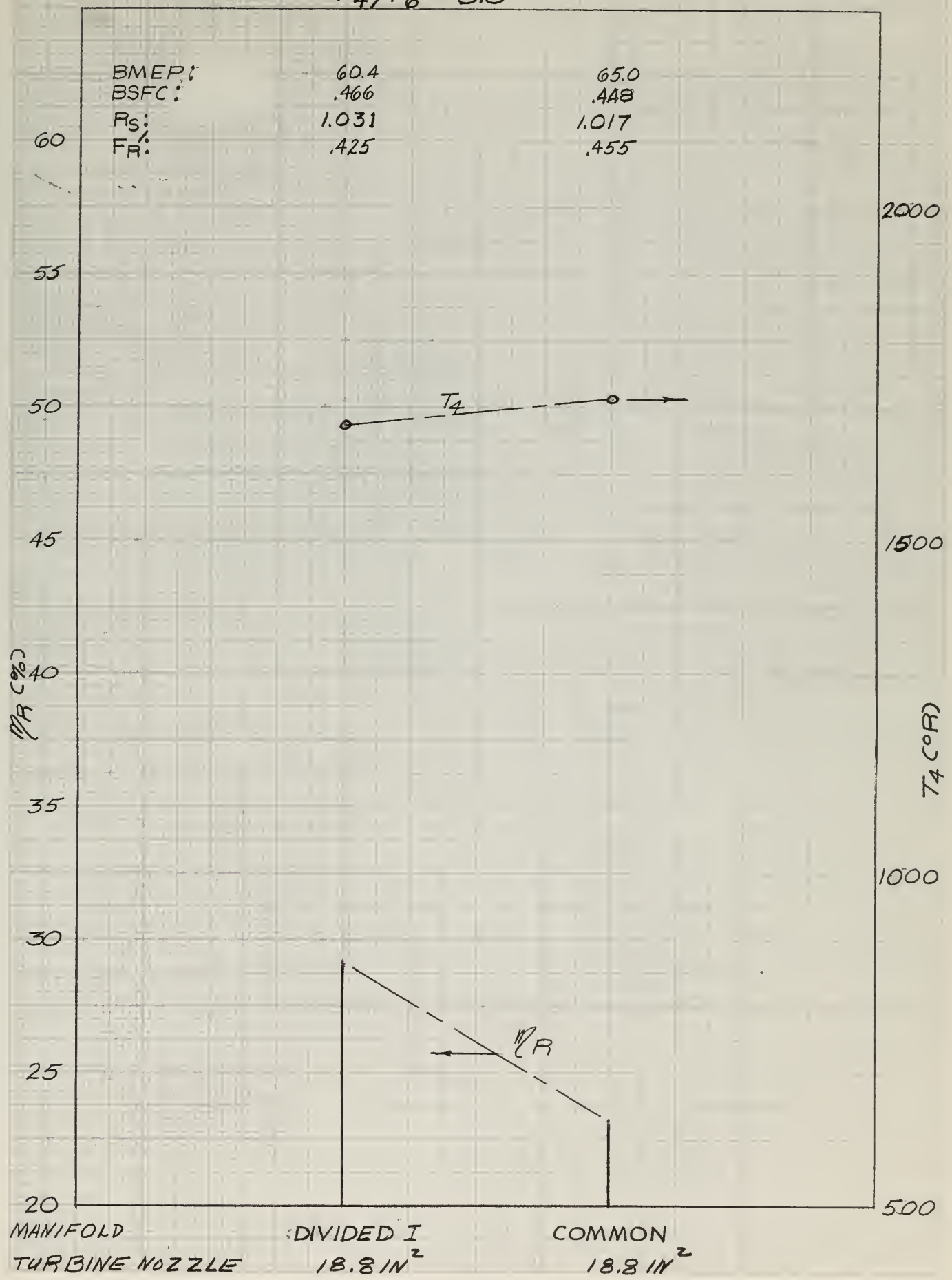

G.E. TURBOCHARGERS FIG. 36

$P_4/P_6 = 3.5$

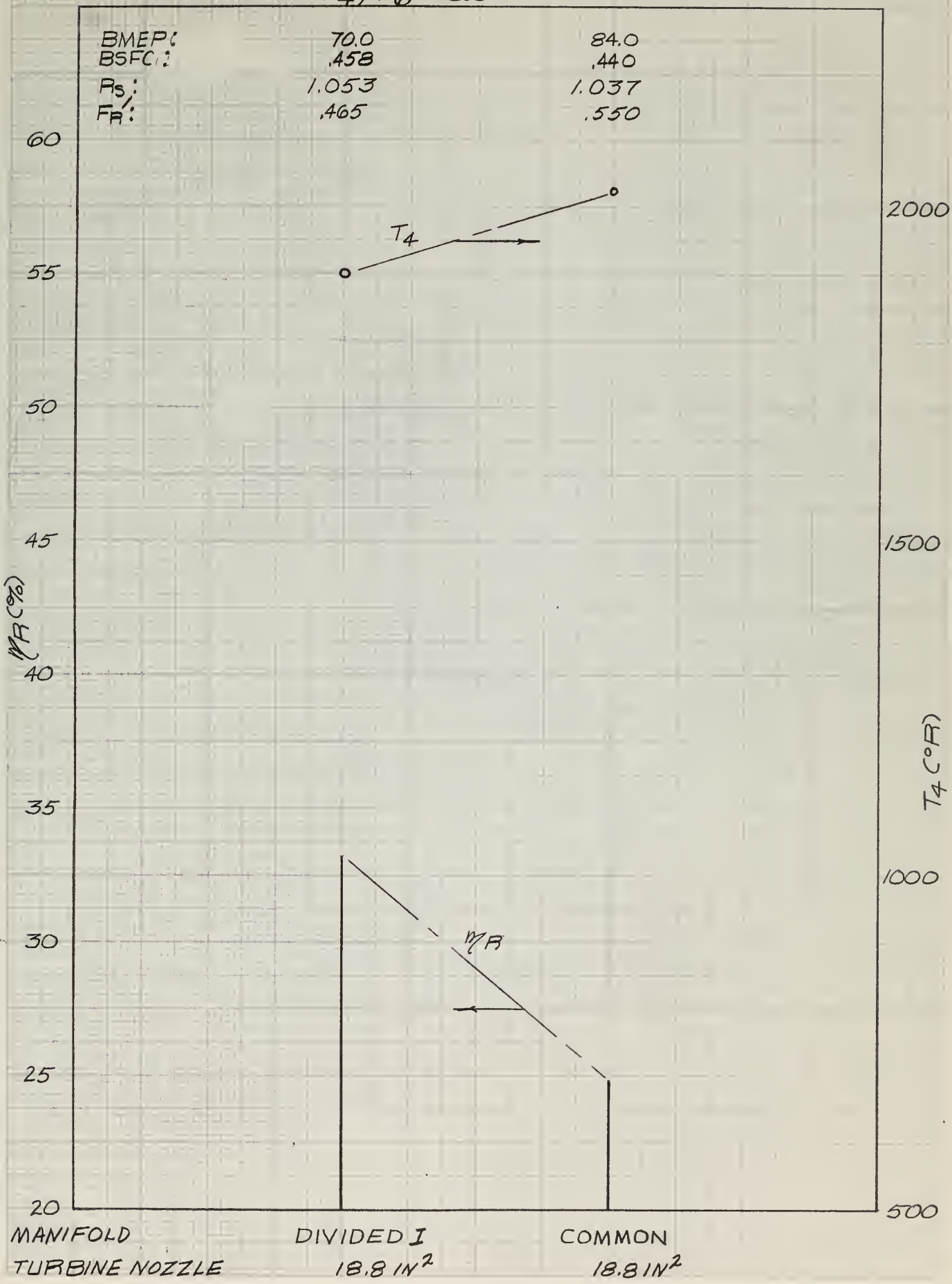

G.E. TURBOCHARGERS FIG. 37

$P_4/P_6 = 4.0$

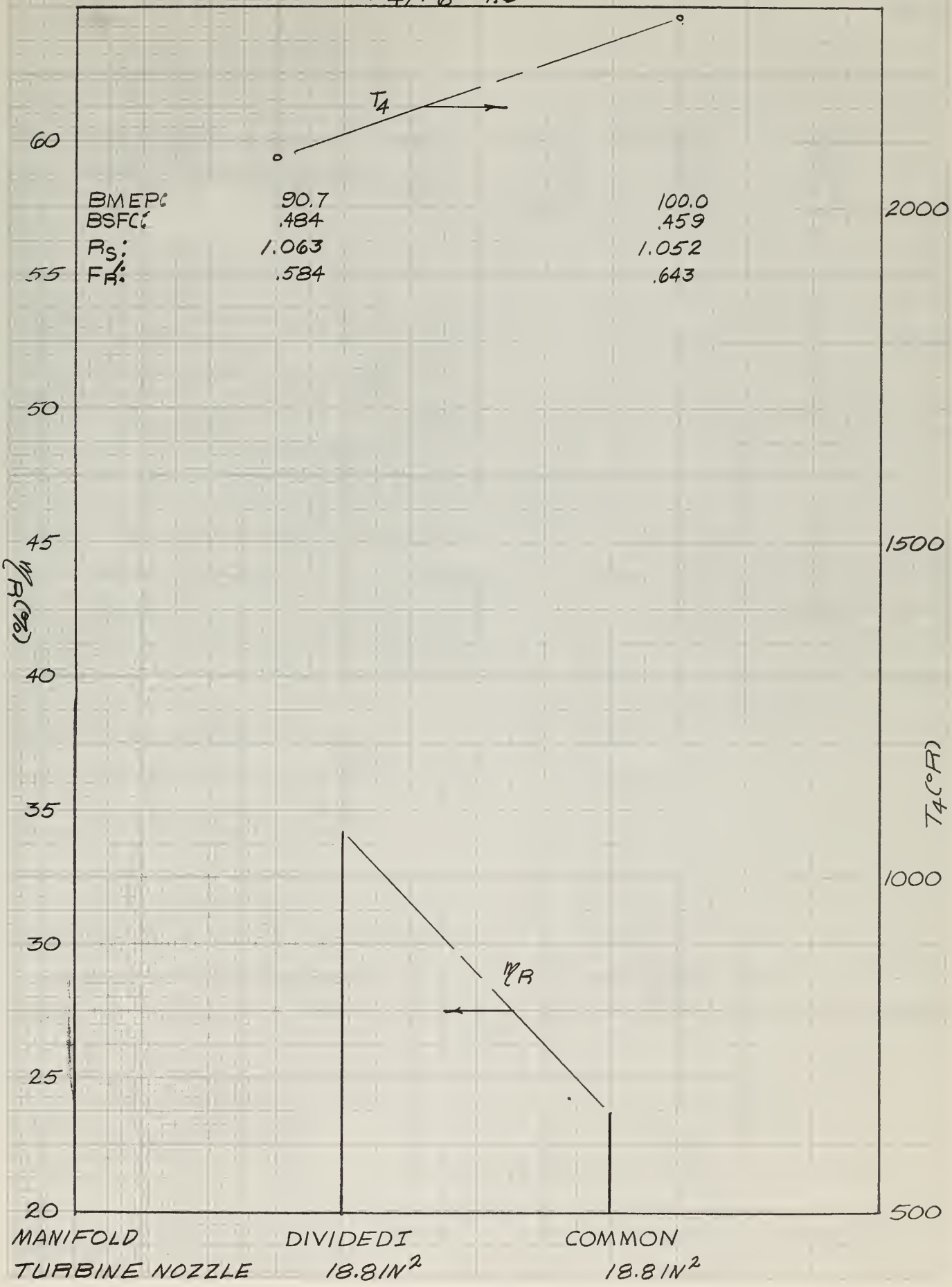

BMEP:	90.7	100.0
BSFC:	.484	.459
R_S:	1.063	1.052
F_R:	.584	.643

MANIFOLD TURBINE NOZZLE — DIVIDED 18.8 IN^2 — COMMON 18.8 IN^2

ELLIOTT PULSE TURBOCHARGERS FIG 38

$P_4/P_6 = 3.0$

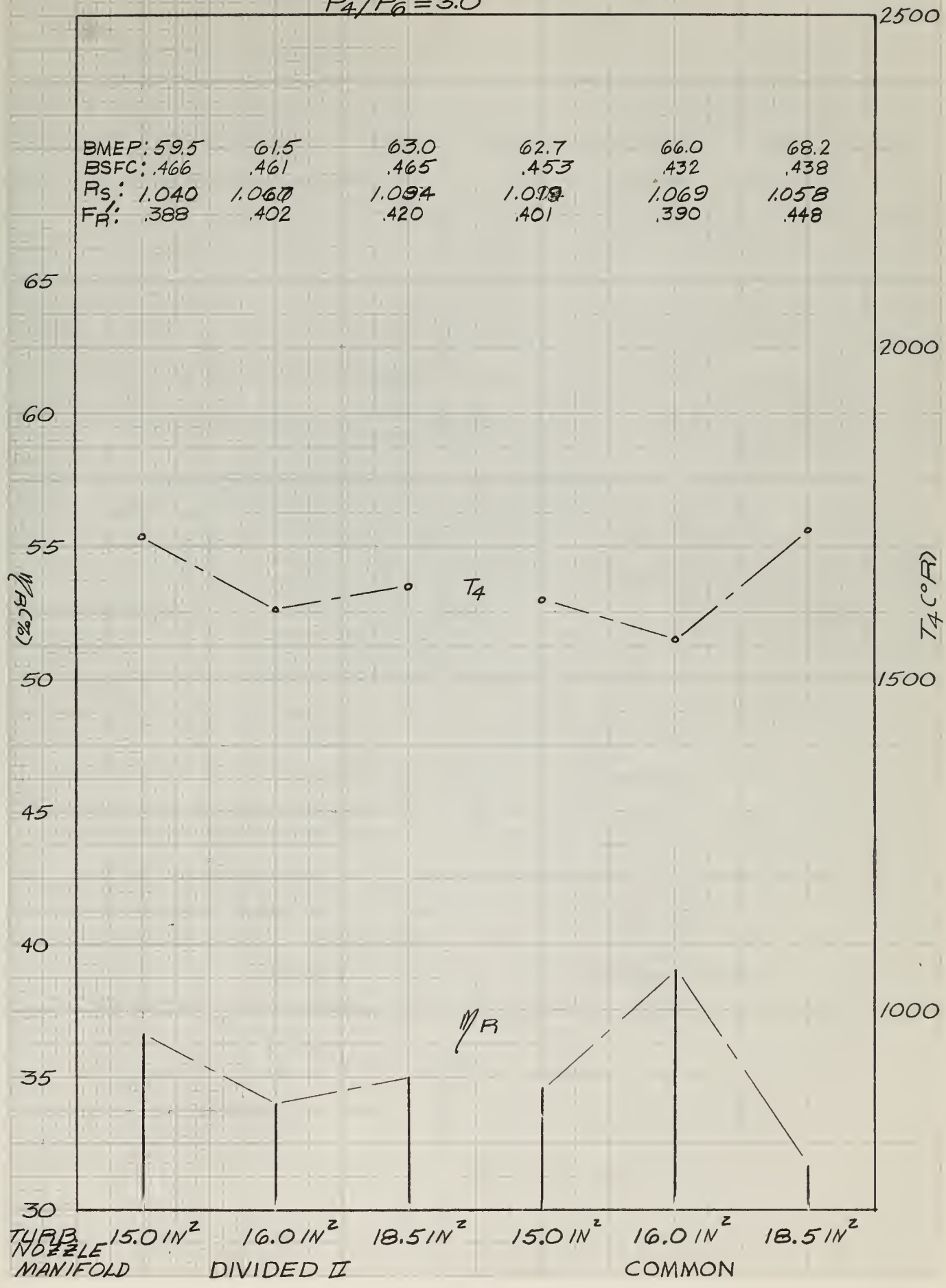

ELLIOTT PULSE TURBOCHARGERS FIG. 39

$P_4/P_6 = 3.5$

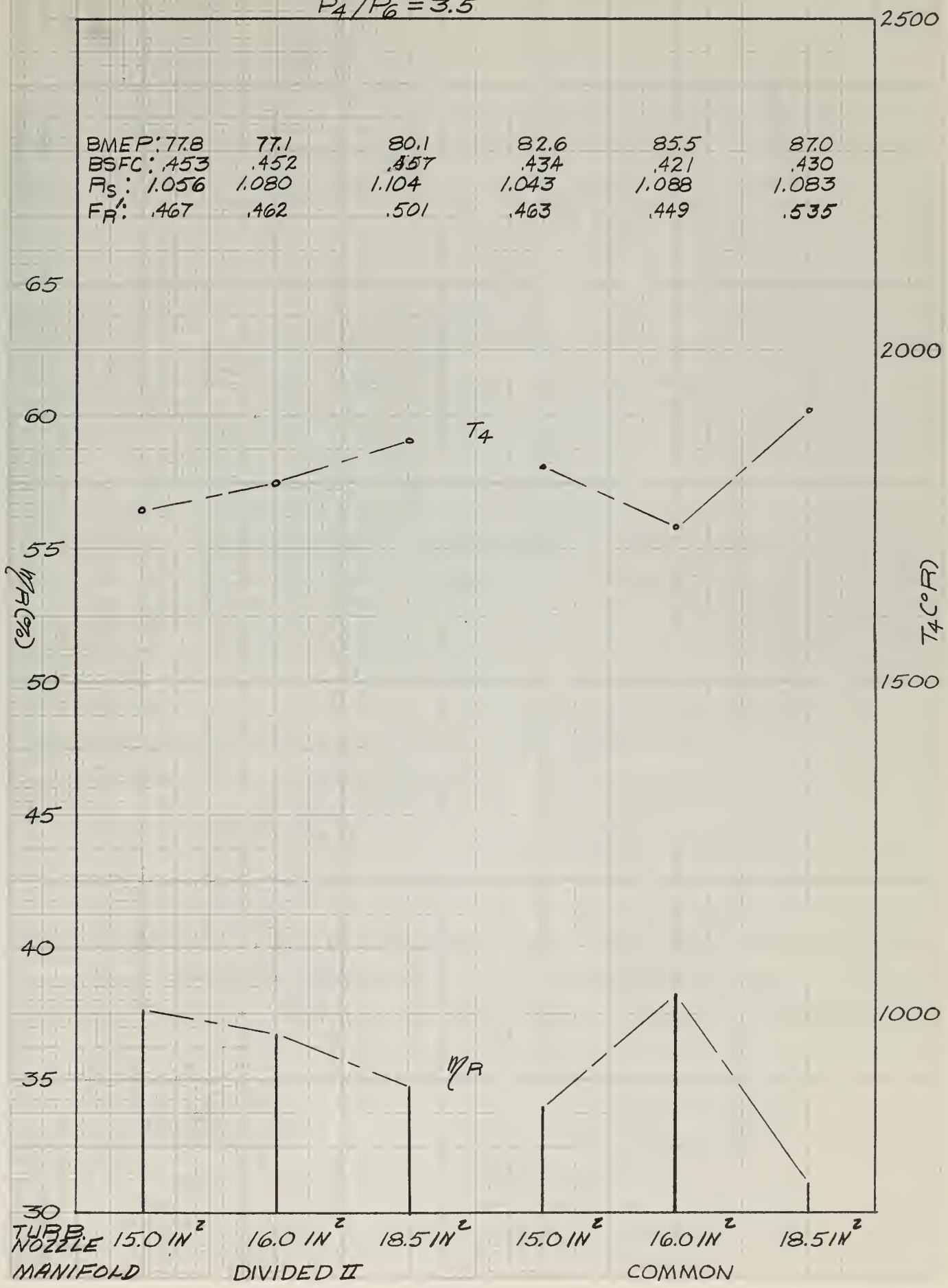

ELLIOTT PULSE TURBOCHARGERS FIG.40

$P_4/P_6 = 4.0$

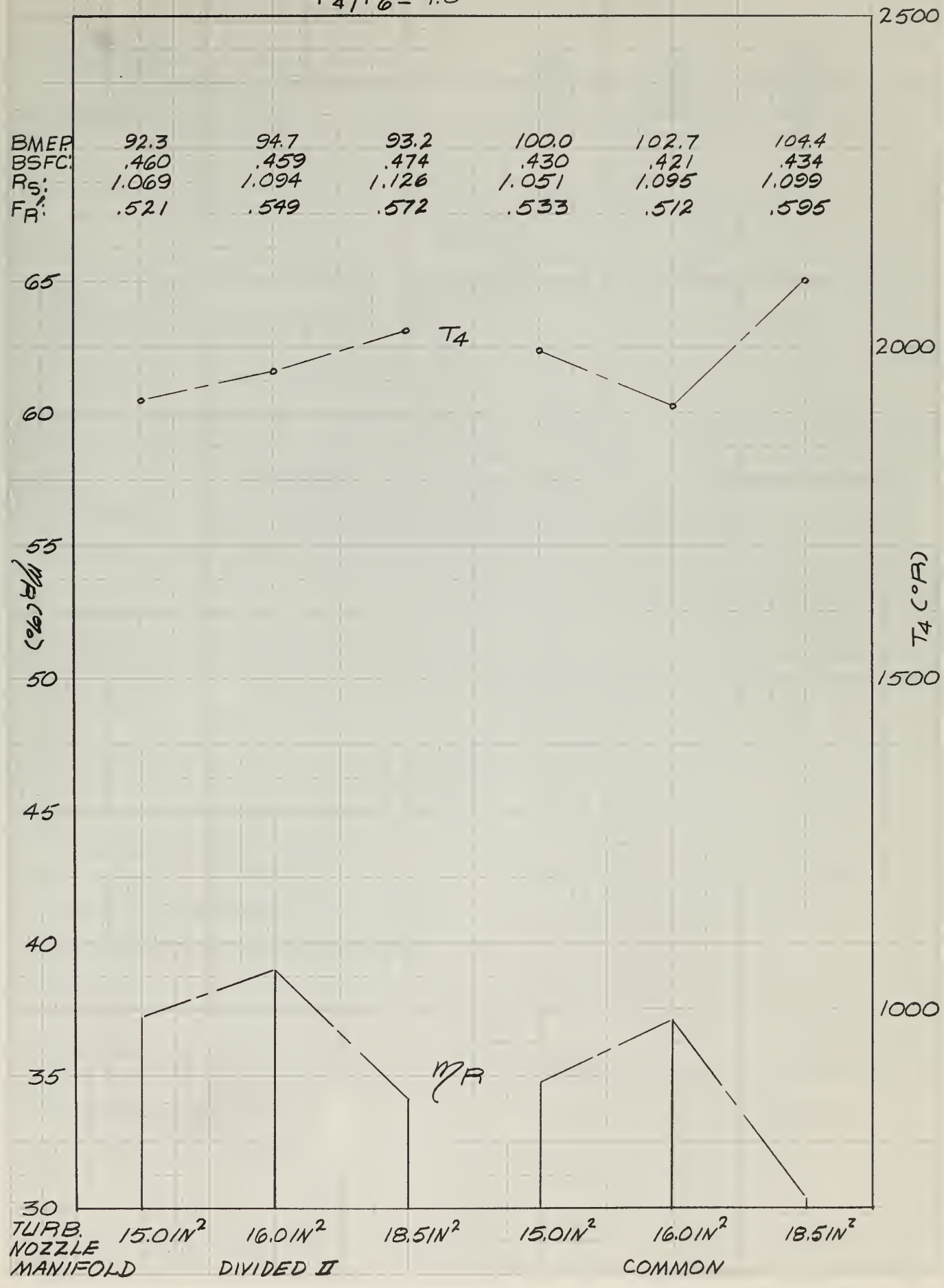

ELLIOTT PULSE TURBOCHARGERS FIG. 41

$P_4/P_6 = 4.5$

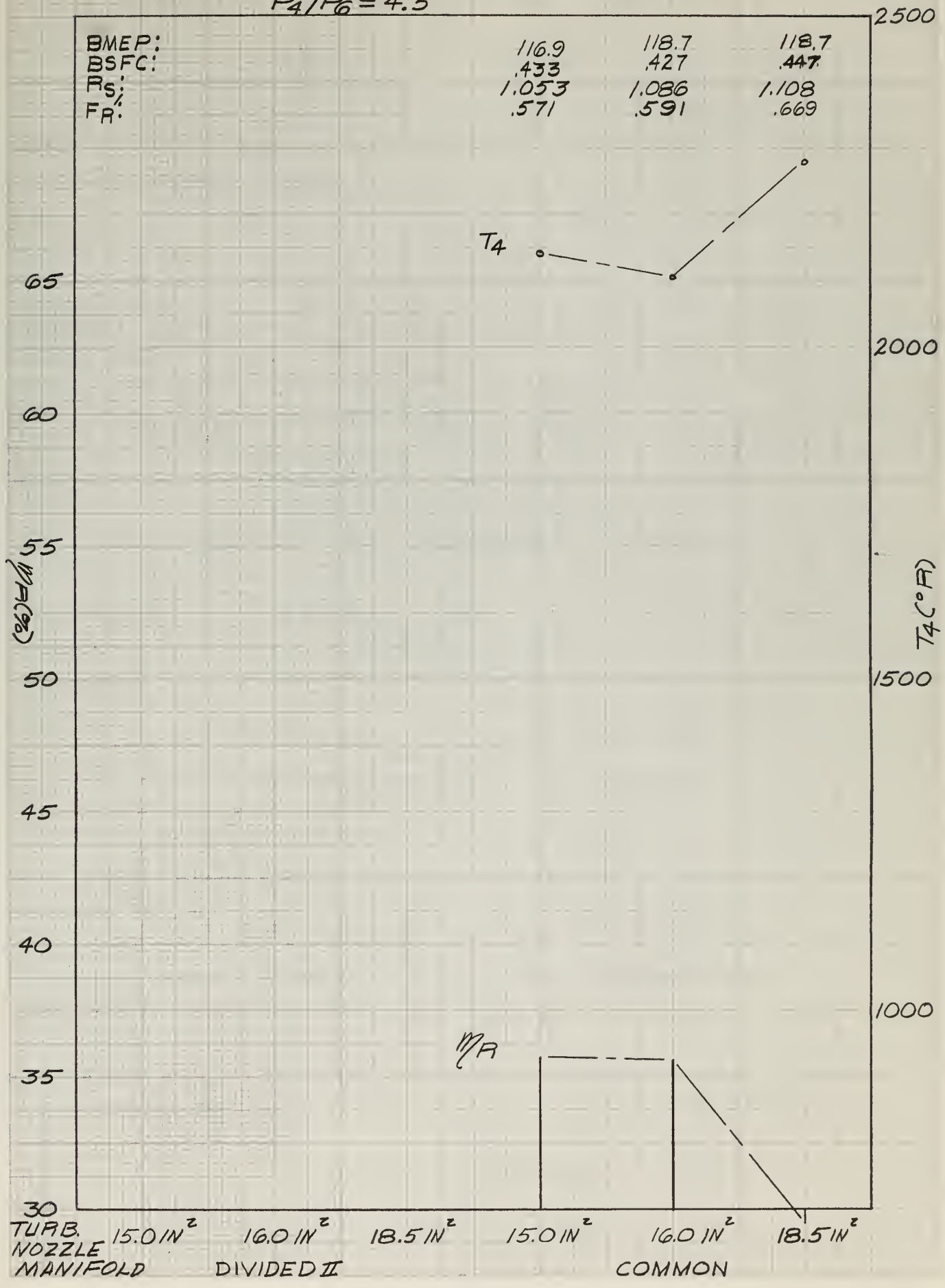

ELLIOTT PULSE TURBOCHARGERS FIG. 42

$P_4/P_6 = 5.0$

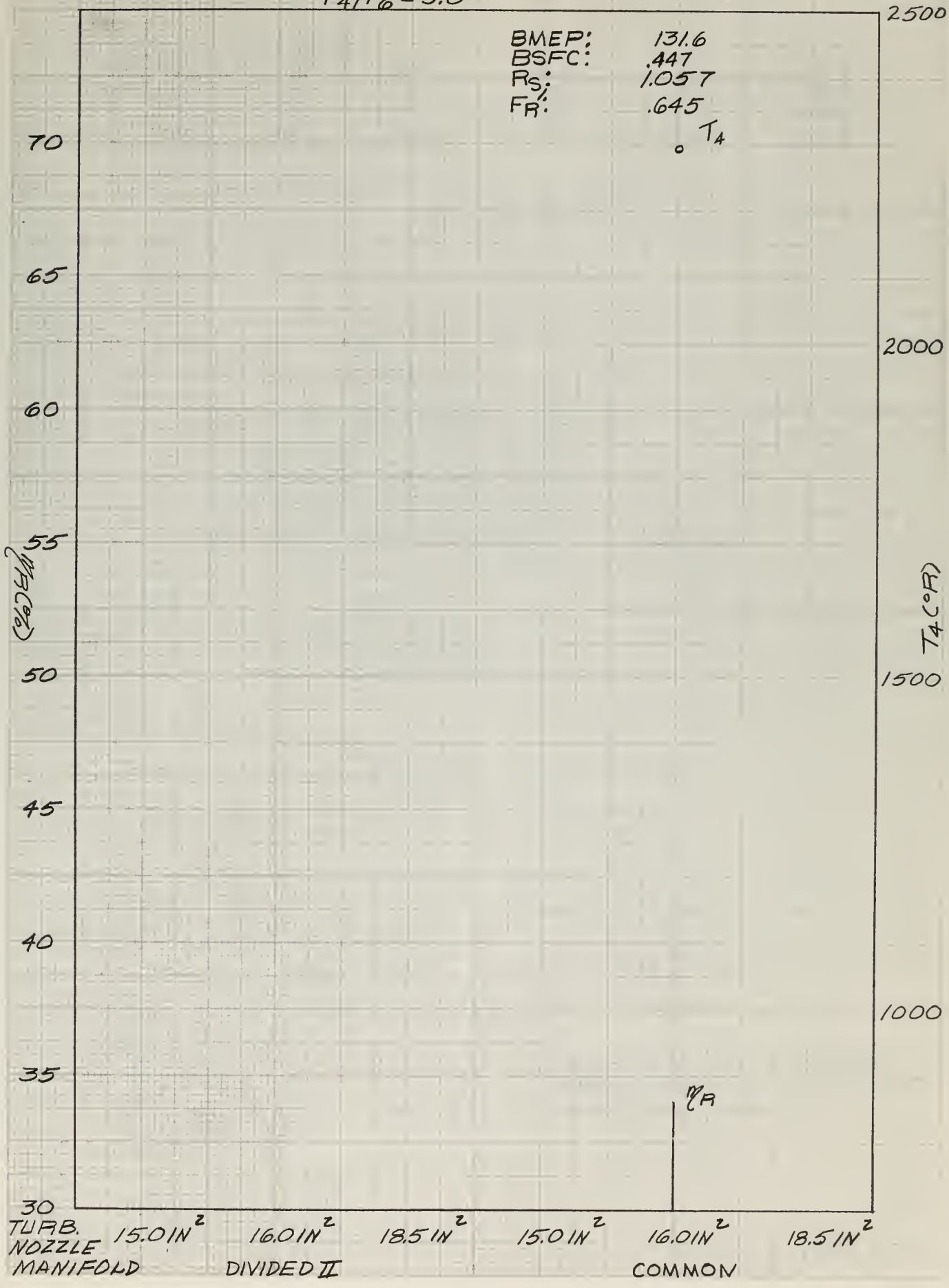

ELLIOTT STEADY FLOW TURBOCHARGERS

FIG. 43

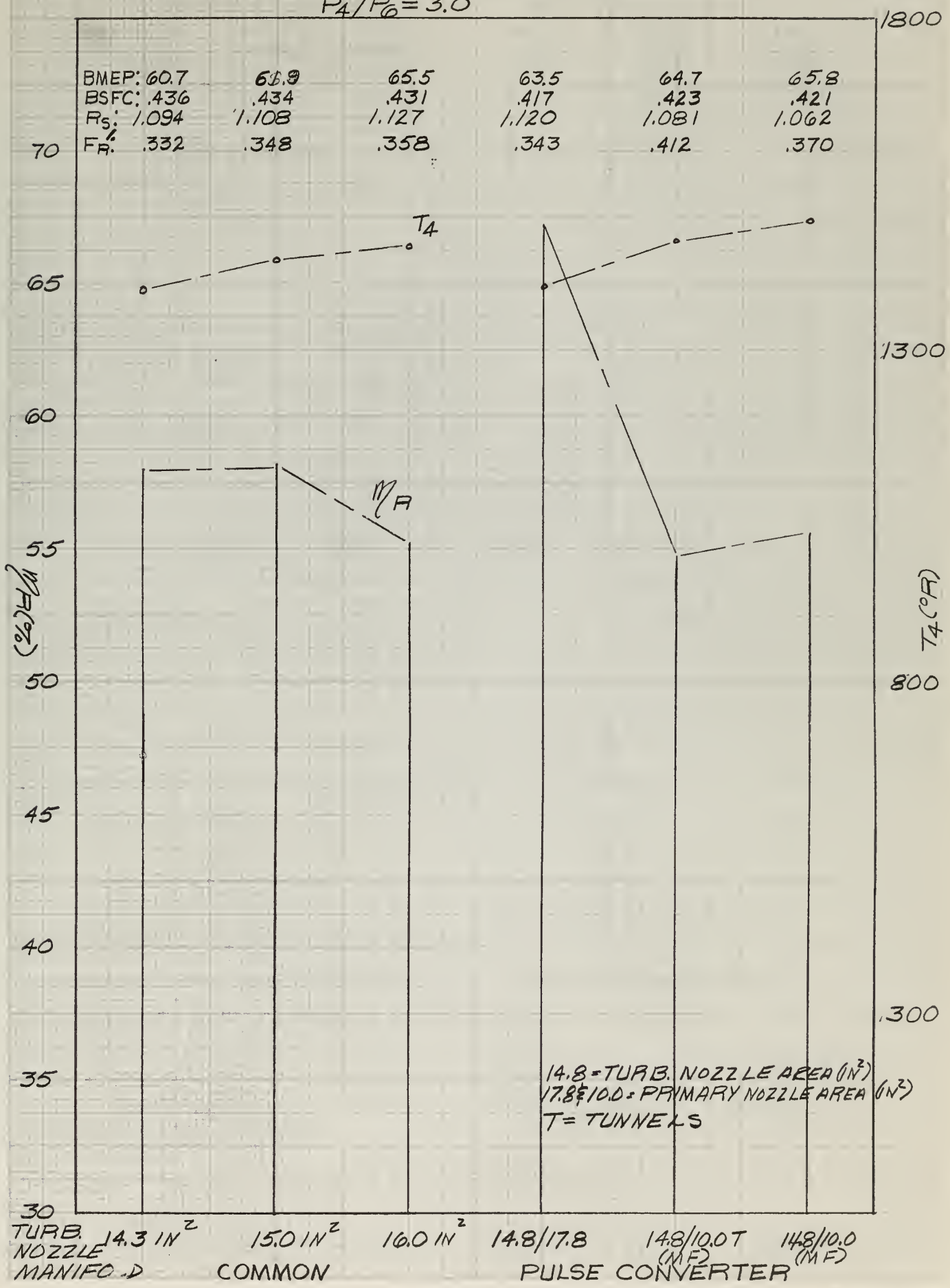

ELLIOTT STEADY FLOW TURBOCHARGERS

FIG. 44

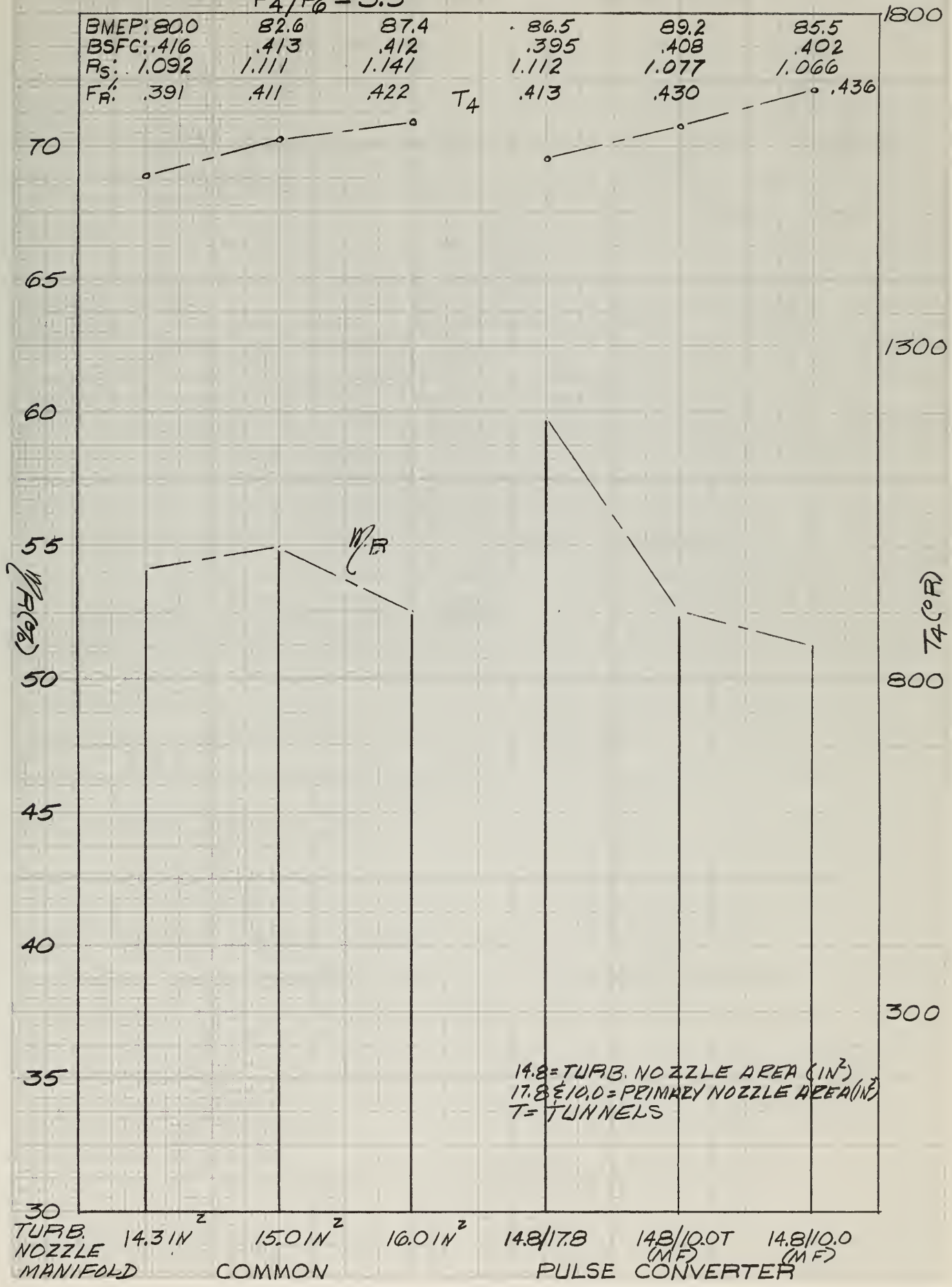

ELLIOTT STEADY FLOW TURBOCHARGERS FIG.45

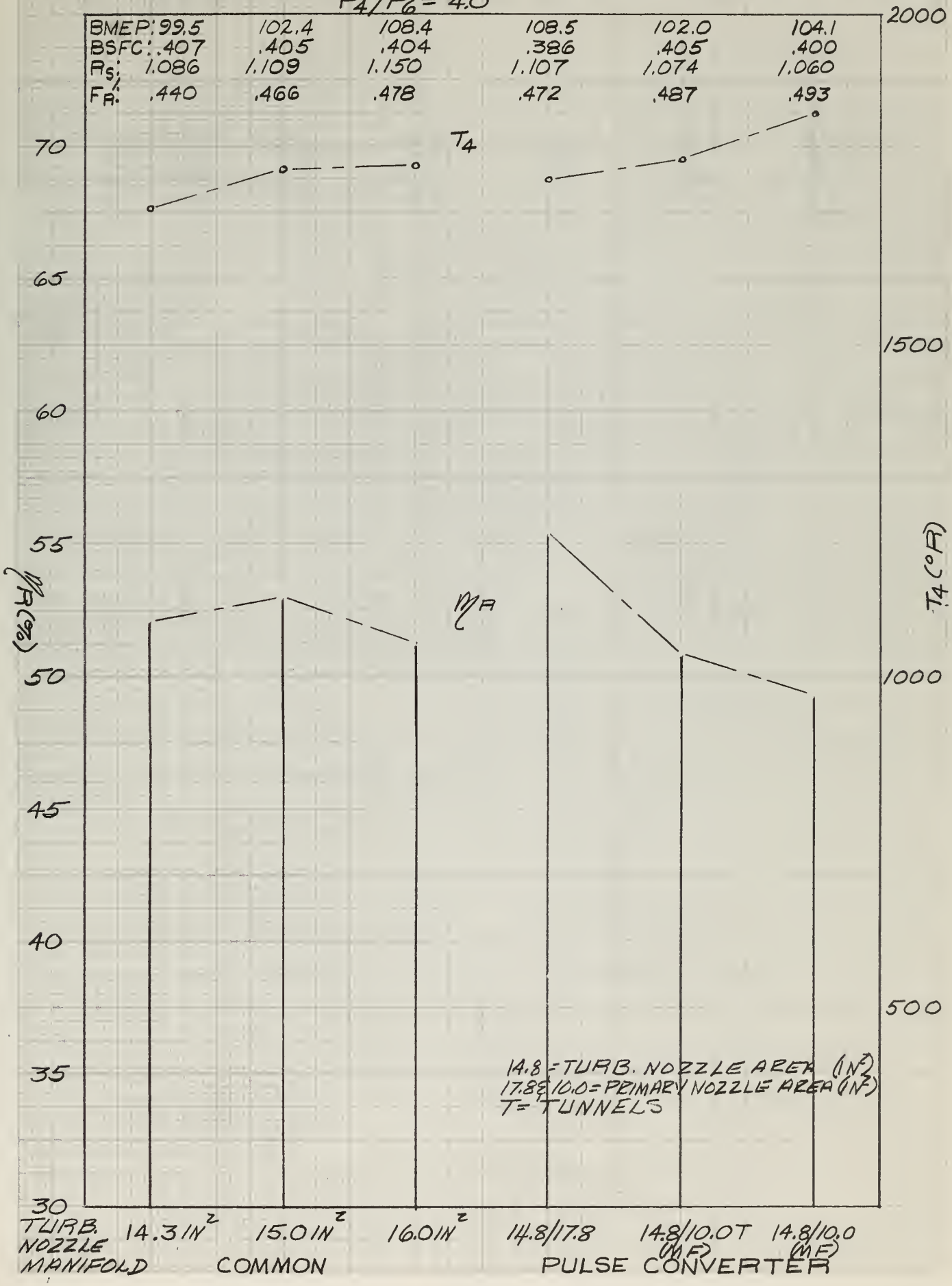

ELLIOTT STEADY FLOW TURBOCHARGERS FIG. 46

$P_4/P_6 = 4.5$

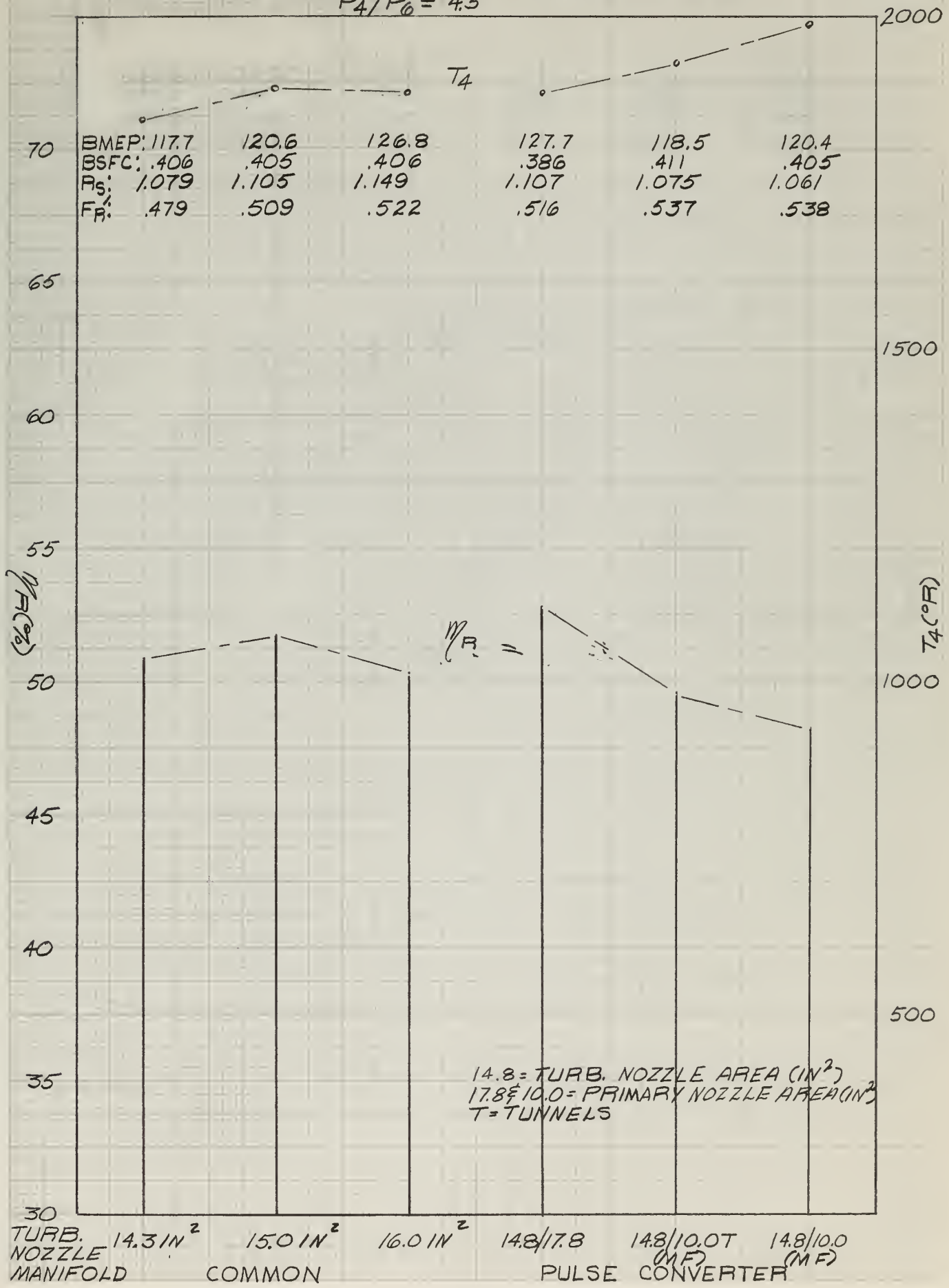

ELLIOTT STEADY FLOW TURBOCHARGERS FIG 47

$P_4/P_6 = 5.0$

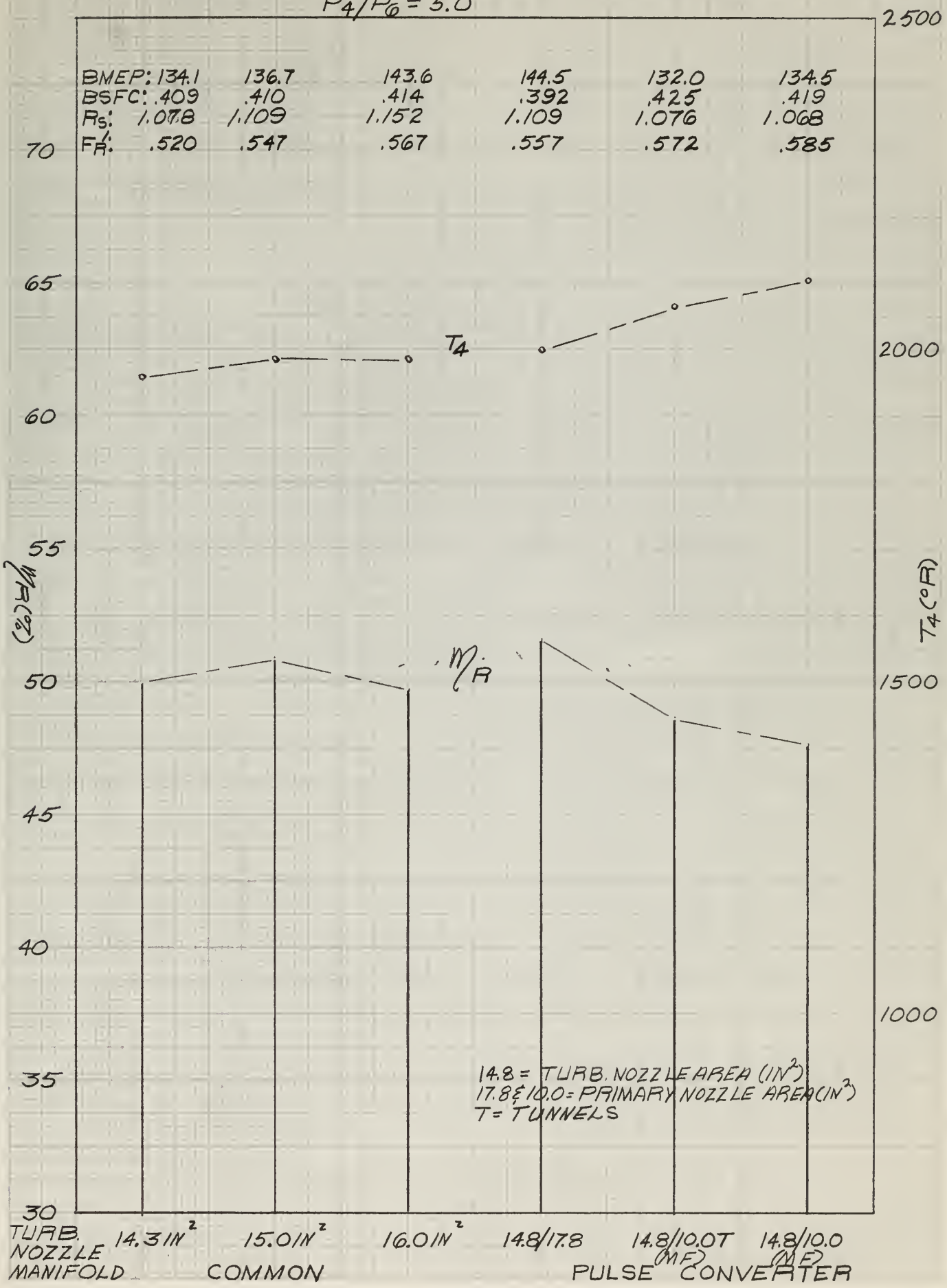

ELLIOTT STEADY FLOW TURBOCHARGERS FIG 48

$P_4/P_6 = 5.5$

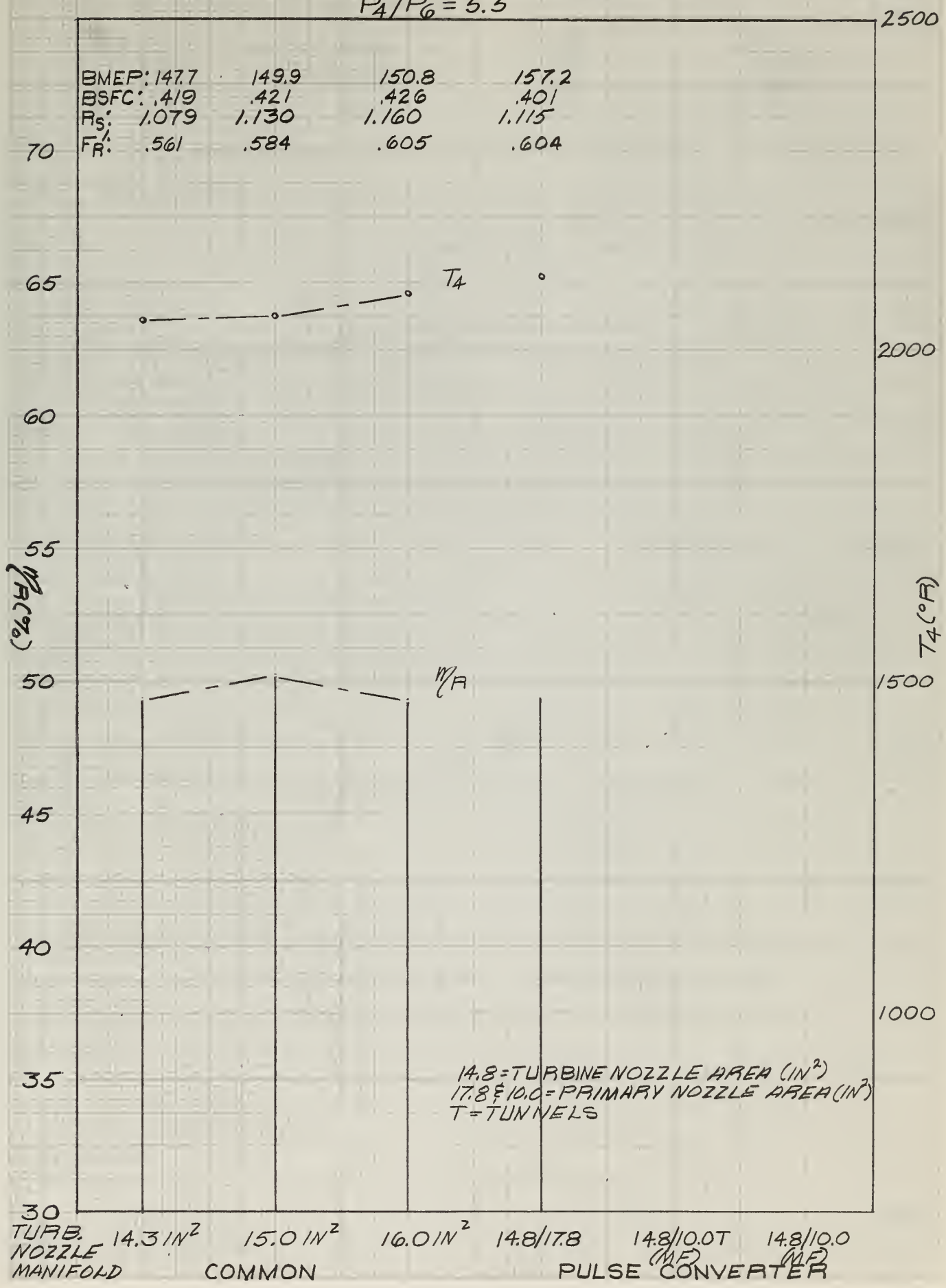

ELLIOTT STEADY FLOW TURBOCHARGERS

FIG 49

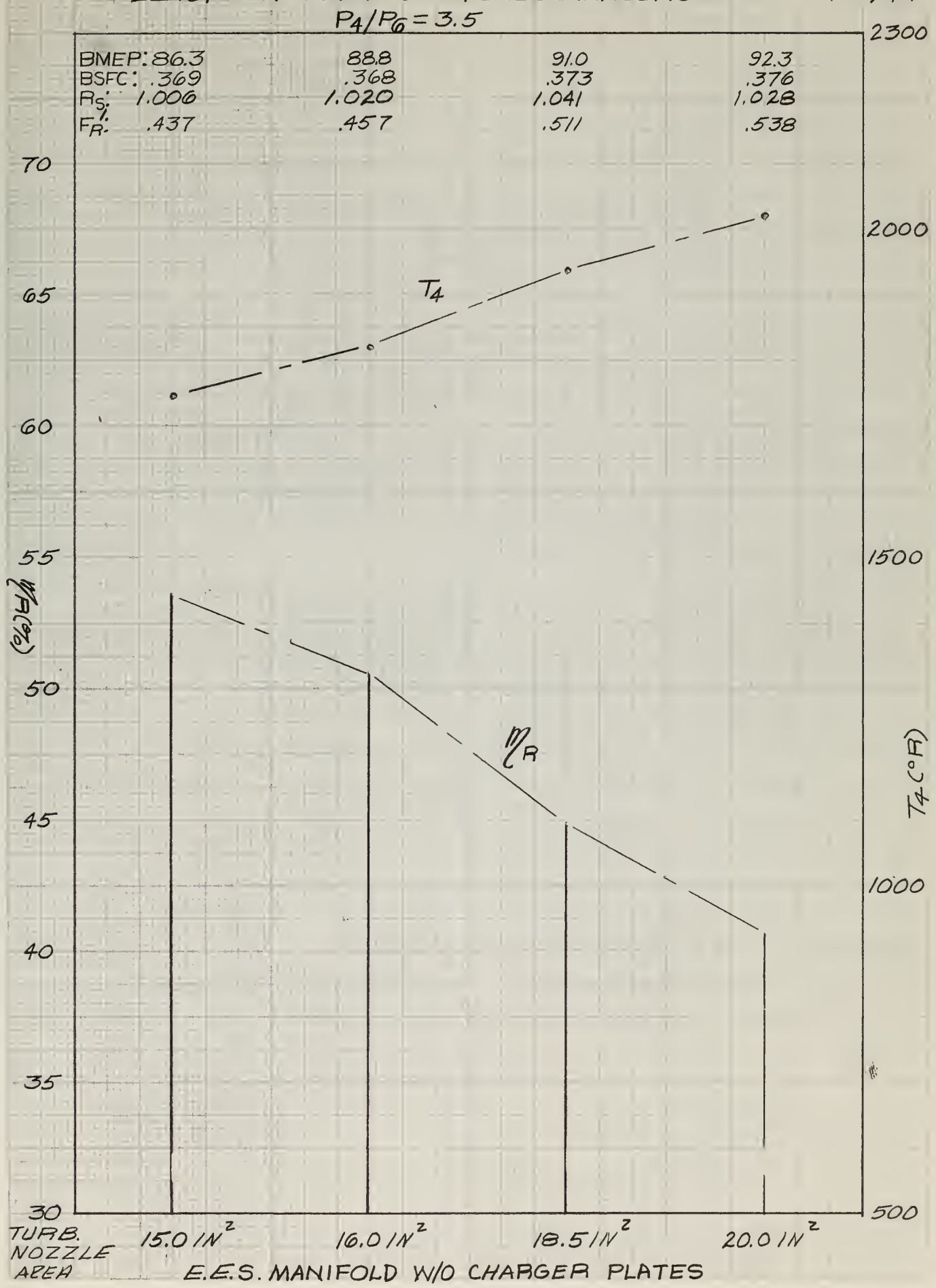

ELLIOTT STEADY FLOW TURBOCHARGERS FIG. 50

$P_4/P_6 = 4.0$

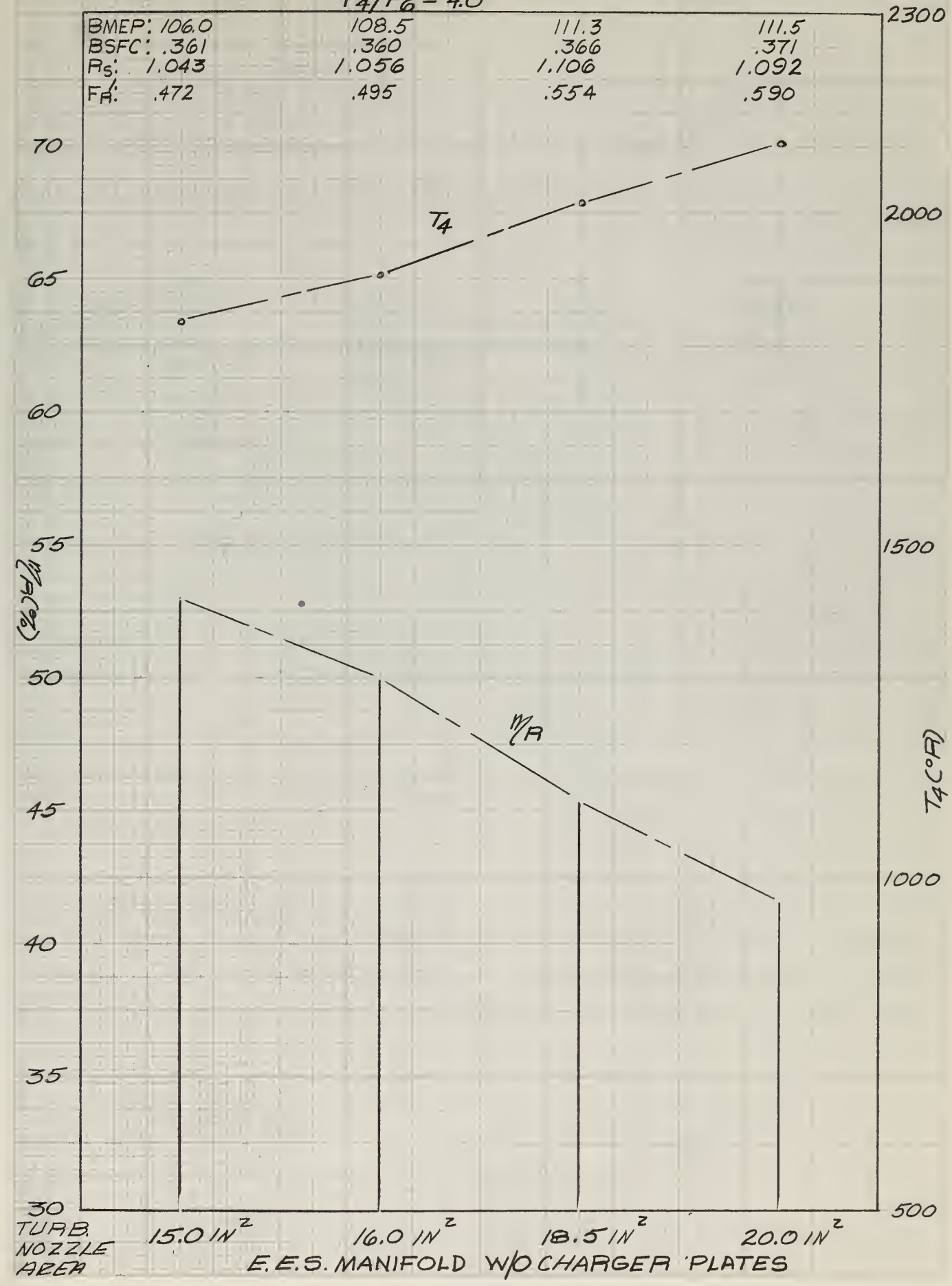

ELLIOTT STEADY FLOW TURBOCHARGERS FIG. 51

$P_4/P_6 = 4.5$

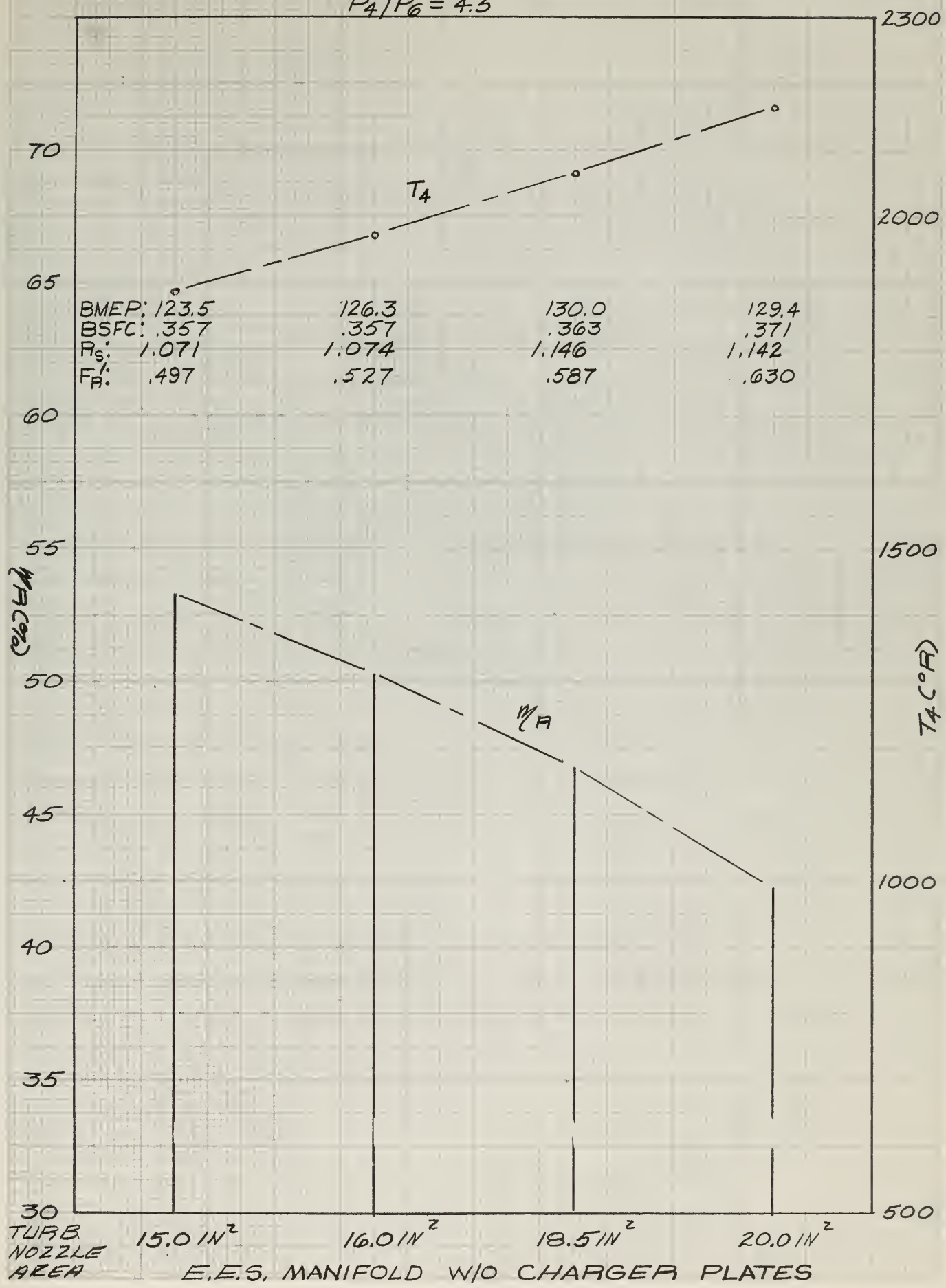

E.E.S. MANIFOLD W/O CHARGER PLATES

ELLIOTT STEADY FLOW TURBOCHARGERS FIG.52

$P_4/P_6 = 5.0$

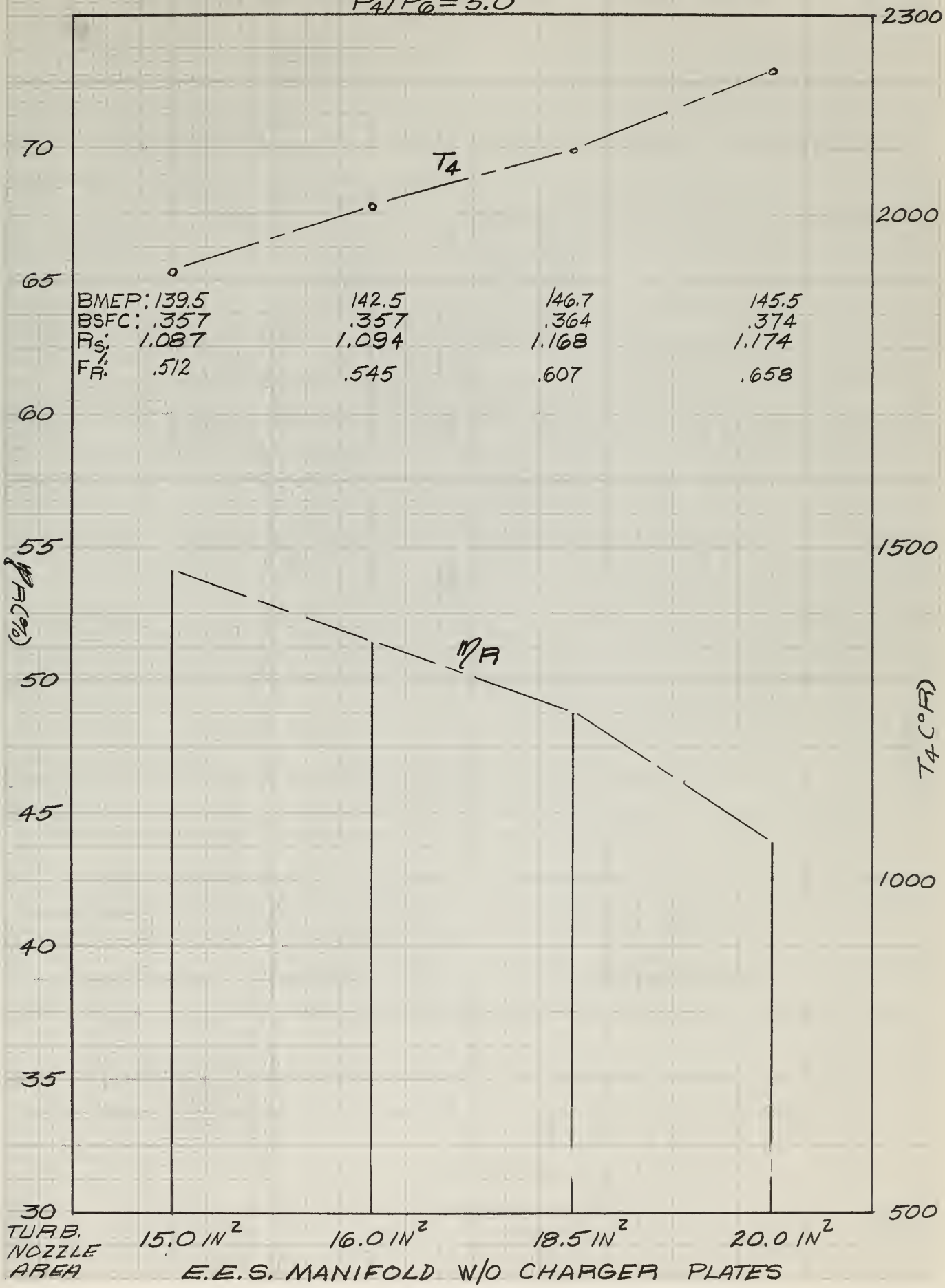

E.E.S. MANIFOLD W/O CHARGER PLATES

ELLIOTT STEADY FLOW TURBOCHARGERS FIG.53

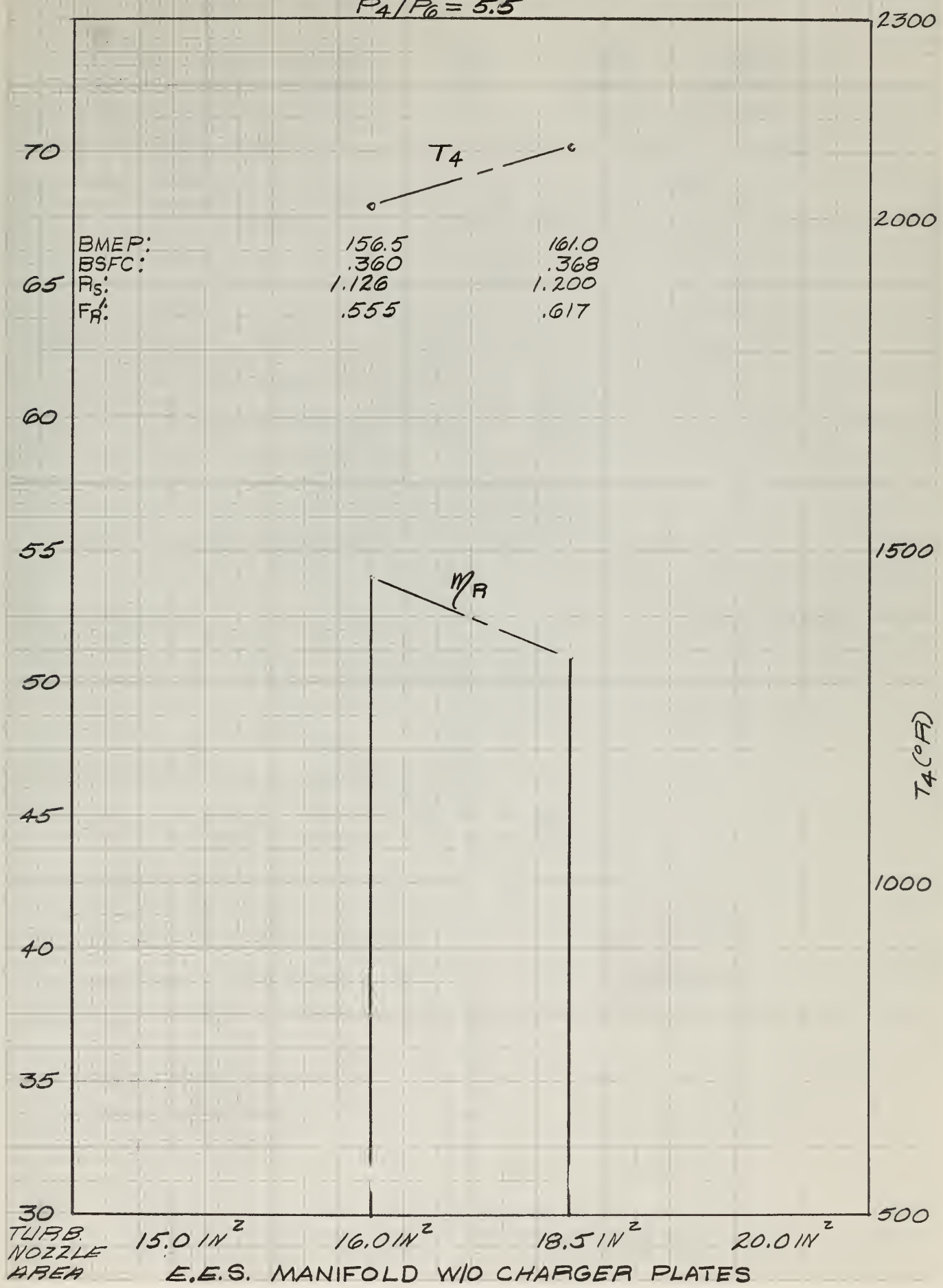

E.E.S. MANIFOLD W/O CHARGER PLATES

ELLIOTT STEADY FLOW TURBOCHARGERS FIG 54

$P_4/P_6 = 3.5$

BMEP:	87.4	87.7	86.0	85.8	86.0
BSFC:	.376	.379	.379	.380	.381
R_s:	.998	.994	1.004	1.006	1.023
F_R':	.475	.492	.476	.476	.474

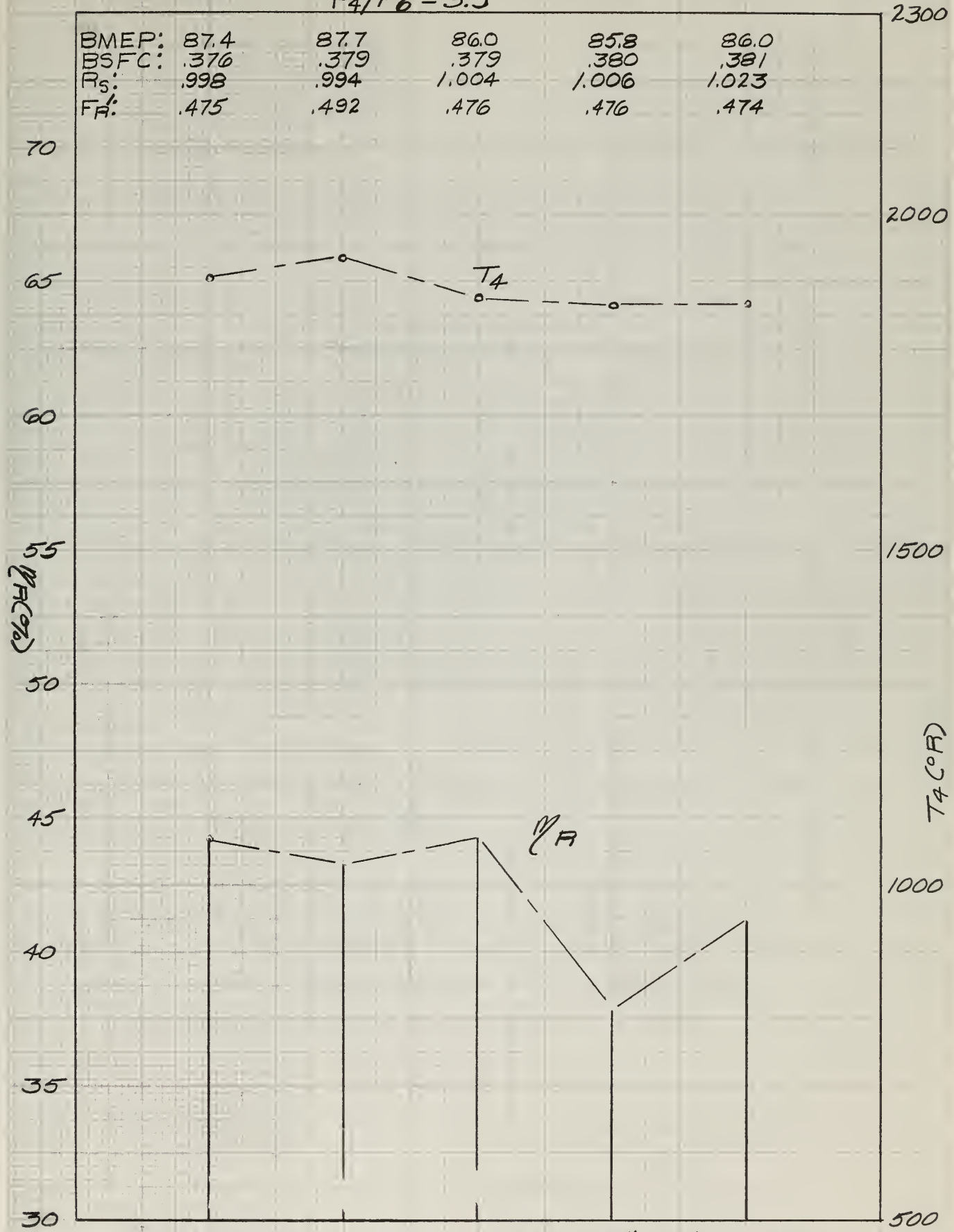

E.E.S TIPS GM. TIPS 17 in EL's. 20 5/8 in. EL's 26 in. EL's
17 in. EL's E.E.S. TIPS
E.E.S. MANIFOLD W/O CHARGER PLATES

ELLIOTT STEADY FLOW TURBOCHARGERS FIG. 55

$P_4/P_6 = 4.0$

BMEP:	103.8	105.5	105.5	104.0	105.4
BSFC:	.370	.373	.370	.374	.374
R_S:	1.014	1.013	1.042	1.032	1.042
F_R:	.500	.526	.517	.517	.525

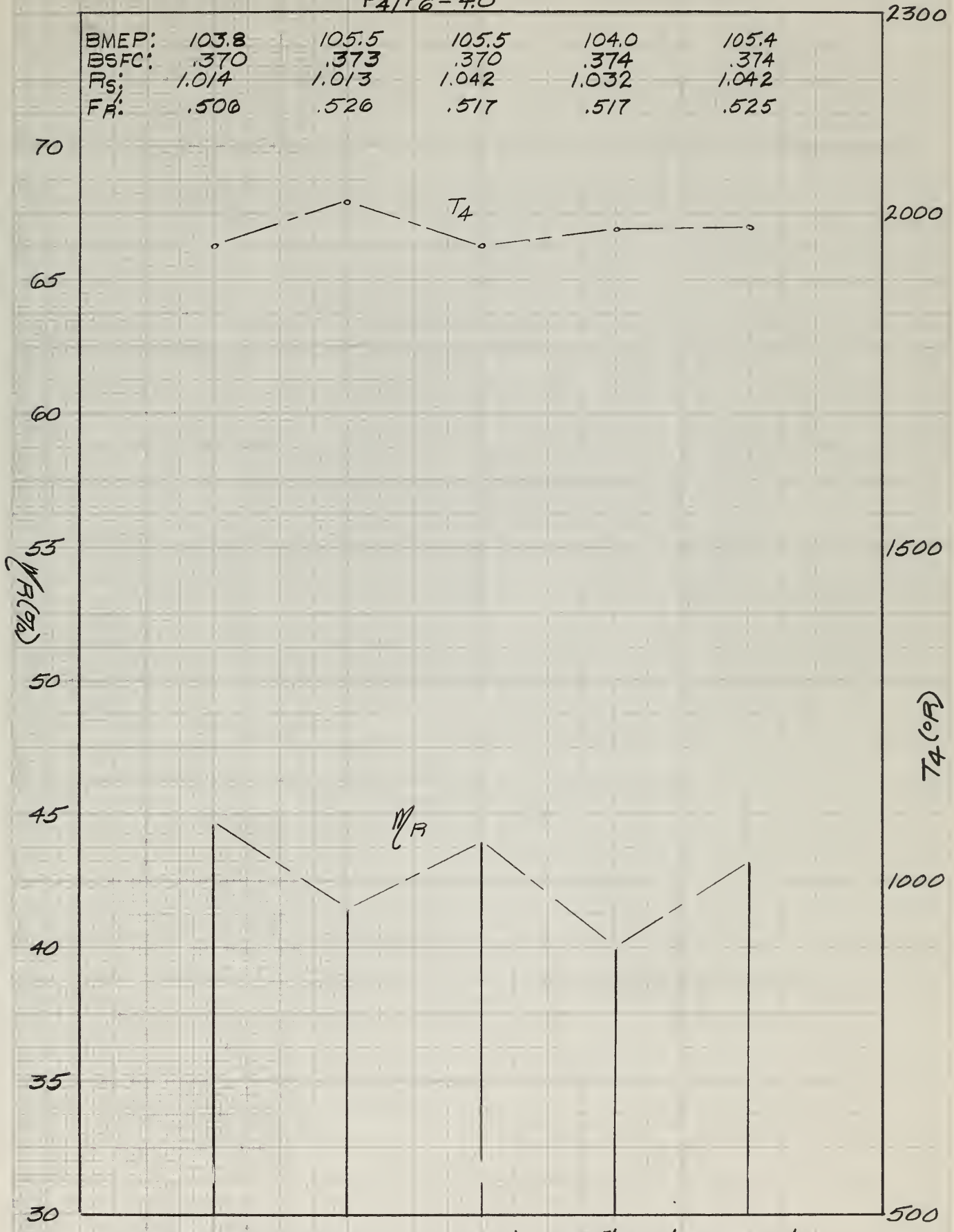

E.E.S. MANIFOLD W/O CHARGER PLATES

ELLIOTT STEADY FLOW TURBOCHARGERS

FIG. 56

$P_4/P_6 = 4.5$

BMEP:	120.7	122.6	124.5	122.0	123.8
BSFC:	.366	.369	.364	.370	.368
R_S:	1.019	1.022	1.076	1.053	1.066
F_R:	.530	.551	.541	.548	.550

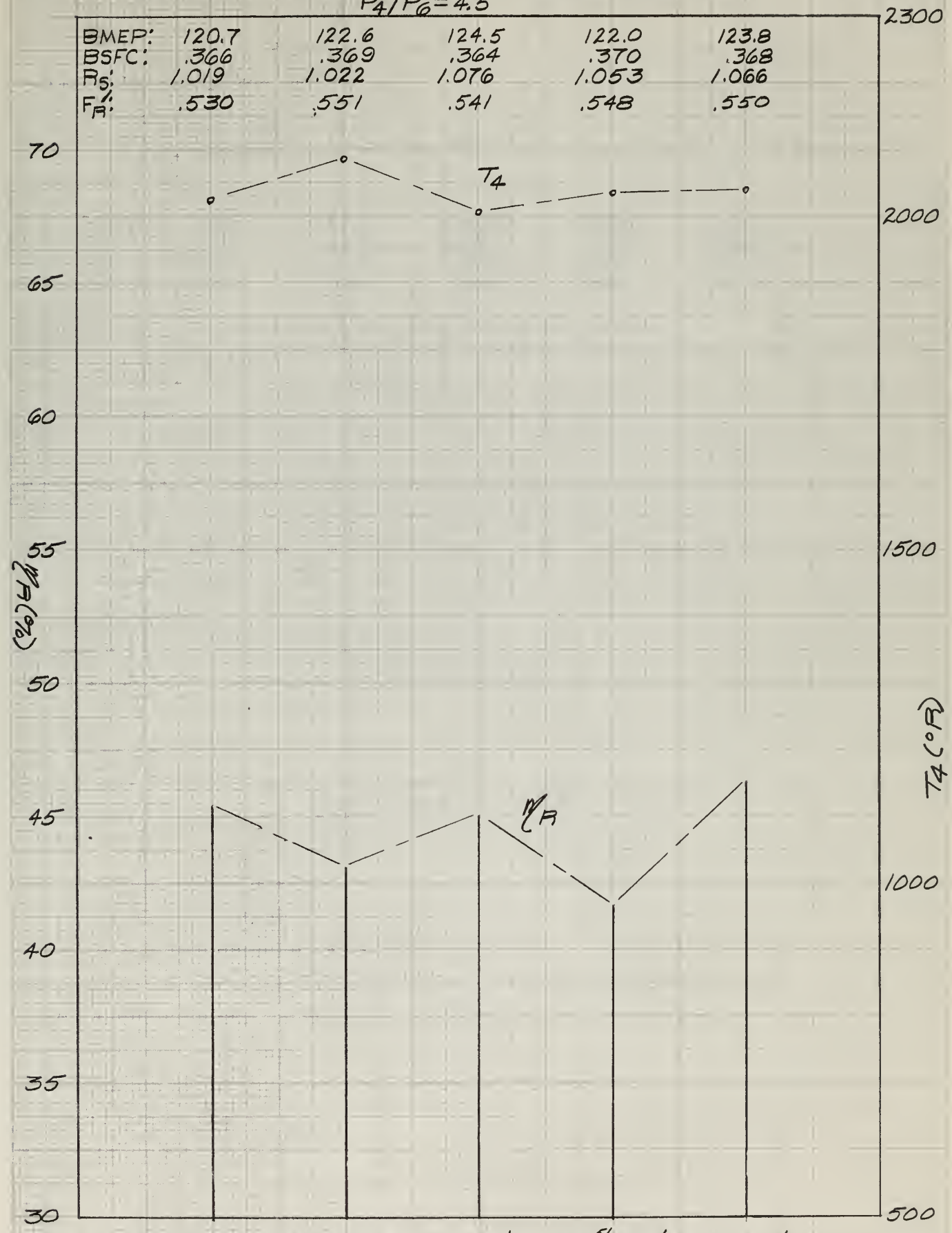

E.E.S. MANIFOLD W/O CHARGER PLATES

ELLIOTT STEADY FLOW TURBOCHARGERS FIG. 57

$P_4/P_6 = 5.0$

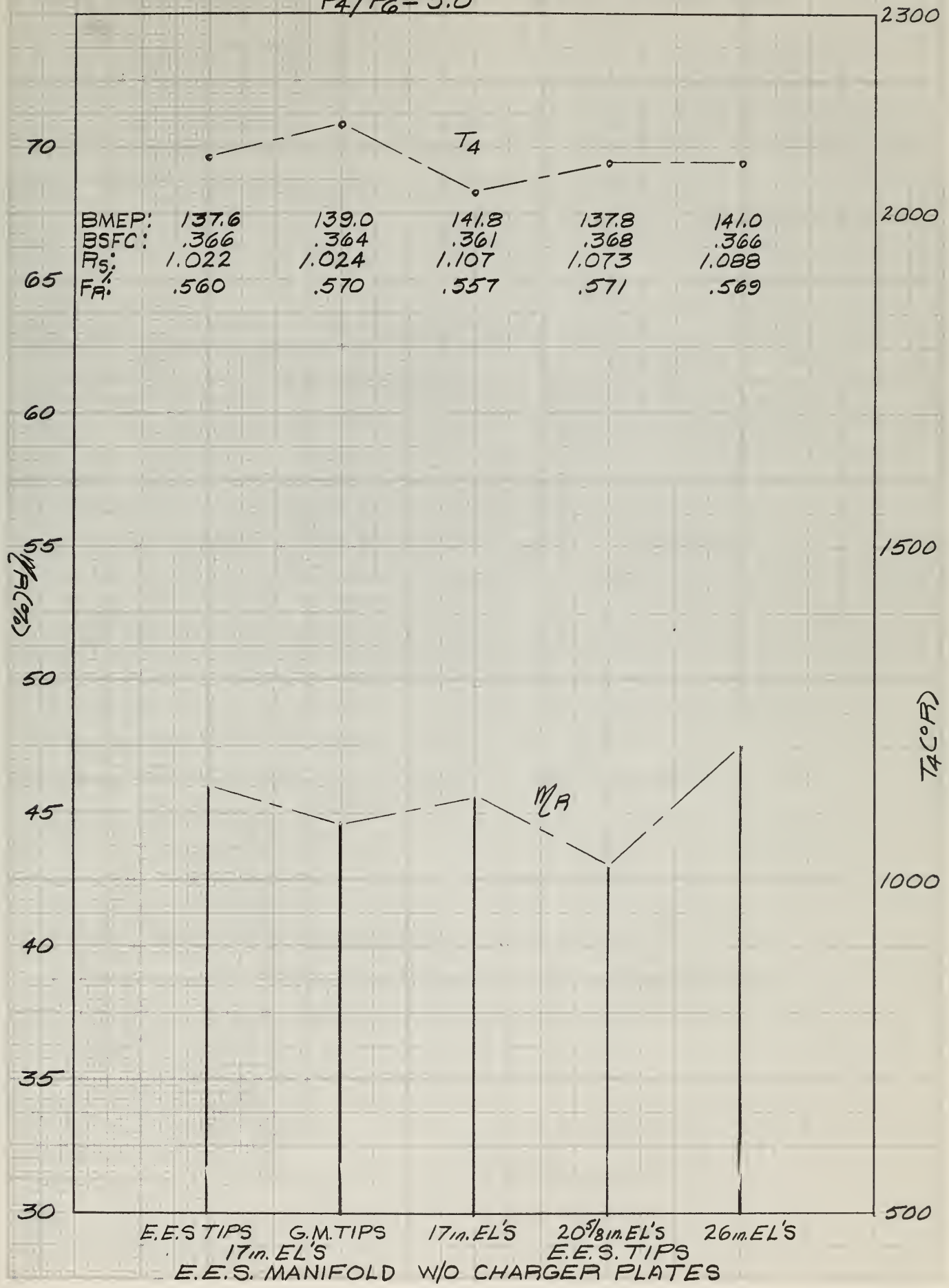

E.E.S. MANIFOLD W/O CHARGER PLATES

ELLIOTT STEADY FLOW TURBOCHARGERS FIG. 58

$P_4/P_6 = 5.5$

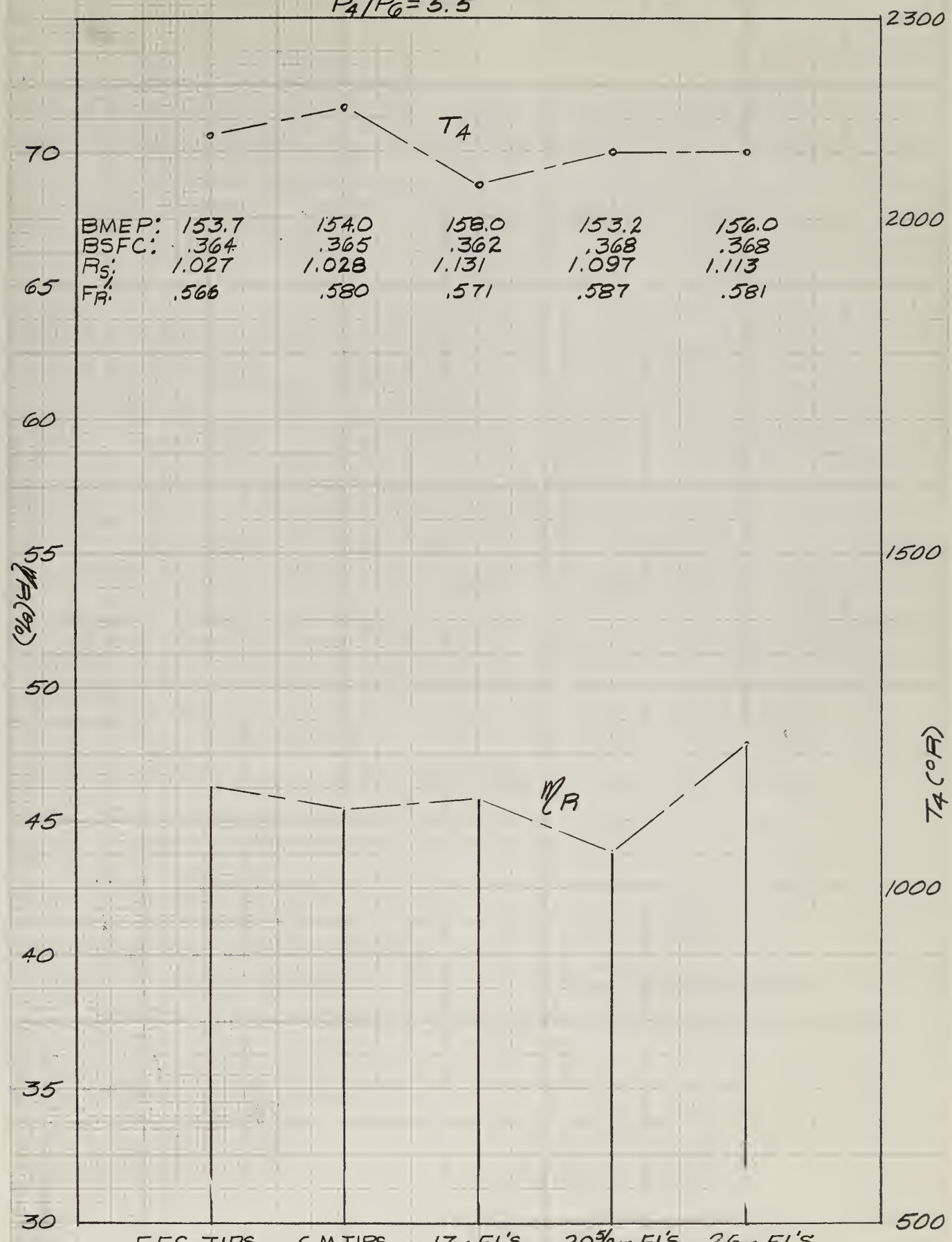

E.E.S. MANIFOLD W/O CHARGER PLATES

ELLIOTT STEADY FLOW TURBOCHARGERS

FIG. 59

$P_4/P_6 = 6.0$

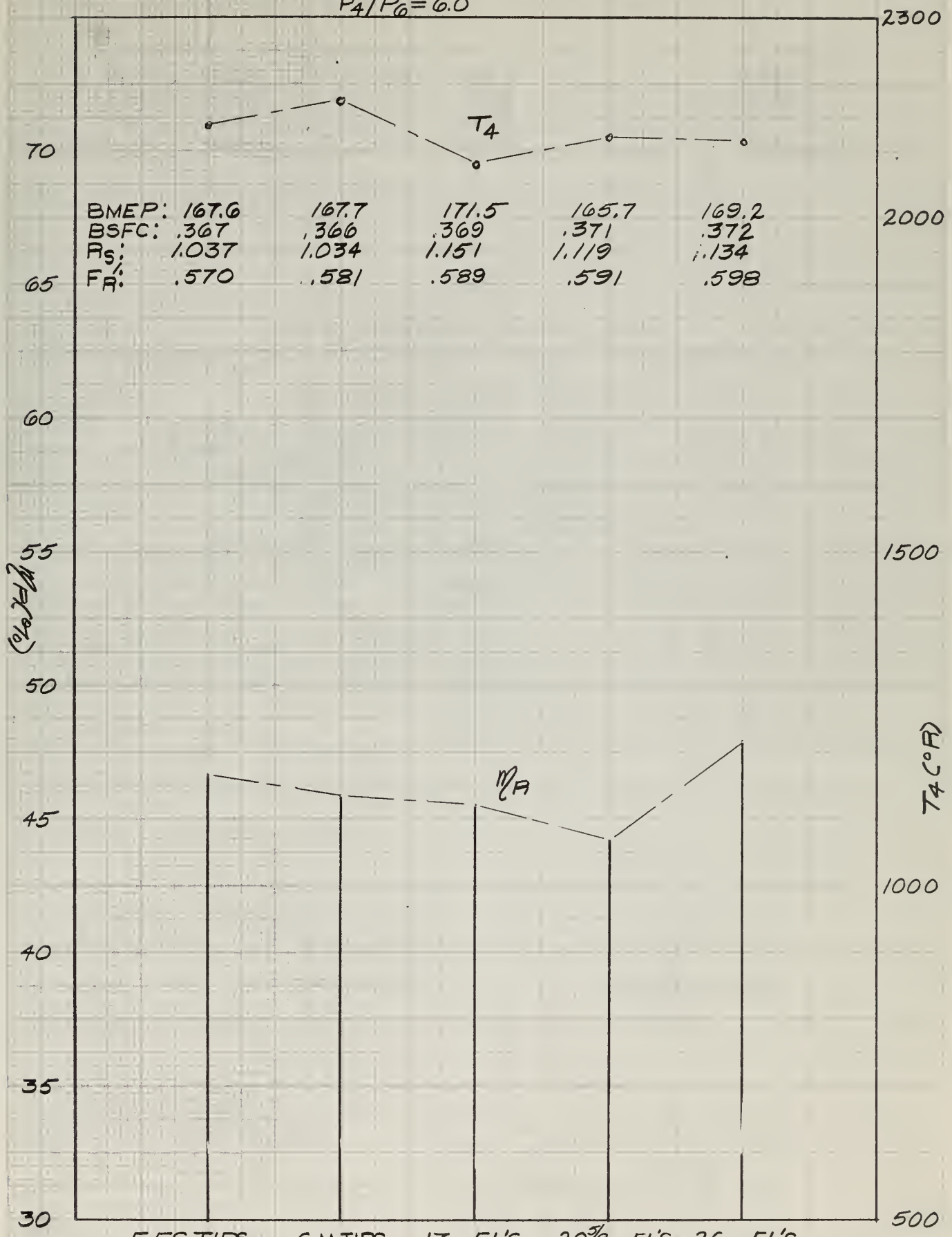

COMPARISON OF ELLIOTT STEADY FLOW OPTIMA FIG. 60

$P_4/P_6 = 3.5$

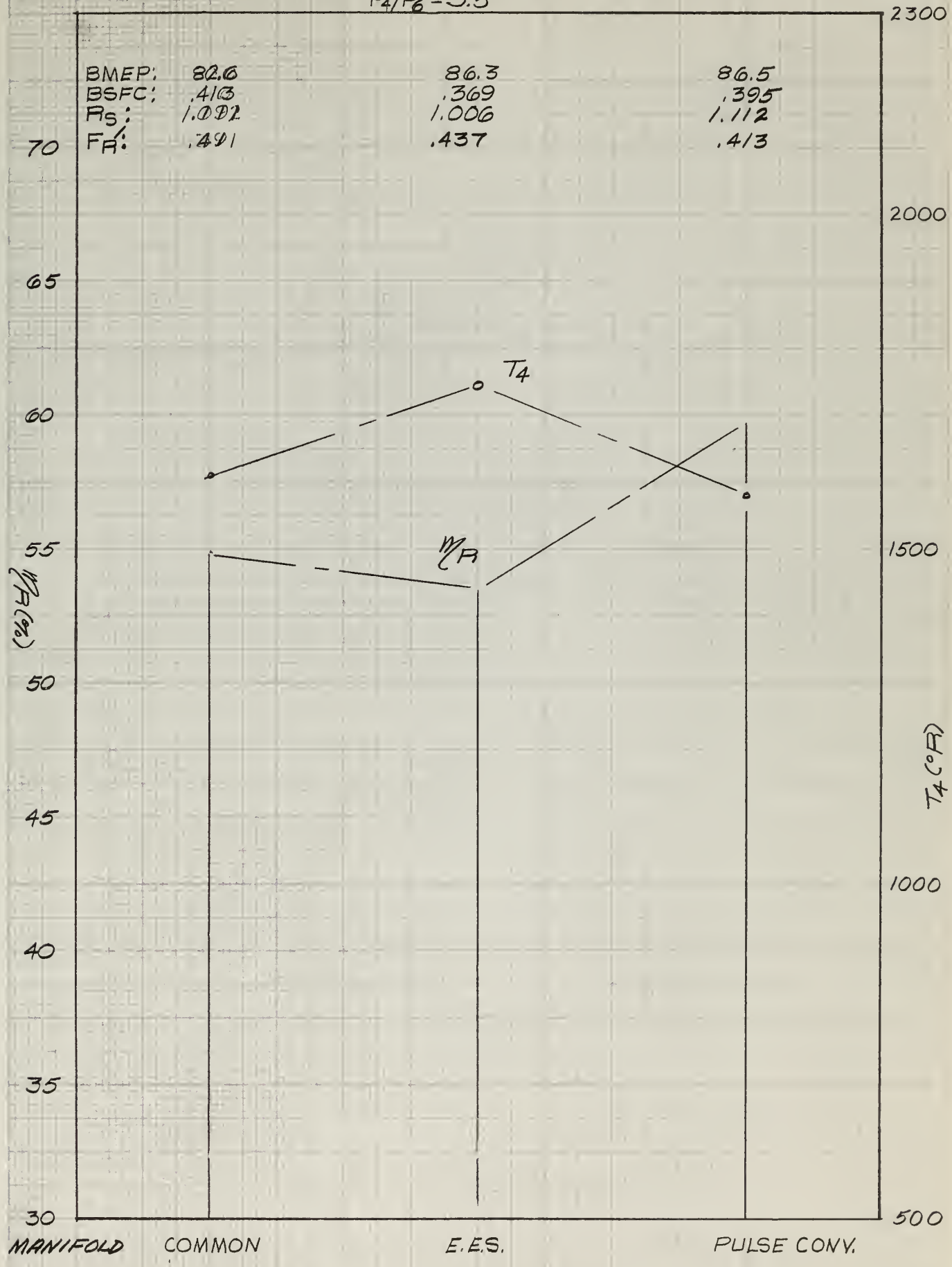

COMPARISON OF ELLIOTT STEADY FLOW OPTIMA FIG. 61

$P_4/P_6 = 4.0$

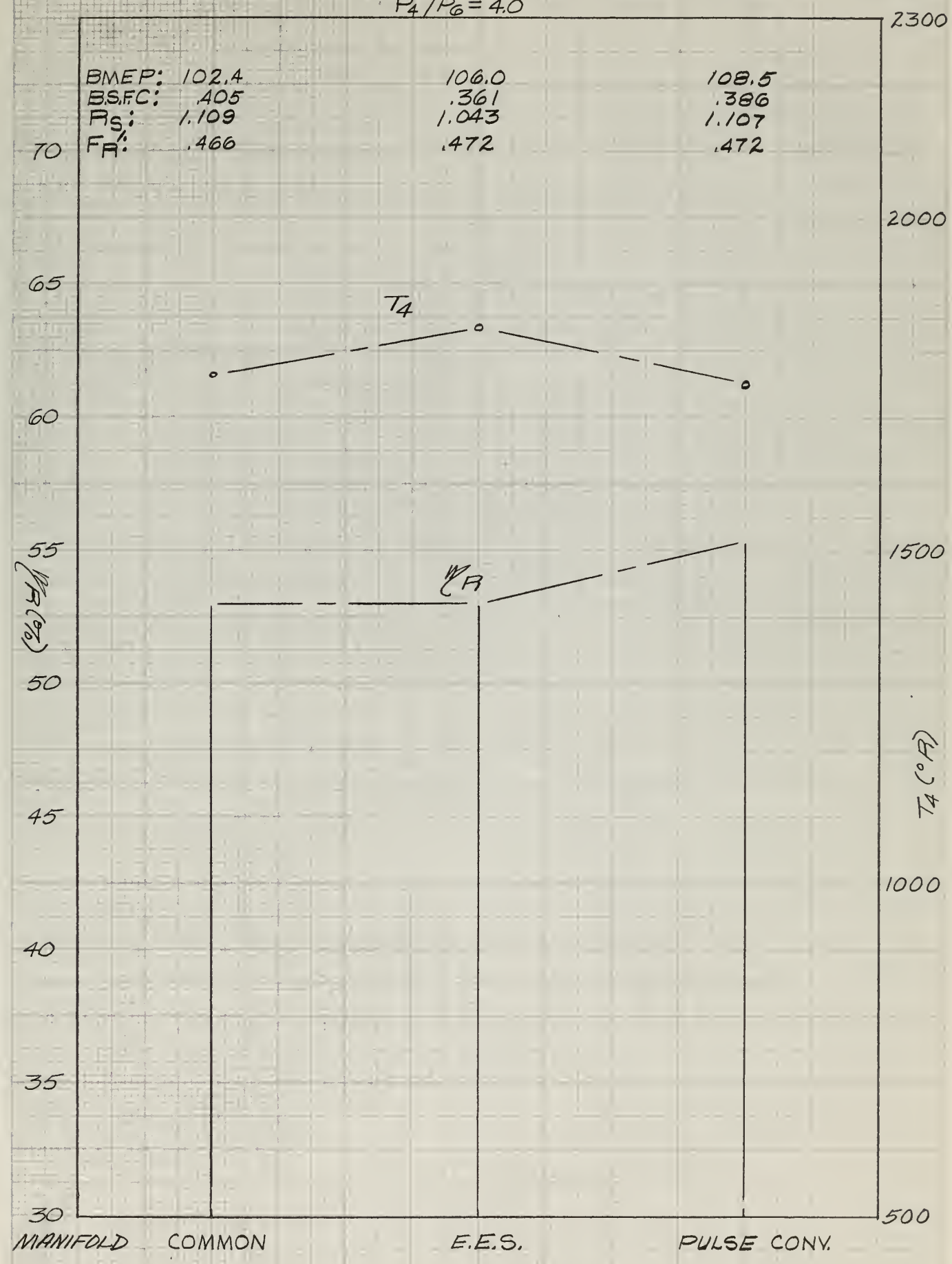

COMPARISON OF ELLIOTT STEADY FLOW OPTIMA FIG. 62

$P_4/P_6 = 4.5$

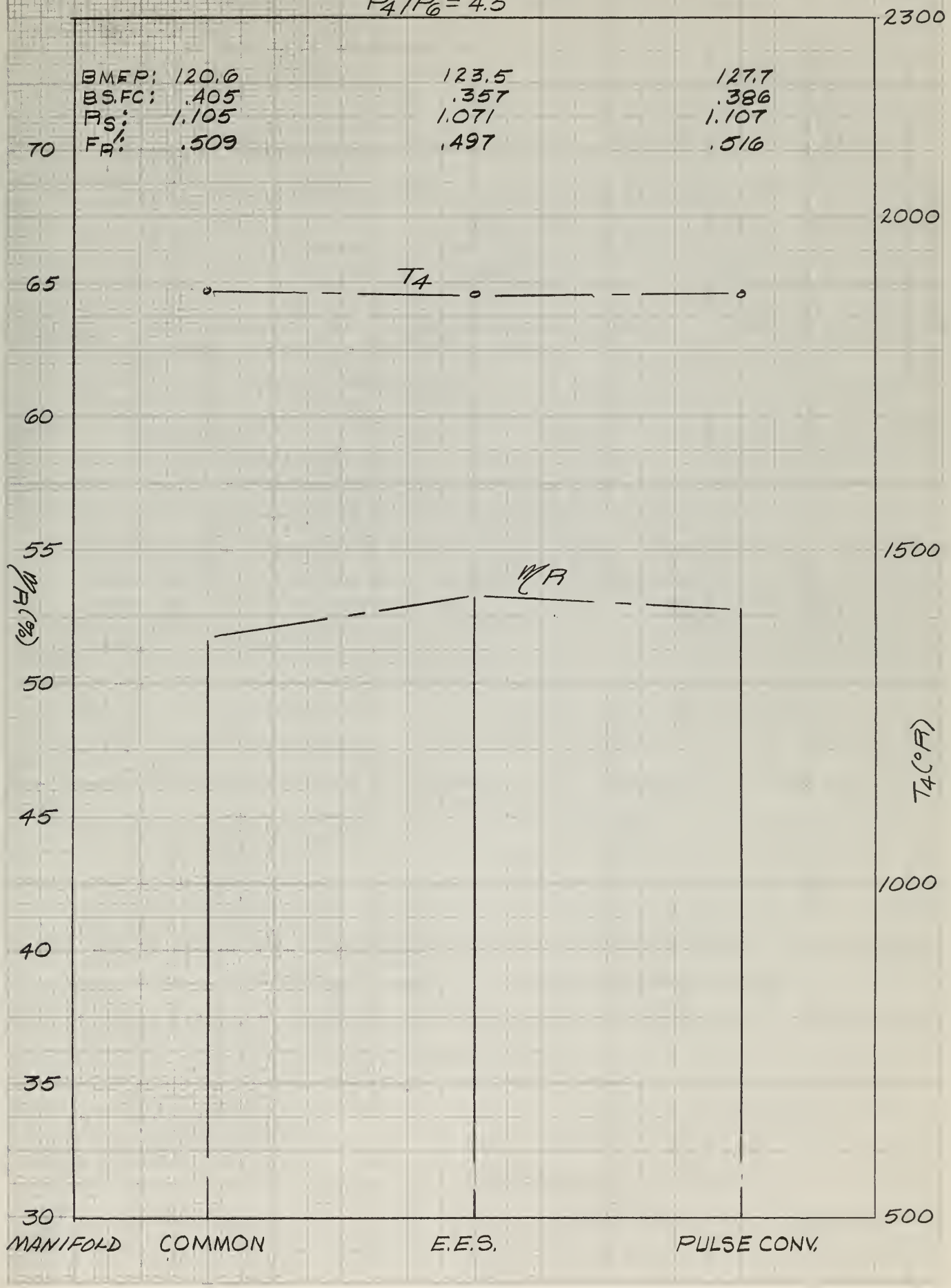

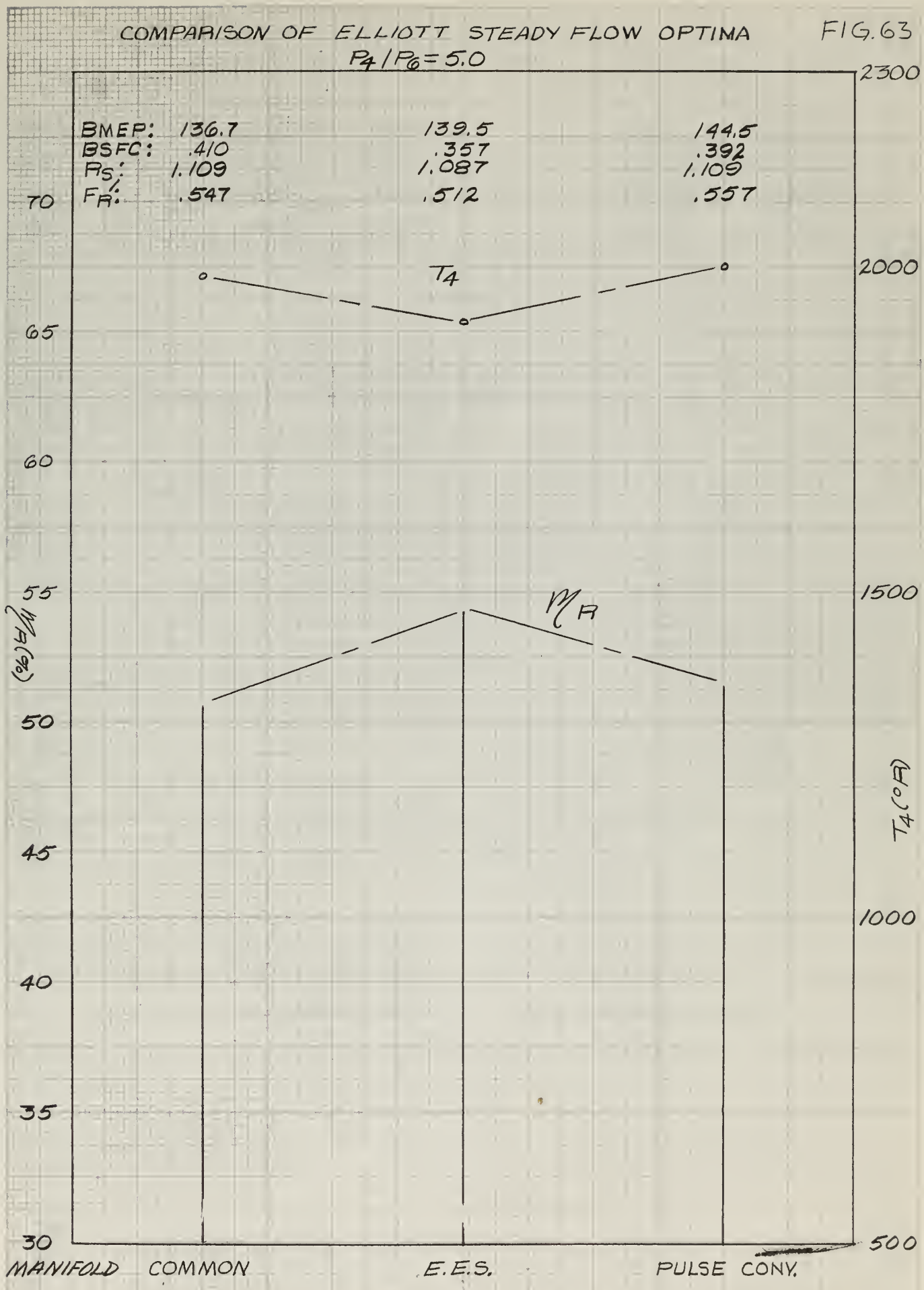
COMPARISON OF ELLIOTT STEADY FLOW OPTIMA
FIG. 63
$P_4/P_6 = 5.0$
BMEP: 136.7 139.5 144.5
BSFC: .410 .357 .392
R_S: 1.109 1.087 1.109
F_R': .547 .512 .557
T_4
M_R
M_R (%)
T_4 (°R)
70
65
60
55
50
45
40
35
30
2300
2000
1500
1000
500
MANIFOLD
COMMON
E.E.S.
PULSE CONV.

DELAVAL "STEADY FLOW" TURBOCHARGERS FIG 64

P4 / P6 = 3.2

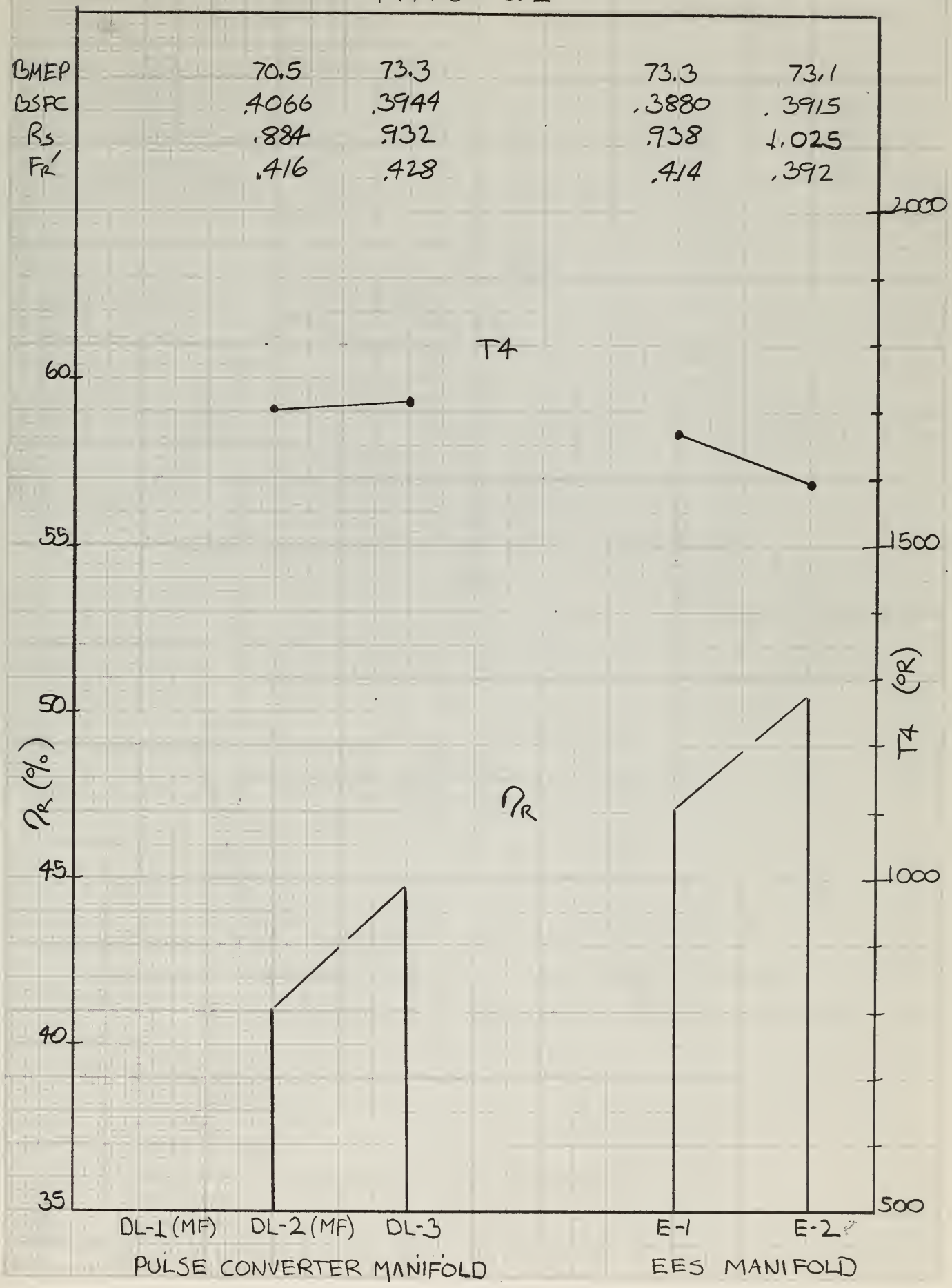

DELAVAL "STEADY FLOW" TURBOCHARGERS FIG. 65

P4 / P6 = 3.7

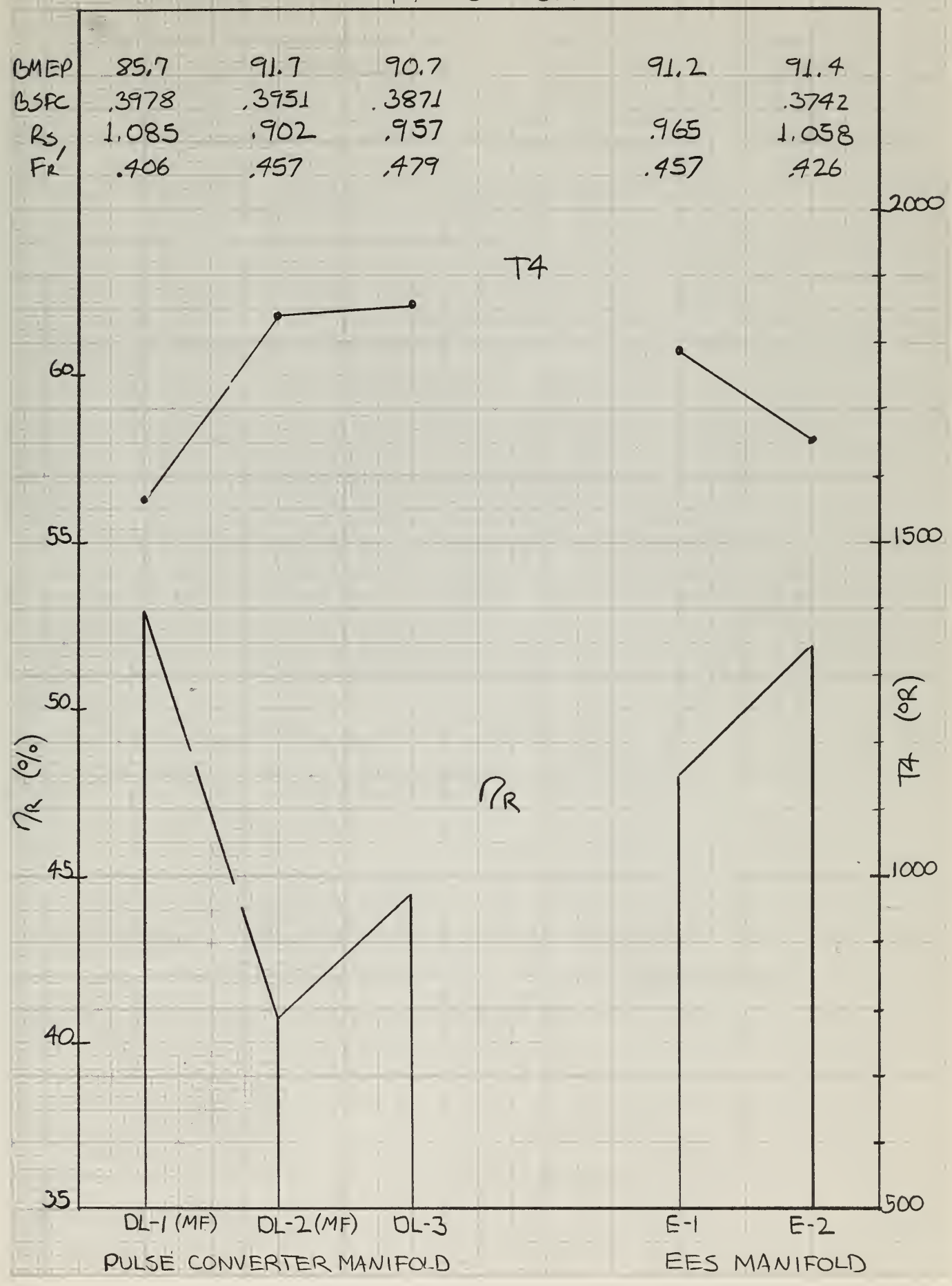

DELAVAL "STEADY FLOW" TURBOCHARGERS FIG. 66

$P_4 / P_6 = 4.2$

BMEP	101.5	101.2	106.3	107.4	108.8
BSFC	.3938	.3942	.3850		.3660
R_s	1.091	.923	.983	.999	1.088
F_R'	.446	.494	.519	.494	.452

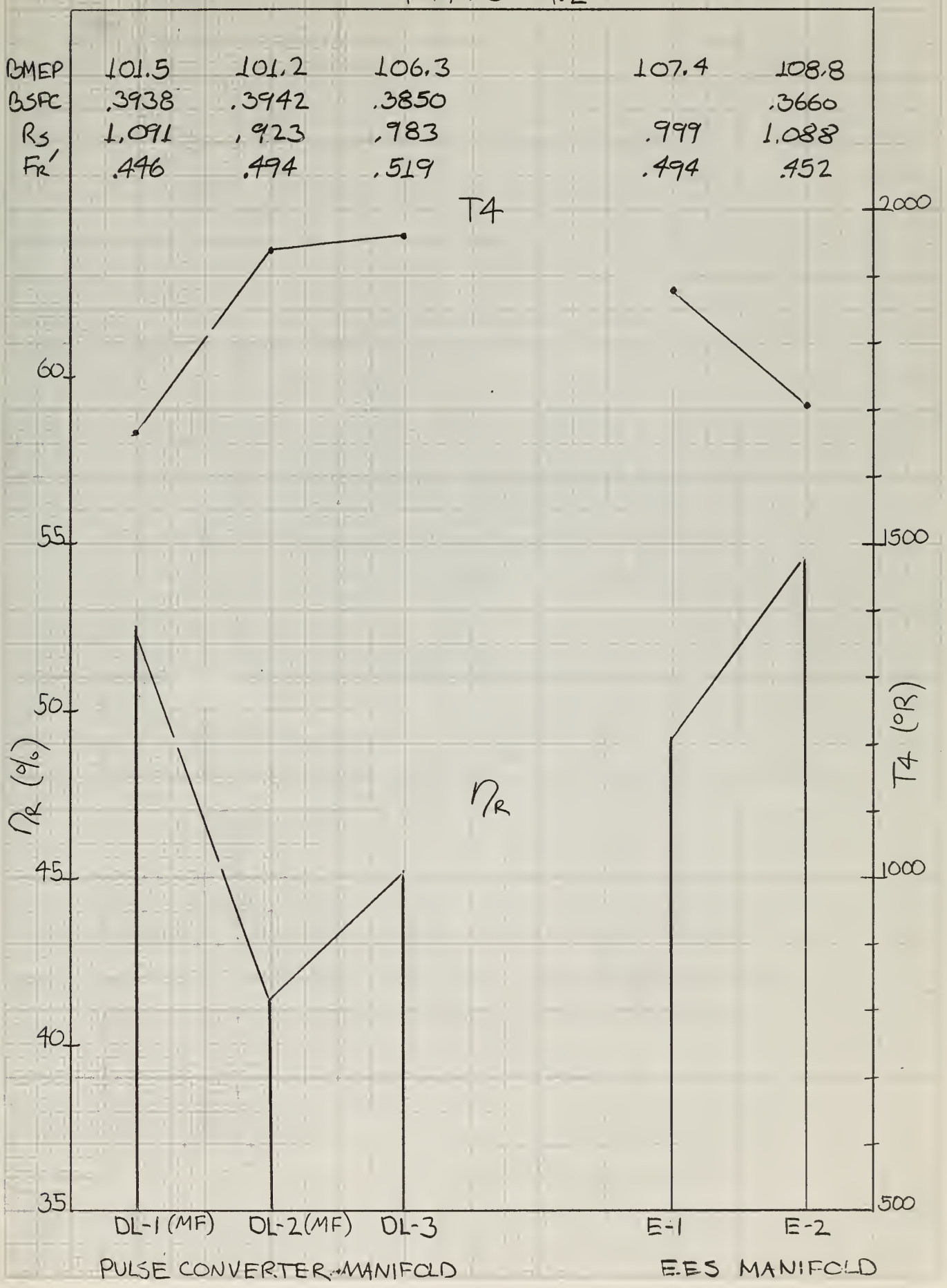

DELAVAL "STEADY FLOW" TURBOCHARGERS FIG.67

P4 / P6 = 4.7

BMEP	116.4	115.7	123.0	123.0	125.6
BSFC	.3950	.3967	.3863		
R_S	1.130	.944	1.012	1.031	1.115
F_R'	.479	.526	.553	.525	.476

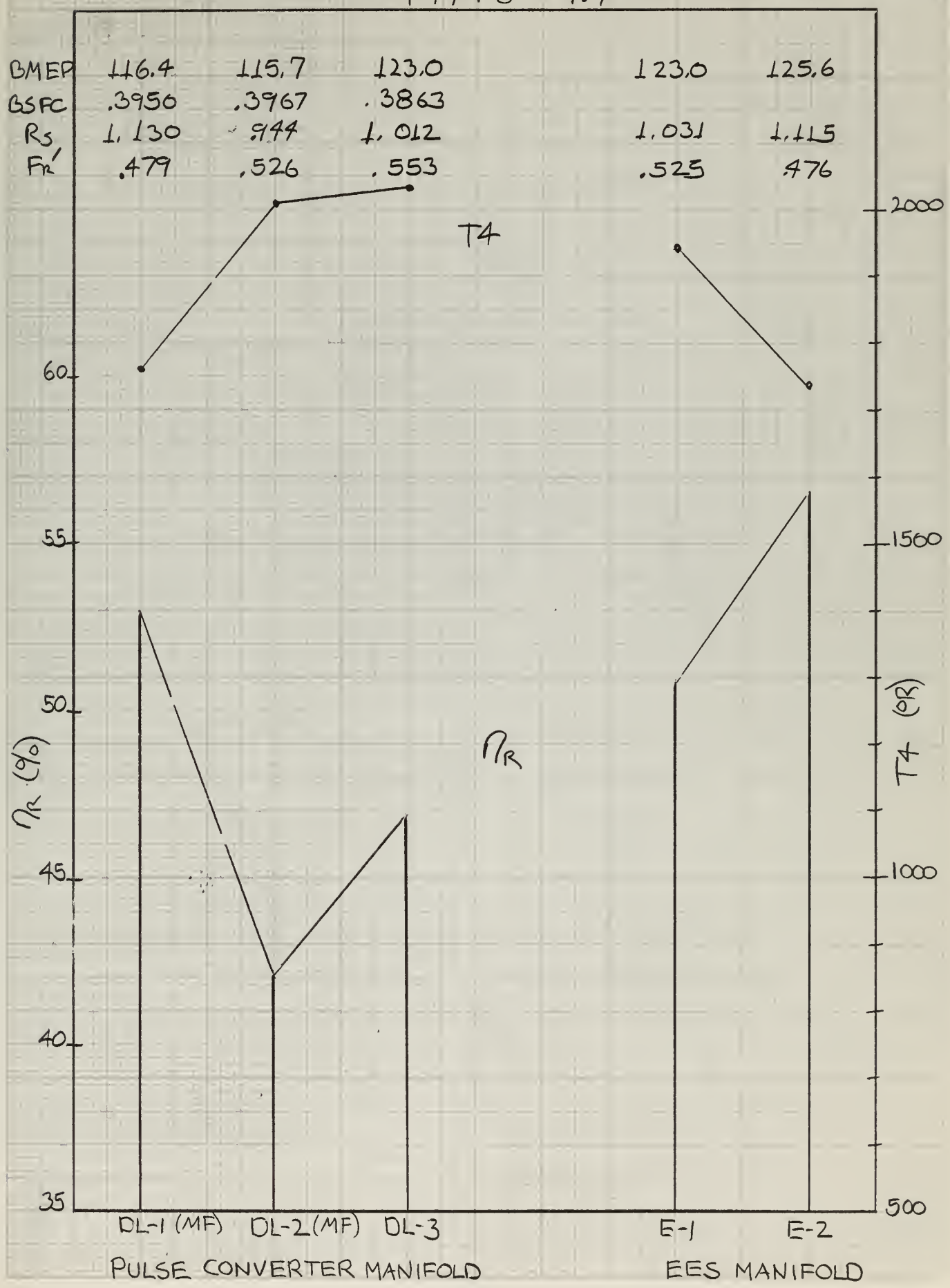

DELAVAL "STEADY FLOW" TURBOCHARGERS FIG.68

P4/P6 = 5.2

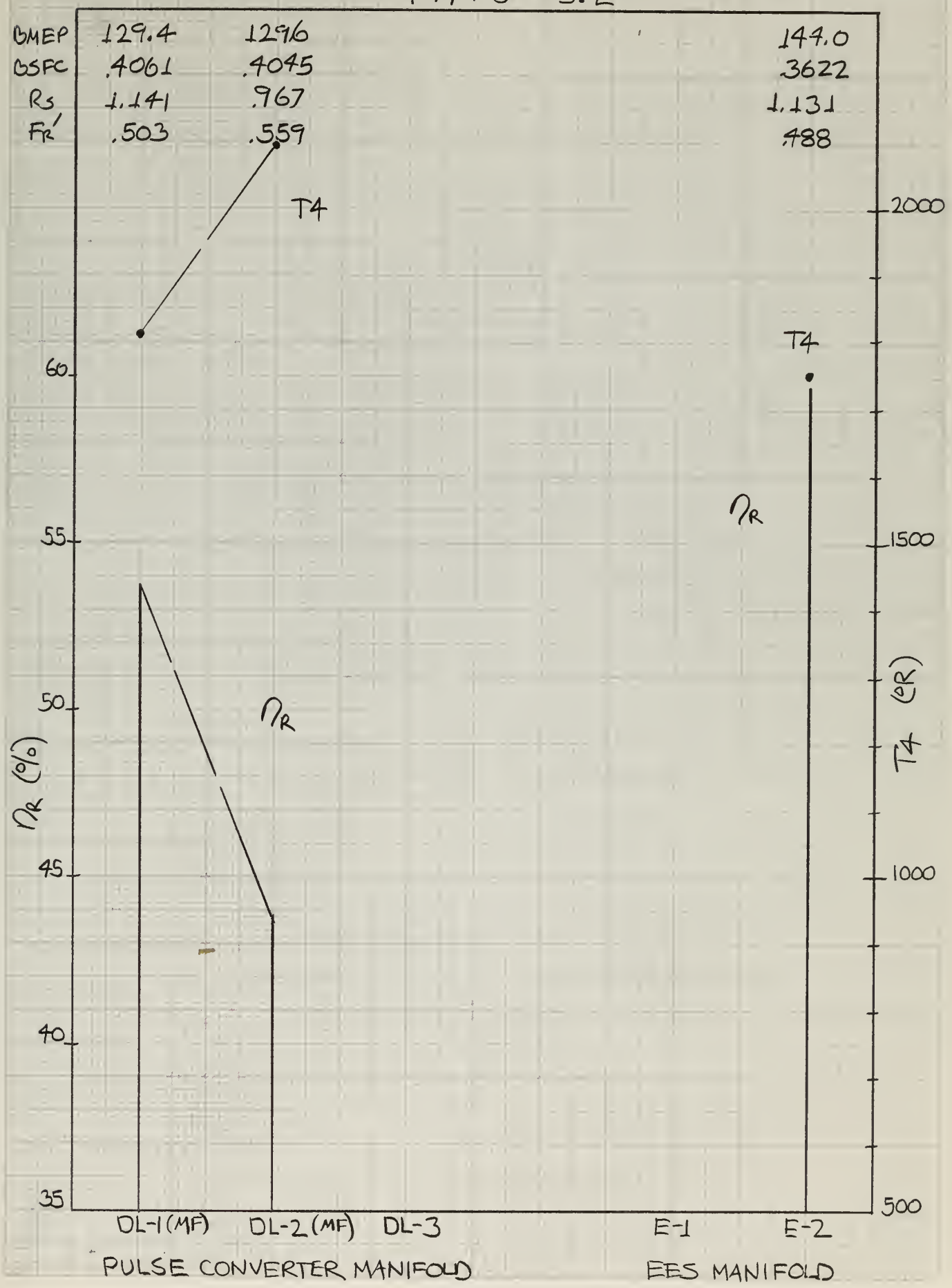

DELAVAL "STEADY FLOW" TURBOCHARGERS FIG69

$P_4 / P_6 = 5.7$

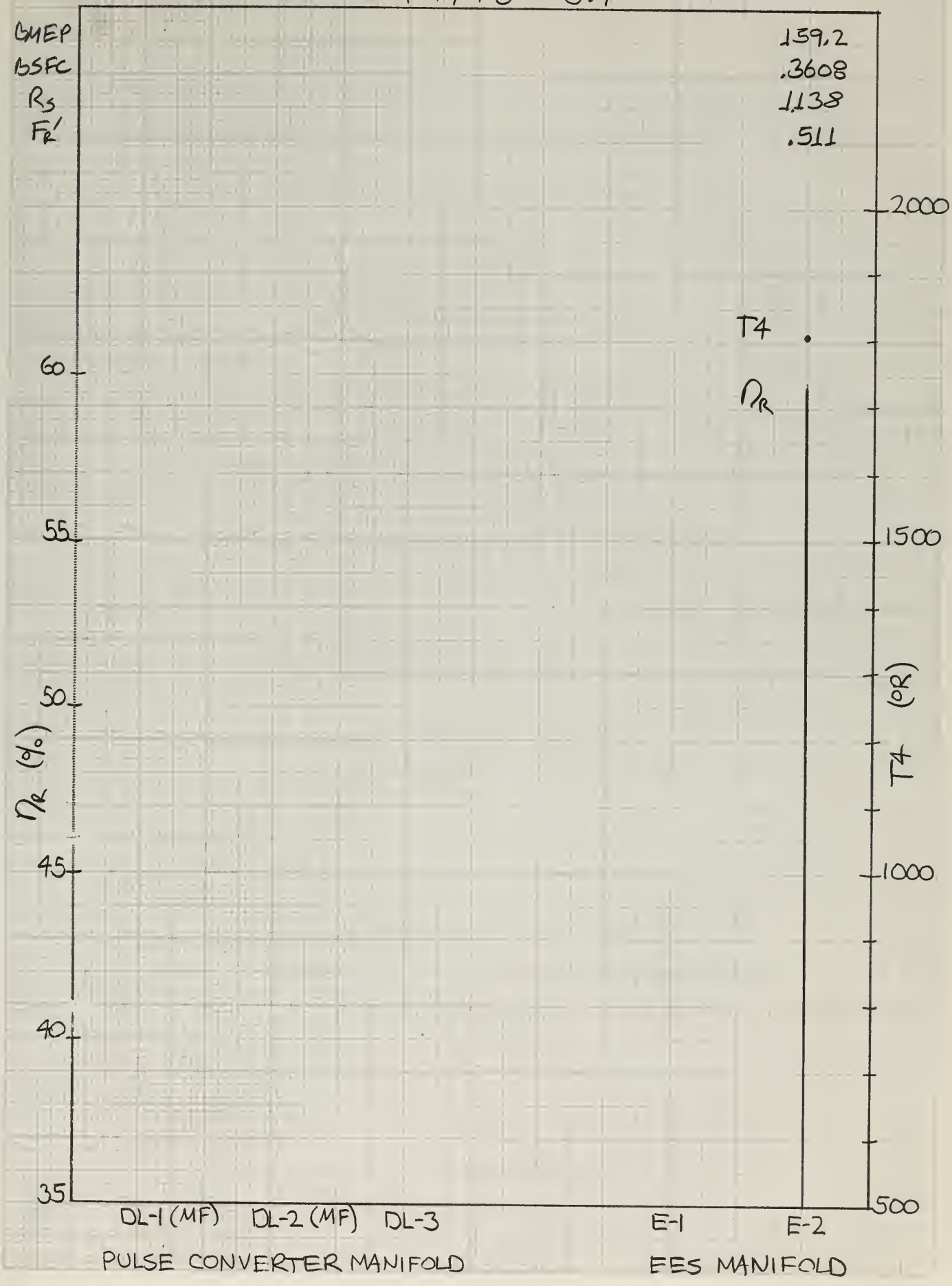

DELAVAL "STEADY FLOW" TURBOCHARGERS
P4 / P6 = 6.2

FIG. 70

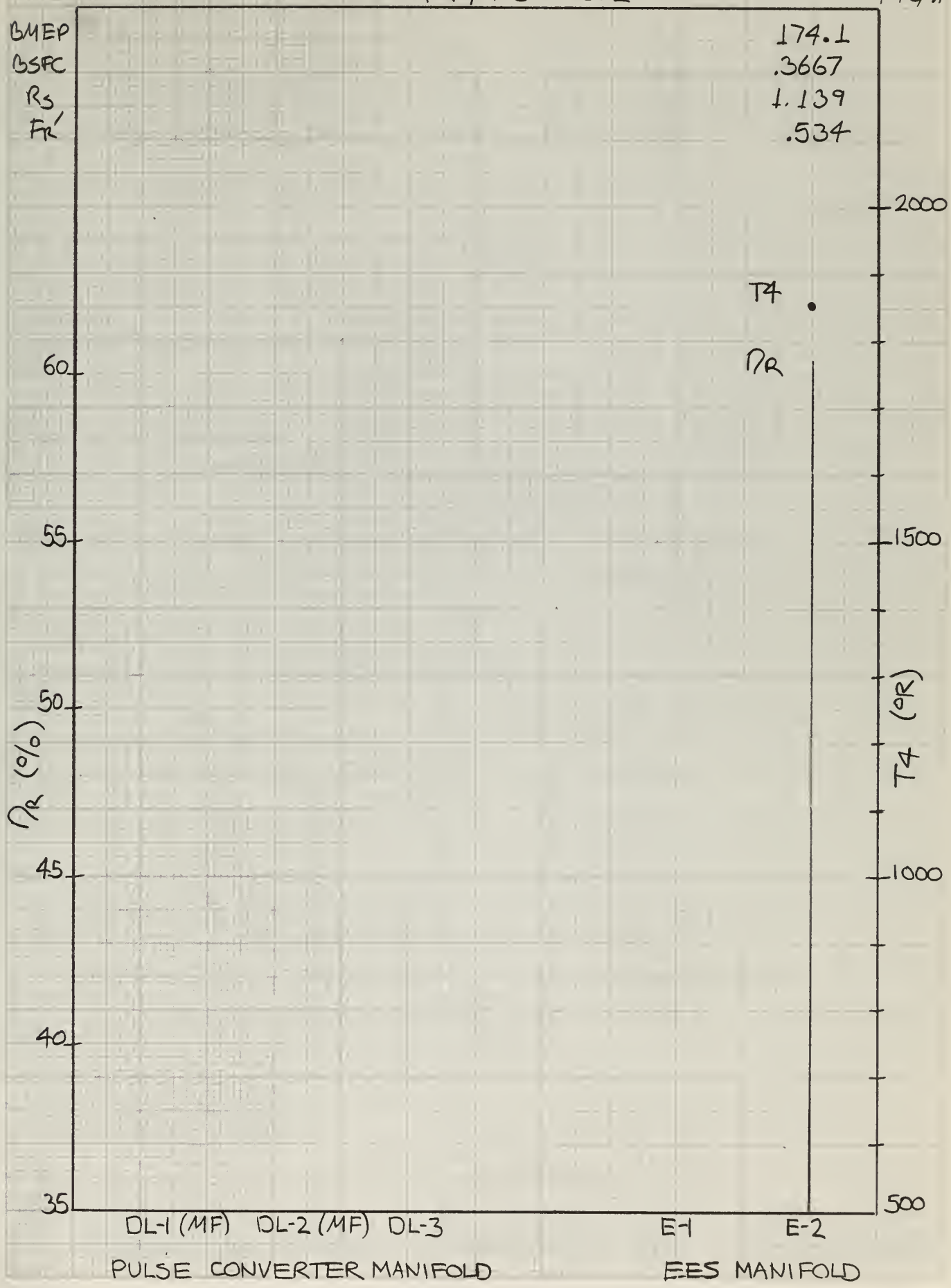

FIG. 71

DELAVAL TURBINE - EES MANIFOLD $P_4/P_6 = 3.2$

BMEP (PSI)	71.5	72.7	73.1	71.3	71.0	71.8	73.1
BSFC	.3972	.3932	.3910	.3988	.3984	.3963	.3915
R_S	.996	.989	.984	1.018	.989	.984	1.025
F_R	.395	.403	.407	.393	.388	.399	.392

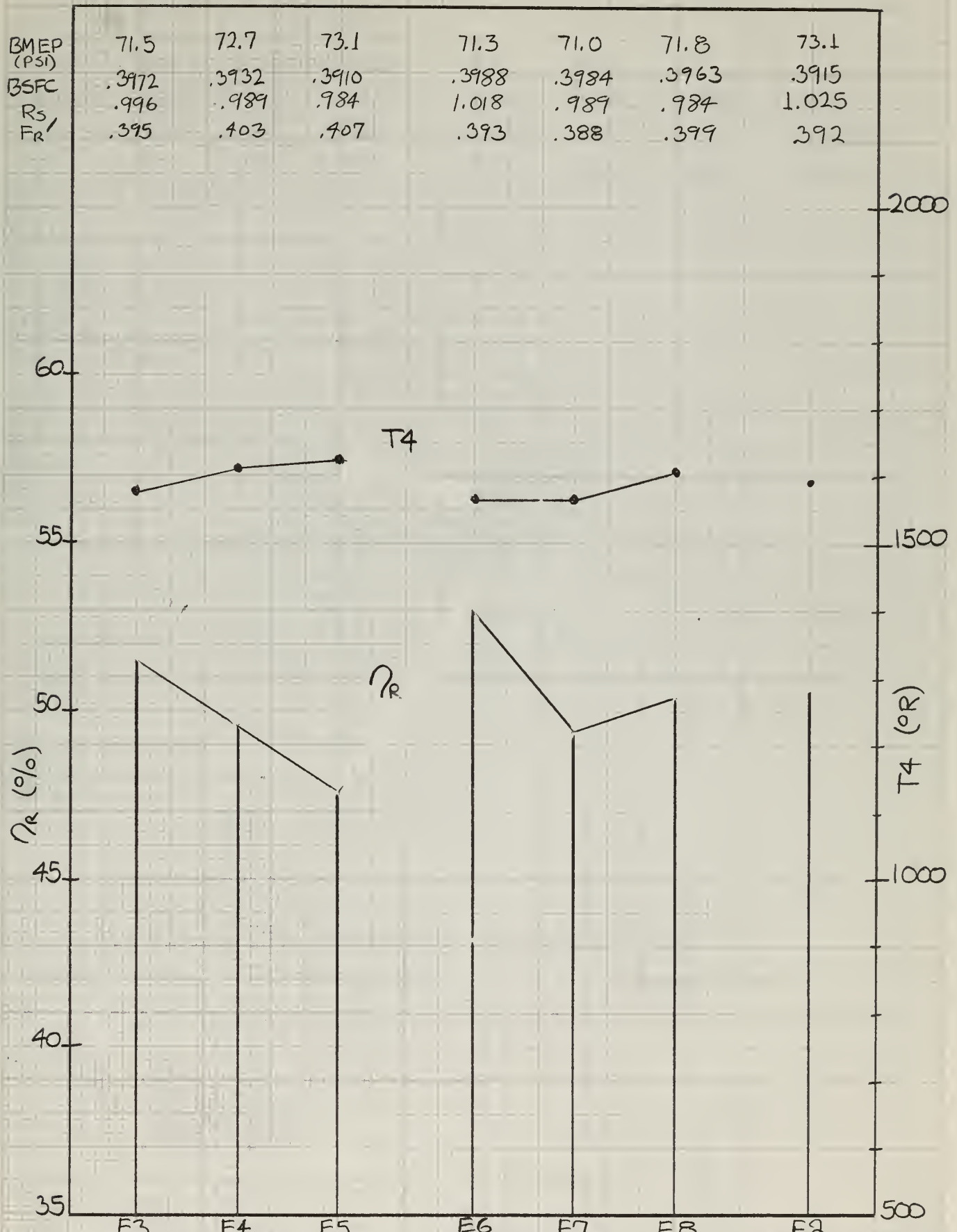

FIG. 72

DELAVAL TURBINE - EES MANIFOLD $P_4/P_6 = 3.7$

BMEP	90.1	91.2	92.2	89.3	89.3	90.5	91.4
BSFC	.3782	.3764	.3745	.3818	.3806	.3792	.3742
R_S	1.023	1.023	1.017	1.035	1.031	1.021	1.058
F_R'	.429	.433	.445	.426	.424	.433	.427

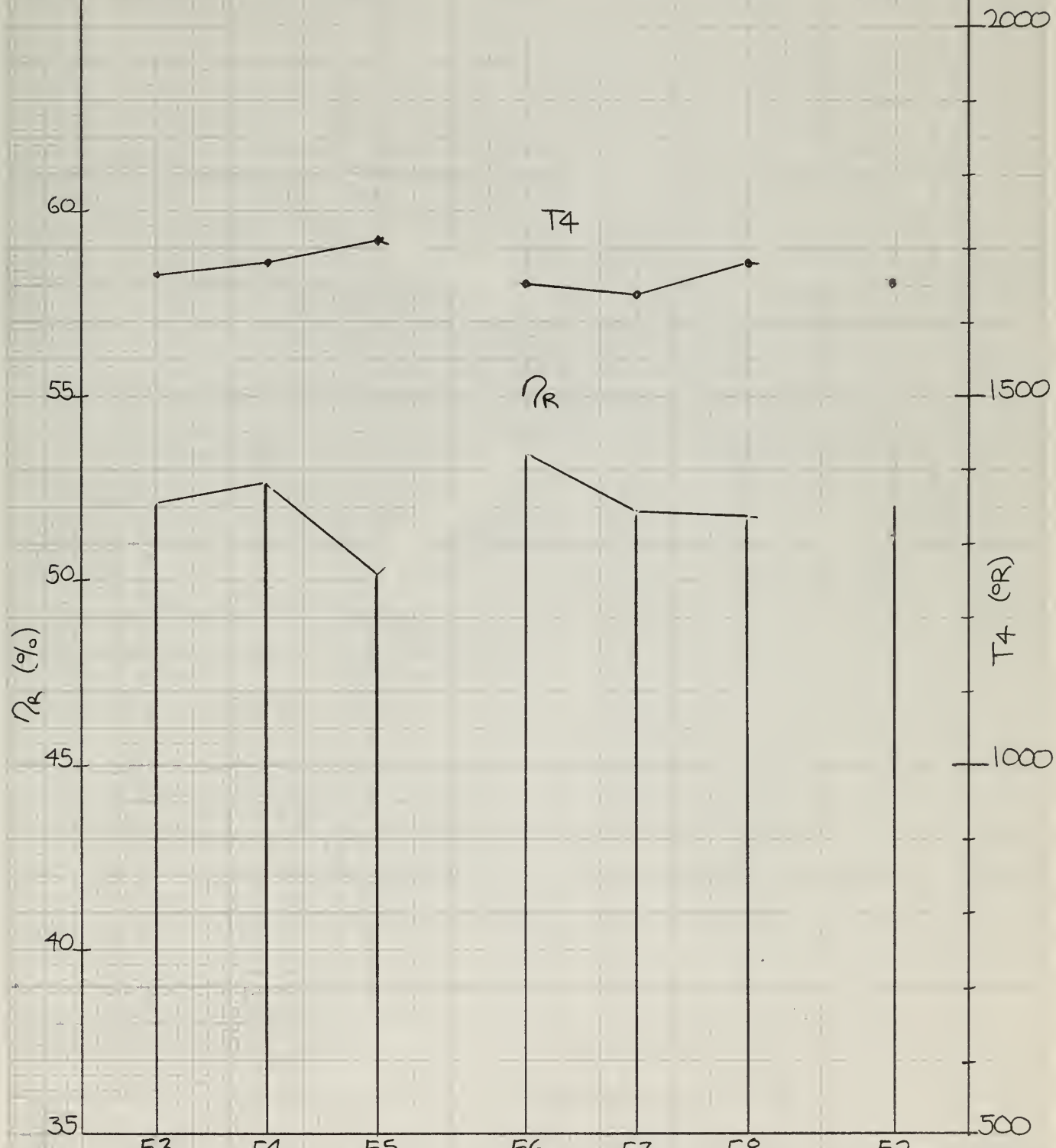

FIG. 73

DELAVAL TURBINE – EES MANIFOLD $P_4/P_6 = 4.2$

	E3	E4	E5	E6	E7	E8	E2
BMEP	107.0	108.0	109.4	106.0	107.0	108.0	108.8
BSFC	.3718	.3702	.3688	.3738	.3719	.3697	.3660
R_S	1.050	1.052	1.044	1.053	1.062	1.052	1.088
F_R'	.456	.461	.476	.451	.447	.460	.458

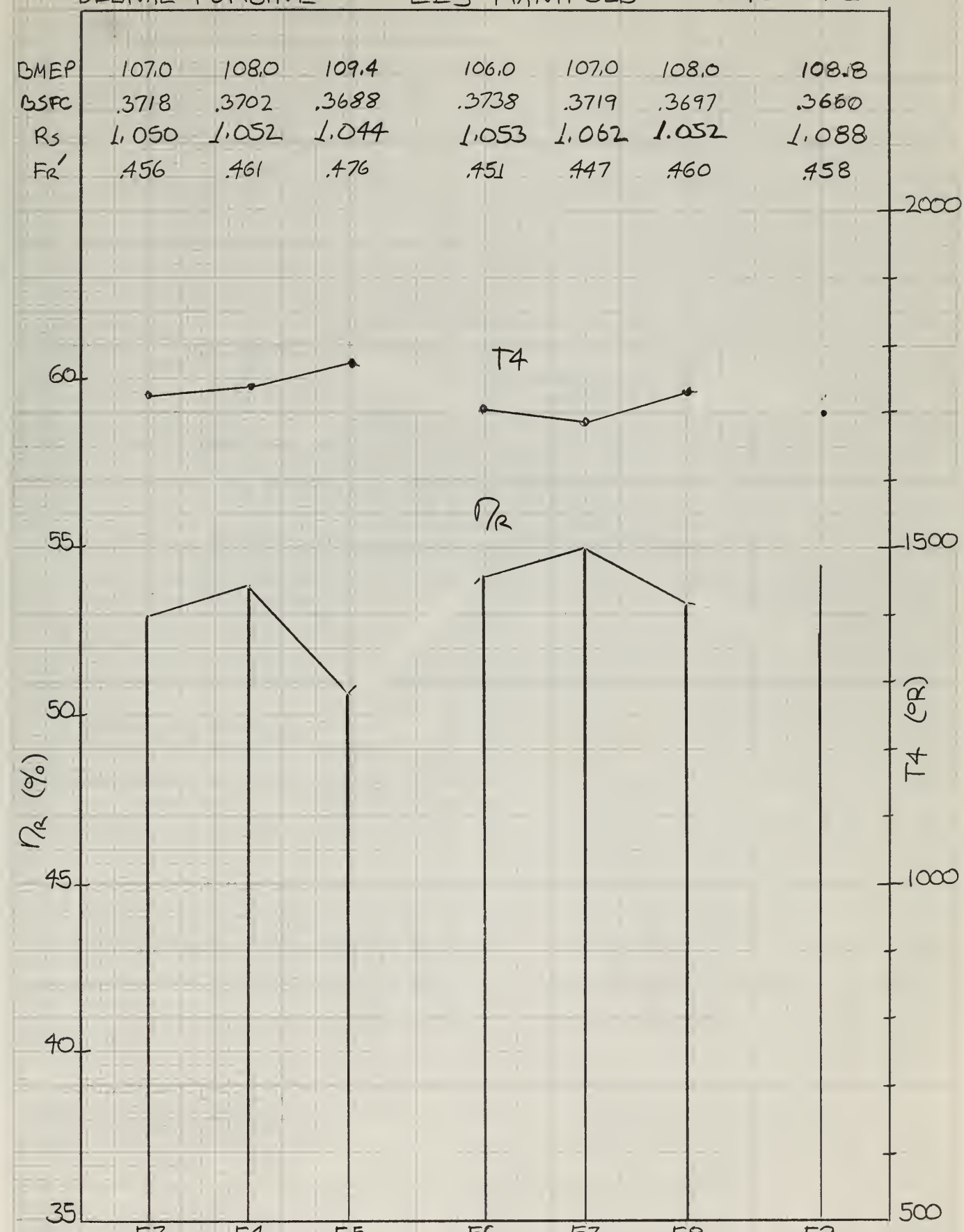

E3 E4 E5 — CHARGER PLATE – 40.8 IN² — E6 E7 E8 — CHARGER PLATE – 23.0 IN² — E2 NO CHARGER PLATE

PLATE SPACING – 3" 6" 9" 3" 6" 9"

FIG. 74

DELAVAL TURBINE – EES MANIFOLD $P_4/P_6 = 4.7$

BMEP	123.1	124.4	125.6	123.0	124.3	124.7	**125.6**
BSFC	.3689	.3678	.3665	.3693	.3674	.3656	
R_s	1.074	1.072	1.066	1.068	1.082	1.077	**1.115**
F_R'	.480	.487	.498	.475	.471	.464	**.476**

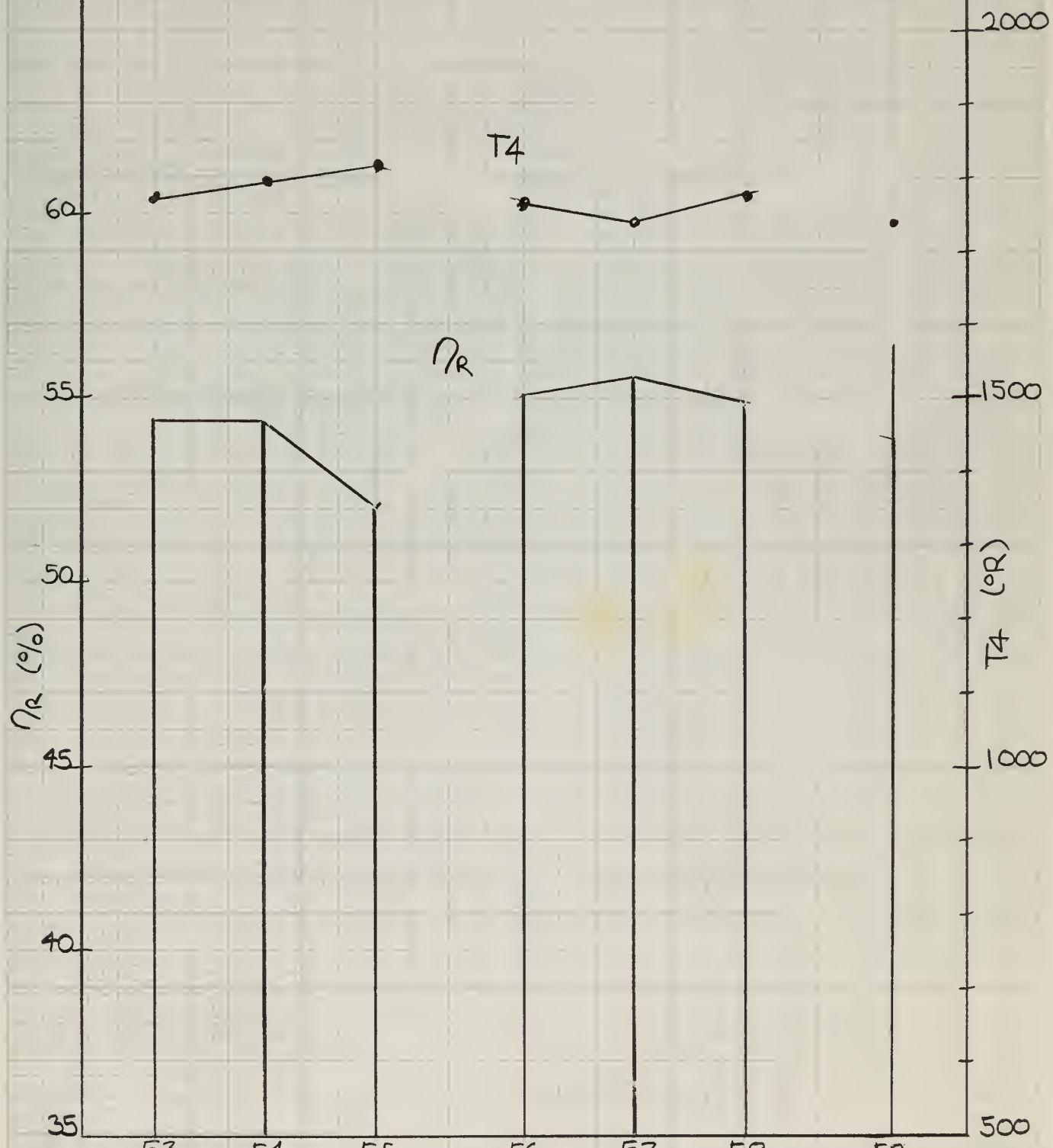

FIG. 75

DELAVAL TURBINE – EES MANIFOLD $P_4/P_6 = 5.2$

BMEP	139.0	139.4	142.4	139.2	140.8	142.0	144.0
BSFC	.3694	.3685	.3669	.3688	.3667	.3645	.3622
R_s	1.094	1.091	1.085	1.087	1.103	1.097	1.131
F_R'	.500	.509	.520	.495	.490	.505	.488

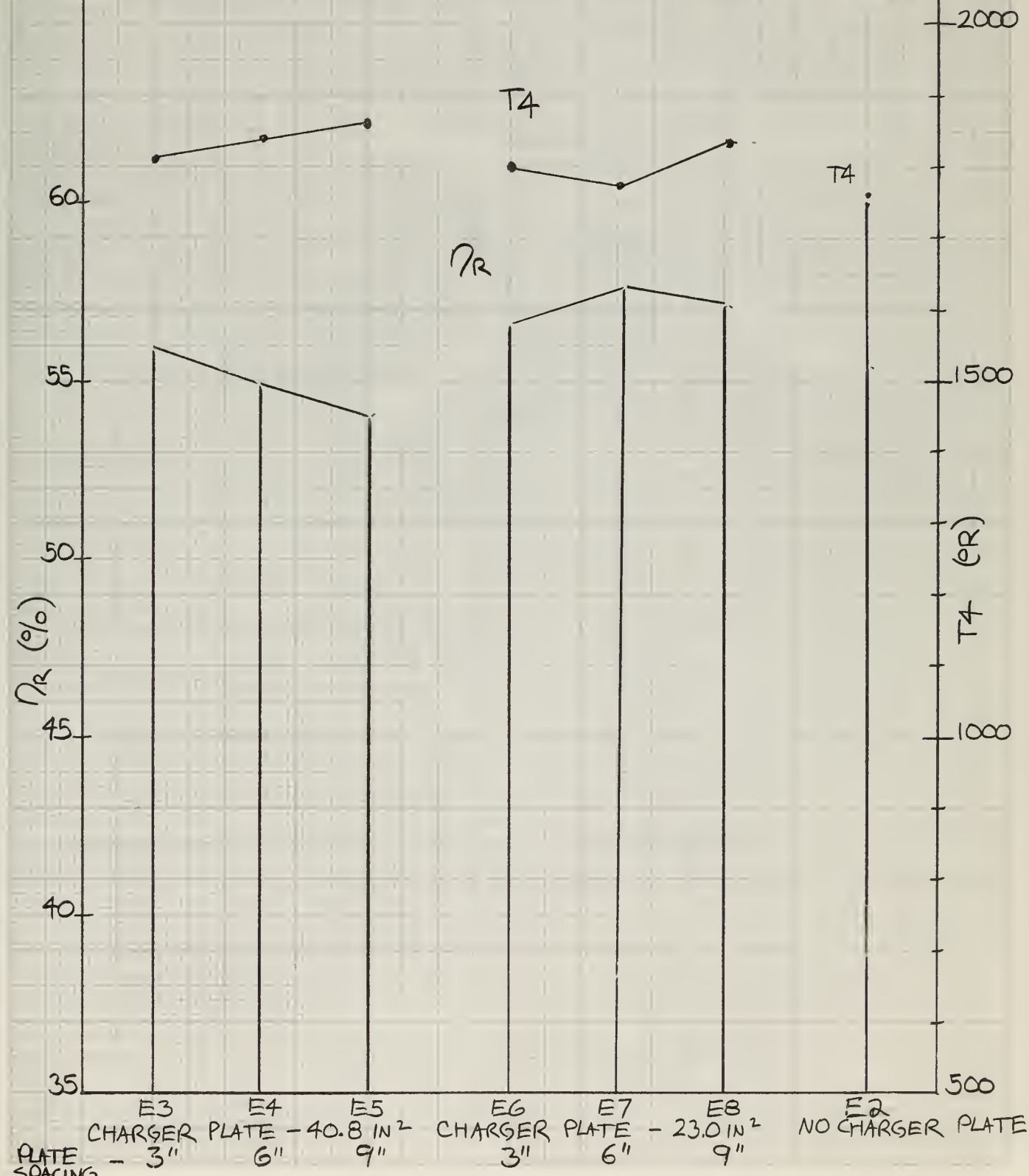

FIG. 76

DELAVAL TURBINE - EES MANIFOLD $P_4/P_6 = 5.7$

	E3	E4	E5	E6	E7	E8	E9
BMEP	154.8	157.0	157.1	154.4	156.4	159.7	159.2
BSFC	.3720	.3709	.3698	.3708	.3684	.3670	.3608
R_s	1.111	1.108	1.099	1.104	1.124	1.108	1.138
F_R'	.520	.536	.538	.512	.509	.526	.511

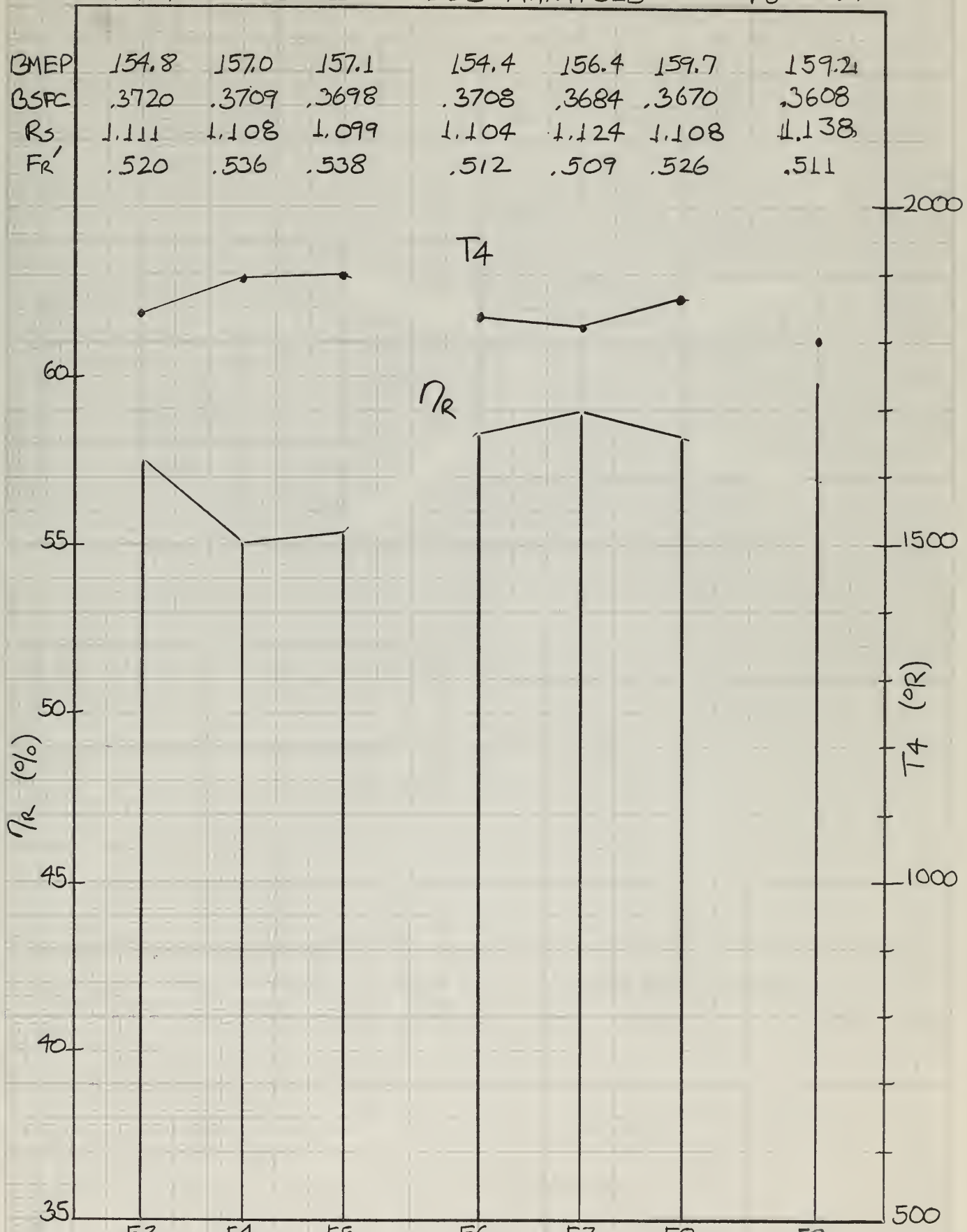

FIG. 77

DELAVAL TURB. — EES MANIFOLD $P_4/P_6 = 6.2$

BMEP	168.9	171.2	171.4	168.7	173.9	175.4	174.1
BSFC	.3763	.3761	.3748	.3755	.3756	.3731	.3666
R_s	1.124	1.121	1.112	1.117	1.141	1.110	1.139
F_R'	.536	.559	.558	.529	.517	.530	.534

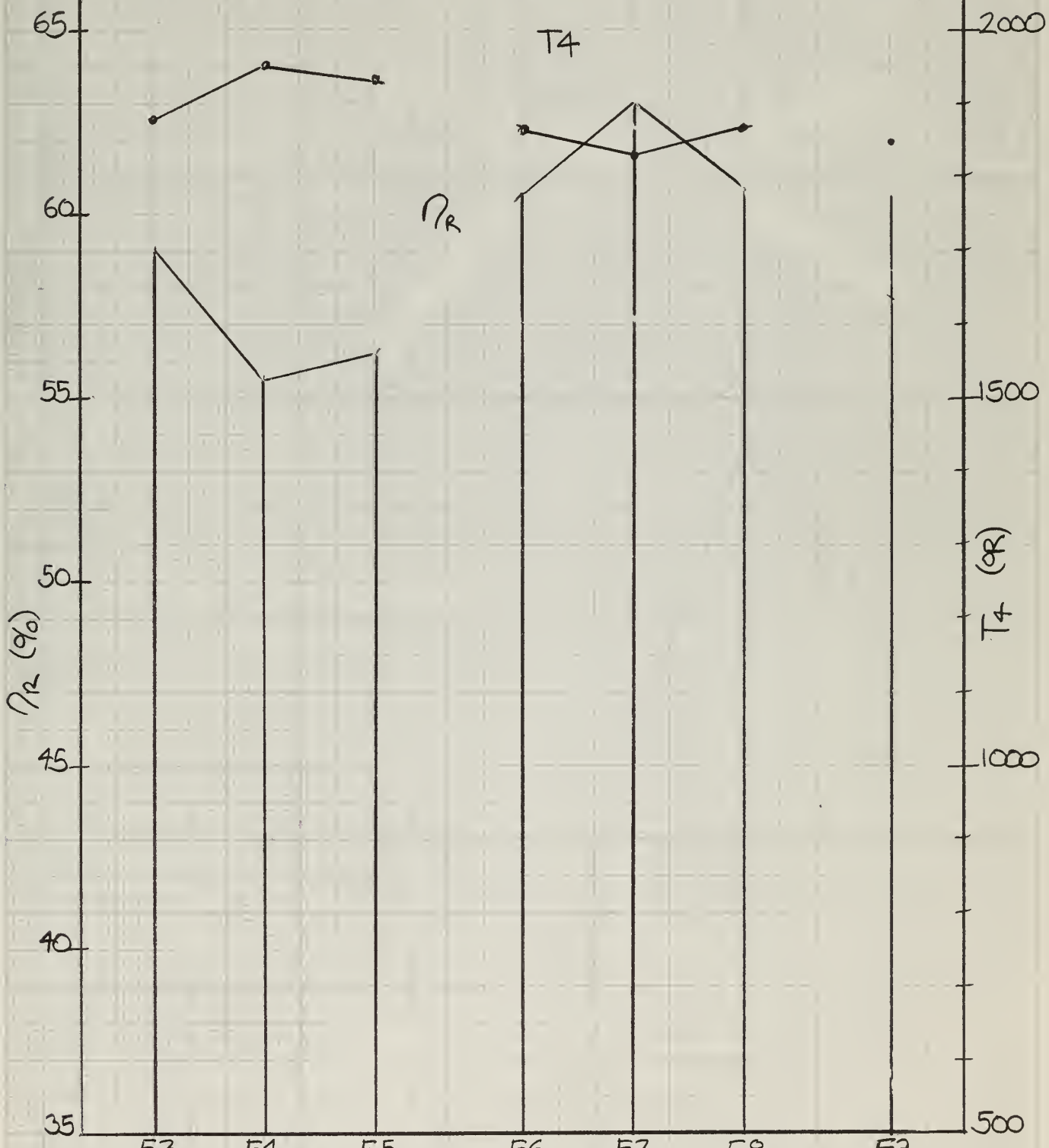

DELAVAL STEADY-FLOW TURBOCHARGERS
8 CYL. ENGINE

FIG. 78

BMEP	53.2	56.2	54.1	71.2	74.6	71.2
BSFC	.502	.463	.487	.471	.433	.452
F_R'	.793	.679	.686	.756	.636	.665

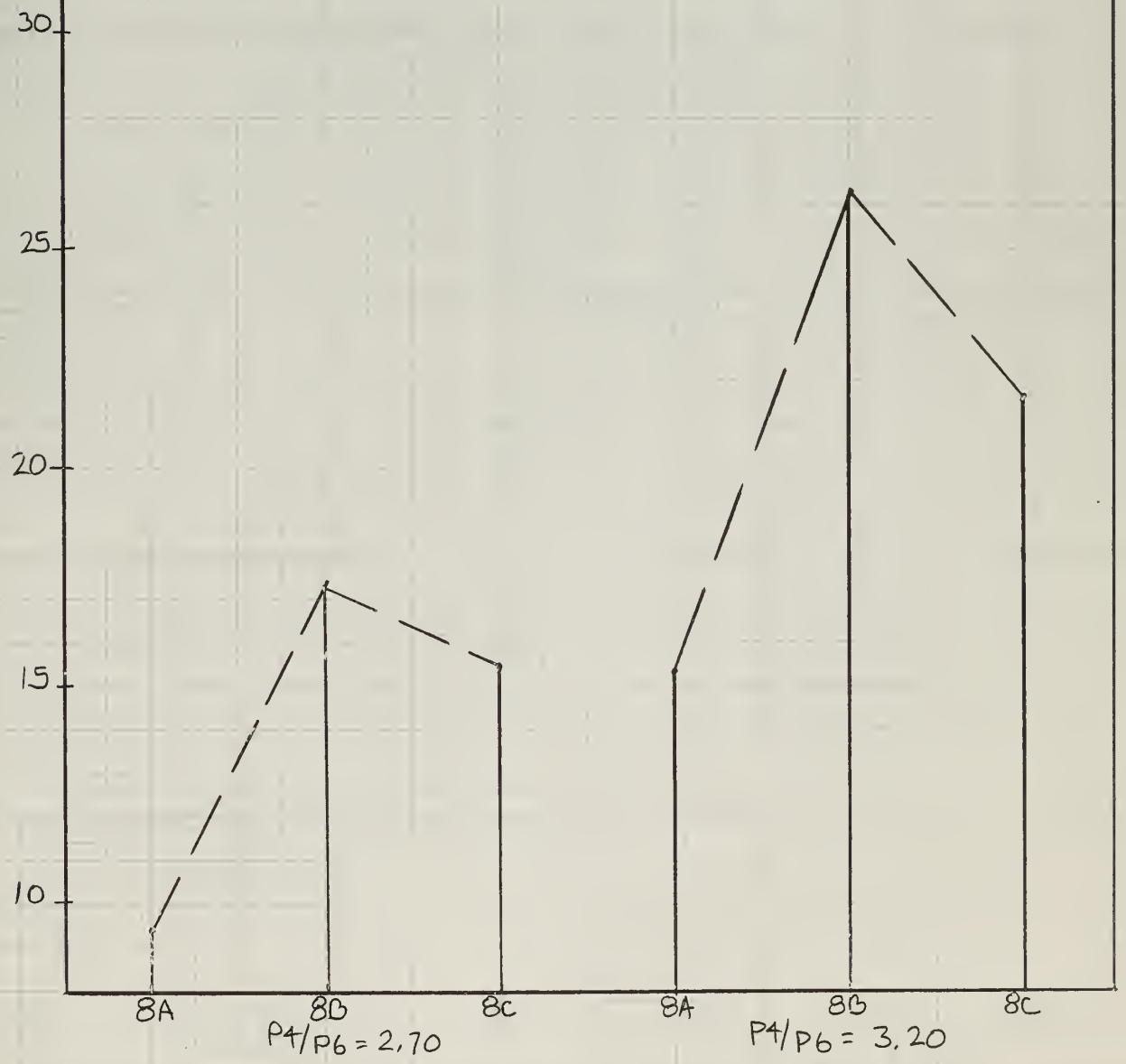

DELAVAL "STEADY FLOW" TURBOCHARGERS
8 CYL. ENGINE

FIG. 79

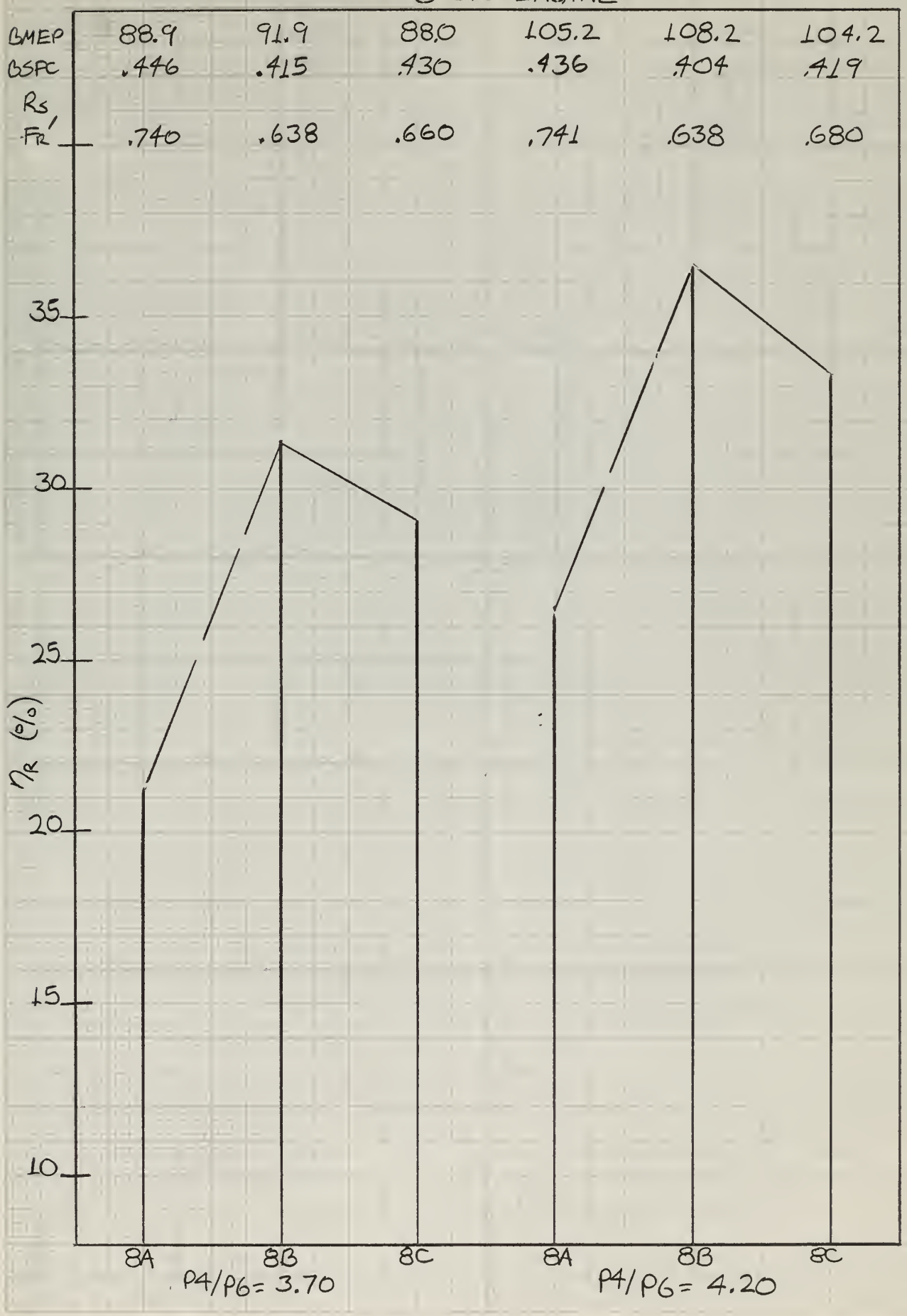

DELAVAL "STEADY FLOW" TURBOCHARGERS FIG. 80
8 CYL. ENGINE

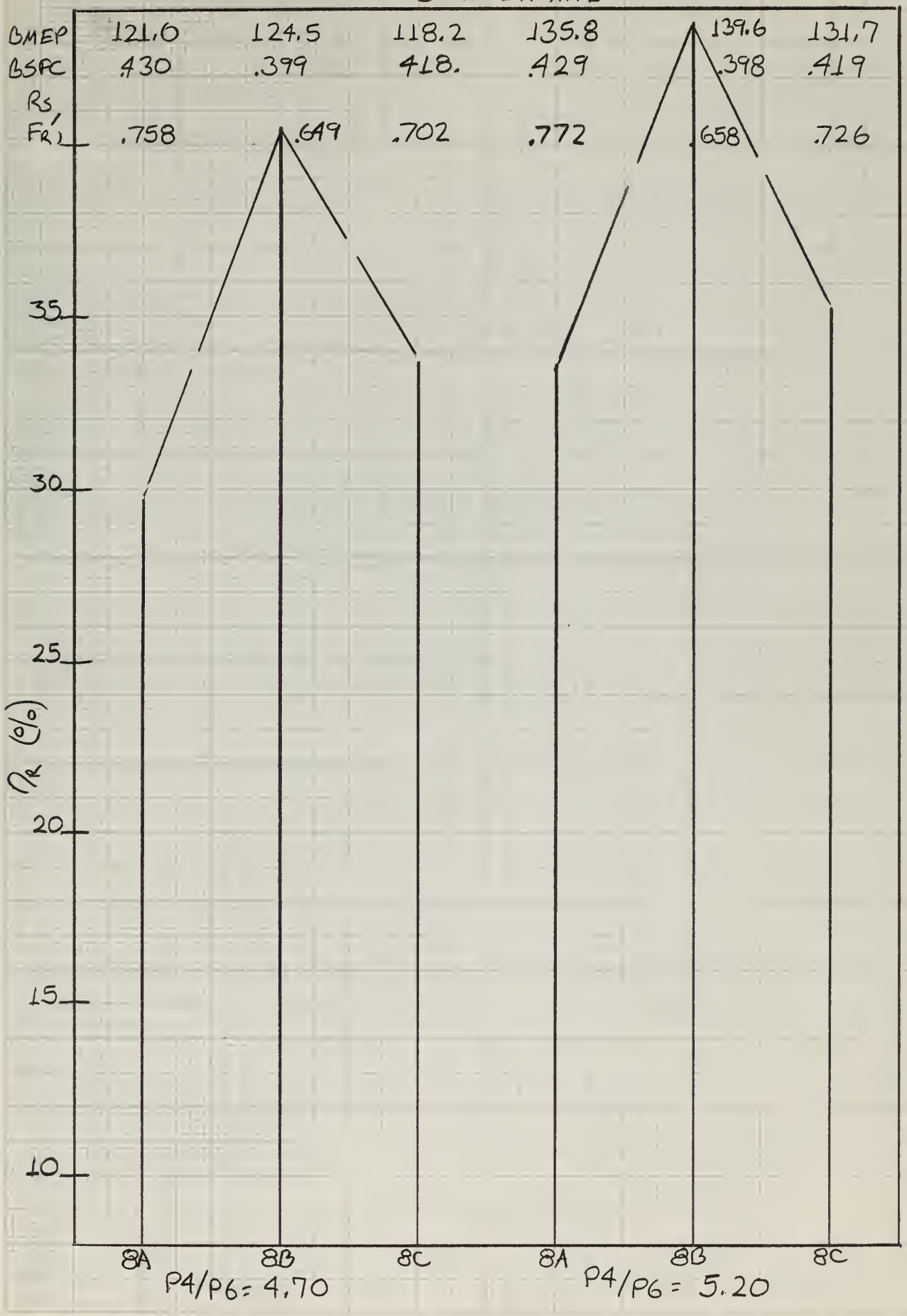

DELAVAL "STEADY FLOW" TURBOCHARGERS FIG. 81

8 CYL. ENGINE

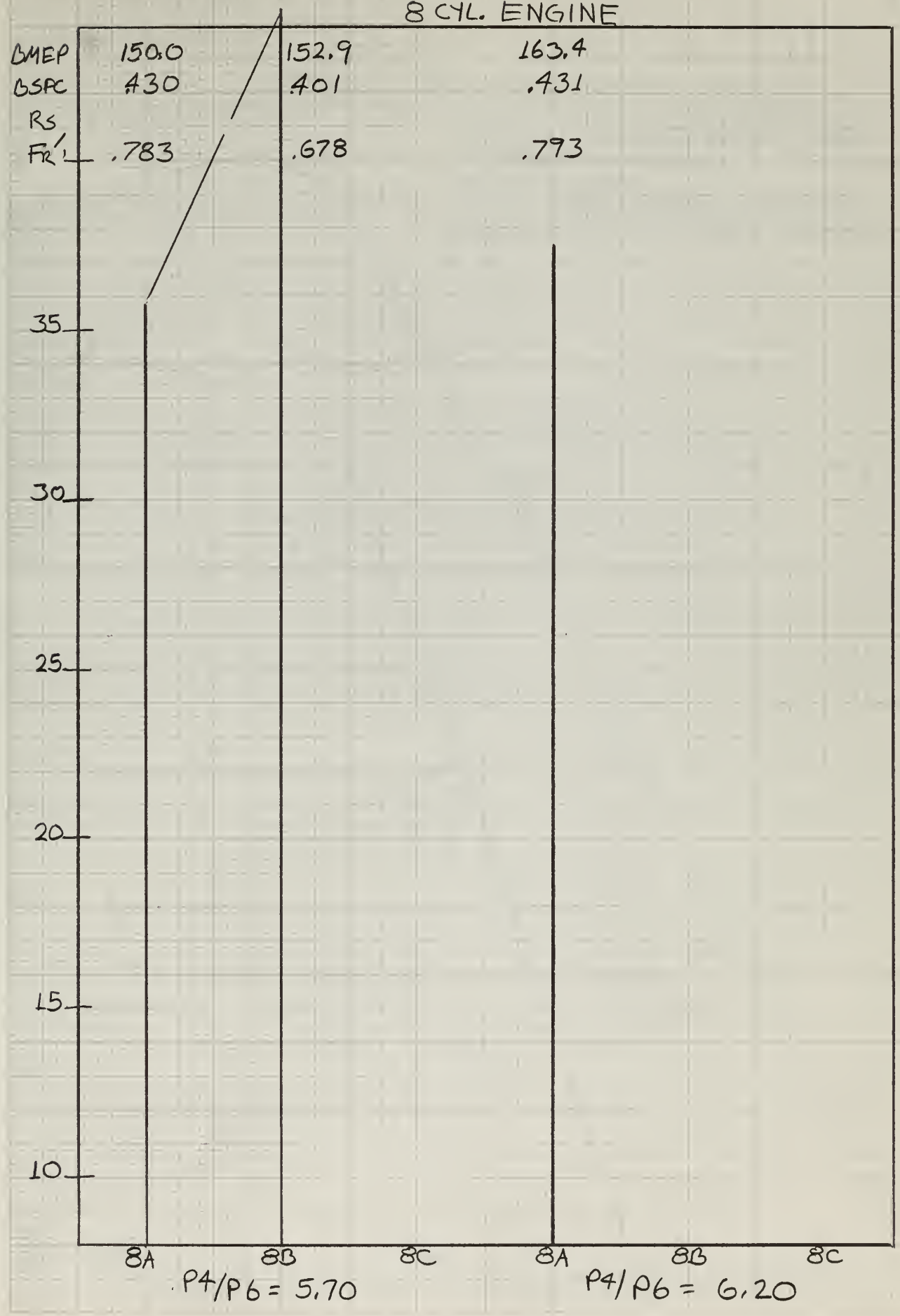

FIG. 82

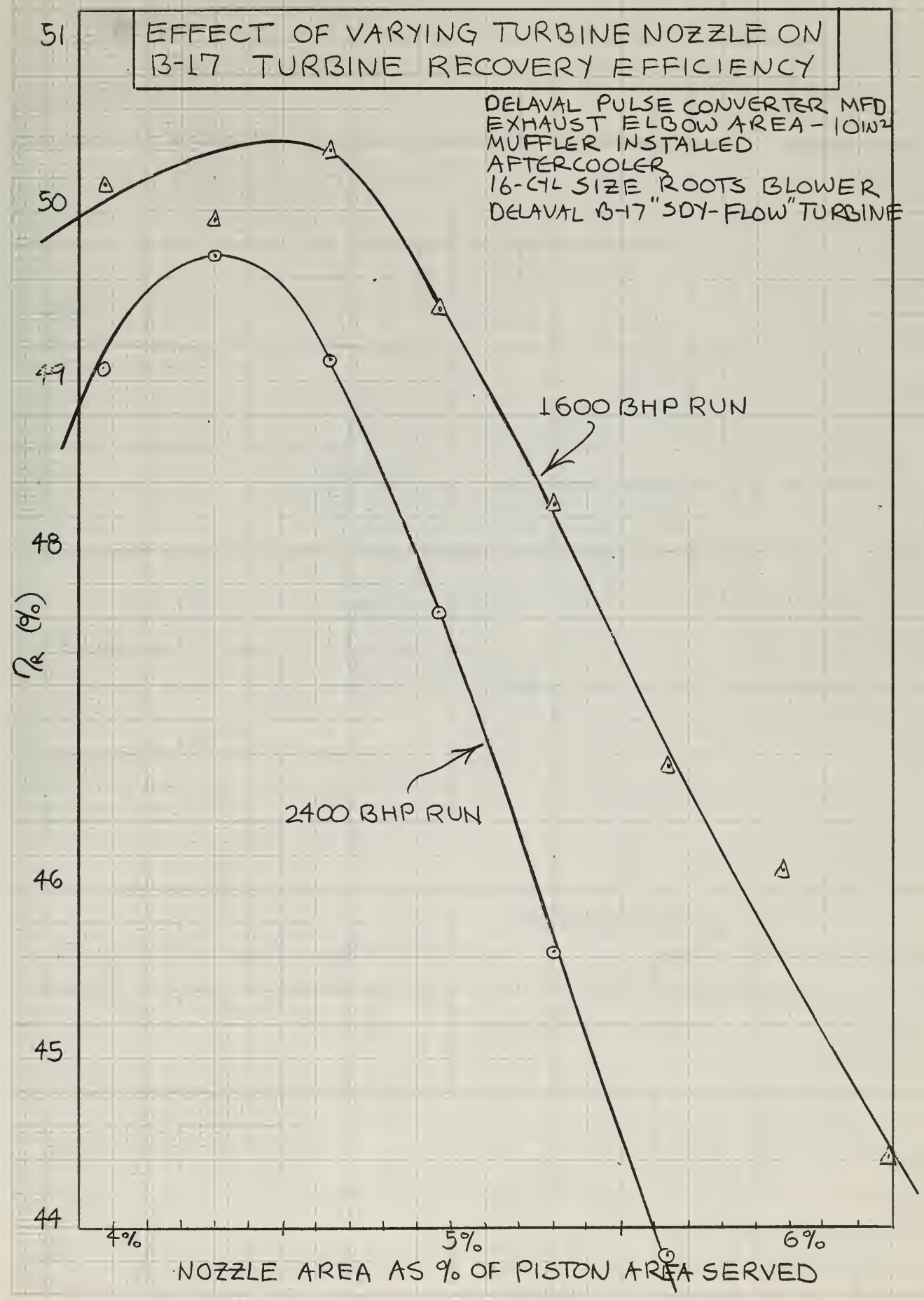
EFFECT OF VARYING TURBINE NOZZLE ON B-17 TURBINE RECOVERY EFFICIENCY
DELAVAL PULSE CONVERTER MFD
EXHAUST ELBOW AREA - 10IN²
MUFFLER INSTALLED
AFTERCOOLER
16-CYL SIZE ROOTS BLOWER
DELAVAL B-17 "SOY-FLOW" TURBINE
1600 BHP RUN
2400 BHP RUN
51
50
49
48
46
45
44
ηc (%)
4%
5%
6%
NOZZLE AREA AS % OF PISTON AREA SERVED

FIG. 83

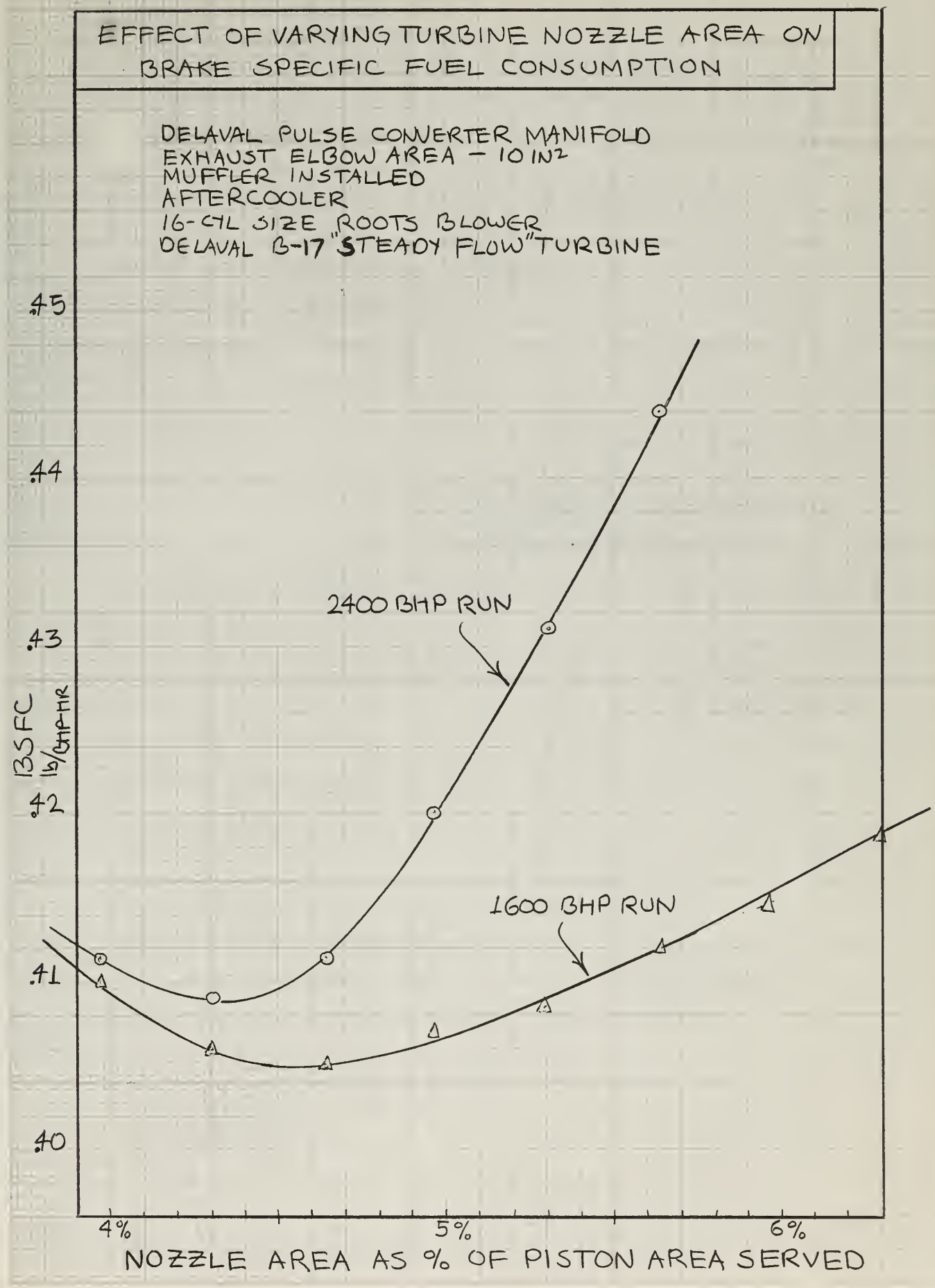
EFFECT OF VARYING TURBINE NOZZLE AREA ON BRAKE SPECIFIC FUEL CONSUMPTION
DELAVAL PULSE CONVERTER MANIFOLD
EXHAUST ELBOW AREA – 10 IN²
MUFFLER INSTALLED
AFTERCOOLER
16-CYL SIZE ROOTS BLOWER
DELAVAL B-17 "STEADY FLOW" TURBINE
.45
.44
.43
.42
.41
.40
BSFC lb/BHP-HR
2400 BHP RUN
1600 BHP RUN
4%
5%
6%
NOZZLE AREA AS % OF PISTON AREA SERVED

FIG. 84

DELAVAL PULSE CONVERTER MANIFOLD
WITH DELAVAL B-17 TURBOCHGR

EXHAUST ELBOW AREA – 10 IN²
EXHAUST ELBOW LENGTH – 26 IN
TURBINE NOZZLE AREA – 42 IN² (4.3%)
MUFFLER INSTALLED
LARGE SIZE ENGINE DRIVEN BLOWER
AFTERCOOLER INSTALLED

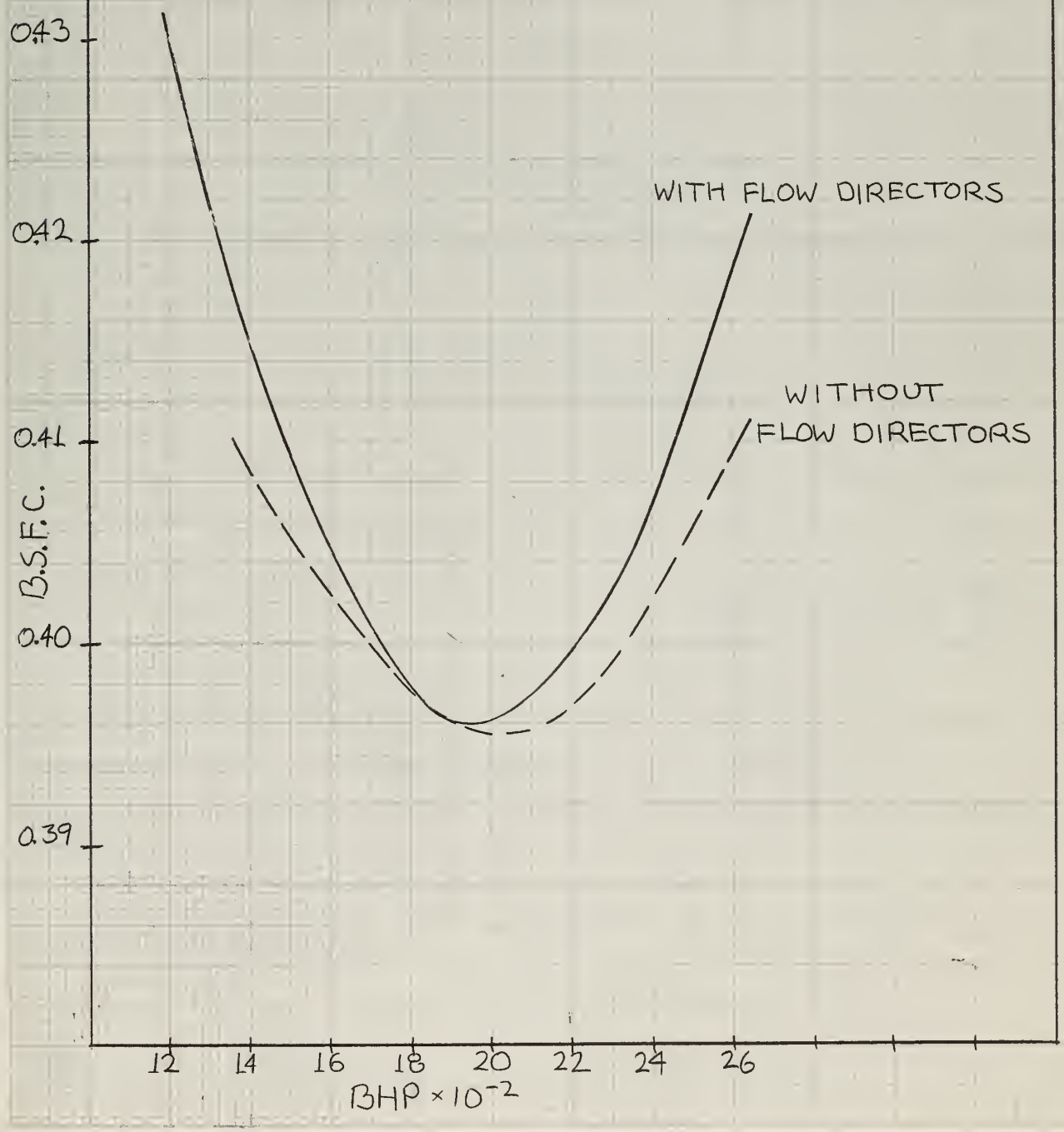

FIG. 85

DELAVAL PULSE CONVERTER MANIFOLD
WITH DELAVAL B-17 TURBOCHARGER

EXHAUST ELBOW LENGTH — 26 IN
TURBINE NOZZLE AREA - 38 IN^2 (4.09%)
MUFFLER BY-PASSED
SMALL SIZE ENGINE-DRIVEN BLOWER
AFTER COOLER INSTALLED

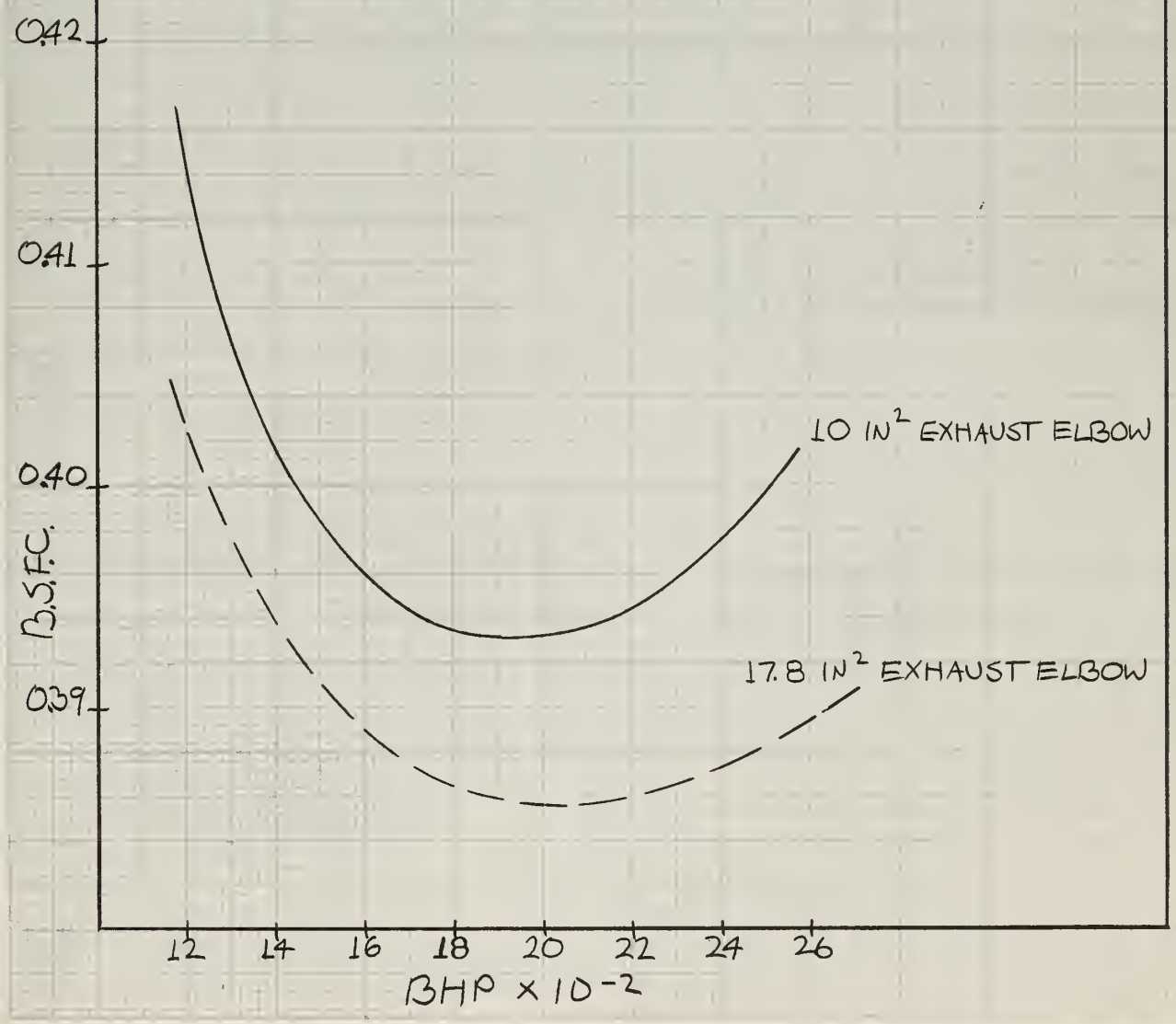

FIG. 86

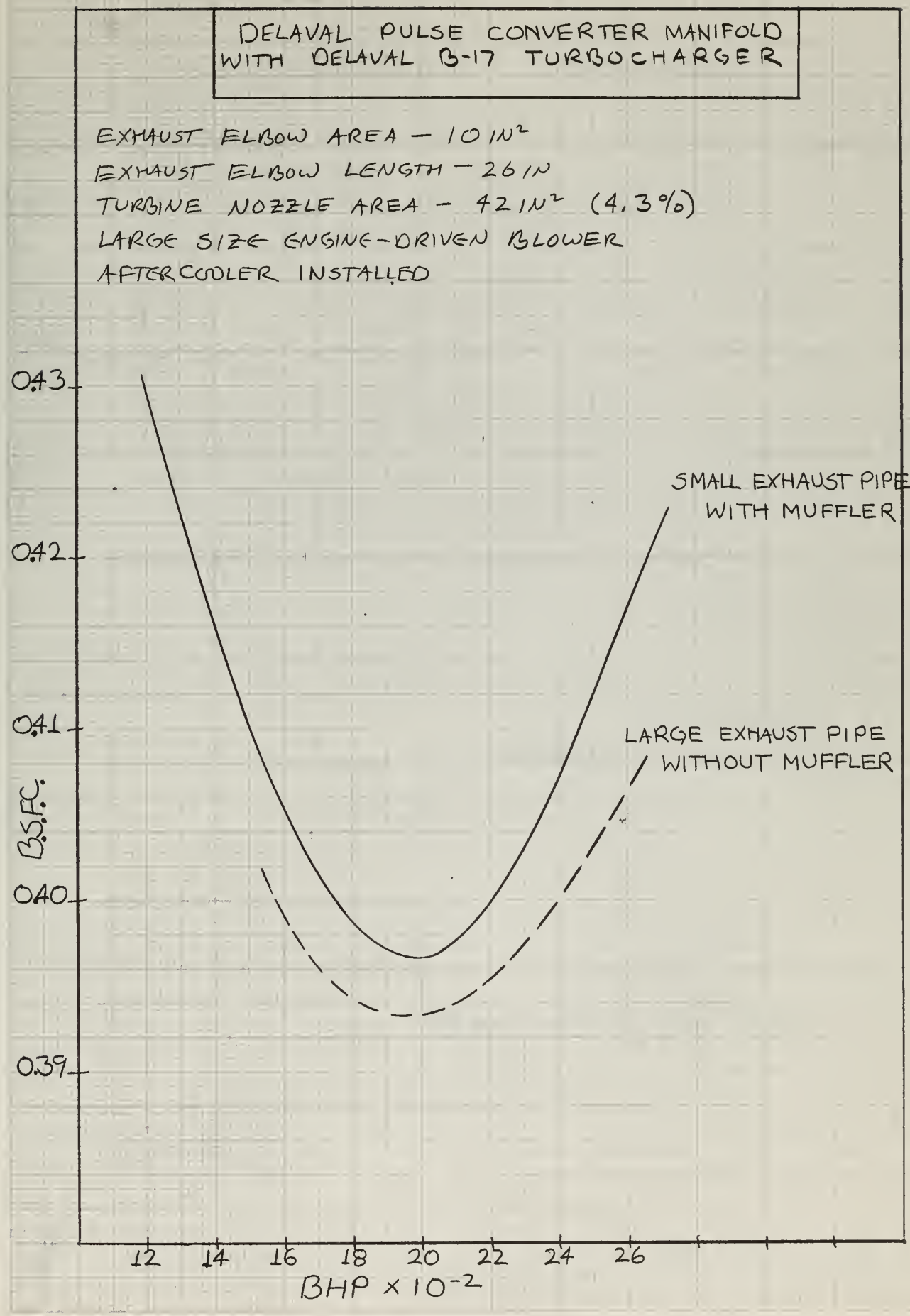
DELAVAL PULSE CONVERTER MANIFOLD
WITH DELAVAL B-17 TURBOCHARGER
EXHAUST ELBOW AREA – 10 IN²
EXHAUST ELBOW LENGTH – 26 IN
TURBINE NOZZLE AREA – 42 IN² (4.3%)
LARGE SIZE ENGINE-DRIVEN BLOWER
AFTERCOOLER INSTALLED
0.43
0.42
0.41
0.40
0.39
B.S.F.C.
SMALL EXHAUST PIPE WITH MUFFLER
LARGE EXHAUST PIPE WITHOUT MUFFLER
12
14
16
18
20
22
24
26
BHP x 10⁻²

FIG. 87

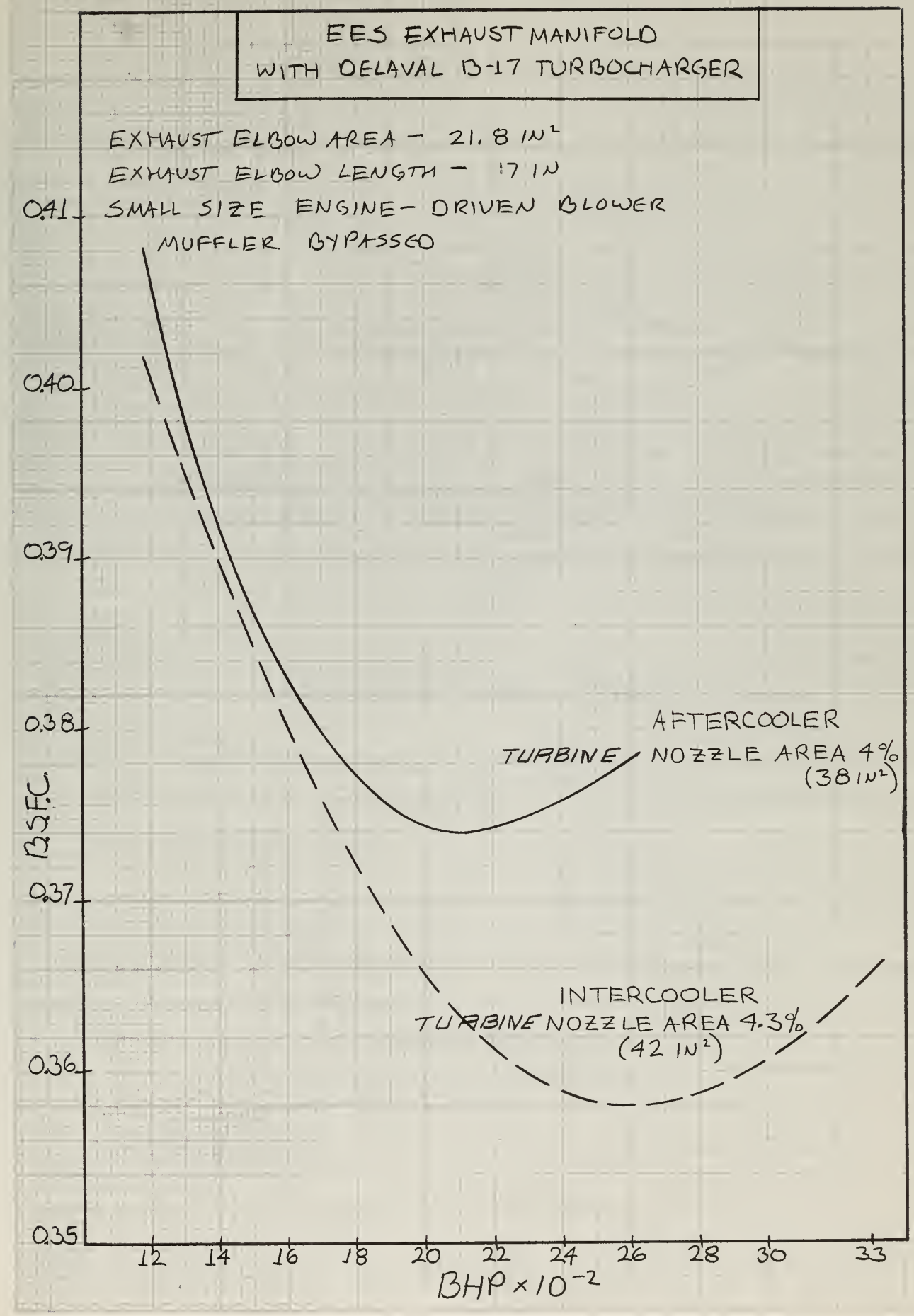
EES EXHAUST MANIFOLD
WITH DELAVAL B-17 TURBOCHARGER
EXHAUST ELBOW AREA - 21.8 IN²
EXHAUST ELBOW LENGTH - 17 IN
SMALL SIZE ENGINE-DRIVEN BLOWER
MUFFLER BYPASSED
AFTERCOOLER
TURBINE NOZZLE AREA 4%
(38 IN²)
INTERCOOLER
TURBINE NOZZLE AREA 4.3%
(42 IN²)
BSFC
0.41
0.40
0.39
0.38
0.37
0.36
0.35
12
14
16
18
20
22
24
26
28
30
33
BHP x 10⁻²

FIG. 88

EES EXHAUST MFLD + DELAVAL B-17 TURBINE

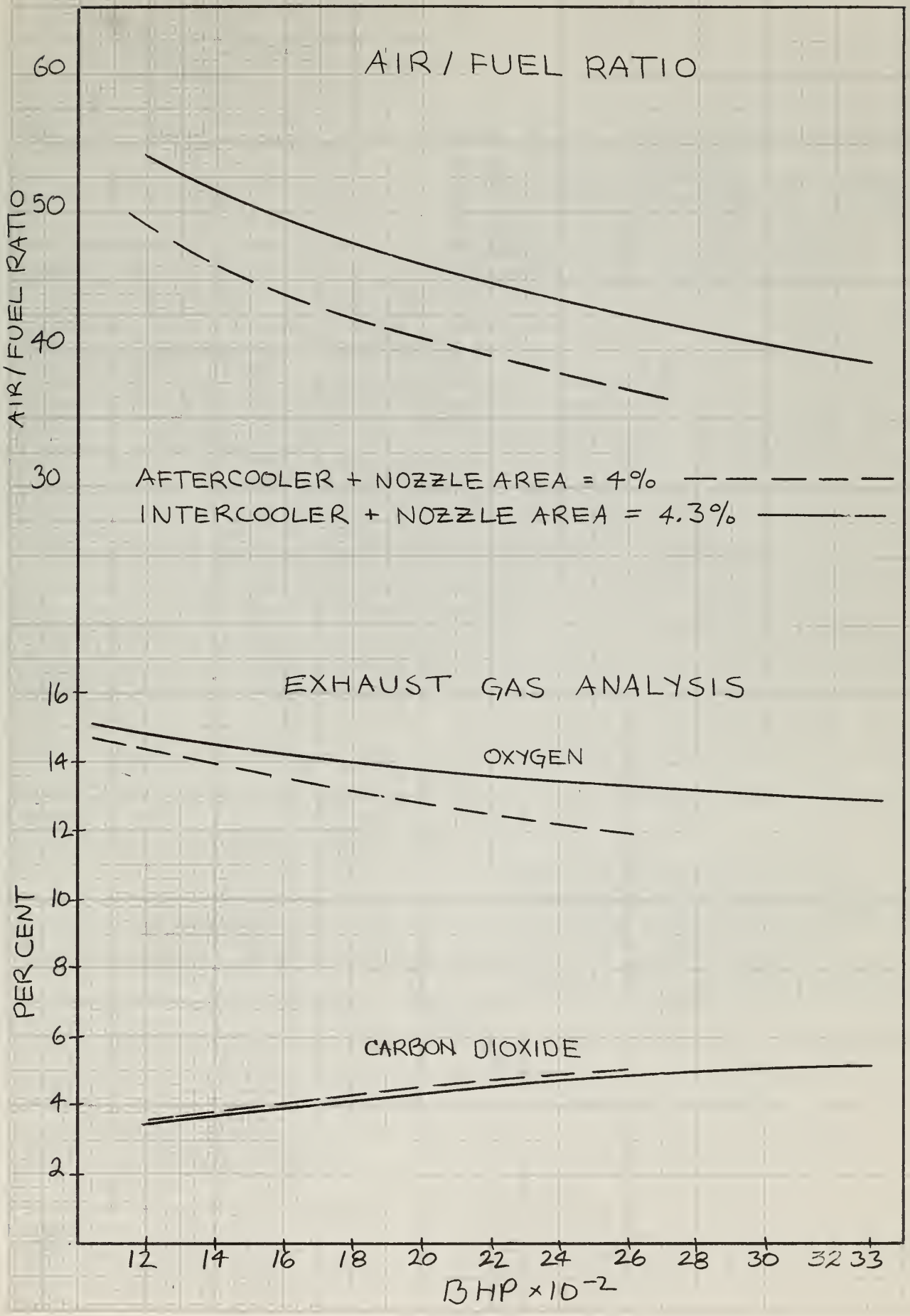

FIG. 89

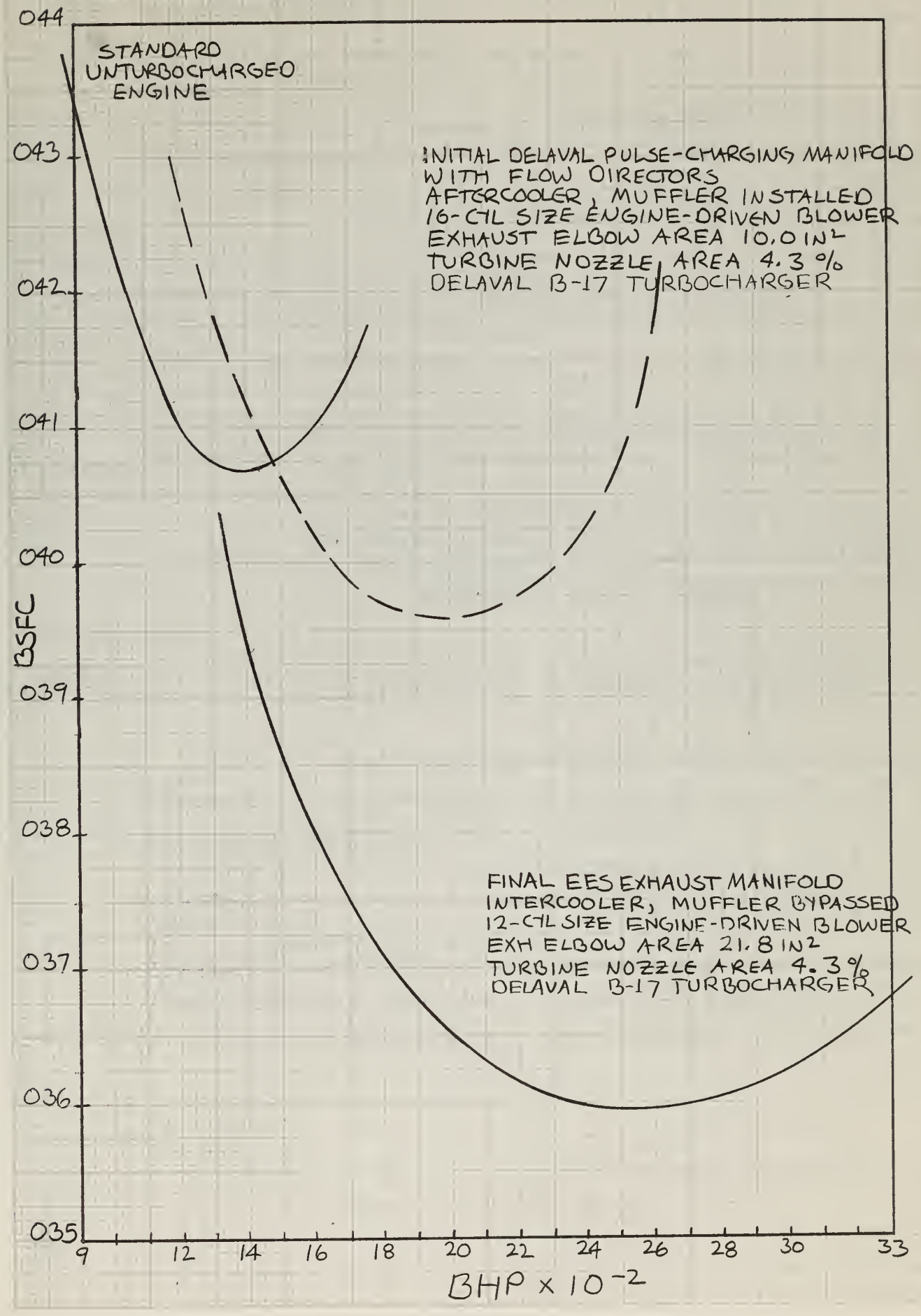
044
043
042
041
040
039
038
037
036
035
BSFC
STANDARD UNTURBOCHARGED ENGINE
INITIAL DELAVAL PULSE-CHARGING MANIFOLD
WITH FLOW DIRECTORS
AFTERCOOLER, MUFFLER INSTALLED
16-CYL SIZE ENGINE-DRIVEN BLOWER
EXHAUST ELBOW AREA 10.01 IN²
TURBINE NOZZLE AREA 4.3%
DELAVAL B-17 TURBOCHARGER
FINAL EES EXHAUST MANIFOLD
INTERCOOLER, MUFFLER BYPASSED
12-CYL SIZE ENGINE-DRIVEN BLOWER
EXH ELBOW AREA 21.8 IN²
TURBINE NOZZLE AREA 4.3%
DELAVAL B-17 TURBOCHARGER
9
12
14
16
18
20
22
24
26
28
30
33
BHP x 10⁻²

SCHEMATIC ARRANGEMENT OF DIVIDED MANIFOLD

FIG. 90

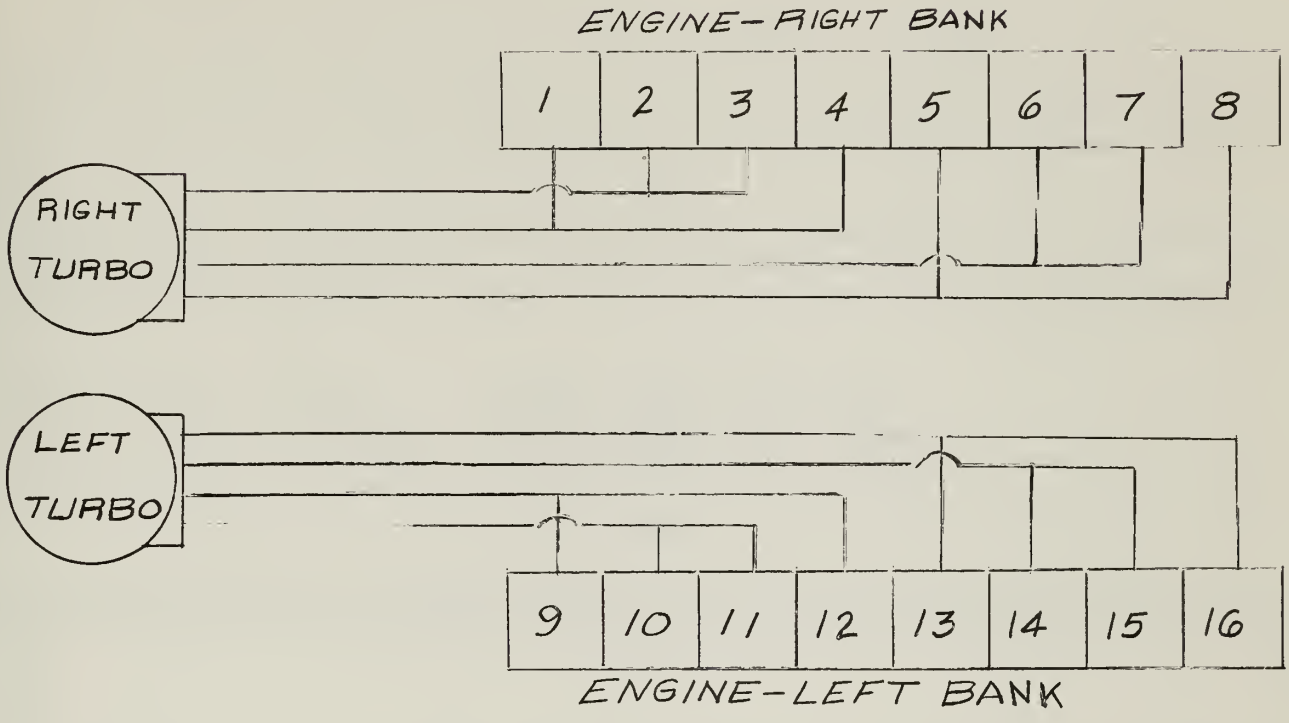

SCHEMATIC ARRANGEMENT OF COMMON MANIFOLD

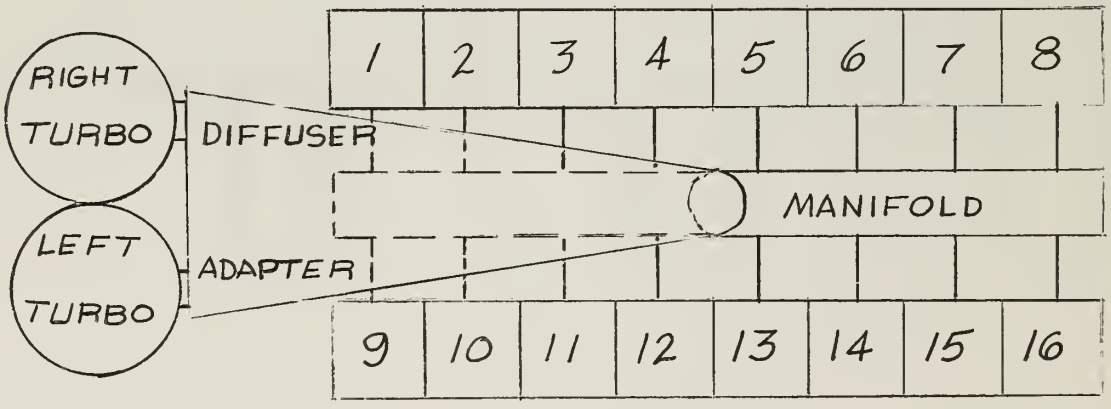

FIG. 92

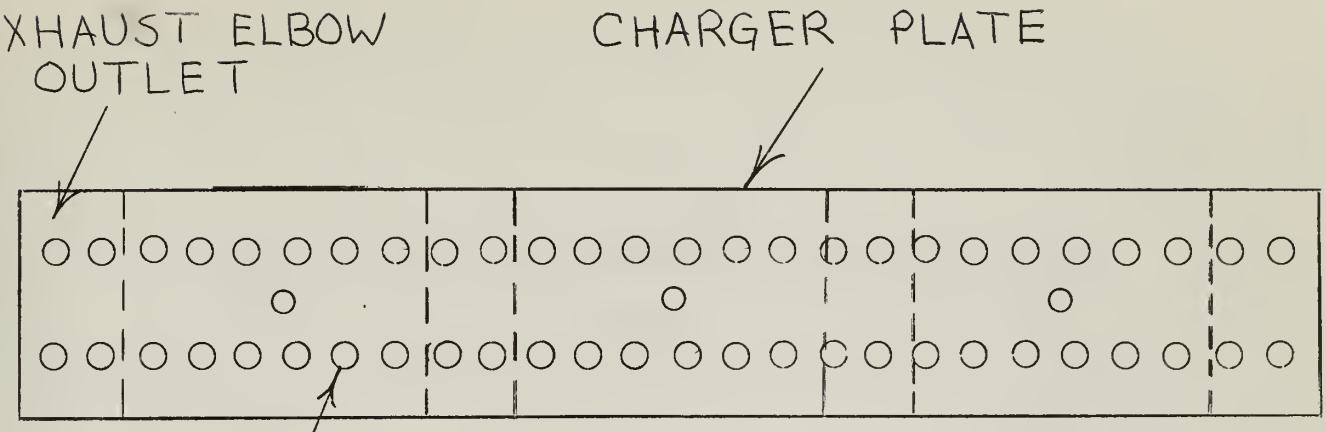

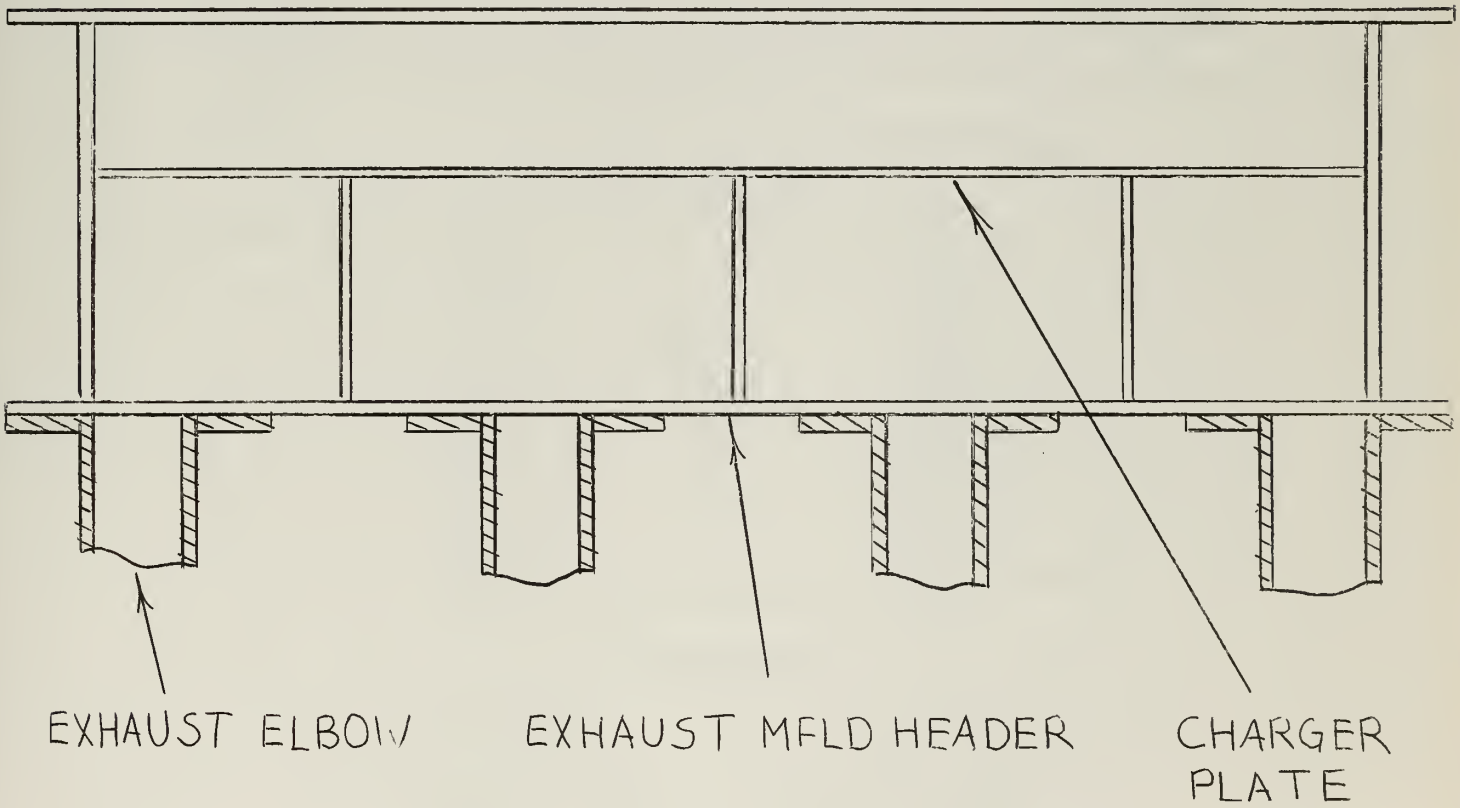

ARRGT. OF CHARGER PLATE FLOW AREA

(NOT TO SCALE)

SCHEMATIC OF MEASURING INSTR. LOCATION

FIG. 93

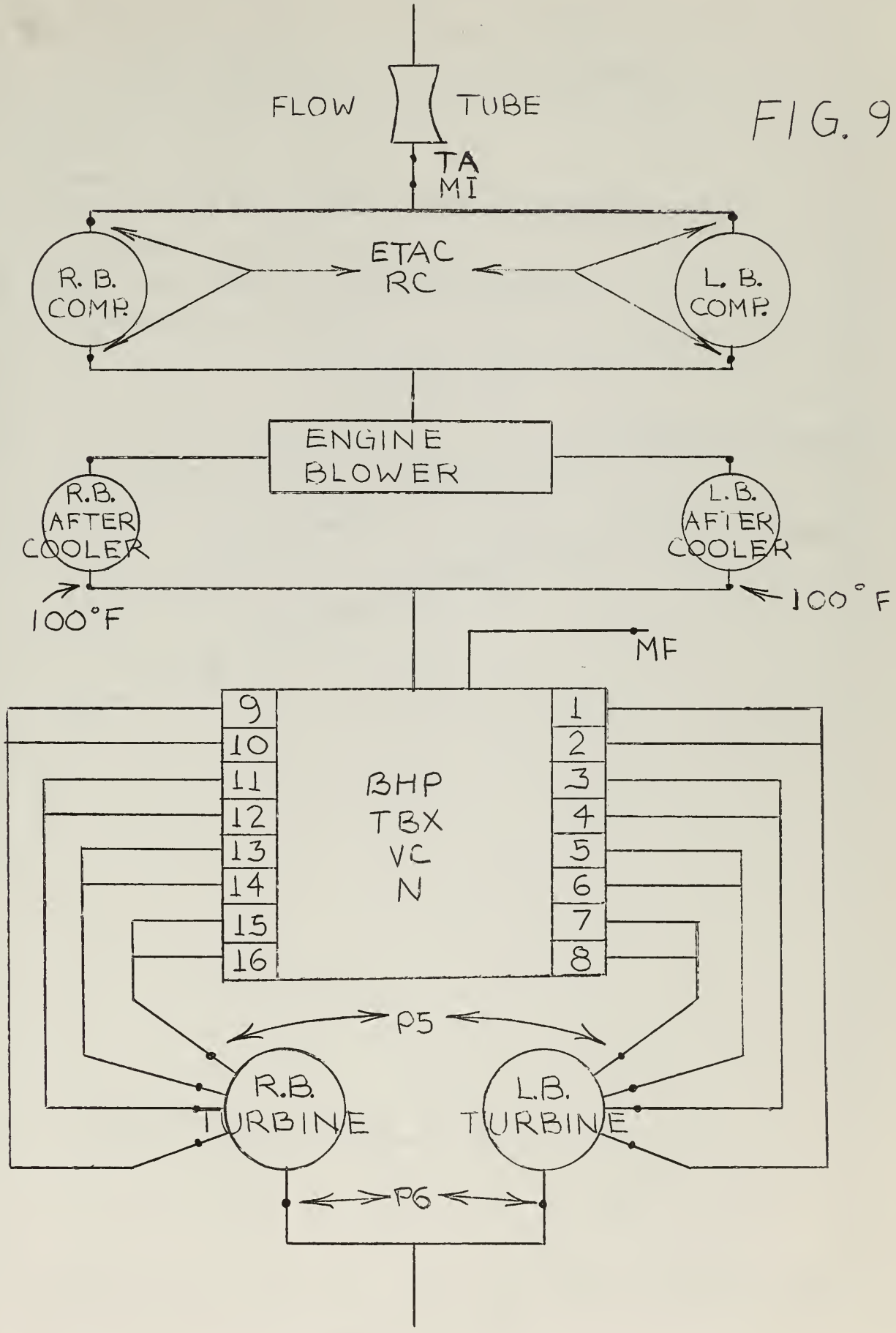

FIG. 94

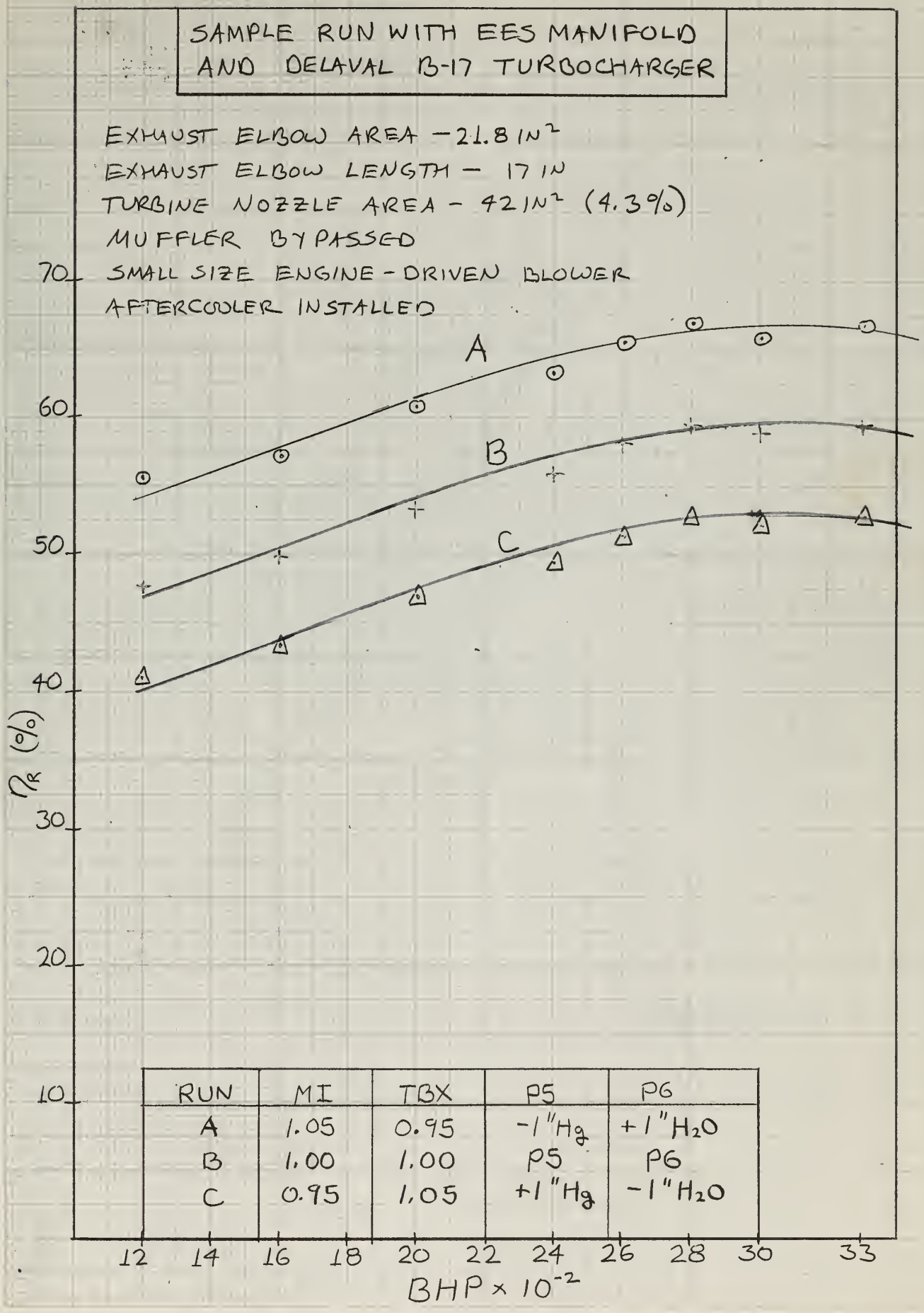
SAMPLE RUN WITH EES MANIFOLD AND DELAVAL B-17 TURBOCHARGER
EXHAUST ELBOW AREA – 21.8 IN²
EXHAUST ELBOW LENGTH – 17 IN
TURBINE NOZZLE AREA – 42 IN² (4.3%)
MUFFLER BYPASSED
SMALL SIZE ENGINE-DRIVEN BLOWER
AFTERCOOLER INSTALLED
A
B
C
70
60
50
40
30
20
10
η_R (%)
12
14
16
18
20
22
24
26
28
30
33
BHP × 10^{-2}
RUN | MI | TBX | P5 | P6
A | 1.05 | 0.95 | -1 "Hg | +1 "H₂O
B | 1.00 | 1.00 | P5 | P6
C | 0.95 | 1.05 | +1 "Hg | -1 "H₂O

FIG. 95

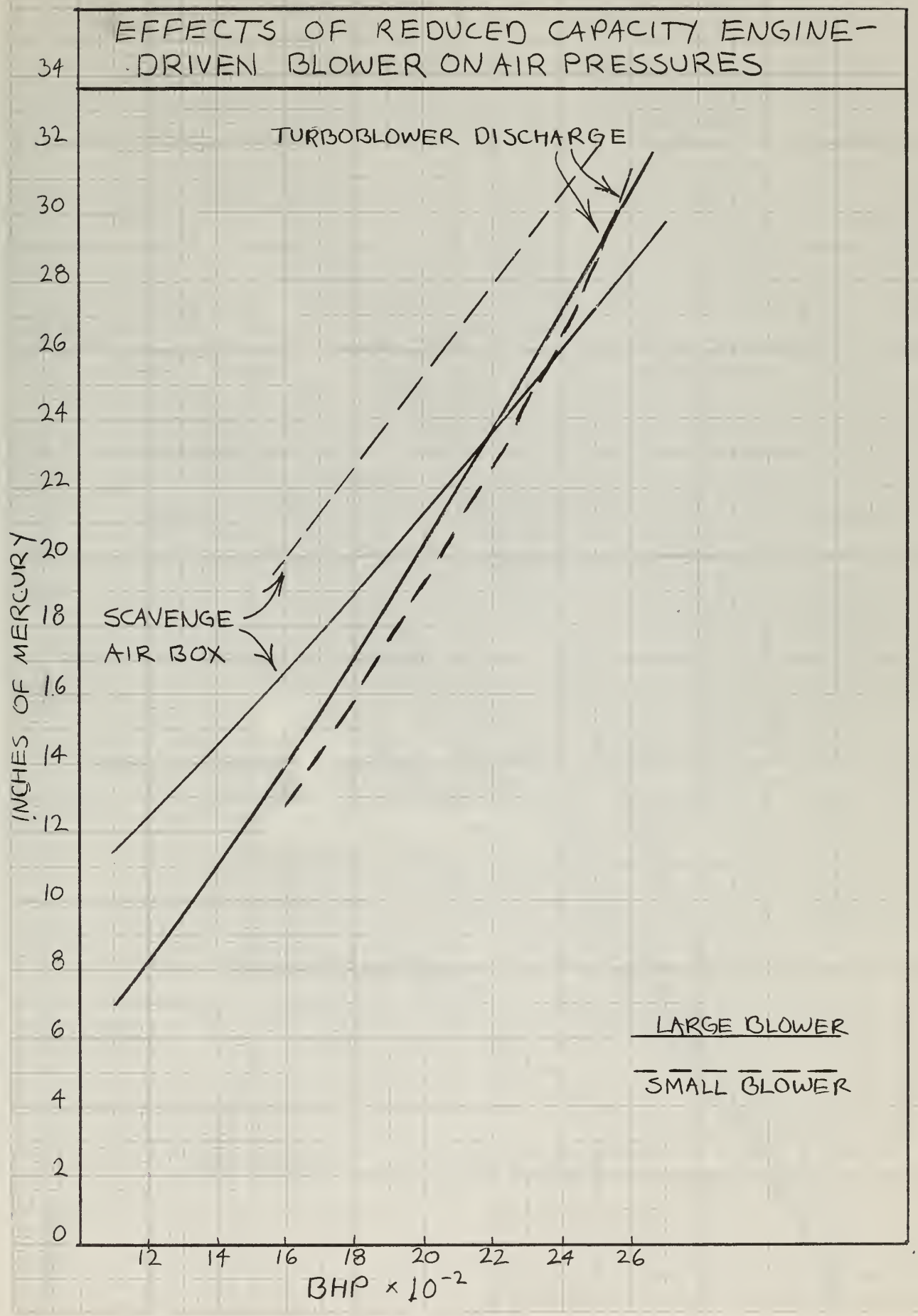
EFFECTS OF REDUCED CAPACITY ENGINE-DRIVEN BLOWER ON AIR PRESSURES
TURBOBLOWER DISCHARGE
SCAVENGE AIR BOX
INCHES OF MERCURY
34
32
30
28
26
24
22
20
18
16
14
12
10
8
6
4
2
0
12
14
16
18
20
22
24
26
BHP × 10⁻²
LARGE BLOWER
SMALL BLOWER

WORK RATIO VS. PRESSURE RATIO

FIG. 96

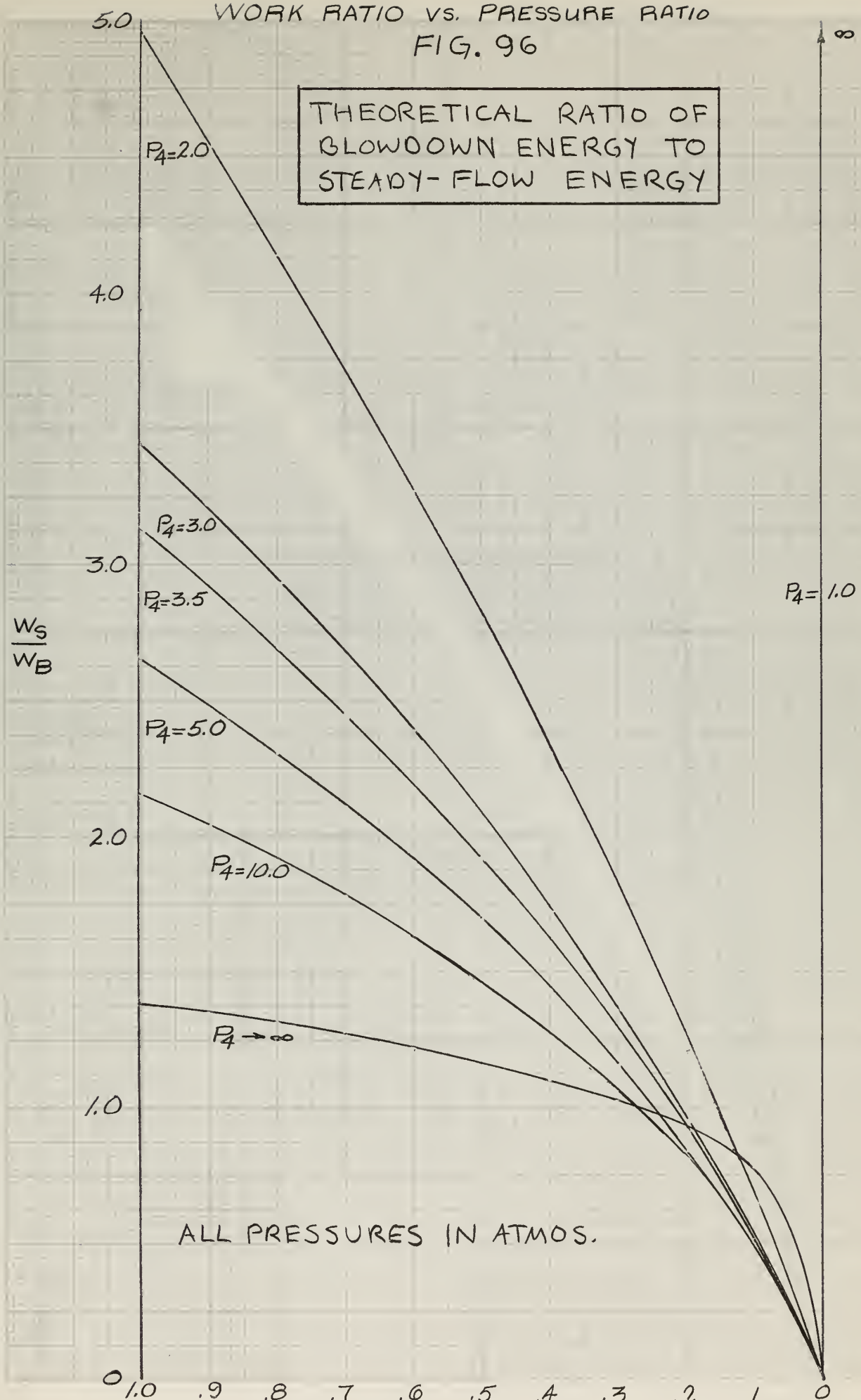

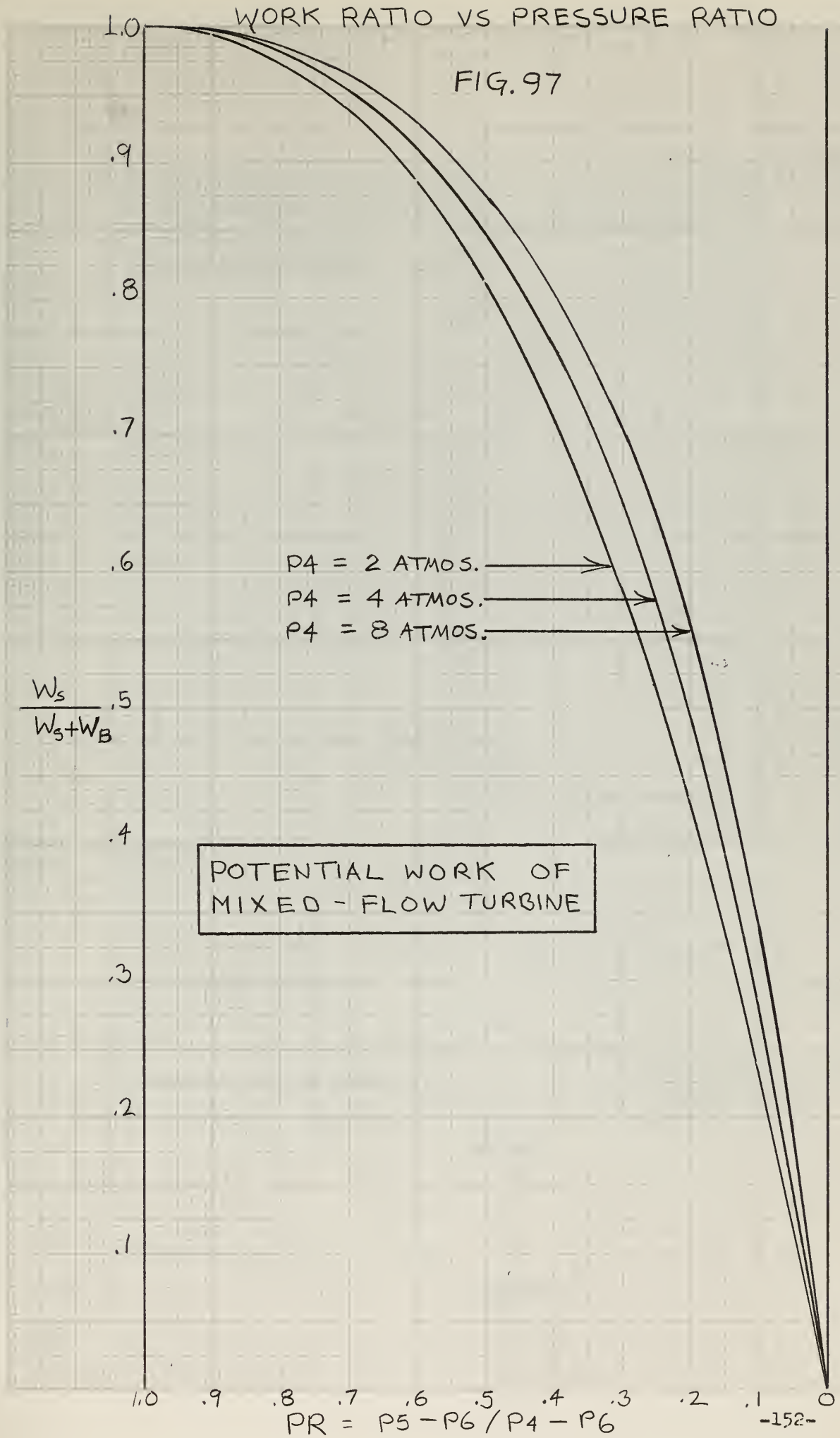
WORK RATIO VS PRESSURE RATIO
FIG. 97
1.0
.9
.8
.7
.6
.5
.4
.3
.2
.1
0
P4 = 2 ATMOS.
P4 = 4 ATMOS.
P4 = 8 ATMOS.
$\frac{W_S}{W_S+W_B}$
POTENTIAL WORK OF MIXED - FLOW TURBINE
1.0 .9 .8 .7 .6 .5 .4 .3 .2 .1 0
PR = P5 − P6 / P4 − P6

DELAVAL PULSE CONVERTER MANIFOLD

FIG. 98

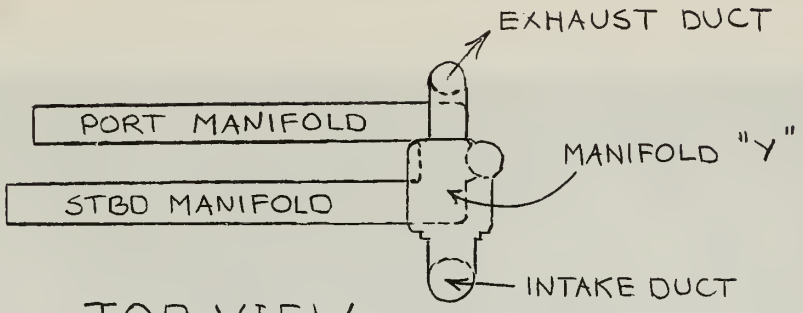

TOP VIEW

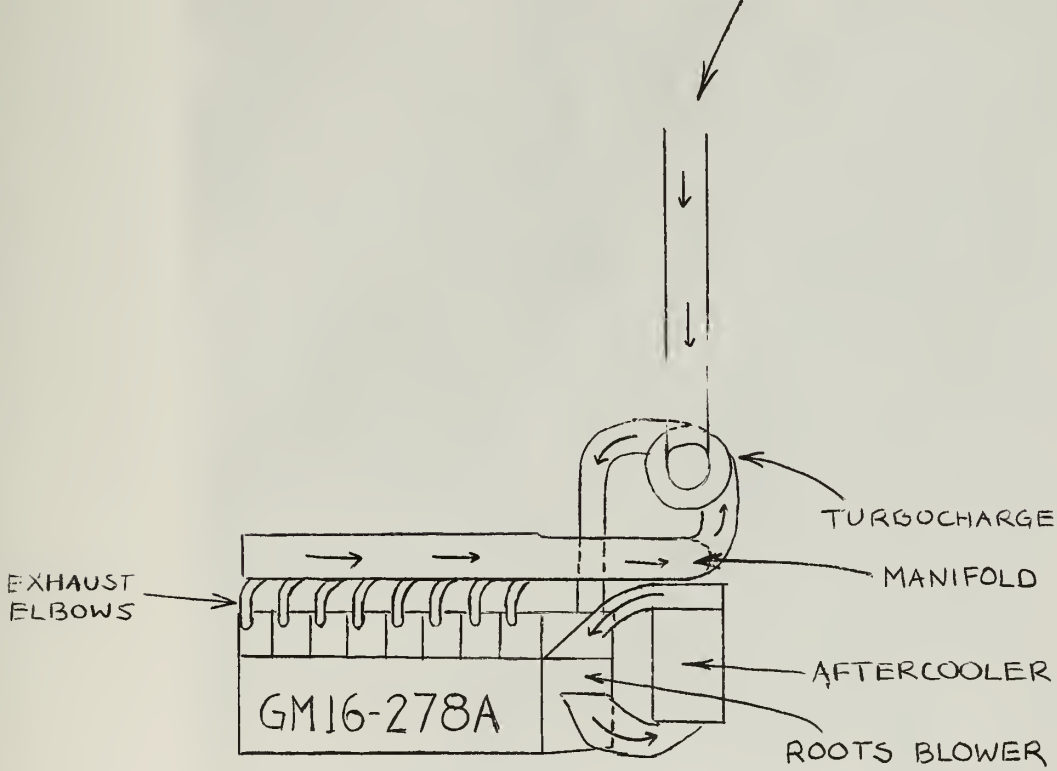

SIDE VIEW

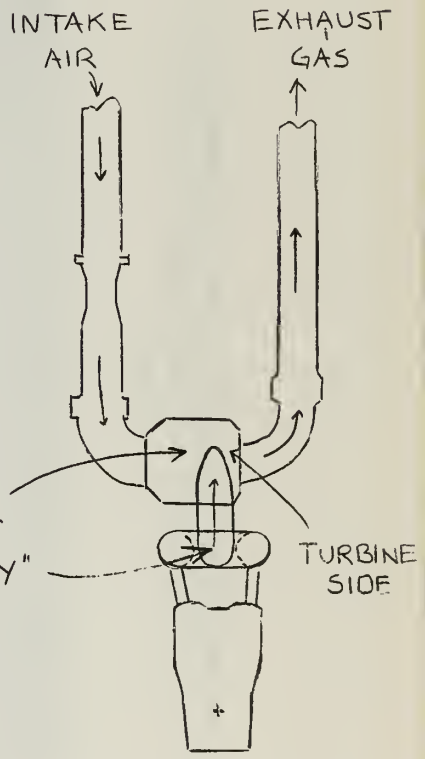

END VIEW

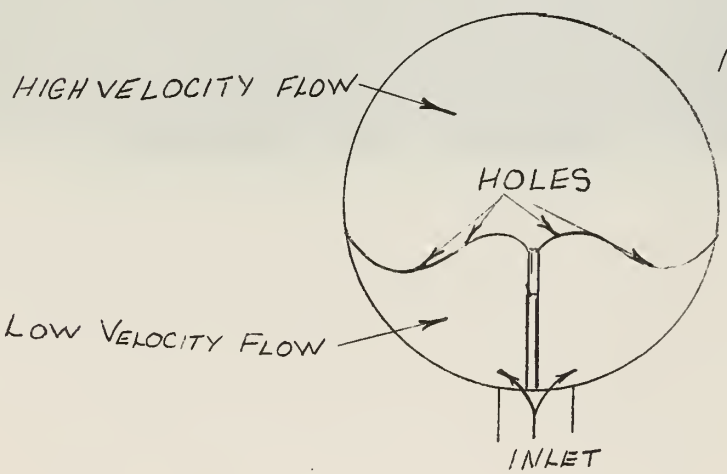

MANIFOLD CROSS SECTION

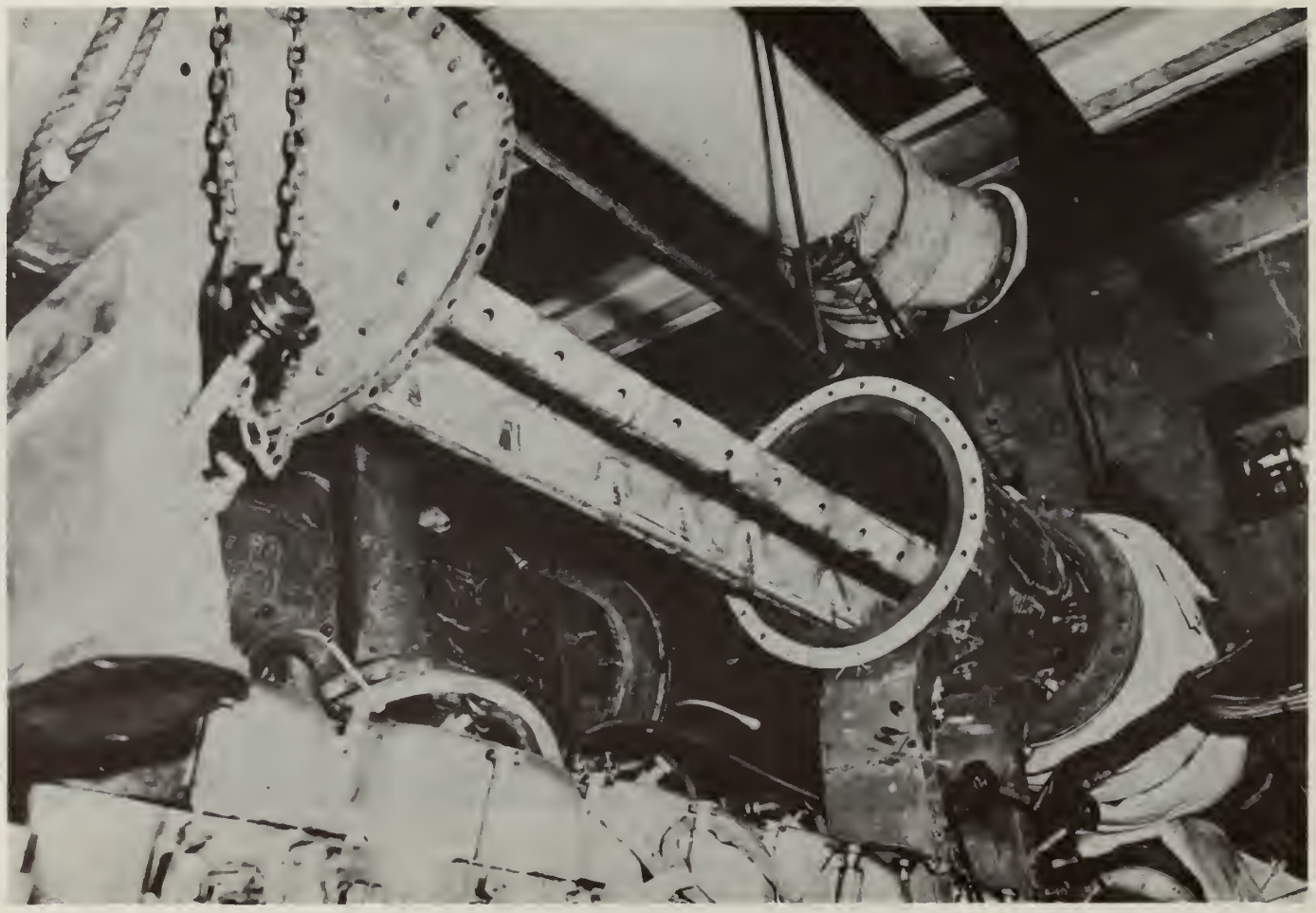

Plate I
De Laval Pulse Converter Exhaust Manifold
Showing Assembly of Flow Directors and Manifold Sections

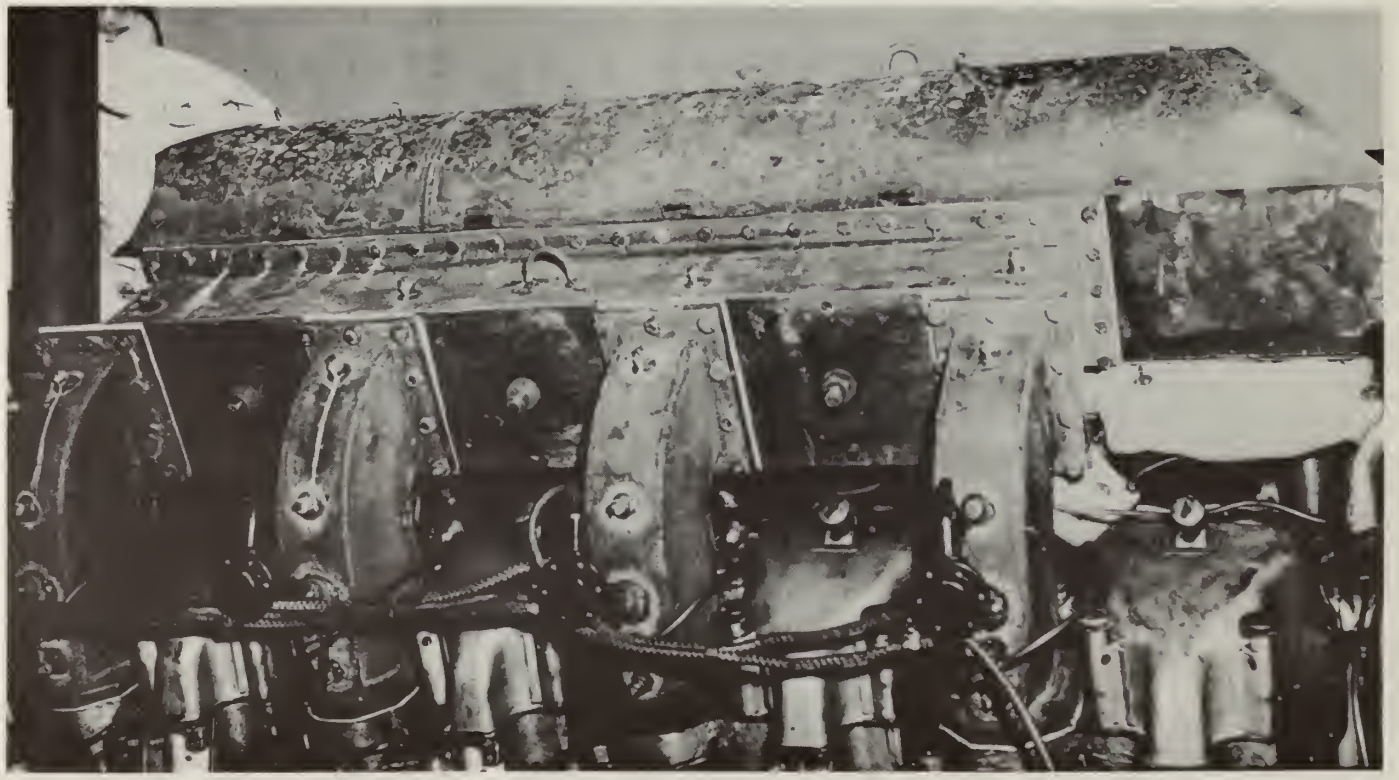

Plate II
EES Pulse Charging Exhaust Manifold
Showing Short Exhaust Elbows, Header and Common Manifold

CHAPTER V

CONCLUSIONS AND DISCUSSION OF RESULTS

1. General Introduction

2. Pulse Turbochargers

3. Steady Flow Turbochargers

   a. Elliott Model H561-2S Turbocharger with General Motors Common Manifold

   b. Elliott Model H561-2S Turbocharger with DeLaval Pulse Converter Manifold

   c. Elliott Model H561-2S Turbocharger with EES Manifold

   d. Cross comparison of best runs with Elliott Model H561-2S Turbocharger with the Common, Pulse Converter & EES Manifolds

   e. DeLaval Model B-17 Turbocharger with DeLaval Pulse Converter Manifold

   f. DeLaval Model B-17 Turbocharger with EES Manifold

   g. Cross comparison of runs with DeLaval Model B-17 Turbocharger with the Pulse Converter and EES Manifolds

   h. Comparison of best runs with DeLaval Model B-17 Turbocharger and Elliott Model H561-2S Turbocharger and the EES Manifold

   i. DeLaval Model B-8 Turbocharger with DeLaval Manifold and GM-8-268A Diesel Engine

4. Summary

1. General Introduction

There is much discussion of what constitutes a proper exhaust system in the technical literature. Universal recognition of the large power potential present in the exhaust gases has given rise to many practical and theoretical schemes for capturing this power. Unfortunately, too many of the laboratory schemes have not been or cannot be applied in a practical way. In addition, many of the practical schemes are extremely inefficient; the hypothesis apparently being that any recovery of the lost power, since it represents a net gain, is satisfactory. Plots of theoretical exhaust power available, horsepower recovered and recovery efficiency (η_R) for the GM 16-278A engine and GM 8-268A engine at various loads and operating under the constraint of the numerous exhaust geometries previously described are found in Chapter IV. These plots also show the breakdown of theoretical power into blowdown power (P_{EXH1}), steady flow power (P_{EXH2}) and "bypass" or scavenge power (P_{SC}).

Although η_R, as defined, is a measure of the amount of exhaust power recovered it is not an absolute independent index. An exhaust turbocharger system cannot be realistically considered independently, but must be considered to be dependent upon the engine-exhaust manifold system of which it is an integral part.

The selection of turbocharger characteristics to match engine operating characteristics is discussed in great detail in textbooks and the published literature. It is not our intention to discuss this

problem here. Instead, we shall use this as our point of departure in considering those factors in the engine exhaust system which can be altered to improve both engine and exhaust turbine performance. This analysis is biased to the extent that we consider the exhaust turbine to be an accessory of the engine and not vice versa.

It has long been recognized that the exhaust manifold is a controlling factor for the amount of engine airflow, cylinder scavenging, cylinder charge dilution, engine back pressure, etc. It is further recognized that often insufficient attention has been given to exhaust manifold design. The justifying argument being that the engine performs well and there are practical limitations, etc. We readily accept the fact that practical execution of many laboratory truths is difficult if not presently impossible. We are, therefore, concerning ourselves with those changes and/or modifications which are relatively easy to accomplish.

There are three basic types of exhaust turbines: (1) the pulse or blowdown type, (2) the mixed flow type and (3) the steady flow type. We are concerned with types (1) and (3) in this analysis.

In the following analysis and discussion of test results, several attempts to convert the geometry to mixed-flow (i.e. to convert blowdown kinetic energy to pressure and temperature) will be described. These attempts were, in general, unable to produce significant mixed-flow. They were, therefore, steady-flow configurations in actual practice. In the interest of clarity and consistency of definition, we will use (MF) to assist the reader in determining when the geometry is quasi-mixed-flow.

As stated above, we are considering the exhaust turbine to be an engine accessory. We are, therefore, concerned with evaluating the performance of the complete system. In order to do this objectively, we must establish criteria for comparison. The most obvious criteria are that the engine is running smoothly and steadily, that the cylinder pressures and temperatures are within the design limits, and that the engine is delivering the desired output. In the following analyses the reader may assume that these criteria are all met unless a specific statement to the contrary is made. The final criterion and the most important from a practical viewpoint, after the others have been met, is economy of operation. The index for this criterion is, quite obviously, B.S.F.C. In the following text it has been necessary to make both qualitative and quantitative comparisons of the various configurations. Since we are considering both the overall system and the exhaust turbine performance, we are interested in determining which configuration is best, which are good, poor,etc.

"Best" performance without modifying description will denote performance which satisfies all operating criteria satisfactorily with the added stipulation that the B.S.F.C. is the best (lowest) observed. The text of each analysis will leave no doubt as to whether the best performance being discussed is the best with a particular geometric configuration or the best performance observed overall, etc. Therefore, "best" performance implies specifically satisfactory operation at a local or overall optimum B.S.F.C. The final criteria in evaluating overall system performance is B.S.F.C.

Best turbine performance will in all cases apply to the observed values of η_R and will denote the local or overall optimum η_R. It will be found that poor turbine performance (low η_R) will normally be observed when engine performance is poor (high B.S.F.C. or failure to meet previously stated satisfactory operating criteria).

The foregoing discussion of the bases for comparison is intended to facilitate the reader's understanding of the text and to preclude lengthy, repetitive statements regarding the bases for comparative evaluations.

2. Pulse Turbochargers

The geometric description and general results are found in Appendices A, B, and C and Figures 2A through 9B of Chapter IV. Data plots versus overall exhaust pressure ratio (P_4/P_6) are plotted in Figures 35 through 42.

The performance of the General Electric Model 7SRD3C turbocharger with Divided Manifold I was completely unsatisfactory. The tests were terminated because of high fuel consumption. The extensive qualitative work of TSU, contained in Reference 28, demonstrated that a divided manifold was capable of greater air flow than any other manifold he tested. In the tests with the General Electric 7SRD3C turbochargers, this condition did not hold.

The tests with the Elliott Model H-504-MP-4S turbochargers, with Divided Manifold II, showed a substantial improvement in both engine and exhaust turbine performance. Divided Manifold II was identical in design with Divided Manifold I except the I.D. of Manifold II was increased from 3 3/4" to 4 1/4". Results of these tests must also be declared unsatisfactory, however.

The tests with Divided Manifold II did result in realizing the highest specific air flow (lbm/BHP.hr) of any tests made. These results indicate coarse agreement with the work of TSU. The change in performance between Divided Manifolds I and II indicates that the qualitative results of TSU can be realized in a practical application. The results further indicate that maximum air flow and best turbine efficiency occur at approximately the same turbine nozzle area.

With Manifold II, specific air flow decreases markedly (7.5% - 6.5%) with increasing turbine nozzle area. When viewed in this way, the specific air flows of Divided Manifolds I and II are compatible. This data also supports the TSU results which show divided manifolding to have superior throttled performance over common type manifolds.

Even though the specific air flow was greater than for any other tests, the performance of the pulse turbochargers was extremely poor.

The best engine and exhaust turbine performance was obtained with the Elliott pulse turbocharger (Divided Manifold II) and a turbine nozzle ring of 16.0 $in.^2$ area. This area corresponds to a dimensionless nozzle ratio of 3.32% of the piston area served. When the Elliott pulse turbochargers were run as steady flow machines, with the Common Manifold, engine performance was much improved and exhaust turbine performance was equal to or better than that with Divided Manifold II. This bizarre result indicates that the Divided Manifold as configured is not permitting the exhaust pressure pulses, with the resultant high velocity flow, to reach the pulse turbine but is instead acting as a multi-tube "common" manifold. The fact that the Elliott pulse turbochargers were able to sustain 2600 BHP with the Common Manifold and 16.0 in. turbine nozzle area compared with 2000 BHP with Divided Manifold II at lower B.S.F.C., (6.8% - 11.2%) and a lower specific air flow (1.2% - 4.4%) than with Divided Manifold II is further evidence that this divided manifold is improperly designed.

Flow of exhaust gases is a complex high temperature compressible flow problem involving heat losses, area changes, friction and complex stagnation state changes. When the exhaust valve lifts, the exhaust flow immediately chokes the exhaust valve passage and remains choked until the pressure in the nozzle divided by the pressure at the exhaust passage is greater than $\frac{2}{k+1}^{(\frac{k}{k-1})}$. The Mach No. of the exhaust flow through the exhaust valve and the primary nozzle remains relatively high during the early part of the blowdown precess when most of the cylinder charge is exhausted. With a common type manifold, the Mach No. is greatly reduced upon entering the exhaust header, and the flow is essentially incompressible with small losses. The length of the exhaust flow passages and exhaust elbows is short so the compressibility losses are therefore small. In a long, small diameter tube such as those of Divided Manifolds I and II, the compressibility losses are high because of the length of the tubes and relatively high Mach No. Further, high velocity diffusion is an inefficient process compared with high velocity throttling. It is imperative that a high velocity compressible flow not be needlessly accelerated and decelerated to minimize losses in stagnation pressure. Divided Manifolds I and II are both guilty of these faults; I more so than II.

The exhaust valve flow area/cylinder is $\approx$ 11.84 in.^{2}, the exhaust elbow flow area is $\approx$ 21.8 in.^{2}, the flow area of Divided Manifold I is $\approx$ 11.0 in.^{2} and Divided Manifold II is $\approx$ 14.17 in.^{2}.

Comparing Divided Manifolds I and II with the laboratory results of TSU:

	I		II		TSU	
$\frac{\text{EXH. FLOW AREA}}{\text{EXH.VALVE AREA}}$	$\frac{11.0}{11.84}$	= .93	$\frac{14.17}{11.84}$	= 1.195	$\frac{1.225}{.84}$	= 1.46
$\frac{\text{EXH. FLOW AREA}}{\text{EXHAUST ELBOW AREA}}$	$\frac{11.0}{21.8}$	= .458	$\frac{14.17}{21.8}$	= .65	$\frac{1.225}{1.225}$	= 1.000

From the test results of TSU, it appears that a divided manifold flow tube should have approximately the same area as the exhaust elbow to which it is connected. Additional investigation is required to obtain the quantitative design ratios for optimum divided manifold design.

The pulse turbocharger tests indicate that the turbochargers were never operating in the pulse flow for which they were designed. The G.E. turbochargers with their large (18.8 $in.^2$) turbine nozzle rings produced such low compressor output pressures that the power drain of the Roots-type blower in maintaining the scavenge pressure differential resulted in excessive fuel consumption. The G.E. pulse turbochargers, when operated steady flow, produced not only low pressure ratios, but reduced the air flow to the engine to such an extent that the tests had to be terminated because of excessive temperatures.

The tests with the Elliott pulse turbochargers were more successful. The reduced nozzle area runs provided the first indications

of an optimum turbine nozzle area. This same optimum nozzle ratio will be demonstrated more positively in the discussion of test results with the remaining turbocharger - manifold combinations.

In summary, the slightly better performance of the Elliott turbocharger is considered to be of negligible interest. The fact that this turbocharger had almost identical performance in both geometries, one of which was unequivocally a steady flow environment, conclusively proves that the Divided Manifolds were unable to deliver high velocity pulsing flow to the turbines. The design of the Elliott turbine obviously permitted greater flow variation than that of the G.E. turbines. A point which is of no practical interest in this analysis.

3a. General Motors Common Manifold with Elliott Model H561-22 Steady Flow Turbochargers

The geometric descriptions and general results are found in Appendices A, C, and Figures 10A thru 12B of Chapter IV. Data plots versus overall exhaust pressure ratio (P_4/P_6) are plotted on Figures 43 thru 48.

The performance of the Elliott turbochargers with the G.M. Common Manifold was excellent. Turbocharger performance was very consistent with each of the three turbine nozzle rings tested (14.3 in.^{2}, 15.0 in.^{2} and 16.0 in.^{2}). Specific air flow (lbm air/bhp.hr) was highest with the 14.3 in.^{2} turbine nozzle ring. At 1200 BHP $\frac{\dot{M}_I\ 14.3}{\dot{M}_I\ 16.0} = 1.051$ and at 3000 BHP $\frac{\dot{M}_I\ 14.3}{\dot{M}_I\ 16.0} = 1.025$; the change in turbine nozzle ring area was 11.19%, indicating that specific air flow is relatively insensitive to turbine nozzle ring area changes between 2.97% and 3.32% of piston area served. P_4 and P_5 decreased 2.8 - 2% and 8% - 10%, respectively, with increasing turbine nozzle area. Compressor pressure ratio also decreased with increasing turbine nozzle area. The pressure reductions, pressure ratio reductions, and air flow reductions resulted in a corresponding reduction in exhaust power available (P_{EXH}) and exhaust power recovered (P_T).

When evaluated at the same engine load, η_R is a maximum at 15.0 in^2 turbine nozzle area, but the differences are essentially negligible. When compared at constant overall exhaust pressure ratio, (P_4/P_6),

the 15.0 in.^{2} turbine nozzle area is again the optimum but the variation is still small. This data indicates a slightly different optimum nozzle ratio than that obtained from the pulse turbocharger tests. The optimum point is not a sharp peak but instead covers a relatively broad range of values.

The recovery efficiency of the turbine (η_R) decreases (16.9%) steadily with increasing BHP. This data gives the first indication of what we shall term "excess power" in the exhaust. It is also the first positive proof that η_R is only an index and not an absolute performance measure. The following table summarizes the important results of these tests:

TURBINE NOZZLE RING AREA		14.3 in.^{2}	15.0 in.^{2}	16.0 in.^{2}
$\frac{\dot{m}_{i30}}{\dot{m}_{i12}}$	=	1.387	1.427	1.42
$\frac{P_{T30}}{P_{T12}}$	=	2.93	3.06	3.25
$\frac{P_{EXH30}}{P_{EXH12}}$	=	3.47	3.59	3.69
$\frac{RC_{30}}{RC_{12}}$	=	1.551	1.537	1.565
$\frac{P_{EXH12}}{PT_{12}}$	=	1.73	1.705	1.80
$\frac{P_{EXH30}}{PT_{12}}$	=	2.045	1.995	2.04

From the previous table, and an examination of Figures 10A thru 12B in Chapter IV, the extreme non-linearity of P_{EXH} with increasing engine load is quite obvious. Examination of these figures and the above table indicates further that P_T, while non-linear, is not as non-linear as P_{EXH}. The increase in specific enthalpy of the exhaust gases with increasing engine load is greater than the required increase in enthalpy of the inlet air flow. This means that the recovery efficiency (η_R) is not constant. The turbocharger is self-sustaining throughout the range of operation with all three turbine nozzle rings. It is operating in an environment wherein the breathing characteristics of the engine-manifold combination and the turbo-compressor are in equilibrium. That is to say, the air flow delivered to the engine by the compressor is sufficient in quantity and at a pressure sufficiently high to provide adequate supercharging for high power output and provide satisfactory scavenging at an acceptable value of B.S.F.C. The problem, as seen by the turbine, is that as turbo-compressor pressure ratio increases, air flow increases, engine power output increases, and the turbine is flooded with energy. The turbine is simply driven away from its optimum operating point. Even though the turbine recovers increasingly more energy, it recovers it less and less efficiently. If a wastegate or other flow control device were employed to restrict turbine mass flow to the design flow, more energy per lb_m of gas delivered to the turbine could be recovered. The mass flow of gas diverted from the turbocharger would then be available for use in another turbomachine of arbitrary application, or P_5 could be reduced, thereby improving engine performance.

This geometric configuration, although far from optimum, is nonetheless an excellent example of the kind of engine performance which can be attained by adding a reasonably well matched turbocharger, increasing the fuel system capacity and adding a heat exchanger (inter/aftercooler).

3b. DeLaval Pulse Converter Manifold with Elliott Model H561-2S Steady Flow Turbochargers

The geometric descriptions and general results are found in Appendices A, C, and Figures 13A through 15B of Chapter IV. Data plots versus overall exhaust pressure ratio (P_4/P_6) are plotted on Figures 43 through 48. This manifold system was tested in three different configurations: (1) at maximum exhaust elbow area (17.8 $in.^2$) without internal flow directors (tunnels); (2) at reduced (10.0 $in.^2$) exhaust elbow area with flow directors (tunnels) (MF), and (3) at reduced (10.0 $in.^2$) exhaust elbow area without flow directors (tunnels) (MF).

The tests conducted with these configurations resulted in the lowest B.S.F.C. attained thus far. In configuration 3, the intent was to determine whether accelerating the exhaust flow prior to entering the manifold would raise the manifold pressure profile and thereby increase the turbine output. Performance in this configuration was paradoxical. As previously stated, B.S.F.C. was low, η_R was fair, yet the configuration could sustain no more than 2600 BHP. From 2200-2600 BHP engine operation became increasingly rough and unsteady until operation was terminated at 2600 BHP.

In configuration 2, B.S.F.C. was higher than with 3 (1.2 - 2.5%), η_R was slightly lower (3.9% - 2.0%), but engine operation was much rougher and was also terminated at 2600 BHP.

These two configurations can be considered together. Configuration 2 provided an exhaust elbow area of only 10.0 $in.^2$, This area is

only ≈ 84.5% of the exhaust valve flow area. As air flow (M_I) and exhaust pressure (P_4) increase with increasing engine load, the flow conditions between the exhaust valves and the exhaust elbows are analogous to those of the cylinder proper. That is to say the problem of inducing the flow of a large quantity of fluid through a small orifice in a short time. In addition, the cylinder must be scavenged and filled with fresh charge. With a throttling orifice downstream and small included volume between the orifice and the exhaust valves, the resistance to flow from the cylinder created by the exhaust elbow will reach a point where the flow cannot leave the cylinder in the allotted time. The residual gas fraction will increase (5.8%), flow of cooling scavenge air will be retarted and cylinder charging will be adversely affected. Rough engine performance will result and did.

It can be stated unequivocally, that regardless of what may be done with the flow afterwards, the critical flow area must be the exhaust valve. Choking flow must not be permitted to occur at any other point (such as the exhaust elbow). In a given flow path from cylinder to manifold, the smallest flow area must be the exhaust valve and this too should be as generous as possible.

Configuration 1 is the only one of the three which merits consideration from an analytical point of view. The unsatisfactory results with flow directors and reduced exhaust elbow area left only configuration 1 as a reasonable test mode. In this configuration, the maximum exhaust elbow area (17.8 $in.^2$) possible with this manifold was used. It must be interjected at this point that the 17.8 in^2 exhaust

elbow area is less than the maximum (21.8 $in.^2$) permitted by the engine design. This point will be of interest in later analysis.

Configuration 1 is essentially a common manifold application with reduced (18.3%) exhaust elbow area. The installation easily sustained 3000 BHP with the best B.S.F.C. (4.8% - 2%) observed thus far. All tests were conducted with a single fixed geometry turbine nozzle ring of 14.8 $in.^2$ flow area (3.07%) of piston area served.

At the lower power outputs, η_R was definitely the highest observed to date. Although as engine output increased, the performance of the three configurations tended toward similar values with configuration 1 definitely superior. This condition conclusively indicates that configurations 2 and 3 are unsatisfactory because of their adverse affects on engine performance. In view of the fact that configurations 2 and 3 were completely unsatisfactory, little can be gained here from further comparison.

3c. E.E.S. Manifold with Elliott Model H561-2S Steady Flow Turbochargers

The geometric descriptions and general results are found in Appendices A, C, and Figures 16A thru 24B of Chapter IV. Data plots versus overall exhaust pressure ratio (P_4/P_6) are plotted on Figures 49 through 59. This test geometry was further modified to provide for removal of the exhaust muffler and installation of an 18" I.D. exhaust pipe, the standard 16-cylinder size engine-driven Roots blower (6860 cfm) was replaced by a 12-cylinder size engine-driven Roots blower (5350 cfm) and the heat exchanger was used as an intercooler instead of an aftercooler.

The reduction in turbine back pressure caused by the removal of the muffler created the obvious improvement of a greater turbine expansion ratio. The 16-cylinder blower was replaced with the 12-cylinder blower to reduce the power drain of the Roots blower. Because of the reduced volume rate of flow of the 12-cylinder blower, the heat exchanger was converted into an intercooler to increase the density of the flow entering the Roots blower.

This geometry represents the best performance attained with the Elliott steady flow turbochargers. This geometry was tested with fixed geometry turbine nozzle rings of 15.0, 16.0, 18.5 and 20.0 $in.^2$ area.

The 15.0 and 16.0 $in.^2$ turbine nozzle rings gave identical B.S.F.C. B.S.F.C., η_R, $\dot{M}_I$, P_4, P_5, P_{EXH}, P_T, and RC all decreased with increasing turbine nozzle ring area. The 15.0 $in.^2$ turbine nozzle ring

area produced the best results of any of the four turbine nozzle rings tested in all categories save one. The 15.0 $in.^2$ turbine nozzle ring test resulted in only 2700 sustained BHP. The limitation was the compressor and not the turbine. The turbine drove the compressor to and through its surge line. This resulted in unstable engine flow conditions and corresponding instability of engine operations.

Test were conducted with exhaust elbow lengths of 17.0 in., 20 5/8 in. and 26 in. to determine what effect variations in exhaust elbow length would have on exhaust pipe tuning. Tests with the shortest length, 17.0 $in.^2$, resulted in the best fuel economy (2.6% - 4.2%) and greatest air flow (16.8% - 18.1%). Tests with the 20 5/8 in. elbow caused a moderate drop in η_R and $\dot{M}_I$ and an increase in B.S.F.C. Tests with the 26 in. length resulted in a moderate increase in η_R, the same B.S.F.C. as the 20 5/8 in. length, and $\dot{M}_I$ only slightly less than the basic tests at 17.0 in. exhaust elbow length. Since the improved turbine performance was obtained at the expense of engine B.S.F.C., it must be considered unsatisfactory. The turbine improvement is so small that it must be concluded that exhaust manifold tuning plays a minor role in a turbocharged multi-cylinder engine exhaust system. See Figures 54 through 59.

The final tests of this geometry involved two different fuel injector designs of nearly identical capacity. The results of these tests show that turbine performance will mirror a change in the engine combustion process. In this particular case, the data points labelled

"G.M. Tips" plotted on Figures 56 through 61 show a decrease in engine performance and a corresponding decrease in turbine performance.

This geometry with the 15.0 $in.^2$ turbine nozzle ring and the shortest (17.0 in.) exhaust elbow gave the best performance obtained with the Elliott steady flow turbochargers. This performance was excellent. B.S.F.C. rivalled that of the unsupercharged engine, η_R was very consistent at $\approx 53 + \%$, the turbocharger easily sustained a maximum load of 3300 BHP; the limiting condition at this point was the capacity of the fuel injectors. Engine operation was smooth and steady. At 15.0 $in.^2$ turbine nozzle area even better performance might have been obtained had the turbocompressor been better matched to engine operating conditions.

3d. Cross Comparison of Best Tests with Elliott Model H561-2S Steady Flow Turbochargerw with the Common Pulse Converter and E.E.S. Manifolds

The respective geometries have previously been described. Comparative data plots versus overall exhaust pressure ratio (P_4/P_6) are plotted on Figures 60 through 63.

The many geometric variations have been previously discussed and evaluated. We are interested here in comparing the best run from each of the three manifolds in order to determine what factors exert the most influence on engine and turbine performance.

The first similarity discernible is that the best results with each individual manifold came when the manifolds were configured as simple common manifolds without any internal hardware. The second similarity is that the best B.S.F.C. occurred with turbine nozzle rings of 3.075 - 3.11% of piston area served (common 3.11%, pulse converter, 3.075% and E.E.S. 3.11%).

Within the general statement that all manifolds were operated as common are a few geometric differences. The Common and E.E.S. Manifolds had an exhaust elbow area of 21.8 $in.^2$; the pulse converter manifold had an exhaust elbow area of 17.8 $in.^2$. The pulse converter manifold had two headers (one for each bank) vice the conventional single collection header. The engine was operated intercooled with a Roots blower of reduced capacity with the E.E.S. manifold.

TSU in his qualitative manifold studies (Reference 28) determined that simply increasing the size of a common manifold would improve the performance of a naturally aspirated engine until a certain size was reached. Unfortunately, this critical size is impossible to translate from his results into a general design criterion. After this size is reached, further increases in size will adversely affect engine performance. It is our contention that two dimensionless area ratios are of importance in manifold design. These are: (1) exhaust manifold flow area/piston area served and (2) exhaust manifold flow area/exhaust valve area served. A comparative table of the three manifolds tested follows.

	COMMON	E.E.S.	PULSE CONVERTER
$\frac{\text{MANIFOLD FLOW AREA}}{\text{PISTON AREA SERVED}}$	15.95%	18.91%	47.1%
$\frac{\text{MANIFOLD FLOW AREA}}{\text{EXHAUST VALVE AREA SERVED}}$	81.3%	96.3%	240.0%

	TSU QUASI-OPTIMUM	
BY EXTRAPOLATION	$\frac{\text{MANIFOLD AREA}}{\text{PISTON AREA SERVED}}$	20%
	$\frac{\text{MANIFOLD FLOW AREA}}{\text{EXH. VALVE AREA SERVED}}$	105.2%

It is our allegation (on an admittedly small data sample) that the E.E.S. manifold is near optimum for this engine and that the Common and Pulse Converter Manifolds are too small and too large respectively. Crudely applying the data of TSU to this engine, the resulting manifold would be a circular tube of 15.92 in. diameter with 21.8 $in.^2$ exhaust

elbows. Further experimental work is required to develop reliable design ratios and relationships for exhaust manifolds.

The following table shows the performance at identical engine outputs for the Common and Pulse Converter Manifolds referred to that of the E.E.S. Manifold. A + means "better than"; a - means "worse than" the E.E.S. Manifold

	$\dot{M}_I$	B.S.F.C.	η_R
Pulse Conv.	(+17.1 to + 2.9)%	(-6.7 to -8.7)%	(+11.5 to -4.2)%
Common	(+20.0 to 7.2)%	(-11.7 to -13.9)%	(+2.1 to -5.9)%
	P_{EXH}	P_T	RC
Pulse Conv.	(+4.8 to -1.8)%	(+16.5 to -6.0)%	(0.0 to -6.6)%
Common	(+7.5 to +3.5)%	(+9.7 to -2.6)%	(-3.5 to -6.6)%
	f	e_s	R_s
Pulse Conv.	(+18.3 to +7.0)%	(+7.8 to +1.8)%	(+11.0 to +1.5)%
Common	(+23.7 to +12.7)%	(+7.8 to +1.8)%	(+10.9 to +1.5)%
	P_4	P_5	
Pulse Conv.	(+7.8 to +5.9)%	(+6.1 to +1.7)%	
Common	(+7.8 to +6.8)%	(+4.1 to +1.1)%	

The above table shows that even though the E.E.S. manifold gave the best overall performance, it was not the best in all respects. Unfortunately, this type of mixed result is the usual rather than a special result.

It is significant that as engine load increased, the change in B.S.F.C., η_R, RC, P_{EXH} and P_T showed the increasing superiority of the

E.E.S. manifold. Also, as engine load increased, the values of f, e_s, R_s and P_5 tended toward common values, thereby indicating that the E.E.S. manifold's region of best operation was the higher engine output region. Even so, the consistently superior performance throughout the range of operation demonstrates conclusively the effect of the exhaust manifold on system performance.

3e. DeLaval Pulse Converter Manifold and DeLaval Model B-17 Steady Flow Turbochargers

In this series of runs the following geometric parameters were varied:

(1) the area of the turbine nozzles was changed

(2) the manifold was used both with and without flow directors

(3) high and low turbine back pressure runs were made

(4) both large and small size engine-driven blowers were used

(5) the area of the exhaust elbows was varied.

The geometric description and general results are found in Appendices A and D and Figures 25A through 27B of Chapter IV. Data plots versus overall exhaust pressure ratio (P_4/P_6) are found in Figures 64 through 70.

The DeLaval Model B-17 turbocharger consisted of a mixed flow centrifugal compressor with axial inlet and radial and axial discharge and a single-inlet steady-flow full-admission centripetal turbine with radial inlet flow and axial discharge. The two wheels were combined into a single "monorotor" casting. DeLaval literature* claims that this arrangement eliminates parasitic losses such as leakage between the compressor and turbine. Our test data indicates quite the opposite. Considerable leakage did occur between the compressor and turbine. This is more fully discussed in Appendix H.

* Diesel Engine Catalog, Vol. 24, 1959 Edition, Diesel Progress, Los Angles, 1959, p. 314.

The engine exhaust flowed into the turbine nozzle box through a single tangential inlet. Inside the box there were nozzle guide vanes which could be adjusted to change the effective nozzle area. The guide vanes directed the flow of gases radially inward into the turbine blades.

The pulse converter manifold is described in Appendix A. This system was designed to convert the pulsating portion of the exhaust energy into a pressure rise in such a manner that the turbine inlet pressure would be higher than the mean engine exhaust back pressure. This would allow the turbine to operate at a high expansion ratio without adversely affecting engine scavenging.

Three full scale runs were conducted with this manifold and turbocharger:

In run DL1, the manifold was operated as a pulse converter with flow directors installed. The area of the exhaust elbows was 10 $in.^2$ and their length was 26 in. Turbine nozzle area was 42 $in.^2$ (4.30% area ratio). An aftercooler was used, the standard 16-cyl. size Roots blower was used and the muffler was bypassed.

In run DL2, the Roots blower was replaced with the one usually used with the 12-cylinder engine. In addition, the turbine nozzle area was decreased to 38 $in.^2$ (3.97% area ratio).

In run DL3, the flow directors were removed; eliminating the pulse conversion feature. The area of the exhaust elbows was increased to 17.8 in^2.

Shorter, less well documented, runs were made to evaluate the effects of individually varying the geometric parameters previously listed.

Two experiments were conducted to evaluate the effects of varying the area of the turbine nozzles. In a 1600 BHP run, the area was varied from 38 $in.^2$ to 60 $in.^2$ (3.97% to 6.30% area ratio). In a 2400 BHP run, the area was varied from 38 $in.^2$ to 54 $in.^2$ (3.97% to 5.63% area ratio). The results of these runs are shown in Figures 82 and 83.

Both recovery efficiency and B.F.S.C. reached well defined optimum points. As expected, the runs with the smaller nozzle areas produced generally higher efficiencies and better fuel economy. Conversely cylinder pressure and turboblower RPM were lower in the runs with the larger nozzle areas.

As the nozzle area was increased beyond the optimum point, the turbine recovered less power. In the 2400 BHP runs, the recovered power at the largest nozzle area was 11.6% less than that recovered at the optimum nozzle area. This caused the turboblower to slow down (an 800 RPM drop). This decreased the density of the fresh air charge and the mass rate of air flow decreased by 6.5%. In addition, the compressor ratio decreased by 7.6%; to maintain a power load of 2400 BHP (BMEP = 126 psi) substantially more fuel was required (8% more). The reduced turboblower output led to a reduction in maximum cylinder pressure (an 8% drop). Exhaust valve opening pressures and temperatures increased, however. It is felt that this was due to the increase in the amount of fuel injected and the reduced cooling effect caused by the decrease in air flow. The pressure at turbine inlet decreased, however.

The pressure ratio across the turbine (P_5/P_6) decreased by 8%. This led to a reduction in the amount of steady-flow energy theoretically available in the exhaust gas (an 8.9% decrease). Since the turbine was a steady-flow device, this would explain the reduction in recovery eff.

The area ratios for maximum recovery efficiency and minimum fuel consumption were almost identical. In the 2400 BHP run, this ratio was 4.30%. The mechanism which varied the area of the turbine nozzles was only able to decrease the area ratio to 3.97%. At this level it appears that the turboblower was limiting the recovery performance of the turbine. Between the ratios of 4.30% and 3.97%, there was little difference in the air flow, compressor pressure ratio and turboblower RPM. This indicates that the turbo compressor was unable to absorb any more power. Intermittent compressor surging began to occur at this point. This led to generally poorer scavenging which was reflected in an increased demand for fuel. Exhaust gas temperatures and pressures rose and the total energy theoretically available in the exhaust gas increased. However, the inability of the compressor to absorb any more power automatically lowered the computed turbine recovery efficiency. It would have been most helpful if the actual turbine potential could have been measured with a dynamometer.

In runs DL2 and DL3, the performance of the flow directors is measured. Figures 64 through 67 show that run DL3 had markedly improved operating conditions. Removing the flow directors and enlarging the elbow area increased scavenging efficiency by from 3.4% (at 1300 BHP)

to 4.8% (at 2600 BHP). Scavenging ratio was increased by from 4.6 to 7.2%. The amount of residual exhaust gas retained was decreased by from 6.4 to 7.0%. This improvement in scavenging appears mainly due to a lowering of P_5 of by from 6.2 to 9.2%. In turn, this improved scavenging led to a 3% improvement in fuel economy. Moreover, at equal pressure ratios (P_4/P_6) run DL3 developed considerably more BMEP than did run DL2 (3.8 to 6.3%).

The reduction in fuel flow led to generally lower pressures and temperatures. This lowered the theoretically available exhaust energy. Yet, in run DL3 the recovery efficiency increased considerably (5.3 to 11.6%). It is felt that some of this improvement may be fictitious. In examining the two runs we note that air flow, compressor efficiency, compressor pressure ratio and turbine power remain substantially constant. It appears that once again the turboblower may have been unable to absorb any more power from the turbine. Therefore the decrease in theoretical energy automatically raised recovery efficiency. This is the same phenomenon that was previously discussed in the runs with variable nozzle areas, although the direction of the change is opposite.

It is, however, obvious that the removal of the flow directors and the enlargement of the exhaust elbow areas was highly beneficial. Figures 84 and 85 show the effect of individually removing the flow directors and enlarging the elbow areas. It appears that the area enlargement made the major contribution towards improving performance.

It appears that recovery efficiency is, at best, only an index of turbine performance. In a turboblower supercharged engine a compromise must be made between engine scavenging and turbine performance. A low engine back pressure improves scavenging. Yet, to maximum turbine performance a high inlet pressure is desirable. Generally engine back pressure and turbine inlet pressure are the same. In run DL2, we see that the turbine was easily able to recover sufficient energy to drive the compressor. In fact, it appears that the inlet pressure was somewhat more than the turbine actually required for good performance. The turbine was unable to use this "excess" pressure and it was detrimental to engine scavenging. In run DL3, we see considerable improvement in engine scavenging. Yet the turbine was still able to perform satisfactorily with the lower inlet pressure. Obviously, run DL3 was successful due to the better matching of turbine and engine requirements.

In the earlier runs of this series, an exhaust muffler was used. This produced a turbine back pressure of 35 " H_2O at 2600 BHP. It was felt that a reduction in back pressure would improve both turbine and engine performance. Accordingly, the exhaust pipe was increased from 15 in. I.D. to 18 in. I.D. and the muffler was bypassed. This resulted in a turbine back pressure of only 8.5 " H_2O at 2600 BHP.

The scavenging pressure ratio ($P_{airbox}/P_{exhaust}$) was increased considerably (4.2% at 1600 BHP to 6% at 2600 BHP). Maximum cylinder pressure was slightly lowered (15 psi) and turbine inlet temperature was lowered about 40°F. The improved scavenging led to a significant improvement in fuel economy (see Figure 86).

Obviously, reducing turbine backpressure is entirely beneficial. In many circumstances, however, the presence of an exhaust muffler is not dictated by purely engineering considerations. When possible, in marine engines for instance, every effort should be made to reduce back pressure by dispensing with a muffler.

It became apparent that at high power loads the engine-driven blower was a parasitic power absorber which served no useful purpose. This blower was only needed for starting and during periods of light load. At high power loads, the blower imparted only a small pressure rise to the incoming air. At 2600 BHP the pressure rise across the blower was only 2.5 " H_g.

In an attempt to minimize this power drain, a blower of reduced capacity was installed. This was the blower usually used with the GM V-12 engine and was similar in construction, but of reduced capacity. The original blower had a capacity of 6860 CFM; the new one only 5350 CFM.

The performance of the new installation is shown in Figure 95. At power levels above 2200 BHP the turboblower discharge pressure was higher than the scavenge air box pressure. At 2600 BHP this amounted to 2 " H_g. The engine-driven blower was unloaded and possibly even returned some power to the shaft.

However, the engine performance was disappointing. Evidently the small capacity blower restricted air flow. Air flow was down some 13.5% at 2600 BHP. Turbine inlet temperature was increased by 75-130°F. There was no significant change in B.S.F.C.

In order to capitalize on the reduced power drain with the smaller blower, it is necessary to reduce the volume of the air flowing through it. This was later done by cooling the air before it entered the blower to decrease the volumetric rate of flow without decreasing mass flow. This will be discussed later.

3f. E.E.S. Manifold and DeLaval Model B-17 Steady Flow Turbochargers

In this series of runs the following geometric parameters were varied:

(1) the aftercooler was replaced with an intercooler

(2) "charger-plates" were installed in the exhaust header boxes

The geometric descriptions and general results are found in Appendices A & D and Figures 28A through 30B of Chapter IV. Data plots versus overall pressure ratio (P_4/P_6) are found in Figures 64 through 77.

The DeLaval Model B-17 turbocharger has been discussed previously in this chapter. The EES manifold is described in Appendix A and shown in Plate II. Essentially it was a common manifold with generous direct-flow passages. The exhaust elbows were connected in groups of four to rectangular headers which in turn opened into the manifold proper. Perforated plates ("charger plates") could be inserted in the rectangular headers.

Eight full scale runs were conducted with this manifold and turbocharger:

In run E1, the manifold was operated without charger plates. The area of the exhaust elbows was 21.8 $in.^2$ and their length was 17 in. Turbine nozzle area was 38 $in.^2$ (3.97% area ratio). An after cooler was used, the 12-cylinder size Roots blower was used and the muffler was bypassed.

In run E2, the aftercooler was replaced with an intercooler. The nozzle area was increased to 42 $in.^2$ (4.30% area ratio).

In the E3, E4 and E5 series of runs, a charger plate was placed in each exhaust header. Each charger plate had 52 1-in. diameter holes (40.8 $in.^2$ flow area). Tests were made with the charger plates 3 in., 6 in. and 9 in. from the exhaust elbow outlets (see Fig. 92).

In the E6, E7 and E8 series of runs, the charger plates had 52 3/4-in. diameter holes (23.0 $in.^2$ flow area).

Runs E1 and E2 provide graphic proof of the effectiveness of the intercooler. See Figs. 64 through 67. Air flow was dramatically increased (7.3% at 1300 BHP to 11% at 2600 BHP). Scavenging was also considerably improved. Scavenging ratio was increased by from 6.3 to 9.5%. Scavenging efficiency was increased by from 4.7 to 6.6%. See Fig. 88. This led to considerable improvement in fuel economy (up to 5.6% improvement). See Figure 87.

The increased air flow caused a sharp drop in exhaust temperature. This lowered the value of the energy theoretically available in the exhaust gases. The power required to drive the compressor increased proportionately with the increased air flow. This, coupled with the reduction in theoretical available energy, led to a considerable improvement in recovery efficiency (by from 5.8 to 11.8%). As discussed elsewhere, this improvement in recovery efficiency may be somewhat ficititious, but there is no disputing that the overall engine performance improved.

The next six runs were undertaken to evaluate the effects of placing perforated "charger plates" inside the exhaust manifold headers.

These plates were designed to restrict the flow of exhaust gas so as to increase the pressure level of the air charge retained in the cylinder. In effect, they hoped to achieve a more advantageous manifold by changing the effective length of the exhaust elbows.

The first run was run E3 in which the flow area of the charger plates was 40.8 $in.^2$ and they were placed 3 in. from the exhaust elbow outlets. While the pressure in the air box increased as desired, the increase was very slight (up to 0.7% at 1300 BHP and up 2% at 3300 BHP as compared with run 32). The slight increase in this pressure was matched by a greater increase in P5 (up 3% at 3300 BHP). The net effect was poorer, rather than better, scavenging. Scavenging ratio dropped 3.2% at 1300 BHP and 1.4% at 3300 BHP. This led to an increased demand for fuel to maintain the same BMEP (up 1.45% at the lowest pressure ratio (3.2) and up 3.8% at the highest pressure ratio (6.2).

Both the pressure and the temperature of the exhaust gas were raised which led to a moderate gain in power recovered (4%). However, the poorer scavenging of the engine made it impossible to effectively utilize this increased power input to the compressor. Air flow was actually reduced by up to 5% as compared with run E2.

The other runs in this series had the charger plates spaced at 6 in. and 9 in. As might be expected, their performance was somewhat better than that with the 3 in. spacing. Scavenging was improved, but it appears that this was due to placing the charger plates further down stream where the gas velocity was lower. It was certainly not due to raising the pressure in the air box since these pressures were actually lower than in run E2.

In the E6, E7 and E8 series the flow area of the charger plates was some 42% less than in the E3, E4 and E5 series. Predictably, scavenging and fuel economy suffered even more than with the larger flow area runs. See Figures 71 through 77.

In summary, it appears that this entire series of experiments with the charger plates was rather fruitless. The EES Manifold was a good manifold primarily because it was correctly sized to the area of the exhaust valves and because it had large short exhaust elbows. Placing restrictions in the exhaust manifold did little to increase pressures in the air box and did a great deal to restrict flow and raise the pressures at manifold inlet. Since this manifold was basically a good one, performance did not suffer greatly. However, without exception, every performance criterion did suffer and none were improved.

3g. Comparison of DeLaval Pulse-Converter Manifold and EES Manifold As Used With The DeLaval Steady-Flow Turbine

The following four runs summarize operations with the DeLaval steady-flow turbine:

Run	Manifold	Elbow Area	Nozzle Area	Cooler	Roots Blower
DL1	DeLaval (MF)	10	42	after-	large
DL2	DeLaval (MF)	10	38	after-	small
E1	EES	21.8	38	after-	small
E2	EES	21.8	42	inter-	small

Run DL1 was the first and best run with the DeLaval manifold. Runs DL2 and E1 contrast the two different manifolds when each was operating under identical conditions of restricted air flow. Run E2 was the best run with the EES manifold.

Air flow was severely restricted in runs DL2 and E1 by the presence of the small Roots-blower and the absence of any intercooling. At 2600 BHP, the air flow in run DL1 was 702 lb/min. In run DL2, it was only 605 lb/min. In run E1, it was still only 596 lb/min. In run E2, it had increased up to 662 lb/min.

In runs DL2 and E1, air flow, compressor pressure ratio and power delivered to the compressor were virtually identical between the two runs (differences less than 2%). These two runs, therefore, afford an opportunity to evaluate the two different manifolds under similar operating conditions. See Figures 64 through 67.

It is evident that the EES manifold utilized its air flow much more successfully than did the DeLaval manifold. Scavenging was much

superior with the new manifold. Scavenging ratio was up to 11% higher. Scavenging efficiency was up to 9.6% higher. Residual gas retained was up to 12% lower. This was primarily due to generally lower P5's (up to 9.2% lower). This improved scavenging was reflected by substantial improvements in fuel economy (up to 8.7% improvement).

In the DeLaval manifold, the exhaust pressures and temperatures were considerably higher than with the EES manifold. This raised the value of the energy theoretically available in the exhaust gas considerably (up to 20% higher). However, it appears that once again the inability of the compressor to absorb any more energy limited turbine recovery. Since the power recovered was essentially constant between the two manifolds, the higher theoretical energy in the DeLaval manifold automatically lowered its turbine recovery efficiency. The EES recovery efficiency was up to 11.5% higher.

The EES manifold was superior to the DeLaval manifold because the engine and turbine requirements were more closely matched. In the DeLaval manifold, the high exhaust back pressure penalized engine scavenging without any compensating effect on turbine recovery. In the EES manifold engine, scavenging and turbine recovery complemented each other rather than competed with one another.

It is rather difficult to compare the best run with the DeLaval manifold and the best run with the EES manifold (runs DL2 and E2). Run DL1 was a mixed-flow run and was conducted with the large Roots blower and an aftercooler while run E2 was a steady-flow run and was conducted

with the smaller Roots blower and an intercooler. The use of the intercooler brought the air flow up to within 5% of the run with the big blower. See Figures 65 through 68.

The EES manifold produced a tremendous gain in the ability of the engine to utilize its air flow effectively. The residual exhaust gas retained was decreased by a full 22%. This led to gains in fuel economy of up to 12% at equal BMEP's and up to 10.8% at equal pressure ratios (P4/P6). Moreover, at equal pressure ratios the EES manifold developed up to 11.2% more BMEP.

Finally, it appears that the main problem with the DeLaval manifold was that it was designed with the wrong flow area at the wrong place. As was discussed previously, the very small exhaust elbow area (10 $in.^2$) developed choked flow in the elbows. The effect of this on engine scavenging was disastrous. The DeLaval manifold proper, on the other hand, was excessively large. It provided the turbine with more inlet pressure than could be effectively utilized. Both engine scavenging and the compressor itself limited the amount of power that the compressor could absorb. The extra turbine pressure was bought at the price of engine scavenging and yet the turbine was unable to deliver any extra power as compensation. See Figure 89.

3h. Comparison of Best Runs With DeLaval B-17 Steady-Flow Turbocharger and Elliott H-561-2S Steady-Flow Turbochargers and the E.E.S. Manifold

The comparison which follows will demonstrate the performance of two very different systems. The Elliott model H-561-2S turbochargers were operated in parallel. The discharge end of the E.E.S. manifold was Y-connected to the turbocharger inlets. Each turbocharger, therefore, received the exhaust flow from one bank of cylinders and supplied the air for one bank of cylinders.

The DeLaval turbocharger was a single unit. The discharge of the manifold was connected directly to the inlet of the single turbocharger and the single turbocompressor supplied intake air to both cylinder banks.

For purposes of comparison, we shall use the Elliott model H-561-2S as the standard. The following table shows the comparative performance. a + means the DeLaval is "better than" the Elliott, a - means the DeLaval is "worse than" the Elliott.

η_R	P_{EXH}	P_T
(-8.1 to + 1.3)%	(+ 4.0 to - 1.0)%	(- 4.1 to + 6.2)%
f	e_S	R_S
(+6.9 to + 5.0)%	(+ 3.1)%	(+ 4.5 to +3.5)%
$\dot{m}_i$	B.S.F.C.	RC
(+3.6 to + 4.8)%	(- 2.2 to - .3)%	(0.0 to + 1.5)%

All turbine parameters show change of sign; $\Delta RC \approx$ constant, but the DeLaval installation shows definitely improved engine scavenging. The Elliott installation retains a similar edge in B.S.F.C. The improved scavenging is accounted for by virtue of the increased nozzle area of the DeLaval installation (4.30%) as contrasted with the Elliott nozzle area of 3.11% of piston area served. Improved engine scavenging was always noted in previous analyses as turbine nozzle area increased.

Both of these runs represent excellent performance. To attempt to find a best run between them would be valueless because of the similarity of the results. Since the turbochargers and minor ducting differences are the only geometric differences between these runs, the differences in performance (minor though they may be) can only be attributed to the differences between the turbochargers. As previously stated, it is not our intention to discuss the details of turbine-engine matching. Therefore, we will state that these runs are representative of the kind of performance that can be obtained with a near optimum manifold. The performance of these runs also demonstrates the improvement which can be realized by improving the engine exhaust manifold.

3i. 8-Cylinder Engine and DeLaval Manifold and DeLaval Model B-8 Steady-Flow Turbocharger

The geometric descriptions and general results are found in Appendix E and Figures 31b through 34b of Chapter IV. Data plots versus overall exhaust pressure ratio (P4/P6) are found in Figures 78 through 81.

This series of experiments was based on runs with the General Motors Model 8-268A Diesel Engine. This engine was a V-8 with an unsupercharged rated BHP of 425 at 1200 RPM. It is generally similar to the GM 16-278A except for size. The DeLaval Model B-8 turbocharger is generally similar in design to the B-17 Model, except for size. The experiments conducted serve mainly to reinforce conclusions developed earlier from the larger engine. Three full scale runs were conducted in this series.

In run 8B, the air in the intake manifold was maintained at 70°F by means of an aftercooler (placed between the compressor and the air box).

In run 8C, no attempt was made to cool the intake air. The temperature of the air varied between 130°F (at 300 BHP) and 280°F (at 800 BHP).

In run 8A, the air in the intake manifold was maintained at 100°F. In addition, the area of the turbine nozzles was increased some 12% over that of the first two runs.

The following table contrasts the first two runs.

	700 BHP		800 BHP	
	B Aftercooled	C Not Aftercooled	B Aftercooled	C Not Aftercooled
Manifold air density lb/ft^3	0.1330	0.1093	1.1460	0.1184
Air flow, lb/min.	127	138	143	155
Fuel consumption lb/bhp-hr	0.400	0.418	0.398	0.421
Measured air-fuel ratio, overall	27.2	28.3	26.9	27.6
Displacement, one cylinder, top of ports to top of liner, ft^3	0.1148	0.1148	0.1148	0.1148
*Wt air charge in cylinder, lbs.	0.0153	0.0126	0.0168	0.0136
Wt fuel charge, 1 cyl, 1 cycle, lbs.	0.000486	0.000508	0.000553	0.000585
**Wt air charge in cyl., lbs.	31.5	24.8	30.4	23.2
Trapping Efficiency	0.806	0.710	0.797	0.691
Cylinder air-fuel ratio	25.3	17.6	24.2	16.05
% Excess air	74	21	66	10

*Assuming cylinder filled with air at air box conditions when cylinder ports are just covered by the piston.

**Utilizing the trapping efficiencies computed by our program.

As can be seen from the table, air flow was reduced by the use of the aftercooler (7.8% less at 800 BHP). However, the density of the air in the intake manifold was greatly increased (23.3% more at BHP). The amount of excess air present in the cylinder was very much larger when the incoming air was cooled. This resulted in a substantial gain in fuel economy. At equal BHP's fuel economy was improved by from 3.4 to 5.6%. The reduced air flow resulted in less power being required by the compressor (i.e. less power recovered by the turbine). In the uncooled run, the higher temperature of the intake air coupled with the increased fuel flow led to considerably higher exhaust temperatures and moderately higher exhaust pressures. This caused a general increase in the amount of energy theoretically available in the exhaust gases. As has been previously discussed in this Chapter, it appears that the specific power in the exhaust gas increased at a more rapid rate than did the increase in energy required by the compressor. Therefore, the turbine recovery efficiencies uncooled were considerably lower than in the aftercooler runs. At equal BHP's, efficiencies were from 7.3 to 21.9% lower. At equal pressure ratios, (P4/P6) efficiencies were from 13.1 to 24.0% lower. See Figures 78 through 81 and Figure 31.

A comparison of runs 8A and 8B provide an indication of the effect of varying the turbine nozzle area. An aftercooler was used in both of these runs to maintain the intake air at a constant temperature. These temperatures were not too dissimilar (100°F for run 8A and 70°F for run 8B). Therefore, it can be assumed that performance differences

were mainly due to the changes in nozzle area. In run 8A, this area was some 12% greater than it was in run 8B. From our analysis, it appears that the nozzle area of run 8B was close to optimum. When this area was exceeded, performance suffered. The effects of increasing the nozzle area beyond the optimum area point were almost identical to the effects previously noted in the variable nozzle area experiments with the large engine and DeLaval manifold and turbine.

As the nozzle area was increased past the optimum point, the turbine recovered less power. At 900 BHP, the recovered power in run 8A was 15.8% less than that recovered in run 8B. This caused the turboblower to slow down (a 1500 RPM drop). This led to a 2% drop in air flow and, more important, an 8.1% drop in compressor pressure ratio. To maintain a power level of 900 BHP, substantially more fuel was required (13.4% more). The decreased air flow, coupled with the increased fuel flow, caused a substantial increase in the temperature of the exhaust gases (12.3%). This resulted in a moderate increase in the amount of energy theoretically available in the exhaust gas (3.8%). The pressure at turbine inlet decreased, however (8.7%). This led to a reduction in the amount of energy recovered by the turbine. The combined effect of increased theoretical energy and decreased recovered energy led to a large drop in computed turbine recovery efficiency (18.9%). See Figure 31 and Figures 78 through 81.

4. Summary

In the previous analyses, three distinct turbine nozzle areas have produced local optimum results. These different areas correspond to three different turbochargers. The Elliott Model H-504-MP-4S Pulse Turbocharger had its best performance at a nozzle ratio of 3.32% of piston area served. The Elliott Model H-561-2S Steady-Flow Turbocharger had its best performance at a nozzle ratio of 3.11% of piston area served. The DeLaval B-17 Steady-Flow Turbocharger had its best performance at a nozzle ratio of 4.30% of piston area served. The range of nozzle ratios tested showed that approximately 3.0% of piston area served was the lower limit of nozzle area ratios. Below 3.0%, any gain in turbine performance is completely overshadowed by losses in engine performance. The upper limit is definitely a function of the particular turbocharger installed. The Elliott geometries reacted unfavorably to increases in nozzle area above 3.11% of piston area served while the DeLaval reacted unfavorably to increases or decreases in area from 4.30% of piston area served. It would seem reasonable from the data thus far presented, that an approximate upper limit would be 4.5 to 5.0% of piston area served. Limits of 3.0 and 4.5 - 5.0% give a sufficient design latitude to produce a satisfactory turbine.

Excess exhaust power is a real problem. If the exhaust turbine is used as the prime mover for a compressor and the engine is to be operated over a wide-load range, the variation in entrance conditions for the turbine will also vary over a wide range. Gas turbine

technology has made great strides in recent years and the efficiency of gas turbines has been greatly improved. There is, however, a limit to the range of entrance conditions which any given turbo-machine can accommodate without marked loss in performance. The same remarks are also applicable to the compressor. The compressor also applies an additional constraint on the turbine. For a given mass flow, the compressor has an operating point fixed by its design. The compressor can only transfer a finite amount of energy to the intake air flow. This then limits the amount of power the turbine can recover regardless of its recovery potential. It has already been demonstrated that specific power in the exhaust increases more rapidly than the required energy increase in the intake air flow.

We have already shown that a high level of performance can be realized with an absolute minimum number of engine modifications. In such a case, with a reasonable turbocharger-engine match, the variations in turbine performance are of only academic interest. With proper attention to manifold design, the overall performance can be significantly improved.

It is a relatively simple mechanical problem to install a waste gate or similar control system in a manifold. Such a control system permits the channelling of excess exhaust gas away from the exhaust turbine, thereby permitting the turbine to operate at its design point. The excess exhaust gases can then be used to drive an additional turbine, passed through a heat exchanger, etc. or simply

dumped to the atmosphere, thereby reducing P_5 with the corresponding improvement in engine performance. There is an obvious requirement for a balance between turbine and engine requirements as P_5 is reduced.

The percentage of total theoretical exhaust power available as steady-flow power varies with P_5/P_4, but in our data, it varied from $\approx$ 50 - 70%. A representative percentage would be 65.0%. In the better runs, approximately 54% of total theoretical exhaust power was required to support the engine. Therefore, with a properly applied turbosystem of two stages, one blowdown at an efficiency of $\approx$ 70% and one steady flow at an efficiency of $\approx$ 85%, we could then recover (.70) (.35) + (.85) (.65) = .80. The power required by the compressor $\approx$ .54 leaving 26% of the theoretical exhaust power available for other uses. To make this power available would require the use of more than one turbine. A possible configuration would be four complete turbosystems, three of which would provide the turbocharging power and the fourth would be able to deliver approximately 20% of the theoretical exhaust power for arbitrary use. At higher engine outputs, this power is not inconsiderable; amounting to 200-250 HP. However, the requirement that the pulse turbine be very close to the engine presents many arrangement and mechanical difficulties.

An alternate proposal would require pulse turbines close to the engine driving turbochargers. This would provide recovery of $\approx$ 25% of the theoretical power, the exhaust gas could then be collected and used to drive two or more identical steady-flow machines which could

recover an additional ≈ 25% of theoretical power. This would permit ≈ 27% to be used for purposes other than supercharging the engine. The arrangement and mechanical problems are substantial. It is extremely questionable whether the increased cost and complexity are worth the power gained from exhaust recovery.

One excellent example, the Wright Turbo-Compound Aircraft engine, gears the turbine output to the engine output shaft. Such an arrangement has substantial possibilities because the entire engine package can be kept small.

The plot on Figure 96 shows the theoretical relationship of steady-flow energy to total blowdown potential as a function of dimensionless pressure ratio: $P_R = \frac{P_5 - P_6}{P_4 - P_6}$. The blowdown energy, W_B, is computed on the basis of a system of unit mass expanding isentropically from P_4 to P_6. As derived in Appendix F, the expression for W_B can be written as $W_B = W_{ID} =$

$$\frac{R_e T_4}{J}\left[\frac{1}{k_e - 1}\left(1 - \left(\frac{P_6}{P_4}\right)^{\frac{k_e - 1}{k_e}}\right) - \left(\left(\frac{P_5}{P_4}\right)^{\frac{k_e - 1}{k_e}} - \frac{P_5}{P_4}\right)\right]$$

The steady-flow energy, W_S, is computed on the basis of the enthalpy difference between points 5 and 6 and embodies a small correction for the stagnation effect produced when the high velocity flow from the exhaust elbows expands into the exhaust manifold proper.

$$W_S = C_{pe}\, J\, T_5 \left[1 - \left(\frac{P_6}{P_5}\right)^{\frac{k_e-1}{k_e}} \right]$$ where $T_5 = T_5 \times$ STAGNATION CORRECTION.

From a relatively crude evaluation of the gas dynamics of the GM 16-278A and other engines, a STAGNATION CORRECTION OF $\approx$ 1.5% is reasonable. This correction will vary with a particular engine geometry. Our value of 1.5% is taken as representative of current design. W_S contains no other allowance for the blowdown from P_4 - P_5. While this blowdown potential exists, if no recovery is made during blowdown, the greatest part of this potential is dissipated and not recoverable in steady-flow.

The plot indicates that when $P_R \approx .3, W_s \approx W_B$. When $P_R > .3$, the relationship between W_S and W_B is controlled by the absolute value of P_4. As $P_4 \longrightarrow \infty$ and $P_r \longrightarrow 1.0$, W_S/W_B tends to a limiting value of ≈ 1.395. This plot demonstrates that at values of $P_R \lessapprox .3$, the blowdown potential is greater than the steady-flow potential. This condition indicates that if blowdown recovery efficiency could approach that attainable in steady-flow, it would be preferable to operate on the blowdown potential. Since this is not now the case, it is currently necessary to operate almost without exception on the steady-flow potential alone.

Figure 97 demonstrates an alternative means of presenting exhaust energy potential. In this plot, total exhaust potential, W, is considered to be the blowdown energy W_B, from 4 to 5, plus the steady-flow energy, W_S, from 5 to 6. $\therefore W = W_S + W_B$. We recognize the artificiality of this summation. Unless the blowdown potential is

directly operated upon, it is essentially lost. It is, nonetheless, a real potential and forms a real part of the total exhaust potential since it is available for possible recovery.

The ratio W_S/W therefore demonstrates the portion of the theoretical maximum available energy which is operated upon by the average exhaust power recovery system.

The conclusions which can be drawn can most usefully be presented by dividing them into those which are directly applicable to the engine and those which are directly applicable to the turbine.

A. Optimum Engine Performance

1. The turbocharger unit must be properly matched to the engine if either unit is to deliver proper performance. This requirement is absolutely paramount and admits of no compromise if the system is to perform well over a large operating range.

2. The size and configuration of the exhaust manifold exerts a controlling influence upon engine performance, particularly the B.S.F.C.

3. An exhaust system should offer no unnecessary restriction to flow such as are found in the Pulse Converter Manifold with flow directors and reduced exhaust elbow areas, the E.E.S. manifold with charger plates, and Divided Manifolds I and II.

4. Systems intended to convert blowdown energy to pressure and temperature must be carefully evaluated for possible adverse effects reflected back into the engine.

5. Attempts to capture blowdown energy by using multiple pipes, separate turbine nozzles, etc. may reduce overall performance unless they are skillfully designed and take into account engine requirements.

B. Optimum Turbine Performance

1. The exhaust manifold has a pronounced influence on turbine performance. Specifically, the flow requirements of the turbine must be made compatible with those of the engine by the manifold. This concept is closely allied with the matching of turbocharger to engine. The manifold, since it exerts a controlling influence on both engine and turbine, must be considered when considering the match of turbocharger to engine.

2. For optimum turbine performance over a wide range of inlet conditions, it is paramount that the turbine be designed to accommodate the range of conditions at reasonable efficiency rather than being designed for extremely high efficiency at a single point. This condition can be alleviated by using a waste gate or similar system.

3. There does not appear to be a general optimum nozzle area. Optimum nozzle area is of the order of $\approx$ 3.1% - 4.3% of piston area served, but the absolute value is a function of the complete engine-exhaust manifold-turbocharger system. Nozzle area exerts a very pronounced effect on overall system as well as turbine performance. It is quite probable that a poor choice of nozzle area could invalidate an otherwise excellent system.

4. As previously stated, η_R is only an index of turbine performance. It is of interest to observe that η_R tends to increase as overall system performance improves. As engine performance improves, B.S.F.C. improves accordingly. Therefore, the amount of energy released to the

exhaust is correspondingly reduced. The demands of the compressor remain substantially fixed. This condition results in higher observed η_R if the turbocharger remains self-sustaining.

Our summarizing and most general conclusion is that for most turbocharged installations greater improvement in total system performance can be realized by improving the exhaust manifold than can be realized from improving the turbine. The difference in performance of the Elliott and DeLaval turbochargers as the manifold was changed demonstrates conclusively the effect of the exhaust manifold. Further, the cross comparison of the Elliott and DeLaval turbochargers indicate that turbine performance is subordinate to the manifold's effects. In summary, a good manifold can overcome many of the effects of a non-optimum turbine, but a good turbine cannot overcome a bad manifold.

CHAPTER VI

RECOMMENDATIONS

It has been demonstrated that the exhaust manifold plays a controlling role in an engine's ability to breathe. The exhaust manifold in conjunction with a turbocharger controls engine output, basic performance and more specifically, the B.S.F.C. It is recommended that further studies be made to determine the manifold size and geometric configuration which will provide the best turbocharged engine performance. It is hoped that such a study would provide design ratios and relationships directly applicable to the general design case.

The results of this thesis create the surface impression that recovery of exhaust power by means other than a turbocharger is not economically feasible in normal engineering applications. A thorough economic study of a series of exhaust power recovery systems would be of great practical and academic value.

APPENDIX A

*DESCRIPTION OF GENERAL MOTORS MODEL 16-278A DIESEL ENGINE AND TEST MANIFOLDS

A standard General Motors Model 16-278A diesel engine with the following characteristics was used:

Number of Cylinders	16
Cylinder Arrangement	40° Vee
Operating Cycle	Two-stroke, uniflow scavenged
Bore, in.	8.75
Stroke, In.	10.5
Rated Speed, RPM	750
Rated Power Output, Normal, BHP	1700 (88.8 psi bmep)
Exhaust Valves Open, ° ATC	89
Exhaust Valves Close, ° ABC	58 $\frac{1}{2}$
Intake Ports Open, ° ATC	134
Intake Ports Close, ° ABC	46
Piston Displacement, per cyl., cu. in.	631.5
Cylinder Swept Volume, Total for Engine at 750 RPM, CFM	4385

The engine was modified as follows:

1. The standard fuel injector assemblies were replaced with units of increased capacity.

2. The standard fuel transfer pump was replaced with a larger unit.

* The majority of this material is taken from References 13, 21 and 22.

3. The standard fuel injector spray tips were replaced with tips with larger orifices.

4. The engine cylinder compression ratio was reduced from the standard value of 15.6:1 to new values of 13.8:1 and 13.0:1.

The five different test manifolds are described below:

1. Divided Manifold I consisted of eight individual tubes of 3.75 in. I.D. Four tubes made up the manifolding for one bank of eight cylinders, and each bank drove its own turbocharger. Each tube was the manifold for two cylinders 180 crank-angle degrees apart. Four tubes were connected to a common header immediately adjacent to the single turbine inlet. The manifold was insulated with asbestos.

2. Divided Manifold II was identical in all respects with Divided Manifold I except that the tubes were of 4.25 in. I.D.

3. The Common or GM Standard Manifold consists of a common header of 14.0 in. I.D. into which all sixteen cylinders exhaust. The manifold has a center outlet. A diffuser-adapter connected the manifold outlet to the inlet casings of the two turbochargers. This manifold was operated uncooled.

4. The Pulse Converter Manifold conformed essentially to a design furnished by the DeLaval Company. It was designed to convert the energy in the cylinder exhaust pulses into effective pressure. In this configuration, each bank of eight cylinders exhausted into its own 17.0 in. I.D. manifold. The outlet ends of the two manifolds were Y-connected to provide a single inlet to the single turbocharger. Inside each manifold, a flow director, or tunnel, was installed.

The flow director covered over the individual cylinder exhaust inlets. Thus the high velocity gas flow in the manifold was confined to the flow director and the exhaust pulses were not dissipated by direct discharge into the relatively larger volume of the manifold proper. The cylinder exhaust elbows ("primary exhaust nozzles") were adjustable so that the flow area could be varied (10 in^2 to 17.8 in^2). The elbows were 26 in. long. See Figure 98 and Plate I.

5. The EES Manifold was essentially a common exhaust manifold with generous direct-flow passages. The manifold was equivalent to a 15.25 in. I.D. tube. The exhaust elbows were as short as possible (17 in.) and their flow areas were as large as possible (21.8 in^2). Each group of four cylinders exhausted to rectangular headers which, in turn, were connected to the main manifold. Perforated pressure charging plates ("adapters") of various sizes could be inserted in the headers to change the effective length of the exhaust elbows.

Plate II is a photograph of a portion of the EES Manifold showing four exhaust elbows, a header box and the common manifold. Figure 92 is a drawing which shows how the charger plates were installed in the rectangular header boxes.

APPENDIX B

*DESCRIPTION OF GENERAL MOTORS MODEL 16-278A DIESEL ENGINE AND GENERAL ELECTRIC MODEL 7SRD3C TURBOCHARGERS

The engine characteristics and modifications are described in Appendix A. The exhaust manifolds used in this series of experiments were Divided Manifold I and the GM Common Manifold; also described in Appendix A.

The intake air was supercharged during two stages of compression. Two General Electric Model 7SRD3C pulse type turbochargers operated in parallel were used for the first stage of compression. The standard engine driven Roots blower provided the second stage of compression. A water cooled heat exchanger maintained the inlet temperature to the engine airbox at 100°F.

The General Electric turbochargers consisted of a single stage compressor and a single stage turbine mounted on a common shaft. The compressor was centrifugal type, and the turbine was designed for axial flow, pulse operation. The turbine employed a fixed geometry nozzle ring of 18.8 in^2 flow area with a single inlet.

The engine power was absorbed by a hydraulic dynamometer. All tests were conducted at 780 RPM.

*The majority of this material is taken from Reference 13.

APPENDIX C

*DESCRIPTION OF GENERAL MOTORS MODEL 16-278A DIESEL ENGINE AND ELLIOTT MODELS H-504-MP-4S AND H-561-2S TURBOCHARGERS

The engine characteristics and modifications are described in Appendix A. The exhaust manifolds used in this series of experiments were Divided Manifold II, the GM Common Manifold, the Pulse Converter Manifold and the E.E.S. Manifold; described in Appendix A.

The intake air was supercharged during two stages of compression. Two Elliott Model H-504-MP-4S or H-561-2S turbochargers operated in parallel were used for the first stage of compression. An engine driven Roots blower provided the second stage of compression. A water cooled heat exchanger was used as an intercooler between stages and as an aftercooler after the second stage of compression. In both configurations, the output air flow from the heat exchanger was cooled to 100°F.

During the earlier tests, the engine-driven blower was the standard blower for the unsupercharged 16-cylinder engine (6860 CFM capacity). During certain tests this blower acted as an air motor; extracting power from the inlet air flow. For comparative purposes, a smaller blower of the size normally used on the GM 12-cylinder engine (5350 CFM capacity) was installed.

The engine power was absorbed by a hydraulic dynamometer. Early tests were conducted at 780 RPM; later tests were conducted at 750 RPM.

---

*The majority of this material is taken from Reference 21.

Two distinct series of tests are involved here. In both series the compressors and turbines were single stage machines mounted on a common shaft. The compressors were identical and of the centrifugal type, but the turbines were different. The Model H-504-MP-4S was a pulse type, axial flow turbine and the Model H-561-2S was a steady, axial flow type.

The pulse type turbocharger was tested with Divided Manifold II and the Common Manifold, the standard engine driven blower and fixed geometry nozzle rings of 15 - 18.5 in^2 flow area.

The steady flow turbocharger was tested with the Common Manifold, the Pulse Converter Manifold with and without tunnels, the EES Manifold with and without charger plates, the standard and reduced capacity engine driven blower, various exhaust elbow (primary nozzle) areas, and fixed geometry turbine nozzle rings of 14.3 - 20.0 in^2 flow area.

APPENDIX D

*DESCRIPTION OF GENERAL MOTORS MODEL 16-278A DIESEL ENGINE AND DELAVAL MODEL B-17 TURBOCHARGER

The engine characteristics and modifications are described in Appendix A. The exhaust manifolds used in this series of experiments were the Pulse Converter Manifold and the EES Manifold; also described in Appendix A.

The intake air was supercharged during two stages of compression. A DeLaval Model B-17 turbocharger was used for the first stage. An engine-driven Roots type blower was used for the second stage. A water cooled heat exchanger was used to cool the air to 100°F. This heat exchanger was used in two different configurations; as an aftercooler, the air was cooled after the second stage of compression and just prior to entering into the engine (see Fig. 90). As an intercooler, the heat exchanger cooled the air just prior to entering the Roots type blower.

The DeLaval Model B-17 turbocharger consisted of a single stage compressor and a single stage turbine mounted on a single shaft. The compressor was of the mixed flow type. The centripetal turbine was of the single-inlet steady flow type. The turbine nozzle vanes were adjustable so that the flow area could be varied (37 in^2 to 60 in^2).

---

*The majority of this material is taken from Reference 22.

During the earlier tests, the engine-driven blower was the standard one used with the 16-cylinder unturbocharged engine (6860 CFM capacity). Although this blower was necessary for starting and during periods of light load, its capacity was not required at higher loads. The exhaust turbocharger supplied sufficient air for the engine and the engine driven blower merely absorbed power. Therefore, during the later tests, a smaller engine-driven blower was installed (5350 CFM capacity). This smaller blower was the size usually used with the GM 12-cylinder engine.

The engine power was absorbed by a hydraulic dynamometer. All tests were conducted at an engine speed of 750 RPM. During all tests, the coolant flow through the air cooler was adjusted so that the outlet air temperature was maintained at 100°F (both in the after-cooler and the intercooler configurations).

APPENDIX E

*DESCRIPTION OF GENERAL MOTORS MODEL 8-268A DIESEL ENGINE AND DELAVAL MODEL B-8 TURBOCHARGER

A standard General Motors Model 8-268A diesel engine was used with the following characteristics:

Number of Cylinders	8
Cylinder Arrangement	In line
Operating Cycle	Two-stroke, uniflow scavenged
Bore, in.	6.50
Stroke, in.	7.00
Rated Speed, RPM	1200
Rated Power Output, Normal, BHP	425 (75.5 psi bmep)
Piston Displacement, per cyl., cu. in.	232.5
Cylinder Swept Volume, Total for Engine at 1200 RPM, CFM	1290

The engine was modified as follows:

1. The engine-driven positive-displacement blower was removed.

2. A DeLaval Model B-8 turbocharger was installed. The turbocharger was equipped with a hydrobooster unit for starting and light load operation.

3. The standard fuel injector assemblies were replaced with units of more than double capacity.

---

*The majority of this material is taken from Reference 19.

4. An air cooler was mounted between the turbocharger and the scavenge manifold.

An electric-motor driven variable-capacity hydraulic pump supplied hydraulic oil to the hydrobooster. The hydrobooster unit consisted of a small hydraulic turbine mounted on the turbocharger shaft. It was used for starting and light load operation (less than 360-400 BHP). At higher engine loads the exhaust turbocharger supplied sufficient air for the engine.

APPENDIX F

DERIVATION OF FORMULAE

FLOW BALANCE

The inlet air flow ($\dot{M}_I$) consists of dry air ($\dot{M}_\alpha$) plus water vapor ($\dot{M}_V$). A constant mass fraction of water vapor of .02 has been assumed for all runs.

$$\therefore \quad \frac{\dot{M}_V}{\dot{M}_\alpha} \equiv .02 \equiv h; \quad \frac{\dot{M}_I}{1+h} = \dot{M}_\alpha$$

Total flow to engine $\equiv \dot{M}_I$

Total flow from engine $\equiv \dot{M}_I + \dot{M}_F$

However, since all of the air supplied is not retained in the engine cylinders, allowance must be made for this "bypass" air.

The trapping efficiency, Γ, has previously been defined as

$$\frac{\text{Mass Retained}}{\text{Mass Supplied}}.$$

$\therefore$ Total mass trapped in engine cylinders/unit time $= \dot{M}_\alpha (1+h) \Gamma = \dot{M}_\alpha' (1+h)$.

Total trapped mass/engine cycle $= \frac{\dot{M}_\alpha}{N} (1+h) \Gamma = M_\alpha' (1+h)$

That flow, which is not trapped in the engine, passes from the inlet air box through the engine cylinders and into the exhaust manifold. This flow is equal to (total flow) - (flow trapped in the engine):

$$\therefore \quad \dot{M}_{SC} = \dot{M}_\alpha (1+h) (1-\Gamma)$$

The flow from the cylinders is simply the trapped flow plus mass of fuel consumed/unit time.

$$\therefore \quad \dot{M}_{EXH} = \Gamma\dot{M}_{\alpha}\,(1+h+F')$$

CONSIDERATION OF CYLINDER CHARGE

The composition of the cylinder charge during compression/ engine cycle

$$M_{CHC} = M_{\alpha}' + M_V + M_R$$

The following definitions apply:

$$M_{\alpha} \equiv \frac{\dot{M}_{\alpha}}{N};\ \Gamma M_{\alpha} \equiv M_{\alpha}'\ ;\ \frac{M_V}{M_{\alpha}} \equiv h$$

$$f \equiv \frac{M_R}{M_{\alpha}'+M_R}$$

$$\therefore \quad M_R = M_{\alpha}'\frac{f}{(1-f)}$$

then $M_{CHC} = M_{\alpha}' + M_{\alpha}'\cdot h + M_{\alpha}'\cdot\frac{f}{(1-f)} = M_{\alpha}'\left(1+h+\frac{f}{1-f}\right) = \frac{M_{\alpha}'}{(1-f)}\left[1+h(1-f)\right]$

The cylinder charge changes only after the injection and combustion of the fuel so that during the expansion process

$$M_{CHE} = M_{\alpha}' + M_V + M_R + M_F$$

Since $M_{\alpha}' + M_V + M_R = M_{CHC} = M_{\alpha}'\cdot\left[(1+h) + \frac{f}{(1-f)}\right]$

$$M_{CHE} = M_{CHC} + M_F = M_{\alpha}'\cdot\left[(1+h) + \frac{f}{(1-f)}\right] + M_F$$

But $F' = \frac{M_F}{M_{\alpha}'}$, thus $M_F = M_{\alpha}'\cdot F'$

$$\therefore \quad M_{CHE} = M_{\alpha}'\left[(1+h) + \frac{f}{(1-f)} + F'\right]$$

Fig. 91

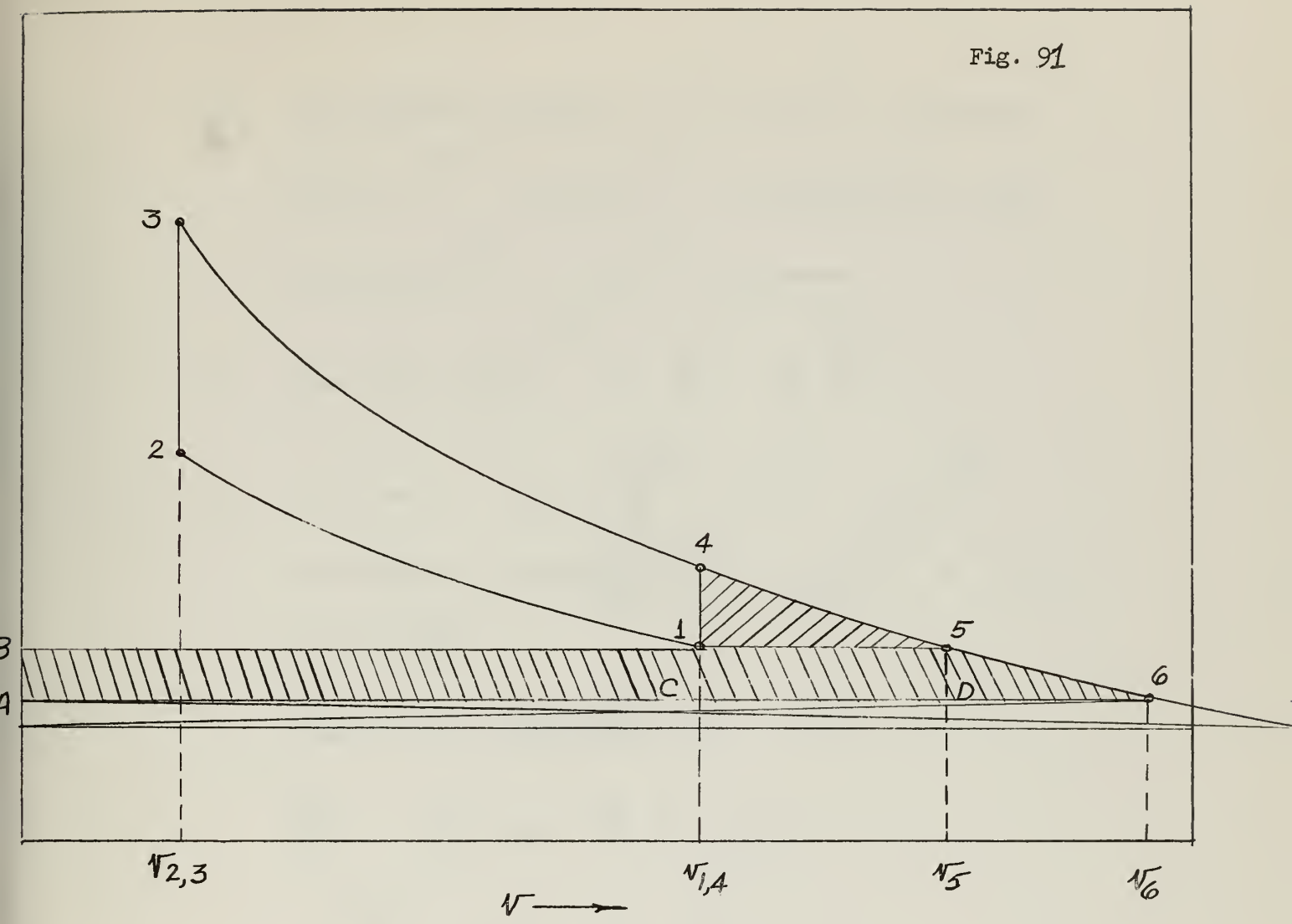

THEORETICAL EXHAUST POWER

The ideal blowdown work = area C-4-5-D-C minus area C-1-5-D-C as shown on Fig. 91.

The derivation* is as follows assuming isentropic expansion:

$$\frac{C_{Pe}}{C_{Ve}} = K_e \; ; \; C_{Pe} - C_{Ve} = \frac{R_e}{J} \quad ; \quad K_e = 1.35$$

(1) $$C_{Pe} - \frac{C_{Pe}}{K_e} = \frac{R_e}{J} \; ; \; C_{Pe}\,(1 - 1/K_e) = \frac{R_e}{J} \; ; \; C_{Pe} = \frac{R_e}{(1 - 1/K_e)}$$

(2) $$C_{Ve}K_e - C_{Ve} = \frac{R_e}{J} \; ; \; C_{Ve}\,(K_e - 1) = \frac{R_e}{J} \; ; \; C_{Ve} = \frac{R_e}{(K_e - 1)}\; J$$

*Taken from Reference 28.

(3) For adiabatic processes: $p.v^{K_e} = P_1 v_1^{K_e} = \text{constant}$

or $P.V.V.^{K_e-1} = P_1 \cdot v_1 \cdot v_1^{K_e-1} = \text{constant, but } Pv = R_e T$

therefore $Tv^{K_e-1} = T_1 v_1^{K_e-1} = \text{constant}$

(4) then $T/T_1 = \left(\frac{v_1}{V}\right)^{K_e-1}$ or $\frac{v_1}{v} = \frac{T}{T_1}^{\frac{1}{K_e-1}}$

(5) but from (3) $P/P_1 = \left(\frac{V_1}{V}\right)^{K_e}$ or $\frac{v_1}{v} = \left(\frac{P}{P_1}\right)^{\frac{1}{K_e}}$

combining (5) and (4) $\left(\frac{T}{T_1}\right)^{\frac{1}{K_e-1}} = \left(\frac{P}{P_1}\right)^{\frac{1}{K_e}}$ or $T/T_1 = \left(P/P_1\right)^{\frac{K_e-1}{K_e}}$

finally $P/P_1 = \left(T/T_1\right)^{\frac{K_e}{K_e-1}}$

$$\frac{W_{ID}}{lbm} = \left[(U_4 - U_5) - \frac{P_5}{J}(v_5 - v_4)\right]$$

$$\text{or } \frac{W_{ID}}{lbm} = C_{Ve}(T_4 - T_5) - \frac{P_5}{J}(v_5 - v_4)$$

Replacing T_5 and $v_5 - v_4$

$$\frac{W_{ID}}{lbm} = \left[C_V\left(T_4 - T_4\left(\frac{P_5}{P_4}\right)^{\frac{K_e-1}{K_e}}\right) - \frac{R}{J}\left(T_4\left(\frac{P_5}{P_4}\right)^{\frac{K_e-1}{K_e}} - T_4\frac{P_5}{P_4}\right)\right]$$

with $C_V = \frac{R_e}{(K-1)J}$ from (2)

$$\frac{W_{ID}}{lbm} = \left[\frac{R_e}{J}\frac{T_4}{(K_e-1)}\left(1 - \left(\frac{P_5}{P_4}\right)^{\frac{K_e-1}{K_e}}\right) - \frac{R_e T_4}{J}\left(\left(\frac{P_5}{P_4}\right)^{\frac{K_e-1}{K_e}} - \frac{P_5}{P_4}\right)\right]$$

$$\frac{W_{ID}}{lbm} = \frac{R_e}{J} \quad T_4 \left[\frac{1}{K-1} \left(1 - \left(\frac{P_5}{P_4}\right)^{\frac{K_e-1}{K_e}}\right) - \left(\left(\frac{P_5}{P_4}\right)^{\frac{K_e-1}{K_e}} - \frac{P_5}{P_4}\right)\right]$$

Multiplying both sides by $\frac{J\dot{M}_{EXH}}{3.3 \times 10^4}$

converts work/lbm to power

$$\therefore \dot{P}_{EXH1} = \frac{\dot{M}_{EXH} R_e T_4}{3.3 \times 10^4} \left[\frac{\left(1 - \left(\frac{P_5}{P_4}\right)^{\frac{K_e-1}{K_e}}\right)}{K_e - 1} - \left(\left(\frac{P_5}{P_4}\right)^{\frac{K_e-1}{K_e}} - \frac{P_5}{P_4}\right)\right]$$

The steady flow work 5-6, P_{EXH2_1} is simply the enthalpy difference.

$$\frac{T_6}{T_5} = \left(\frac{P_6}{P_5}\right)^{\frac{K_e-1}{K_e}} \qquad Y_{T1} = 1 - \left(\frac{P_6}{P_5}\right)^{\frac{K_e-1}{K_e}}$$

$$P_{EXH\ 2} = \frac{\dot{M}_{EXH}}{3.3 \times 10^4} \quad C_{Pe}\ J\ (T_5 - T_6) =$$

$$\frac{\dot{M}_{EXH}}{3.3 \times 10^4} \quad C_{Pe}\ J\ T_5 \quad \left(1 - \frac{P_6}{P_5}^{\frac{K_e-1}{K_e}}\right) = \frac{\dot{M}_{EXH}}{3.3 \times 10^4} \quad C_{Pe}\ J\ T_5\ Y_{T1}$$

in the same manner the power in the bypass air

$$P_{SC} = \frac{\dot{M}_{SC}}{3.3 \times 10^4} \quad C_{P\alpha}\ T_1\ J\ Y_{T2}$$

where $Y_{T2} = 1 - \left(\frac{P_6}{P_5}\right)^{\frac{K_\alpha - 1}{K_\alpha}}$

$P_{EXH} \equiv P_{EXH\ 1} + P_{EXH\ 2} + P_{SC} =$ Total Power Available in the Exhaust System

$$P_T = \frac{\dot{M}_I J}{3.3 \times 10^4} (h_{DISCH} - h_A) = \frac{\dot{M}_I J C_{P\alpha}}{3.3 \times 10^4} (T_{DISCH} - T_A)$$

$$\frac{\text{Work Ideal}}{\text{Work Actual}} \equiv \eta_C = \frac{(T_{ID} - T_A))}{(T_{DISCH} - T_A)} \frac{C_{P\alpha}}{C_{P\alpha}}$$

$$\frac{T_{ID}}{T_A} = (RC)^{\frac{K_\alpha - 1}{K_\alpha}}$$

$$C_{P\alpha} (T_{DISCH} - T_A) = \frac{(T_{ID} - T_A)}{\eta_C} \quad C_{P\alpha} = \text{Work Actual}$$

$$\text{Work Actual} = T_A \frac{\left[(RC)^{\frac{K_\alpha - 1}{K_\alpha}} - 1\right]}{\eta_C} C_{P\alpha}$$

$$\therefore P_T = P_C = \frac{\dot{M}_I J}{(3.3 \times 10^4)} \frac{C_{P\alpha} T_\alpha}{\eta_C} \left[(RC)^{\frac{K_\alpha - 1}{K_\alpha}} - 1\right]$$

The overall exhaust power recovery efficiency $(\eta_R) \equiv$

$$\frac{\text{Power Recovered}}{\text{Ideal Power}} \equiv \frac{P_T}{P_{EXH}}$$

APPENDIX G

DESCRIPTION AND DISCUSSION OF COMPUTER PROGRAM

After several weeks of hand calculations, the need to shift to machine operations became apparent. The calculations were straightforward, but lengthy because of the iterative technique used. A minimum of two man-hours of hand calculations was required for each data point. The number of exponential operations required and the degree of accuracy desired were not consistent with handwork.

After several weeks of working with the curves of Reference 11, it became apparent that these curves could be approximated by a series of straight line segments within our region of interest.

GM 16-278A Diesel Engine

The program for the 16-cylinder engine was written first since the majority of our data was obtained from this engine.

The first problem was the determination of scavenging efficiency (e_s). As previously discussed, we decided to use Figure 11-7 of Reference 27, which is a curve of scavengine efficiency (e_s) versus scavenging ratio (R_s) for two-cycle, poppet exhaust valve engines. It was assumed, and later confirmed, that the range of R_s was small enough to allow approximation of Figure 11-7 by a single straight line in our region of interest. The actual range of R_s was from 0.95 to 1.10. The formula used was:

$$e_s = 0.5\ R_s + 0.2.$$

The next, and major problem, was the interpolation and/or linearization of the curves of Reference 11. Four curves describe the relationship between P_4 and P1 as functions of engine compression ratio (r), relative trapped fuel-air ratio (F_r'), temperature of mixed cylinder charge at start of compression (T1), fraction of residual gas retained (f) and mass percent of water vapor (h). The curves are set up such that each of the above variables produces a correction factor. When these correction factors are multiplied together, the resulting number is the ratio P_4/P_1. In our computer program, these factors are labelled CORR1, CORR2 and CORR3. In an analogous manner, the correction factors for determining the relationship between T_4 and T1 may be found. These correction factors are labelled CORR11, CORR22 and CORR33. The correction factor for humidity effects is unity.

The first parameter to be considered was engine compression ratio (r). Fortunately, the 16-cylinder engine runs were performed at only two different compression ratios: 13:1 and 13.8:1. Separate subprograms within the main program were written for each compression ratio.

The next important parameter was that of relative trapped fuel-air ratio (F_r'). F_r' is used as an input to the curves of Reference 11 to determine CORR1 and CORR11. It was decided to cover the range from $F_r' = 0.300$ to $F_r' = 0.700$. This range was further divided into four subranges: 0.300 to 0.400, 0.400 to 0.500, 0.500 to 0.600 and 0.600 to 0.700. In actual practice, the engine operated between $F_r' = 0.383$ to $F_r' = 0.600$. Linear interpolation within this family of curves was considerably more accurate than the eye interpolation previously used in hand calculations.

It had been previously observed from hand calculations that T1 was equal to $700^{\circ}R \pm 60^{\circ}$. T1 is used as the entering argument to the curves to determine CORR2 and CORR22. These curves also require F_r' as an input. However, in the vicinity of T1 = $700^{\circ}R \pm 60^{\circ}$, the curves are insensitive to relatively large changes in F_r'. Moreover, when T1 = $700^{\circ}R$ exactly, the multiplying correction factor equals unity. Therefore, two linearized approximations were used to cover the cases of T1 < $700^{\circ}R$ and T1 $\geq$ $700^{\circ}R$. These linearized approximations are as accurate as the basic curves themselves for the values of T1 in which we are interested.

Finally, it was necessary to compute CORR3 and CORR33 due to variations in exhaust gas retained (f). These curves are themselves straight lines so no approximation was required.

The last major decision was the degree of iterative accuracy desired and the method of selecting new trial data. It was decided to continue iterating until the controlling temperatures agreed within $0.25^{\circ}F$.. It was also decided to select the new trial temperature by simply averaging the input and output temperatures. Fortunately, these decisions produced accurate results with a minimum expenditure of computer time.

The remaining equations were identical with those used in the hand calculations. Cross checks between hand and machine computations showed close agreement. Due to the length of the hand process, it is felt that the slight disagreements between the two methods (under 4%) are explained by errors in the hand process rather than in the machine operations.

GM 8-268A Diesel Engine

The program for the 8-cylinder engine was exactly the same in principle as that for the larger engine. However, some of the parameters of the smaller engine varied over a greater range of values.

Scavenging efficiency was determined from Figure 11-7 of Reference 27 as before. The formula used was:

$$e_s = 0.426\ R_s + 0.2848$$

Within the actual range of acavenging ratios (0.63 to 0.80) this formula is accurate to within 1%.

The curves of Reference 11 were linearized for the single compression ratio of 15.6:1. Interpolation within the family of F_r' curves was identical with that for the 16-cylinder engine. F_r' varied between 0.630 and 0.796.

T1 varied considerably more in the smaller engine than in the larger. Therefore, it was necessary to increase the number of straight line segments. Separate equations were written for 100° segments between 700°R and 1200°R. These large temperature changes were caused by large variations in air flow. In this engine, the ratio of maximum air flow (high power) to minimum air flow (low power) varied between a low of 2.9 and a high of 3.5. In the 16-cylinder engine, this ratio varied only between 1.4 and 1.8 with consequent reduced cooling effect. It is felt that the larger variations in T1 and F_r' present in the smaller engine were adequately compensated for by the larger number of straight line segments. The maximum possible error introduced in this region is less than 2%.

All other equations were similar to those for the larger engine.

In the final analysis, the program for the 8-cylinder engine was probably only slightly less accurate than that for the 16-cylinder engine. Due to the wider variation in operating conditions, the basic thermodynamic model may itself, however, be somewhat less accurate.

Error Check Procedure

An attempt was made to determine the envelope of possible errors produced by various combinations of parameters. This procedure is discussed in Appendix H.

This procedure was used for three different engine-manifold-turbine geometries of the 16-cylinder engine. The geometries chosen were representative of the large number of geometric permutations.

As stated elsewhere, simultaneous errors ($\pm$ 5% and $\pm$ 1") in the measurements of air flow, air box temperature, turbine inlet pressure and turbine outlet pressure resulted in errors in turbine recovery efficiency of only 10-13%.

Computer Program

The basic program for the 16-cylinder engine is reproduced below. Computer inputs were: air flow, fuel flow, room temperature, engine RPM, turbine inlet pressure, turbine outlet pressure, clearance volume, compressor efficiency, compressor pressure ratio, air box temperature and engine brake horsepower. Computer outputs were: pressure and temperature at exhaust valve opening, turbine inlet and turbine outlet; trapping efficiency, relative trapped fuel-air ratio, mass ratio of fuel to dry air, blowdown energy, steady-flow energy, "bypass" or "scavenge" energy, total theoretical exhaust energy, actually recovered exhaust energy, turbine recovery efficiency and engine brake horsepower.

```
*       XEQ
*       MAD
        PRINT FORMAT GOUGE
        VECTOR VALUES GOUGE = $ (105H    T4     P4     T5     P5     T6
          P6    GAMMA  FR     F      PEXH1   PEXH2  PSC    PEXH       PT
         ETAR     BHP) $
        RE = 53.5
        K1 = 1.35
        K2 = 1.40
        CP1 = .27
        CP2 = .24
        EXP1 = (K1-1.)/K1
        EXP2 = (K2-1.)/K1
START   READ FORMAT DATA 1, MI, MF, TA, N, P5, P6
        READ FORMAT DATA 2, VC, ETAC, RC, R, TBX, BHP
        VECTOR VALUES DATA 1 = $ (6F12.3) $
        VECTOR VALUES DATA 2 = $ (6F12.3) $
        P1 = P5
        MA = MI/1.02
        PE = 144.0*P5*14.7
        RS = MI*RE*TA/N/VC/PE
        X = RS -1.08
        ES = .740 + X/2.
        GAMMA = ES/RS
        FPRIME  = MF* .945/GAMMA/MA
```

```
          FR = FPRIME/.0678

          WHENEVER R .E. 13.0, TRANSFER TO R13

          WHENEVER R .E. 13.8, TRANSFER TO R138

R13       WHENEVER FR .G. .300 .AND. FR .L. .400, CORR1 = 2.10 +
          (FR - .300) * 3.80

          WHENEVER FR .GE. .400 .AND. FR .L. .500, CORR1 = 2.48 +
          (FR - .400) * 3.70

          WHENEVER FR .GE. .500 .AND. FR .L. .600, CORR1 = 2.85 +
          (FR - .500) * 3.60

          WHENEVER FR .GE. .600 .AND. FR .L. .700, CORR1 = 3.21 +
          (FR - .600) * 3.50

          F = .12

GO        MCHC = GAMMA*MA* (1.+(.02)*(1.-F))/N/(1.-F)

          V = VC/MCHC

          T1 = P1*V/.0255

          WHENEVER T1 .L. 700.0, CORR2 = 1.00+(700.0-T1)* .10/80.

          WHENEVER T1 .GE. 700.0, CORR2 = 1.00+(700.0-T1)*.001

          CORR3 = .96+(.10-F)*.80

          P4 = P1*CORR1*CORR2*CORR3

          WHENEVER FR .G. .300 .AND. FR .L. .400, CORR11 = 2.10 +
          (FR - .300) * 3.50

          WHENEVER FR .GE. .400 .AND. FR .L. .500, CORR11 = 2.45 +
          (FR - .400) * 3.40

          WHENEVER FR .GE. .500 .AND. FR .L. .600, CORR11 = 2.79 +
          (FR - .500) * 3.30

          WHENEVER FR .GE. .600 .AND. FR .L. .700, CORR11 = 3.12 +
          (FR - .600) * 3.20

          CORR22 = 1.00+(T1-700.0)*.00038

          CORR33 = .966+(.10-F) * .74
```

```
        T4 = T1*CORR11*CORR22*CORR33

        PR = P5/P4

        PR1 = PR.P.EXP1

        T5 = T4*PR1

        T1A = TBX*(1.-F)+F*CP1*T5/CP2

        DELTAT = T1A-T1

        WHENEVER .ABS.DELTAT .G. .250

        F = (F+(T1-TBX)/(CP1*T5/CP2-TBX))*.50

        TRANSFER TO GO

        OTHERWISE

        TRANSFER TO PWR

        END OF CONDITIONAL

R138    WHENEVER FR .G. .300 .AND. FR .L. .400, CORR1 = 2.07 +
        (FR - .300) * 3.80

        WHENEVER FR .GE. .400 .AND. FR .L. .500, CORR1 = 2.45 +
        (FR - .400) * 3.70

        WHENEVER FR .GE. .500 .AND. FR .L. .600, CORR1 = 2.82 +
        (FR - .500) * 3.60

        WHENEVER FR .GE. .600 .AND. FR .L. .700, CORR1 = 3.18 +
        (FR - .600) * 3.80

        F = .12

WENT    MCHC = GAMMA*MA*(1.+(.02)*(1.-F))/N/(1.-F)

        V = VC/MCHC

        T1 = P1*V/.0255

        WHENEVER T1 .L. 700.0, CORR2 = 1.00 + (700.0-T1) * .10/80.

        WHENEVER T1 .GE. 700.0, CORR2 = 1.00 + (700.0-T1) * .001

        CORR3 = .96 + (.10 - F) * .80
```

```
          P4 = P1*CORR1*CORR2*CORR3

          WHENEVER FR .G. .300 .AND. .L. .400, CORR11 = 2.07 +
          (FR - .300) * 3.50

          WHENEVER FR .GE. .400 .AND. FR .L. .500, CORR11 = 2.42 +
          (FR - .400) * 3.40

          WHENEVER FR .GE. .500 .AND. FR .L. .600, CORR11 = 2.76 +
          (FR - .500) * 3.20

          WHENEVER FR .GE. .600 .AND. FR .L. .700, CORR11 = 3.08 +
          (FR - .600) * 3.10

          CORR22 = 1.00 + (T1 - 700.0) * .00038

          CORR33 = .966 + (.10-F) * .74

          T4 = T1*CORR11*CORR22*CORR33

          PR = P5/P4

          PR1 = PR.P.EXP1

          T5 = T4 * PR1

          T1A = TBX * (1.-F) +F*CP1*T5/CP2

          DELTAT = T1A - T1

          WHENEVER .ABS. DELTAT .G. .250

          F = (F+(T1-TBX)/(CP1*T5/CP2-TBX)) * .50

          TRANSFER TO WENT

          OTHERWISE

          TRANSFER TO PWR

          END OF CONDITIONAL

PWR       ALPHA1 = (P6/P5) .P. EXP1

          ALPHA2 = (P6/P5) .P. EXP2

          T6 = T5*ALPHA1
```

```
YT1 = 1. - ALPHA1

YT2 = 1. - ALPHA2

MEX = GAMMA*MA*(1.02 + FPRIME)

BETA = MEX * RE * T4/3.3E4

DELTA = 1./(K1-1.)

J = 778.

PEXH1 = BETA*(DELTA*(1.-PR1)-(PR1-PR))

PEXH2 = MEX*CP1*T5*YT1*J/3.3E4

PSC = (1.-GAMMA)*MI*CP2*T1*YT2*J/3.3E4

DT = TA*(RC.P.EXP2-1.)/ETAC

PT = MI*CP2*DT*J/3.3E4

ETAR = (PT*100.)/PEXH

PRINT FORMAT DOPE, T4,P4,T5,P5,T6,P6,GAMMA,FR,F,PEXH1,PEXH2,
PSC,PEXH,PT,ETAR,BHP

VECTOR VALUES DOPE = $(1X,F7.2,1X,F4.2,1X,F7.2,1X,F4.2,1X,F7.2,
1x,F4.2,1x,F5.3,1X,F5.3,1X,F5.3,1X,F6.2,1X,F6.2,1X,F6.2,1X,F7.2
1X,F7.2,1X,F6.3,1X,F7.2)$

TRANSFER TO START

END OF PROGRAM

*       DATA

DATA CARDS WITH MI,MF,TA,N,P5,P6,VC,ETAC,RC,R,TBX AND BHP
```

APPENDIX H

DATA RELIABILITY

There are two major factors to be discussed when considering the validity of the results obtained. The first factor is a purely mechanical one in which errors in measuring engine data (inputs to our program) would cause errors in the program output. The second factor is concerned with errors in our basic thermodynamic model.

The following engine data are inputs to our program: MI, MF, TA, N, P5, P6, VC, ETAC, RC, r, TBX and BHP.

1. MI is the mass rate of flow of intake air to the engine. This was measured by a venturi-type flowmeter.

Errors in measurement of MI could come from two sources. First, the measuring instrument might give incorrect values. Second, the mass rate of flow through the compressor (where the flowmeter was physically installed) may not be the same as the mass rate of flow through the engine.

This second situation occurred in the runs with the DeLaval turbine. The DeLaval turbine is a monorotor design; the turbine and compressor impellers are mounted back to back. A short direct leakage path was present between the exhaust and air side. The amount and direction of air leakage depends on the pressure differential between the compressor air and the turbine exhaust. The pressures at the actual leakage path were not measured. However, some indication of their

magnitudes is shown by the values of turbine inlet pressure and compressor discharge pressure. During runs with relatively high turbine back pressure (muffler installed), the turbine inlet pressure exceeded the compressor outlet pressure at all power loads (up to a maximum value of 4" Hg). During runs with relatively low turbine back pressure (muffler bypassed), the compressor discharge pressure exceeded the turbine inlet pressure at power levels above 2100-2200 BHP. Thus at low power levels, the exhaust leaked into the compressor. As power increased, the amount of leakage decreased and finally the air began to leak into the exhaust turbine. It is estimated that the leakage air amounted to 3 to 5% of measured air flow at maximum engine load.

2. MF is the mass rate of flow of fuel to the engine. It was measured by a calibrated rotameter which is assumed to be accurate.

3. TA is the temperature of the air entering the compressor. This is basically the same as room temperature and is assumed to be accurate.

4. N is engine RPM which was held constant throughout the various runs and is assumed to be accurate.

5. P5 is turbine inlet pressure. P6 is turbine outlet pressure. These pressures were measured by mercury and water manometers respectively. We have investigated possible errors in the measurements of these pressures of $\pm$ 1" of mercury and water, respectively.

6. VC is the clearance volume of the engine and is accurate.

7. ETAC is the isentropic compressor efficiency. It was computed from compressor inlet and outlet temperatures and pressures and is considered to be accurate.

8. RC is compressor pressure ratio and is considered to be accurate.

9. r is the engine compression ratio and is considered to be accurate.

10. TBX is air box temperature. Due to the length of the engine, the cylinders furthest from the air box inlet received air some 20°F warmer than the cylinders adjacent to the air box inlet. We have used an average air box temperature for our calculations. We have investigated the effects of this temperature being in error by $\pm$ 5%.

11. BHP is engine brake horsepower and is used only for purposes of identification.

In order to determine the error sign, we processed eight separate data runs with inputs of MI, TBX, P5 and P6 individually varied by $\pm$ 5% or $\pm$ 1". After determining the error direction, we processed two data runs to find the worse possible additive combinations of the above variables.

Figure 94 shows the results of these calculations for a typical engine run. It can be seen that the errors of $\pm$ 5% and $\pm$ 1" results in errors in η_R of 10-13%. The slopes of the curves remain substantially constant.

The evaluation of possible errors in our thermodynamic analysis is more difficult. Approximate relationships have, of necessity, been used. It is not possible to calculate exactly the errors introduced by such approximations.

Uncertainty exists as to the temperature of the fresh cylinder charge (T1). This temperature is a function of the temperature of the air in the intake manifold (TBX), the mixing process and the temperature of the residual exhaust gas. None of the above is known exactly.

As discussed previously, there is a heating effect as the intake air travels down the air box. In some runs the temperatures at both ends of the air box were recorded. In such cases, we have simply averaged the two values. In some runs, however, only the air box inlet temperatures were recorded. In such cases, we have assumed an average air box temperature based on previous experience. It was observed that the total running time of the engine had a strong effect on the values of TBX.

The temperature of the residual exhaust gases is not known accurately. During the blowdown process, the exhaust gas temperature will drop isentropically. The residual gas in the vicinity of the combustion chamber may gain heat while the residual gas near the freshly uncovered cylinder walls will lose heat. Local gas velocities will affect the amount of heat transferred by conduction. The determination of an accurate mean temperature for the residual gases is therefore not possible. We have assumed that the temperature of the residual gases is approximately equal to T5.

The fresh air-residual exhaust gas mixing process is also not known accurately. In uniflow scavenged engines, such as these, the hottest portion of the residual gas leaves the cylinder when the fresh air enters. Some of the incoming fresh air charge mixes with the remaining residual gas, removes heat from it and passes out of the cylinder. The remaining fresh charge mixes with the now further cooled residual. Quite probably, this mixing process is incomplete when the cylinder compression cycle begins.

For purposes of simplicity, we have assumed that (1) only adiabatic mixing occurs between the incoming fresh air at temperature TBX and the residual exhaust gas at temperature T5 and (2) that this mixing has been completed before compression begins.

The amount of retained residual exhaust gas does not exceed 16.5%. Therefore, the inaccuracies discussed above should produce only small errors in the temperature of the final mixture (T1).

The temperature (T4) and pressure (P4) at the moment of exhaust valve opening are computed by the use of Reference 11 and the IBM 7094 digital computer. Reference 11 was a keystone in our thermodynamic analysis. Its own abstract clearly describes its content:

"The limits on reciprocating engine performances are set by the idealized constant-volume cycle. Heretofore, fuel-air cycles have been computed by tracing them out on thermodynamic charts -- a long and tedious process. By programming the thermodynamic characteristics of the fuel-air media and the cyclic processes on a digital computer,

it has been possible to compute the characteristics of fuel-air cycles over a wide range of fuel-air ratios, compression ratios, and initial conditions and present the results in graphic form."

The amount of residual exhaust gas retained (f) is an entering argument to the curves of Reference 11. This varied from run to run and was computed by an iterative process described elsewhere.

APPENDIX I

BIBLIOGRAPHY

1. Birmann, Rudolph The DeLaval Pulse Converter For Two-Cycle Engine, DeLaval Steam Turbine Co. Report #AGT-12 of January 7, 1953.

2. Birmann, Rudolph New Developments in Turbocharging, SAE Preprint of January, 1954.

3. Bohuslav, Hans & Jacobson, Carl A. Supercharging of High Speed Diesels, SAE Preprint #570 of August, 1955.

4. Cook, Harvey A. Digital Computer Analysis and Interpretation of Turbocharged Diesel Engine Performance, SAE Preprint of January 1950.

5. Cozier, John M. & Lang, Wolfgang S. Developing the Turbocharger for Its Application, SAE Preprint of November, 1960.

6. Crowley, John D., Gottschalk, Arthur W. and Nodell William R. The Utilization of the Exhaust Gas Energy in a Two-Stroke Diesel Engine, Massachusetts Institute of Technology Thesis, 1957.

7. Doolittle, J. S. & Ledbetter T. B. Preliminary Report on Estimation of Performance of Two-Cycle Supercharged Diesel Engine, Report to USN EES of 1 January 1957.

8. Doolittle, J.S. & Ledbetter, T. B. Preliminary Report on Diesel Engine Performance with High-Degree of Supercharging, Report to USN EES of 1 January 1959.

9. Doolittle, J. S. & Ledbetter, T. B. Diesel Engine Performance with High-Degree of Supercharging, Report to USN EES of 23 April 1959.

10. Doolittle, J. S. & Ledbetter, T. B. Performance Prediction for the GM 16-278A Diesel Engine with Supplementary Fuel Burned in the Engine Exhaust Gas, Report to USN EES of 26 May 1959.

11. Edson, M. H. & Taylor C. F. The Limits of Engine Performance - Comparison of Actual and Theoretical Cycles, SAE Preprint #633E of January, 1963.

12. Eksergian, Rupen Introduction to Monograph on Exhaust Turbocharging, Journal of the Franklin Institute, July 1953.

13. Harrison, John H. Performance of General Electric Model 7SRD3C Turbochargers with a General Motors Model 16-278A Diesel Engine USNMEL R&D Report 020016B NS-623-301 of 27 January 1956.

14. Hussmann, A. W. & Pullman, W. A. Formation and Effects of Pressure Waves in Multi-Cylinder Exhaust Manifolds, Pennsylvania State College report for the U. S. Navy, ONR Contract # NONR-656(02), Task No. NR-097-195 of December 1953.

15. Hussmann, A. W. & Pullman W. A. Blowdown Energy Utilization by Pre-Exhaust Separation, Pennsylvania State University report for the U. S. Navy, ONR Contract # NONR-656(02), Task No. NR-097-095 of September 1954.

16. Johnson, Lloyd Supercharged Diesel Performance vs Intake and Exhaust Conditions, SAE Transactions, 1953, Volume 61.

17. Meriwether, Ross F. Piston-Turbine Compound Engine, ASME Paper # 63-MD-51 presented 20 May 1963.

18. Reiners, N. M. & Woollenweber W. E. Turbocharging High Speed, High Output Diesel Engines, SAE Preprint # 673 of January 1956.

19. Reynolds, R. W. Test of General Motors Model 8-268A Turbocharged Diesel Engine, USN MEL R&D report 020188C NS-623-301 of 26 August 1957.

20. Schrader, Alan Simulated Turbocharger Operation of a General Motors Model 16-278A Two-Stroke Cycle Diesel Engine, USN MEL R&D report 020016A NS-623-201 of 25 February 1957.

21. Schrader, Alan Summary Report of Turbocharged Operation of a General Motors Model 16-278A Diesel Engine with Elliot Turbochargers, USN MEL R&D report 020016C NS-623-301 of 30 January 1958.

22. Schrader, Alan Summary Report of Turbocharged Operation of a General Motors Model 16-278A Diesel Engine with DeLaval Turbochargers, USN MEL R&D report 510016D NS-623-301 of 28 May 1958.

23. Shapiro, Ascher H. The Dynamics & Thermodynamics of Compressible Fluid Flow, Volume I., The Ronald Press Company, New York, 1953.

24. Smith, H. T. A High Supercharge Two-Stroke Diesel Investigation, SAE Preprint # 401 of October 1954.

25. Sonderegger, H. C. The Blowdown Energy in Piston Engines and its Utilization in Turbines, Pennsylvania State College report for the U. S. Navy, ONR Contract # NONR-656(02), Task No. NR-097-195 of July 1953.

26. Stecker, F. F. Analysis of Suitability of Miller Supercharging System for Application to GM 16-278A Diesel Engine, USN MEL report 2D(1)20174 NS-623-301 of 27 May 1952.

27. Taylor, C. F. & Taylor E. S. The Internal Combustion Engine, 2nd Ed., International Textbook Company, Scranton, Pa., 1962.

28. Tsu, T. C. Improving Engine Performance by Exhaust Pipe Tuning and by Neutralizing Interference between Adjacent Cylinders, Pennsylvania State College report for the U. S. Navy, ONR Contract # N6 ONR-269, Task Order 1, NR-221-002 of January 1951.

29. Wallace, F. J. & Nassif M. H. Air Flow in a Naturally Aspirated Two-Stroke Engine, Proceedings, Institute of Mechanical Engineers, London, 1954.

30. Wiegand, F. J. & Eichberg, W. R. Development of the Turbo-Compound Engine, SAE Transactions, 1954.

31. Williams, T. J. Exhaust Arrangements and their Influence on the Power Output on Internal Combustion Engines, Proceedings, Institute of Mechanical Engineers, London, 1954.

thesP98
Analysis of exhaust turbine performance
3 2768 001 93068 8
DUDLEY KNOX LIBRARY